3-2010

Reverse genetic and cell biological approaches to the study of developmental functions of Class XI myosin in Arabidopsis thaliana

Eunsook Park
University of Tennessee - Knoxville, epark3@mail.tennessee.edu

To the Graduate Council:

I am submitting herewith a dissertation written by Eunsook Park entitled "Reverse genetic and cell biological approaches to the study of developmental functions of Class XI myosin in Arabidopsis thaliana." I have examined the final electronic copy of this dissertation for form and content and recommend that it be accepted in partial fulfillment of the requirements for the degree of Doctor of Philosophy, with a major in Botany.

Andreas Nebenführ, Major Professor

We have read this dissertation and recommend its acceptance:

Albrecht von Arnim, Beth Mullin, Jae Park

Accepted for the Council:

Carolyn R. Hodges

Vice Provost and Dean of the Graduate School

(Original signatures are on file with official student records.)

To the Graduate Council:

I am submitting herewith a dissertation written by **Eunsook Park** entitled "**Reverse genetic and cell biological approaches to the study of developmental functions of Class XI myosin in *Arabidopsis thaliana***". I have examined the final electronic copy of this dissertation for form and content and recommend that it be accepted in partial fulfillment of the requirements for the degree of Doctor of Philosophy, with a major in Botany.

Andreas Nebenführ, Advisor

We have read this dissertation

And recommend its acceptance:

Albrecht Von Arnim

Beth Mullin

Jae Park

Accepted for the Council:

Carolyn R. Hodges

Vice Provost and Dean of the Graduate School

(Original signatures are on the file with official student records.)

Reverse genetic and cell biological approaches to the study of developmental functions of Class XI myosin in *Arabidopsis thaliana*

A Dissertation Presented for

The Doctor of Philosophy

Degree in Botany

The University of Tennessee, Knoxville

Eunsook Park

May 2010

Dedication

This dissertation is dedicated to

my parents

Chan-Hee Park and ***Kwan-Soon Choi***

and

my husband

Jongchan Woo

who love me well

and give endless supports for my life.

Acknowledgements

I am very grateful to my advisor, Dr. Andreas Nebenführ, for shaping me to be an independent cell biologist. His endless patience and meticulous guidance on me were really effective on me to run this long journey successfully. I also would like to deeply appreciate my committee, Dr. Albrecht von Arnim, Dr. Beth Mullin, and Dr. Jae Park. They, including Dr. Nebenführ, have been concerning my progress not only in my research but also in my life. I would like to thank them deeply for their countless and priceless advices to me for my future.

I also would like to express my appreciation to Dr. Mariano Labrador and my friend, Hyuck-Joon Kang, for allowing me to use a stereomicroscope in his lab any time. More than one third of experiments in this dissertation were done with his microscope.

I might not be able to finish my dissertation without many undergraduate students and others who have been participated in the projects in this dissertation. Especially, I deeply appreciate the enthusiastic participation and successful accomplishment of undergraduate students, Nilou Soltanian, Annabel Rodriguez, Kevin Kuo, and Peter Anthopolos, in many parts of this dissertation. Star Loar, a former lab technician, also deserve my deep gratitude since I could finish most laborious work with her great help.

My deepest gratitude goes to my family and friends. My husband, Jongchan Woo, is very special to me. He is a good mentor, a tough critic, as well as an excellent husband to me. Without his support on me, I couldn't have finished this work. My precious family, my parents and my sister, Eunkyoung, and my brother, Sunghyun, have been supporting me every time. I always

think I am very lucky to have such great parents who always trust me and have no questions on my decisions. I am deeply grateful to my roommate, Prakitchai Non Chotewutmontri and Sommai Gai Janekitkarn, for taking care of me after Jongchan's graduation. My excellent friends, Hyuck-Joon Kang and Bijoyita Roy also deserve my deep appreciations.

Finally, I specially thanks to Dr. Ilha Lee, my role model as a great advisor and mentor, for opening my eyes to the exciting world of Biology.

Abstract

Myosin proteins function as molecular motors that drive the ATP-dependent movement of cellular components along actin filaments. Vascular plants encode two different types of myosin, referred to as class VIII and class XI. Although class XI myosins have been suggested to function in organelle movement and cytoplasmic streaming, little is known about their cellular function in detail.

The *Arabidopsis* genome encodes 13 class XI myosin genes. The reasons for the relatively large number of myosin XI isoforms present within a single plant species are unknown. To investigate the function of these gene products in the cell, we determined the spatial and temporal gene expression patterns by constructing promoter-reporter plants. Myosin genes are expressed in a variety of tissues with substantial overlap between family members. To study the biological function more intensively, homozygous T-DNA insertion lines were isolated for all 13 genes. Interestingly, five mutants showed phenotypes related to root hairs. *mya2*, *xi-b*, and *xi-k* showed shorter root hairs than in wild type while *xi-h* and *mya1* produced a higher density of root hairs on the epidermis. MYA1 and XI-K are the most similar isoforms among the 13 myosins and their double mutant showed an additive phenotype with extremely short root hairs suggesting that these two myosins have partially redundant functions. Interestingly organelle movements, especially those of peroxisomes, were reduced in *mya1 xi-k*.

Tip growth is the key growth mechanism in root hairs and pollen tubes. Many kinds of vesicles are trafficking toward (or backward from) the apical dome of root hairs to supply membrane and cell wall material as well as energy for growing tips. These movements along the

shank of the hair occurred with velocities around 2 to 3 μm/s for *Arabidopsis thaliana*. In *xi-k* mutants, root hairs grew more slowly and terminated sooner than in wild type. Interestingly, this reduction of growth rate was correlated with a fluctuation of YFP-RAbA4b accumulation at the tip of growing root hairs. Other markers, including PI4P lipid and ER, as well as calcium and actin dynamics did not show significant differences. A YFP-XI-K construct driven by its native promoter could rescue the mutant phenotype and revealed accumulation of this myosin in the tip of growing root hairs. The distribution of YFP-XI-K in the root hair tip partially overlapped with CFP-RHD4-labeled vesicles at the subapex and YFP-RabA4b vesicles at the apex of root hairs, suggesting that myosin XI-K might be involved in the accumulation of unidentified vesicles in the tip of growing root hairs.

Characterization of two mutants that showed ectopic root hair growth in the epidermis, resulting in a higher density of root hairs than wild type, *mya1* and *xi-h*, were initiated with two analyses. At first, staining pattern of promoter-reporter constructs of three key transcription factors, *WER*, *EGL3*, and *GL2* were observed in *mya1*. Although variation in individual samples was too large to conclude, *GL2* staining patterns in *mya1* occasionally were unorganized. Increasing sample population and detail study is necessary. Secondly, effects of phosphate deficiency were observed with the *mya1* and the *xi-h* in series of phosphate concentrations ranging from 1μM to 300μM. The *xi-h* mutant showed insensitivity on root hair production upon phosphate deficiency, suggesting a potential function of XI-H in the response to phosphate deficiency. Confirmation of these results and further study of the MYA1 and the XI-H is essential. In summary, this study established a systematic approach to investigate the biological function of class XI myosins in plant development and significantly increases our understanding of the function of XI-K myosin in root hair tip growth.

Table of Contents

List of Tables

List of Figures

List of Movies

List of abbreviations

PCR	Polymerase chain reaction
RT-PCR	Reverse transcription polymerase chain reaction
CFP	Cyan fluorescent protein
YFP	Yellow fluorescent protein
FRET	Fluorescence resonance energy transfer
GUS	ß-glucuronidase
CaMV35S	Cauliflower mosaic virus 35S promoter
cDNA	Complementary DNA
DIC	Differential interference contrast
DMSO	Dimethyl sulfoxide
EDTA	Ethylenediaminetetraacetic acid
EST	Expressed sequence tag
EtBr	Ethidium bromide
KO	Knock out
MT	Microtubule
MS	Murashige and Skoog plant basal medium
PM	Plasma membrane
SEM	Standard error of the mean
SD	Standard deviation
WT	Wild type
X-gluc	5-bromo-4-chloro-3-indol-ß-D-glucuronide
UAS	Upstream activation sequences
TOM	Triple organelle marker

CHAPTER I. Introduction: myosins and root hairs

◆ *Section 2 of this chapter (Cytoskeleton and root hair growth) was submitted as a chapter in a book on the Cytoskeleton in Plant Cells (Bo Liu, Ed.) to be published by Springer 2010.*

I.1. PLANT MYOSINS AND THEIR FUNCTIONS

Myosins are actin-dependent motor proteins known to function in cytoplasmic contractile processes in muscles and many other mechanisms of eukaryotic motility such as cell migration, cytokinesis, phagocytosis, maintenance of cell shape, and organelle trafficking(Berg et al., 2001). A myosin molecule contains one or two heavy chains of masses ranging from about 110 to 250 KDa and different numbers of light chains of masses about 15 to 20 KDa, which bind to the heavy chains (Korn, 2000). All myosin heavy chains consist of three domains, a motor domain that moves along actin filaments and binds and hydrolyses ATP, a neck domain that contains IQ motifs and binds to light chains such as calmodulins or related calcium-binding proteins, and a tail domain that varies in function (Hasson and Mooseker, 1995). In many cases, the N-terminus of myosins also contains a small domain in front of the motor domain. The myosins constitute one of the largest protein families in eukaryotes with diverse functions that are reflected in their various tail domain structures (**Figure. I.1.**). To date, 2,269 myosins in 35 classes of myosin have been identified from 328 species of eukaryotes based on amino acid sequences of the motor domain (Odronitz and Kollmar, 2007). Members in a class show the same domain structure which suggests the coevolution of head and tail domains (Korn, 2000).

Among the 35 classes of myosins, plant-specific myosins are grouped in only two classes, VIII and XI (Odronitz and Kollmar, 2007). Phylogenetic analysis showed that class XI might have originated from class V suggesting that class XI might have similar functions in plants as class V in non-plant species (Odronitz and Kollmar, 2007).

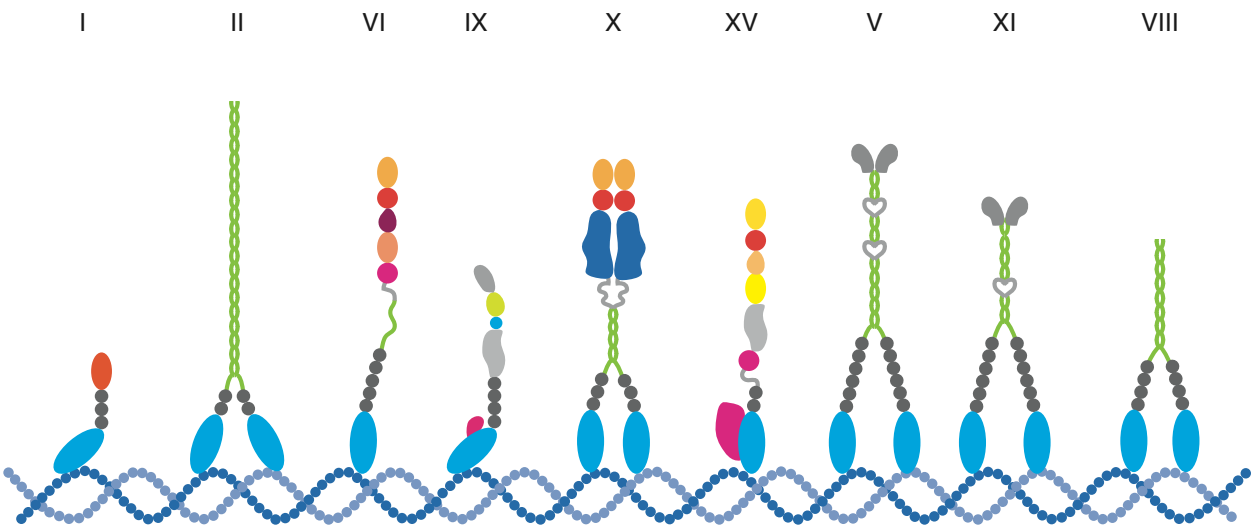

Figure I.1. Structure of myosin is distinct between different classes in eukaryotes

A figure from Krendel and Mooseker 2005 (Krendel and Mooseker, 2005) was redrawn to include plant-specific myosins, class XI and VIII. Note that myosins were classified based on the amino acid sequences of their N-terminal motor domain (blue). However, domain organization of the proteins (represented by different colored shapes) is distinct across the classes while consistent within a class.

I.1.1. Plant myosins: evidence of myosin function in plant cells

Intensive studies to investigate myosin functions have been performed with several classes of myosins, such as class II, V, and VI, in non-plant systems including human cells (Krendel and Mooseker, 2005). These studies confirmed myosin functions in cell motility and organelle transport. On the other hand, the function of plant-specific myosin has been relatively less studied. Involvement of myosin in organelle movements was initially suggested from myosin inhibitor studies. 2,3-Butanedione monoxime (BDM) is generally used as an inhibitor of myosin activity. BDM is known to stabilize the ADP-P_i bound state of myosins and thus inhibit of the release of P_i to produce the power stroke of muscle myosin (McKillop et al., 1994). It has been widely used to support myosin function in various cells including plant cells. Cytoplasmic streaming in lily pollen tubes and root hair cells were inhibited and organization of actin filaments was partially disrupted by treatment with BDM (Tominaga et al., 2000; Yokota et al., 2000). BDM treatment caused an altered tension of the actin cytoskeleton in cultured soybean cells (Grabski et al., 1998), and it also disturbed the distribution patterns of actin filaments in maize root epidermis (Šamaj et al., 2000). In tobacco BY-2 cells, movement of Golgi stacks was inhibited by BDM (Nebenführ et al., 1999), in addition, chloroplast avoidance movements in Arabidopsis leaf cells under high light were also blocked by BDM (Paves and Truve, 2007), suggesting that myosins function in organelle movements. BDM treatments were shown to results in aberrant morphology of the new cell plate in the stamen hair of *Tradescantia virginiana* (Molchan et al., 2002) and in inhibition of auxin-induced cell division by disturbing the actin cytoskeleton and organelle trafficking in tobacco VBI-0 cells (Holweg et al., 2003).

Although it has been suggested that BDM affects other kinase-related proteins besides

myosins (Grabski et al., 1998), direct evidence for these other effects is still lacking. Thus, the studies introduced above might be sufficient to postulate an important role of myosin in plant growth and development.

I.1.2. Plant myosins: Class VIII

Arabidopsis ATM1 is the first myosin identified experimentally in plants (Knight and Kendrick-Jones, 1993). Later one more class VIII myosin, ATM2, was identified in Arabidopsis (Kinkema et al., 1994) and two class VIII myosins each were isolated in maize and sunflower (Liu et al., 2001). As genome projects expanded, 53 myosins in this class were identified experimentally or by annotation in 26 species up to date (Odronitz and Kollmar, 2007).

Typically, Class VIII myosins contain an N-terminal motor domain, four IQ motifs, a putative coiled-coil region, and a tail region (**Figure. I.2.A**). This domain organization is highly conserved among members of this class. Every member of identified (or predicted) myosins in this class has the same domain structures spanning about 115 amino acids (Kinkema et al., 1994; Knight and Kendrick-Jones, 1993; Liu et al., 2001; Odronitz and Kollmar, 2007). Class VIII myosins are distinct from other myosins with their relatively long N-terminal region prior to the motor domain, moreover, their C-terminal tail region is class-specific without any characterized domain structures. The C-terminal region contains many potential phosphorylation sites and at the very end of the C-terminus, they present clusters of basic residues which have been suggested to be involved in binding to phospholipids (Knight and Kendrick-Jones, 1993). A polyclonal antibody was raised against this class-specific tail, including the coiled coil region, of *Arabidopsis* ATM1 to investigate its localization in cells (Reichelt et al., 1999). This study

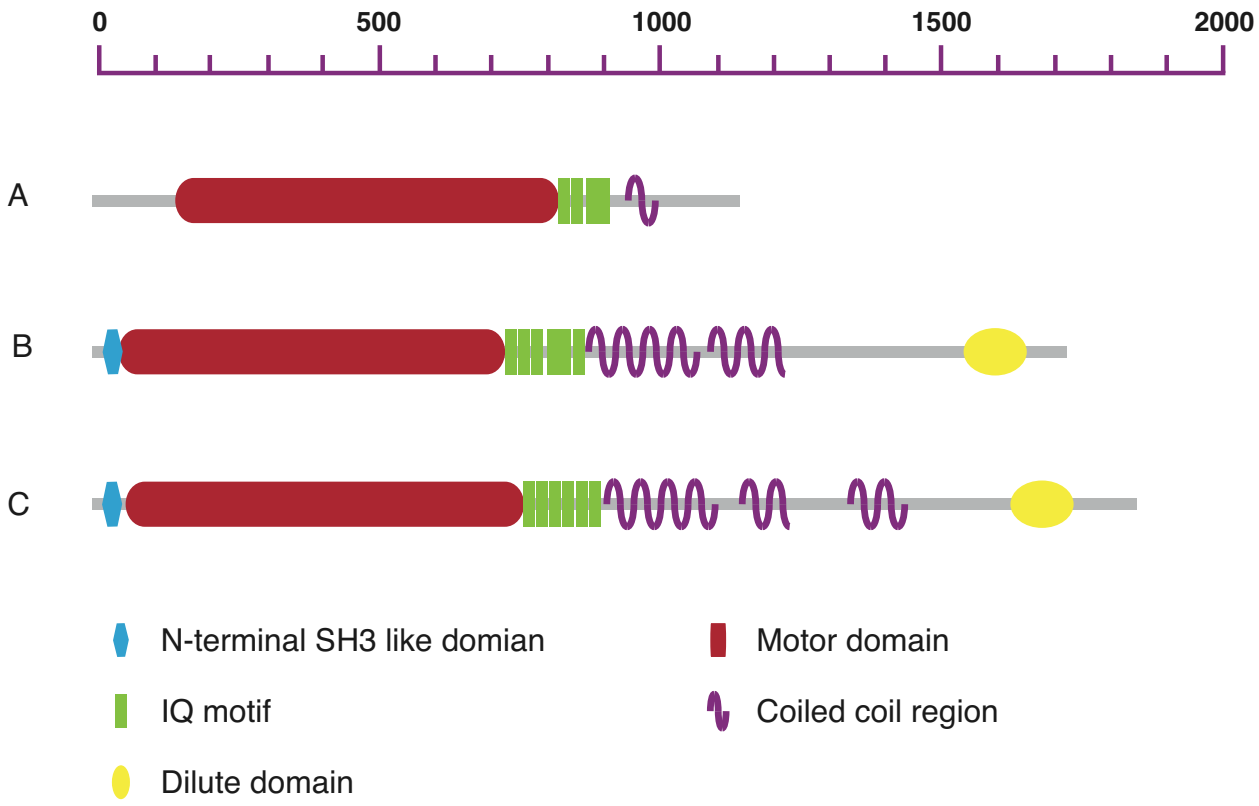

Figure I.2. Myosin domain structures

Representative domain structures of three classes of myosins are shown.

A. ATM1, a class VIII myosin in *Arabidopsis thaliana*

B. MYA1, a class XI myosin in *Arabidopsis thaliana*

C. Myo5A, a class V myosin in human

revealed that class VIII myosins are predominantly localized as spots around the plasmamembrane of cells, which were later identified as plasmodesmata (Baluska et al., 2001), and at cell plates during cytokinesis in cress and maize root epidermis (Reichelt et al., 1999). Overall, it has been suggested that myosin VIII might be important for anchoring of actin filaments at sites of intercellular communication (Baluska et al., 2001; Reichelt et al., 1999). Localization of myosin VIII at the plasmodesmata has been recently confirmed with GFP-ATM1 fusions that lack the motor domain (Golomb et al., 2008). Myosin function in protein delivery to plasmodesmata was also supported by ectopic overexpression of the tail domains of class VIII myosin in tobacco leaves (Avisar et al., 2008a). The Hsp70 homolog (Hsp70h) from *beet yellow virus* targets plasmodesmata of its host, tobacco leaves. Overexpression of truncated myosin VIII abolished Hsp70h localization at the plasmodesmata, suggesting that myosin VIII functions in targeting of Hsp70h to plasmodesmata (Avisar et al., 2008a).

In addition to their function at plasmodesmata, myosin VIII has been suggested to contribute to endocytosis. Immunolocalization studies with a polyclonal antibody showed punctate structures of various sizes throughout the cytoplasm (Reichelt et al., 1999), moreover, GFP-fused ATM tails partially colocalized to endosomal markers, such as FM4-64, FYVE, BRI1, and ARA6 in tobacco leaf epidermis (Golomb et al., 2008; Sattarzadeh et al., 2008). Arabidopsis encodes 4 genes in class VIII myosin, *ATM1*, *AMT2*, *VIII-A*, and *VIII-B*. Although all of them showed their localization at the plasmodesmata and cytoplasmic punctate structures, ATM1 and VIII-A are preferentially localized at the plasmamembrane while ATM2 and VIII-B are mostly localized to endosomal compartments suggesting that different isoforms might have functional preferences while they can substitute for each other (Avisar et al., 2008a; Golomb et al., 2008; Sattarzadeh et al., 2008).

I.1.3. Plant myosin: Class XI

I.1.3.1. Resemblance of class XI myosin in plants with class V in non-plant eukaryotes

The class XI myosins consist of an N-terminal motor domain followed by six IQ motifs, a coiled coil region, and a globular C-terminal tail, which contains a dilute domain (**Figure. I.2.B**). It has been confirmed that myosin motor domains and C-terminal cargo-binding domains co-evolved, resulting different domain structures across the classes, but conservation within a class (**Figure. I.1.**) (Korn, 2000; Odronitz and Kollmar, 2007). Class XI myosin and class V myosin share several of features that suggest their evolutionary linkage. The domain organization of both class V and class XI myosins are identical (**Figure. I.2.B and C**). Both classes contain six repeats of the IQ motif, to which calmodulins bind. In addition, among the 35 classes of myosins, only these two classes contain a dilute domain in the C-terminal cargo-binding globular tail (Odronitz and Kollmar, 2007). Class V myosins were proposed to be one of the "ancient" myosins together with class I myosins, which are present in most taxa of eukaryotes (Odronitz and Kollmar, 2007). The resemblance of class V and XI suggests that class XI myosin might share similar mechanisms and functions with myosin V. Class V myosins have been found to bind several kinds of cargo including melanosomes, early endosomes, peroxisomes as well as vacuoles (reviewed in (Li and Nebenführ, 2008). Taken together with the evidence from myosin inhibitor treatments, this suggests that class XI myosins function in organelle movements.

I.1.3.2. Functional studies of class XI myosins: localization of myosins

Immunolocalization studies using an antibody raised against a class XI-specific peptide in the head domain of a *Zea mays* myosin showed that these motors are associated with several

organelles in cells (Liu et al., 2001). Further analyses with a class-specific antibody raised against a peptide in the tail domain demonstrated that this antibody colocalized with mitochondria, plastids, and the molecular chaperone subunit TCP-1α in maize (Wang and Pesacreta, 2004). However, a relationship between a specific isoform of myosin XI and specific organelles was not identified, leaving the function of myosin XI unclear. Recently, it has been shown that MYA2 localizes to peroxisomes using an antibody raised against a peptide in the MYA2 tail region (Hashimoto et al., 2005). However, a subset of antibodies did not colocalize with peroxisomes but showed small punctate compartments suggesting either cross reactivity of the antibody with other isoforms in class XI or dual localization of MYA2 to two different membrane compartments. Recently, several groups have shown the subcellular localization of class XI myosins of *Arabidopsis thaliana* by transient expression of constructs with GFP fused to class XI myosin tails which revealed colocalization with various intracellular organelles (Avisar et al., 2009; Li and Nebenführ, 2007; Reisen and Hanson, 2007; Sparkes et al., 2008). However, this localization information may not be very reliable since the results were inconsistent between different studies. For example, MYA1 and MYA2 in one study localized to peroxisomes (Li and Nebenführ, 2007), while they colocalized with peroxisomes and partially with Golgi stacks in another study (Reisen and Hanson, 2007). In addition, YFP-XI-K showed punctate structures partially overlapping with Golgi stacks and mitochondria in one study (Reisen and Hanson, 2007), but appeared to be diffusely localized near the ER in a second report (Avisar et al., 2009). This variation might come from the different truncation points of proteins suggesting that the localization of partial proteins might differ from the original localization information of native protein *in vivo*. It is also possible that myosins of Arabidopsis might not localize properly in tobacco cells.

I.1.4. Myosin, organelle trafficking, and plant development

Although myosin localization to a specific organelle is unclear so far, it is likely that myosin is involved in organelle trafficking in plant cells. Overexpression of myosin tail domains perturbed organelle movements in many studies (Avisar et al., 2009; Avisar et al., 2008b; Sparkes et al., 2008). For example, overexpression of the YFP-XI-K tail of *Arabidopsis* inhibited peroxisome and Golgi movements in tobacco leaf cells in two studies (Avisar et al., 2008b; Sparkes et al., 2008). Curiously, their localization patterns were different in the two reports- punctate patterns reported by Avisar et al. 2008 but diffuse signals near ER reported by Sparkes et al. 2008. Interestingly, expression of YFP-XIK tail in both studies showed neither peroxisome localization nor Golgi localization. RNAi-based knockdown of XI-K in tobacco leaves also showed similar results, suggesting that XI-K regulates organelle movement indirectly. Recently, a *xi-k* mutant has been reported to be impaired in the movements of three organelles, peroxisomes, Golgi stacks, and mitochondria (Peremyslov et al., 2008). Interestingly, this mutant showed shorter root hairs than wild type (Ojangu et al., 2007; Peremyslov et al., 2008) suggesting that XI-K might function not only in organelle trafficking but also in root hair growth. *mya2* mutants also showed the inhibition of same three organelle movements in leaf epidermis, however, it is unclear how inhibition of Golgi and mitochondria movements could be achieved in *mya2* mutants. MYA2 is known to localize to peroxisomes since their specific antibody majorly colocalized to peroxisomes (Hashimoto et al., 2005) and recently MYA2 tail has been reported to interact with small GTPases, AtRabCa and AtRabD1, which were able to colocalize with peroxisomes (Hashimoto et al., 2008). Taken together, although much has been learned about myosin in the past three years, many issues remain regarding myosin function in plant

development and vesicle trafficking. Thus, it is necessary to more systematically figure out the relationship among myosin, organelle trafficking, and plant developmentally characterizing of myosin mutants, observing of organelle movements in mutants, and eventually identifying the subcellular localization of corresponding myosins.

I.2. CYTOSKELETON IN ROOT HAIR GROWTH

Root hairs are highly polarized outgrowths of a subset of root epidermal cells, the so-called trichoblasts. The biological function of root hairs is to increase the surface area of roots in order to facilitate the absorption of water and nutrients from soil. Root hairs are also the site of initial interaction with microorganisms (Geitmann and Emons, 2000). The patterning of root trichoblasts varies between plant species and can also be regulated by environmental factors (Dolan and Costa, 2001). These genetic and environmental regulatory mechanisms have been studied intensively and are reviewed elsewhere (Ishida et al., 2008). Trichoblasts are unique plant cells that first elongate by diffuse growth over their entire surface with the other root cells and subsequently form an outgrowth, the root hair, which elongates only at its very tip.

The mechanism of root hair growth can be conceptually divided into two distinct events: root hair initiation, which breaks the symmetry of the root epidermis and results in the formation of a bulge, and unidirectional root hair elongation by tip growth in which all secretion of new cell wall material occurs in a small area at the tip of the hair. Root hairs are not critical for plant growth, so that plants can grow normally on growth media in the lab even with defective root hairs. This has permitted studies on the molecular mechanisms underlying root hair development

based on mutant screens for defects in root hair growth (Schiefelbein and Somerville, 1990). These mutants showed diverse phenotypes from abnormal length or shape of root hairs to additional root hair initiation. In independent studies, pharmacological analyses using chemicals to disrupt cytoskeletal organization revealed the importance of the cytoskeleton, especially actin filaments, for tip growth (Baluska et al., 2000; Bibikova et al., 1999). More recently, studies with GFP-fused proteins related to root hair growth provided further support for the emerging regulatory network and opened up the additional dimension of temporal dynamics (Carol and Dolan, 2002; Cole and Fowler, 2006; Hepler et al., 2001).

Collectively, these studies have established that three factors are very important for this special type of cell morphogenesis. First, signaling from the trichoblast determination pathway leads to a rearrangement of the cytoskeleton in the root epidermis for bulge formation and ultimately for support of tip growth in the emerging hair (Baluska et al., 2000; Bibikova et al., 1999). Second, polar membrane trafficking is required to provide new plasma membrane and cell wall components to the growing tip (Ovecka et al., 2005). Finally, there is a unique distribution of regulatory factors, primarily calcium (Felle and Hepler, 1997), reactive oxygen species (Monshausen et al., 2007), and pH (Bibikova et al., 1998) which regulate each other to modulate tip growth (Cole and Fowler, 2006). Pollen tubes, the other classical model for tip growth in plants, share a similar growth mechanism that involves similar key regulators (Cole and Fowler, 2006). However, there are also some distinct differences between pollen tubes and root hairs, such as vacuole position and growth rate. It remains to be seen whether a common model can simultaneously explain the specific behavior of root hairs and pollen tubes. However, in this chapter, we will forgo this comparison and focus on the mechanisms of root hair growth.

I.2.1. Root hair Initiation

The first visible step during root hair initiation is that a part of the outer epidermal cell starts swelling in response to local signaling. The position of the initial swelling depends on the plant species. For example, *Arabidopsis* root hairs are initiated on the basal part of the trichoblast, i.e. closest to the root tip (Carol and Dolan, 2002), while maize roots form the root hair approximately in the middle of an epidermal cell (Baluska et al., 2000; Fischer et al., 2007). The positioning of root hairs on trichoblasts depends at least partially on hormonal signaling as revealed by mutant analysis. As the first step of root hair initiation, a membrane trafficking effector, ROP-GTPase, and a cell wall loosening enzyme, expansin, accumulate at the initiation site (Molendijk et al., 2001). Both actin and microtubule cytoskeleton then rearrange (Van Bruaene et al., 2004) and local alkalization of the cytosol occurs accompanied by acidification of the cell wall (Bibikova et al., 1998). In addition, the cytosolic calcium concentration increases locally due to a massive uptake of calcium from the environment (Very and Davies, 2000). Finally, actin filaments accumulate and the cell bulges outward and eventually begins tip growth (Ishida et al., 2008).

I.2.1.1. Selection of the bulge site

Auxin and ethylene signaling appear to be key regulators in determining the position of root hairs, since many root hair defective mutants are directly or indirectly related to auxin or ethylene responses (Guimil and Dunand, 2007). In particular, ethylene signaling mutants showed altered position of root hairs on a trichoblast, suggesting that bulge site selection occurs downstream of a hormone signaling pathway (Masucci and Schiefelbein, 1994). The auxin

transport mutant, *aux1*, also displayed root hairs in an apically shifted position and often carried two root hairs on a cell (Grebe et al., 2002). The apical and basal membrane localization of AUX1 on root epidermal cells appeared to be required for maintaining planar root hair polarity by facilitating the uptake of auxin from more distal cells to maintain a local proximal auxin maximum in the trichoblast (Swarup et al., 2001). Moreover, pharmacological interruption of auxin transport also disrupted proper root hair positioning, supporting the critical role of auxin in determining the root hair position (Grebe, 2004).

How auxin and ethylene signaling affect cytoskeletal reorganization is still not clear. However, ROP-GTPase (Rho-like GTPase of plants) may be part of the signaling cascade. In *Arabidopsis*, immunolocalization of ROP proteins revealed their accumulation under the plasma membrane of the root hair initiation site even before swelling started, and this accumulation was maintained during root hair growth (Fu et al., 2002). This localization, together with evidence that overexpression of ROP-GTPase resulted in multiple root hair formation on a single trichoblast (Yang et al., 2007), further supports the notion that ROP-GTPases are key regulators for root hair initiation. ROP accumulation was not sensitive to cytoskeleton-disrupting drugs suggesting that ROP accumulation is an upstream event of actin and microtubule rearrangement in trichoblasts (Baluska et al., 2000; Molendijk et al., 2001). How localization and activity of ROP-GTPase is functionally regulated by polar auxin transport still remains an open question to be investigated. Recently, a mathematical simulation model hypothesized that the auxin gradient might function to balance the activity of ROPs, so that the root hair can be formed at the proper position of root epidermal cells (Payne and Grierson, 2009). Although there is as of yet little experimental support for this hypothesis, this model is a good starting point to identify the mechanisms that ultimately lead to selection of the bulge site.

I.2.1.2. The cytoskeleton in bulge formation

Root epidermal cells have highly organized transverse cortical microtubule arrays. Once a trichoblast starts root hair formation, this microtubule array becomes irregular and randomized at the site of the future root hair bulge (Baluska et al., 2000). This is correlated with local wall acidification which leads to a change in cell wall formation and ultimately results in wall thinning so that the cell can swell in this region (Bibikova et al., 1998). Remarkably, the apex of the bulge is devoid of microtubules when the root hair swelling is ready to initiate tip growth (Baluska et al., 2000). At the same time, actin filaments at the future bulge site become arranged parallel to the long axis of the cell (Baluska et al., 2000). G-actin and profilin also accumulate at the tip of the root hair bulge, as observed by immunofluorescence in maize (Braun et al., 1999), and a fine actin meshwork later forms within the bulge (Baluska et al., 2000).

Actin mutants, *act2* and *act8*, showed root hair bulges but no proper tip growth suggesting that the actin cytoskeleton does not have a critical role in the early steps of root hair initiation (Kandasamy et al., 2009; Ringli et al., 2002). However, actin mutants often formed multiple sites of root hair bulges implying that actin might be involved in the process of determining the root hair initiation site on the trichoblast (Kandasamy et al., 2009). Lettuce seedlings that were germinated on media containing 10μM cytochalasin B, an inhibitor of actin polymerization, did not produce any root hairs (Takahashi et al., 2003). This result suggests that longitudinal redistribution of actin filaments on the site of root hair emergence is necessary for root hair initiation. However, cytochalasin D treatment of vetch roots did not show any effects on root hair bulge formation (Miller et al., 1999). Note, however, that cytochalasin variants have different side effects beside actin disruption. Thus, it is conceivable that long-term exposure of lettuce roots to cytochalasin B may have induced additional secondary effects that inhibited root

hair development. The actin cytoskeleton is clearly more important in later steps of root hair initiation, namely, during the transition from bulge formation to tip growth since *actin* mutants as well as pharmacological interventions showed that a defect of actin organization prevented the initiation of root hair tip growth (Baluska et al., 2000; Kandasamy et al., 2009; Miller et al., 1999; Ringli et al., 2002).

I.2.2. Root hair tip growth: general considerations and organelle distribution

Once a bulge is established, root hairs continue to increase their surface area only at their tip, away from the root epidermis. *Arabidopsis* root hairs have been reported to be able to grow to a length of about 700μm with the growth rate of 1-2μm/min. However, these parameters can differ significantly depending on growth conditions (Monshausen et al., 2008; Ojangu et al., 2007). Conventionally, root hairs are divided into three zones from the tip toward the root epidermis, apex, subapex, and shank. This subcellular organization of growing root hairs shares some similarity with pollen tubes with some notable differences. In growing root hairs, the dome-shaped apex, where active growth occurs, is predominantly filled with secretory vesicles. Large organelles are prevented from entering this region, presumably by mesh-like short, randomly distributed actin fragments in the subapex (Baluska et al., 2003). Unlike pollen tubes, apex and subapex of root hairs are often not clearly distinguished; the vesicle-filled apical zone is narrower than in pollen tubes and the actin mesh spreads more broadly. A major difference between root hairs and pollen tubes is the position of the large central vacuole. While the vacuole in pollen tubes is located far behind the tip in the shank, the vacuole in growing root hairs can reach into the subapex (Cole and Fowler, 2006).

When root hairs stop growing, the vesicle accumulation in the apex disappears and the vacuole can fill the entire root hair. These characteristic changes in organelle distribution and cell morphology depend strongly on the cytoskeleton which in turn is regulated by a feedback loop involving membrane transport and several signaling molecules.

I.2.2.1. Actin cytoskeleton in root hair tip growth

Actin filaments are fundamental for root hair growth, similar to what was found in other cell types (reviewed in (Hussey et al., 2006; Smith and Oppenheimer, 2005). Visualization of the actin cytoskeleton has been performed with several different probes in fixed or living root hairs. While longitudinal actin bundles along the shank of growing root hairs are relatively consistent in images with different probes, the existence of actin at the subapex and apex is somewhat controversial. Confocal microscopy images of actin visualized with a freeze-shattering technique using actin antibodies showed high actin accumulation at the maize root hair apex (Baluska et al., 2000). Labeling of globular actin (G-actin) by fluorescein isothiocyanate (FITC)-DNase I also showed that G-actin accumulated extensively in the apex in growing root hairs of wheat. This accumulation disappeared and was replaced by thick filamentous actin (F-actin) extending into the tip in fully grown root hairs (He et al., 2006). Co-visualization of G-actin and F-actin by labeling with FITC-DNase I and Tetramethyl Rhodamine Isothiocyanate (TRITC)-Phalloidin, respectively, showed distinct localization of G-actin and F-actin in growing root hairs. While G-actin accumulated at the apex, F-actin was presented in the shank of the growing root hairs and could not penetrate into the apex (He et al., 2006).

GFP-conjugated actin binding proteins also have been used to visualize actin filaments. This technique offers the advantage of revealing F-actin dynamics during root hair growth.

However, this has to be balanced with potential artifacts resulting from over-expression of the labels. Initial experiments with GFP-talin transformed *Arabidopsis* displayed the high accumulation of actin at the apex of growing root hairs (Baluska et al., 2000). In subsequent years, it was revealed that over-expression of GFP-talin could cause severe developmental defects in transgenic plants (Ketelaar et al., 2004). Many studies now employ a fimbrin-based marker to visualize actin dynamics in all cells of several species (**Figure. I.3.A**). The second actin binding domain of fimbrin fused to the C-terminus of GFP (GFP-FABD2) displayed more fine actin filaments than GFP-talin and did not show any obvious developmental defects (Voigt et al., 2005). In contrast to GFP-talin, GFP-FABD2 (or GFP-FABD2-GFP for brighter signals) did not accumulate in the apex of growing root hairs of transgenic *Arabidopsis* seedlings (Sheahan et al., 2004; Wang et al., 2008). However, FABD2-GFP transformed *Medicago truncatula* displayed accumulation of actin at the apex (Miller et al., 1999; Timmers et al., 2007; Voigt et al., 2005), suggesting that actin organization might differ between the species. Recently, a new actin marker, Lifeact has been introduced which is based on the actin-binding domain of yeast ABP1 (Era et al., 2009). Lifeact-Venus revealed a similar actin cytoskeleton as GFP-FABD2, however, it had a better resolution at the root hair tip, so that an irregular actin mesh in the subapex and highly dynamic fine filaments reaching into the tip of the apex could be observed (Era et al., 2009).

Based on results from a variety of cell types, it is generally assumed that a central function of actin filaments is to deliver membrane compartments to the apex of root hairs in order to provide cell wall components and membrane lipids necessary for growth, as well as

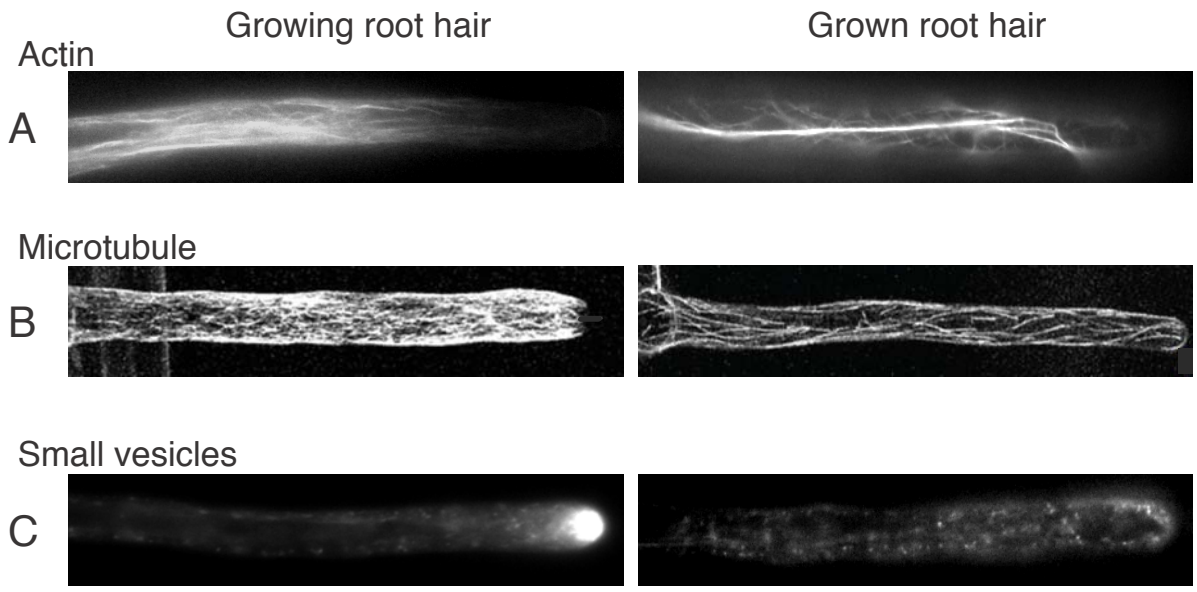

Figure I.3. Distinct distribution of cytoskeletal elements and vesicles during root hair tip growth

A. Actin cytoskeleton, visualized with FABD2-YFP. In growing root hairs, cortical F-actin filaments array mostly longitudinally along the shank and are absent from subapex and apex of root hairs. In contrast, thick bundles of actin cables reach into the apex in fully-grown root hairs.

B. Microtubules, visualized by GFP-MBD. Growing root hairs display longitudinal or helical microtubules along the root hair shank. Note that microtubules do not reach the extreme apex of the growing root hair while they do so in growing root hairs (Reprinted with permission from Van Bruaene et al. 2004).

C. RabA4b-YFP-labeled vesicles accumulate at the tip of growing root hairs. This accumulation is tightly correlated with root hair growth; consequently, fully-grown root hairs lack the accumulation of the RabA4b-YFP vesicles at the tip.

several regulatory factors (Baluska and Volkmann, 2002). The contribution of actin dynamics to root hair tip growth has been exposed by treatment with actin disrupting drugs, Latrunculin B (LatB) (Baluska et al., 2000; Bibikova et al., 1997) and cytochalasin D (Miller et al., 1999). The effect of LatB is dosage-dependent. A one hour treatment with as little as 50 nM LatB reduced root hair growth by 25% while concentrations higher than 500 nM led to complete cessation of root hair growth in *Arabidopsis* (Bibikova et al., 1999). Concentrations of more than 1 μM cytochalasin D also caused cytoplasmic streaming to stop within 30 min and 10 μM cytochalasin D could kill root hairs within 15 min in *Medicago* (Miller et al., 1999). Overall, disruption of actin filaments causes root hairs to stop growing, suggesting that actin organization is critical for tip growth. Genetic studies have corroborated this conclusion. Over decades, numerous root hair mutants of *Arabidopsis* have been isolated in several studies (reviewed in (Guimil and Dunand, 2007) and some of them are mutants of either components of actin filaments or regulators of actin dynamics. For example, *der1*, a mutant of *ACTIN2* (*ACT2*), displayed a cessation of root hair growth after bulging (Ringli et al., 2002) with additional pleiotropic phenotypes in different tissues (Gilliland et al., 2002). ACT8, the isoform most similar to ACT2, also contributes to root hair tip growth. *act8* mutants showed around 50% shorter root hairs than wild type and overexpression of *ACT8* could complement the *act2* mutant phenotype (Kandasamy et al., 2009). Mutation of several regulators of actin dynamics also displayed an arrest of tip growth in root hairs; induced overexpression of AIP1, a F-actin capping protein, resulted in short root hairs (Ketelaar et al., 2007), and overexpression of *PFN1*, an *Arabidopsis* profilin isoform, stimulated root hair tip growth and resulted in root hairs that were twice as long as wild type (Ramachandran et al., 2000). Finally, mutation of *AtFH8*, an *Arabidopsis* group Ie formin

known to regulate actin dynamics, caused an arrest of root hair tip growth after bulge formation (Deeks et al., 2005).

I.2.2.2. Myosin in root hair tip growth

While the actin cytoskeleton has been recognized as an important factor for tip growth, the involvement of myosins, motor proteins that utilize F-actin as a track, was not clear until recently. Based on evidence from pollen tubes and circumstantial evidence from the importance of the actin cytoskeleton (Tang et al., 1989; Yokota et al., 2000), the contribution of myosins to root hair tip growth was proposed (Tominaga et al., 2000). Recent studies with truncated class XI myosins fused to GFP variants at their N-terminus showed their localization on various membrane compartments suggesting a function in intracellular vesicle trafficking (Avisar et al., 2009; Li and Nebenführ, 2007) Direct evidence supporting the involvement of myosin in root hair tip growth was provided by the identification of a mutant of *Arabidopsis thaliana*, *xi-k*. *xi-k* plants showed short root hairs and abnormal trichome branching patterns (Ojangu et al., 2007; Peremyslov et al., 2008). *MYA2*, another one of the 13 class XI myosin genes in *Arabidopsis*, also seems to be involved in root hair tip growth based on the fact that *mya2* mutants also displayed short root hairs (Peremyslov et al., 2008). Interestingly, in these mutants, movements of three organelles, Golgi, peroxisomes, and mitochondria, were dramatically slower than in wild type (Peremyslov et al., 2008). It is still unknown how a single myosin can contribute to the movement of three distinct organelles, particularly, since none of the tested YFP-myosin tail fusions localized to these organelles (Li and Nebenführ, 2007; Reisen and Hanson, 2007; Sparkes et al., 2008). A possible hypothesis is that one of the cargoes of XI-K might be a regulator of cytoskeleton dynamics, thus resulting in defects of movements of many organelles.

In support of this contention, recent observation using variable-angle evanescent wave microscopy and spinning disc confocal microscopy showed that actin turnover might be required for myosin-based mitochondrial trafficking (Zheng et al., 2009). Thus, while it is now firmly established that myosins are involved in root hair tip growth, more research is needed to decipher the mechanism by which myosins operate in this process.

I.2.2.3. Microtubules and root hair tip growth

The organization of microtubules has been initially visualized in root hairs using electron microscopy and immunofluorescence with anti-tubulin antibodies (Lloyd and Wells, 1985; Traas et al., 1985). Later, transgenic plants expressing fluorescent proteins fused to α-tubulin 6 (GFP-TUA6) or to the microtubule binding domain of microtubule associated protein 4 (GFP-MBD), were used to reveal dynamic changes of microtubule organization during root hair growth (Bao et al., 2001; Timmers et al., 2007). After the reorganization event during root hair bulging, dense cortical microtubules (CMTs) are arranged longitudinally along the shank of the root hairs. Similar to the organization of F-actin, CMTs have not been detected in the apex of growing root hairs (**Figure. I.3.B**). Once root hairs are fully grown and the central vacuole approaches the root hair tip, longer and less dense CMTs are arranged longitudinally or spirally along the root hairs and can reach to the very tip of the root hairs (Timmers et al., 2007; Van Bruaene et al., 2004). Endoplasmic microtubules (EMTs) initially have been observed in CLSM images in the interior of root hairs expressing GFP-MBD in *Medicago truncatula* (Sieberer et al., 2002). EMTs displayed a more irregular arrangement than CMTs and predominantly accumulated around the nucleus as well as in the subapex. This distribution later has also been shown to exist in *Arabidopsis* root hairs (Van Bruaene et al., 2004). EMTs in the subapex of growing root hairs are

highly dynamic. While the majority of CMTs array parallel to the shank of root hairs, EMTs at the subapex continuously change their directions and lengths (Van Bruaene et al., 2004).

In contrast to actin filaments, which play a major role in tip growth, microtubules are generally thought of being primarily important for maintaining the direction of root hair growth. Treatment with the microtubule-depolymerizing drug, oryzalin, and the microtubule-stabilizing drug, taxol, showed a loss of directionality of *Arabidopsis* root hair growth (Bibikova et al., 1999). Both taxol and oryzalin-treated root hairs displayed wavy root hairs as well as branched root hairs. Both drugs showed a similar effect on the angular deviation from straight root hairs, however, taxol was more effective in triggering branching than oryzalin (Bibikova et al., 1999), suggesting that the two drugs can distinguish between two distinct roles of microtubules during root hair growth. Analysis of mutants in α-tubulin (*tua6*) (Bao et al., 2001) and in a microtubule-associated protein (*mor1*) (Whittington et al., 2001) also revealed branched or wavy root hair growth, consistent with the pharmacological analysis. Thus, microtubules appear to be required for maintaining a stable polarity for straight growth.

The growth rates of *Arabidopsis* root hairs did not change during treatment with the microtubule disrupting drugs treatments (Bibikova et al., 1999) although *Medicago truncatula* root hairs had only 60% of root hair growth rate of untreated root hairs (Sieberer et al., 2002). Thus, it is likely that microtubules do not play a direct the role in elongating root hair cell surface. Recent studies of mutants in armadillo repeat-containing kinesins (ARKs or MRH2) of *Arabidopsis* showed abnormal root hair growth but no reduced root hair growth rate, further supporting a microtubule function in restricting the elongation zone of root hair tip growth (Sakai et al., 2008; Yang et al., 2007; Yoo et al., 2008).

Given their co-alignment patterns (Geitmann and Emons, 2000) and evidence from other cell types (Collings et al., 2006), an interaction between microtubules and the actin cytoskeleton has been proposed. Using propyzamide to depolymerize microtubules and cytochalasin B to destabilize actin filaments, the interaction between microtubules and actin cytoskeleton has been studied in detail in the root hairs of *Hydrocharis dubia* (Tominaga et al., 1997). Simultaneous treatment with both inhibitors was sufficient to stop cytoplasmic streaming and growth. Washout of Cytochalasin B in the presence of propyzamide did not allow full recovery of the longitudinal actin cytoskeleton indicating that longitudinal microtubules are required to establish the actin cables normally found in the root hair shank (Tominaga et al., 1997). At the same time, actin filaments appeared to be required for normal MT dynamics since longer treatment of root hairs with LatB permitted the formation of MT bundles in the apical or subapical regions (Timmers et al., 2007). A possible candidate for this interaction between actin filaments and microtubules is ARK/MRH2 kinesin, since it could be shown that ARK1/MRH2 can bind to actin filaments in vitro (Yang et al., 2007). Further work will be necessary to confirm this hypothesis.

I.2.2.4. Membrane trafficking and tip growth

To increase the cell size, massive secretion at the tip is required to provide membrane and cell wall components. Additionally, active endocytosis occurs at the apex of root hairs to recycle regulators and remove excess membrane (Ovecka et al., 2005). These membrane trafficking activities are reflected in the accumulation of secretory and endocytic vesicles in the apex of growing root hairs. The small GTPase, RabA4b, has been successfully used as a vesicle marker in root hairs (**Figure. I.3.C**). In growing root hairs, RabA4b-YFP-labeled vesicles accumulated

at the apex of root hairs and LatB treatment released this accumulation coincident with a cessation of growth (Preuss et al., 2004).

It is not surprising that many root hair mutants are defective in genes encoding proteins involved in membrane trafficking (Gilliland et al., 2002). Members of the Ras-like small GTPase superfamily have roles in various endomembrane compartments and several mutants of these proteins showed impaired tip growth. A major example is ROP, a Rho-like GTPase that coordinates actin organization and membrane trafficking by stimulating multiple signaling pathways (Yalovsky et al., 2008). Beside its contribution to root hair initiation (see section I.2.2.2.), ROP-GTPase functions as a critical player in root hair tip growth (Molendijk et al., 2001). ROP-GTPase is normally localized to almost the entire plasma membrane of plant cells but is restricted to the apical plasma membrane of growing root hairs. ROP-GTPase activates phosphatidyl-inositol (PtdIns)-monophosphate kinase (PIPK), a key regulator to maintain tip focused membrane trafficking and actin organization (Yalovsky et al., 2008). It also stimulates NADPH oxidase activity, which leads to the production of reactive oxygen species (Sheahan et al., 2004), a critical factor involved in regulating calcium gradients at the apex of root hairs (Baxter-Burrell et al., 2002). Many regulators of ROP-GTPase activity were also found to be involved in root hair tip growth. An *Arabidopsis* root hair defective mutant, *supercentipede 1* (*scn1*), has a similar phenotype to ROP-GTPase mutants, such that mutants have multiple root hair initiation sites in a cell and root hair tip growth is aborted (Carol et al., 2005). *SCN1* encodes a Rho-GTPase GDP dissociation inhibitor (RhoGDI) that restricts ROP activity to the apex in order to maintain a polarity for root hair growth. Similarly, ROP localization on the plasma membrane is a prerequisite for its function and S-acylation of ROP-GTPase is necessary for its membrane localization (Yalovsky et al., 2008). *TIP1* encodes a S-acyl transferase (Hemsley et

al., 2005) and *Arabidopsis tip1* mutants were initially isolated based on their extremely short, sometimes branched root hair phenotype (Schiefelbein et al., 1993). Since S-acyl transferases tend to modify only specific target proteins, it will be interesting to test whether ROPs are targets for TIP1.

Other regulators of root hair tip growth are specific phosphoinositides that can serve as a recognition landmark for certain cytosolic proteins, thus recruiting them to membrane patches where they then perform their functions. For example, $PI(4,5)P_2$ accumulates in the apical plasma membrane of root hairs and many modifying proteins of this lipids are important for the root hair tip growth mechanism (Cole and Fowler, 2006; Xue et al., 2009). RabA4b interacts with PtdIns-4OH Kinase, PI-4Kβ1 that synthesizes a precursor of $PI(4,5)P_2$ and both proteins colocalize to small vesicles at the apex of growing root hairs (Preuss et al., 2006). A *pi4kβ1/2* double mutant displayed shorter root hairs than wild type, which were often branched or jagged. PI-4Kβ1 also binds to CBL1, a calcium sensor, implying that activity of PI-4Kβ1 is dependent on the calcium gradient present at the root hair apex. Another root hair defective mutant, *rhd4*, showed short and wavy root hairs and RabA4b-YFP accumulation at the apex was altered in the mutants (Thole et al., 2008). *RHD4* encodes PI4P-phosphatase and might function to balance PI4P levels to maintain polar tip growth at the root hair apex. RHD4 might also have a function in actin organization since *rhd4* mutants showed more patchy actin organization and thinner filaments in root epidermal cells compared with wild type, however, the detailed mechanism of this interaction is not yet clear.

I.2.2.5. Signaling factors in tip growth

It has long been known that intracellular calcium gradients in the root hair cytoplasm have an important role in root hair growth (Hepler et al., 2001). Besides a role of calcium as a second messenger in signaling cascades, it has been suggested that calcium might restrict the site of membrane trafficking and also modify the cytoskeleton at the root hair tip so that the root hair can grow straight (Wymer et al., 1997). For example, calcium can affect F-actin polymerization by controlling actin-binding protein activity, such as profilin, actin-depolymerizing factor (Radford and White), or villin (reviewed in Hussey et al., 2006). In support of this, profilin also accumulates in the root hair tip (Baluska et al., 2000) and can lead to sequestration of G-actin in a calcium dependent manner (Kovar et al., 2000). Calcium may also control tip growth by several other mechanisms in addition to a modulation of F-actin dynamics. For example, G-actin accumulation at the apex of wheat root hairs as visualized with FITC-DNase I could be disrupted by treatment with dibromo-l,2-bis(o-aminophenoxy)ethane-N,N,N',N'-tetraacetic acid (BAPTA) (He et al., 2006). BAPTA is well known to rapidly dissipate calcium gradients at the growing root hair tip and consequently stops root hair tip growth (Felle and Hepler, 1997). It was also shown that membrane trafficking is regulated by the calcium gradient since treatment with the calcium ionophore A23187 caused the release of the accumulation of RabA4b-YFP from the apex and a stop of root hair growth (Preuss et al., 2006). Despite these insights, the precise mechanism by which calcium regulates tip growth is still unknown. Given the role of calcium as a key regulatory factor for many cellular events, it is likely that the calcium gradient coordinates tip growth by acting through multiple regulatory factors at the same time.

Similar to pollen tubes, the tip-focused calcium gradient in root hairs has been shown to oscillate within a range from 0.2 μM to more than 1.5 μM (Bibikova et al., 1997; Wymer et al., 1997). These calcium oscillations are tightly correlated with the cell growth rate (Monshausen et

al., 2008). Recent studies have investigated this connection in more detail by using the ratiometric calcium marker, yellow Cameleon 3.6 (Monshausen et al., 2008). This study demonstrated that root hair growth rate oscillations are typically followed by cytosolic calcium oscillation at the root hair apex with about 5 sec lag time. This observation suggests that a high concentration of cytosolic calcium at the root hair apex restricts root hair growth. This hypothesis was supported by observations that treatment with 200 μM La^{3+}, a blocker of Ca^{2+} channels, led to an acceleration of root hair growth. Similarly, treatment with 10 μM A23187, a calcium ionophore, blocked root hair growth (Monshausen et al., 2008). Cytosolic calcium gradients are accompanied by pH changes and a ROS gradient in the cytosol as well as in the cell wall space. ROS are also considered a critical factor to sustain polar growth, since *rhd2*, a mutant of *Arabidopsis* NADPH oxidase, displayed short root hairs and the typical calcium gradient in root hair tip was absent (Foreman et al., 2003). Given that addition of external ROS can recover the root hair elongation and ROS can activate calcium channels, it is likely that accumulation of ROS at the tip is required to open calcium channels at the plasma membrane of the root hair apex in order to increase the cytosolic calcium concentration at the tip (Foreman et al., 2003). Interestingly, unlike animal NADPH oxidase, plant NADPH oxidases have two EF hand motifs at their N-terminus suggesting their regulation by calcium (Sagi and Fluhr, 2001). Indeed, RHD2 can be activated by calcium in the growing root hair, resulting in a positive feedback loop (Sagi and Fluhr, 2001; Takeda et al., 2008). This inter-dependence of calcium and ROS signaling leads to alternating oscillations of ROS and Ca^{2+}gradients in the growing root hair tip, which appears to be necessary for maintaining polar root hair growth (Monshausen et al., 2007).

I.2.3. Conclusion

Root hairs are very dynamic cells which can grow relatively fast compared to other plant cells. They are also unique in their asymmetric outgrowth from a part of root epidermal cells. The growth of root hairs is regulated by a highly elaborate mechanism that involves many components, such as the cytoskeleton, membrane trafficking, and signaling factors. Two distinct steps of root hair development, root hair initiation and tip growth, are regulated in different ways by the regulatory factors (**Figure. I.4.**). However, there are common rules for this regulatory system. First, signals from genetic and environmental cues are translated into a change of the cytoskeleton. Second, the dynamic cytoskeleton rearrangement results in polar trafficking of membrane compartments to facilitate surface increase at the tip. These processes are coordinated by signaling factors that help to maintain cell polarity and allow growth only at the root hair tip. Importantly, these functional steps are all interdependent, so that they reinforce each other in a series of interlocking feedback loops (**Figure. I.5.**).

ROPs are critical for both maintaining cell polarity and growth of root hairs since they determine the site of exocytosis and maintain calcium oscillation by activating ROS production which in turn activates calcium channels. The feedback loop of calcium and ROS oscillation is translated into the distinct organization of the actin cytoskeleton in different region of root hairs. High calcium concentration prevents F-actin formation at the apex but allows formation of a dynamic actin mesh in the subapex. Further back in the root hair, F-actin cables parallel to the shank of root hairs deliver organelles to the subapical region. Among these organelles, Golgi stacks provide membrane compartments that contain key regulators to the tip of root hairs. As a result, vesicles accumulate in the apex and exocytosis occurs preferentially at the tip. Exocytosis

of calcium channels reinforces the calcium oscillations thereby stabilizing the feedback system. At the same time, PtdIns 4,5-P_2 (PIP_2), a derived membrane lipid that is deposited at the apex by exocytotic vesicles, activates ROP proteins to stimulate ROS production, while ROP activity is spatially limited by interaction with RhoGDI in the subapex. Remarkably, ROPs activate PIP-kinase to produce PIP_2 in the membrane, resulting in a positive feedback loop that stabilizes ROP activity at the apex. The net result of these interdependent feedback loops is a series of stable oscillation that ensures polar growth over long periods.

Every factor in this regulatory network plays a pivotal role, so that slight imbalances of any of these factors affect the entire system, resulting in failure of normal root hair growth. Recent studies have identified many of the genes responsible for root hair development and their functions, and made big strides in revealing the underlying molecular mechanisms of root hair development. However, it should be emphasized that many details still need to be clarified. For example, the precise role of myosins on root hair development, as well as the contribution of endocytosis to tip growth still remain in question. Further genetic, cell biological, and biochemical studies to investigate the dynamic interplay of the various factors involved in root hair growth combined with the collection of quantitative data and computational modeling will be necessary to elucidate these and other questions.

Figure I.4. Cellular architecture during root hair development

Schematic representation of root hairs during four stages of root hair development. Upper panels show actin filaments (grey lines) and secretory vesicles (black dots). Lower panels show microtubules (darker grey lines) and the tip-focused calcium gradient (darker color represents higher calcium concentration).

A. Early events after bulge site selection. Note the fragmentation of actin filaments and the local loss of microtubule organization.

B. Initial outgrowth and bulge formation. Actin filaments begin to form a dense mesh behind the tip region where vesicles accumulate and the calcium gradient forms.

C. Tip growth. Cytoskeletal elements are mostly longitudinal along the shank but do not reach into the apex. Vesicle accumulation and calcium accumulation are maximal at the apex.

D. Fully grown hair. Vesicle accumulation and calcium gradient at the tip disappear and longitudinal actin filaments and microtubules reach into the apex.

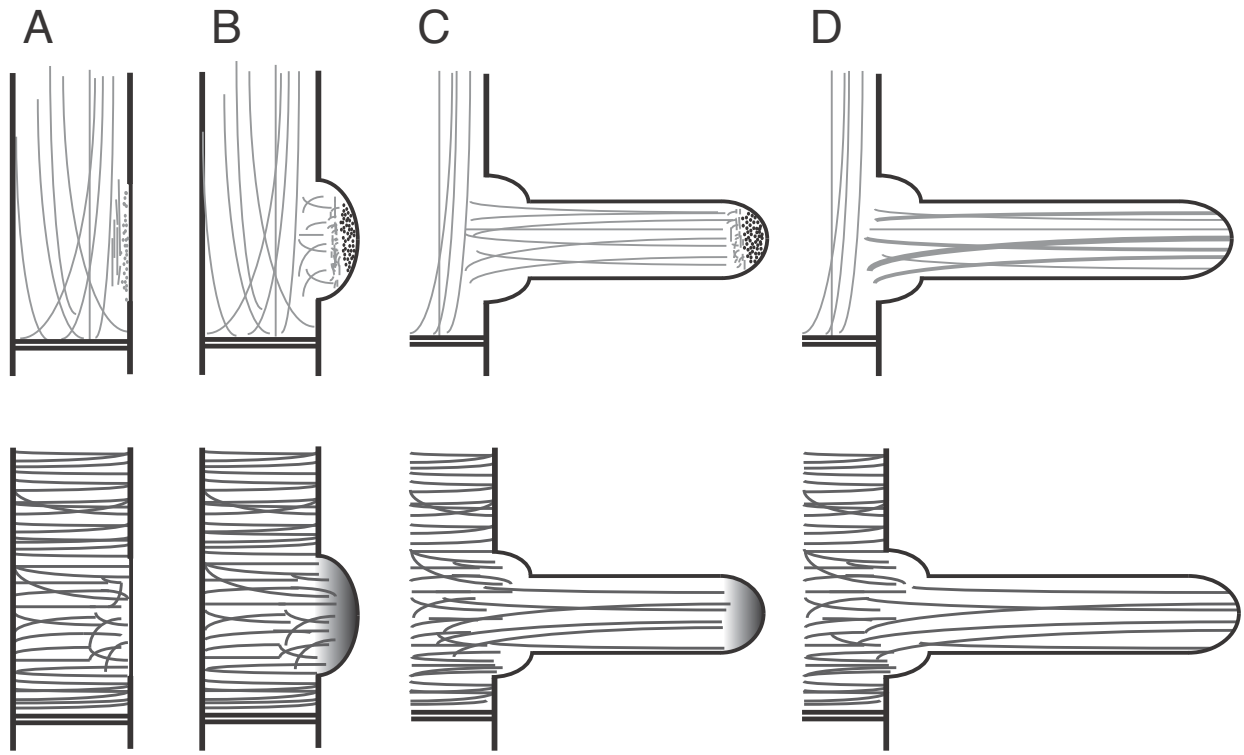
A
B
C
D

Figure I.5. Self-reinforcing feedback regulation of tip growth

Simplified model of regulatory mechanisms that affect the actin cytoskeleton in different areas of the root hair during tip growth. For details see text.

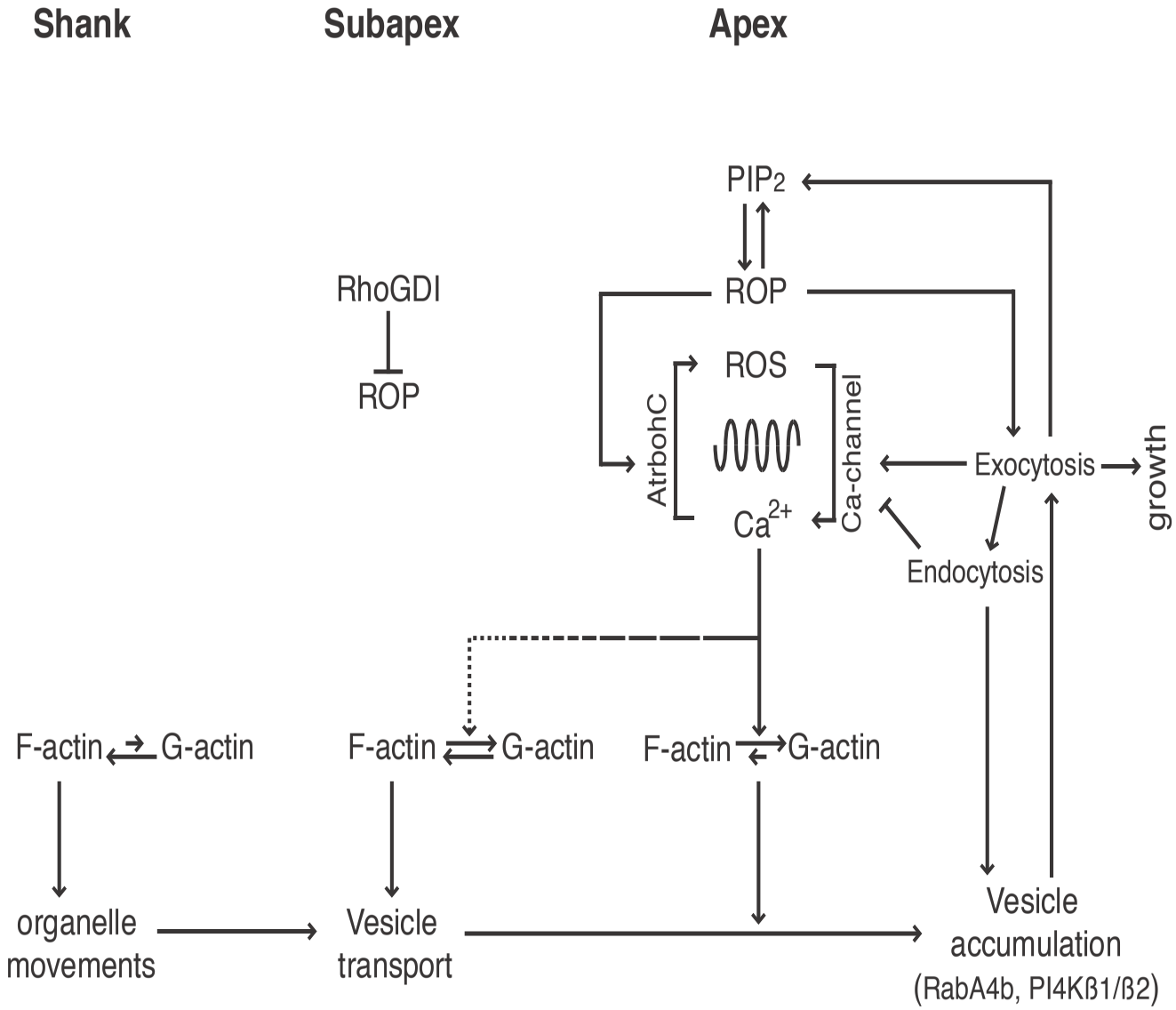
Shank
Subapex
Apex
PIP2
RhoGDI
ROP
ROP
ROS
AtrbohC
Ca-channel
Exocytosis
growth
Ca2+
Endocytosis
F-actin
G-actin
F-actin
G-actin
F-actin
G-actin
organelle movements
Vesicle transport
Vesicle accumulation
(RabA4b, PI4Kß1/ß2)

I.3. MOLECULAR GENETIC MECHANISM OF ROOT HAIR POSITIONING

Although the morphology of plants differs greatly between species, there are four fundamental structures found in all flowering plants: root, leaves, flowers and seeds. The plant root is a critical organ for plants that allows them to survive by absorbing water and nutrients from the soil. Conceptually, roots can be divided into four different zones: a meristematic zone, a cell elongation zone, a root hair initiation zone, and a maturation zone (**Figure. I.6.A**). In the meristematic zone, cell divisions produce new cells and newly divided cells determine their fates. Cells then increase in length in the elongation zone. The root hair initiation zone can be viewed as a part of the maturation zone since cell differentiation occurs at this point, so that individual cells have their own morphologies. However, very young epidermal cells initiating root hair production still can elongate, thus, the root hair initiation zone could be considered as a transition state from cell elongation zone to maturation zone. Root hairs increase the surface area of the root and therefore aid in the fundamental function of this organ. In most species, not every epidermal cell forms a root hair. Many studies have been conducted to identify genes and their relationships to elucidate the elaborate signal cascade of regulatory mechanism that lead to root hair positioning.

I.3.1. Variations in root hair patterning in plants

Distinctive distribution patterns of root hairs are observed depending on the species (Clowes, 2000; Dolan and Roberts, 1995; Tsai et al., 2003). Three patterns are represented in

Figure I.6. *Arabidopsis* root architecture

A. Arabidopsis seedling grown on a vertical plate. Four different zones can be shown conceptually depending on cell morphogenesis. Root apical meristem at the tip of root produces new cells by cell division and those cells keep dividing to form tissues depending on the position in meristematic zone. In elongation zone, cells, whose fate is already determined, increase their length and they start producing root hairs. Root hair growth continues on early stage of maturation zone.

B. Cross-section of root hair initiation zone. *Arabidopsis* has simple root architecture where epidermis, cortex, and endodermis exist as single layers of cells around the vascular bundle in the center.

A

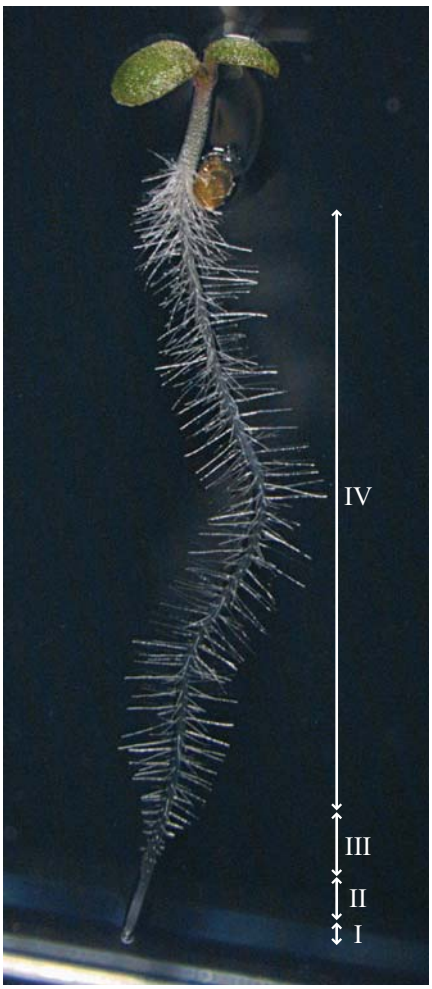

IV Matere zone

III Root hair initiation zone

II Cell elongation zone

I Meristematic zone

B

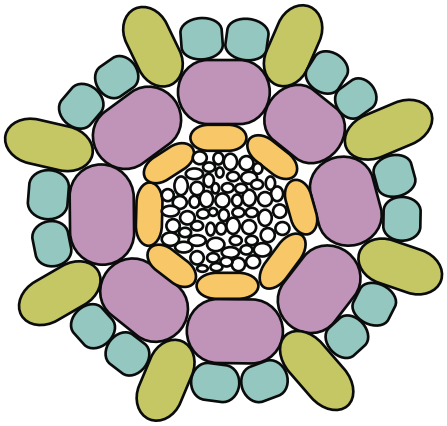

Trichoblast

Atrichoblast

Cortex

Endodermis

vascular plants based on the distribution of root hairs on the root epidermis (**Figure. I.7.**). Type I plants have root hairs randomly distributed (**Figure. I.7.A.**). In type I distribution, every root epidermal cells has the potential to produce root hairs but only a few actually form root hairs. This type of distribution occurs in most dicots and monocots, as well as in ferns (Clowes, 2000). Since all root epidermal cells can produce root hairs, there is no regular pattern for this type. Type II patterns are observed in many lower ferns and monocots (Clowes, 2000). Plants with this type have two differently sized root epidermal cells arrayed along the longitudinal axis and only short cells produce root hairs (**Figure. I.7.B.**). Finally, many eudicots show a type III root hair pattern (**Figure. I.7.C.**). Usually, epidermal cells divide a file of root hair-producing cells (trichoblast or H-cell) and non-hair cells (atrichoblast or N-cell.). Interestingly, type I can be additive to other patterns. For example, *Echium plantagineum L.* showed root hairs on every epidermal cell but root hairs were of two different lengths (Tsai et al., 2003). *Echium* is a type III plant that still has information of H-cells or N-cells, thus the epidermis can produce long hair cells on some files of epidermis and short hairs on the other files of cells. In most species, the molecular machinery of patterning is not yet clear. However, regardless of types, it has been thought that the upstream machinery of fate determination regulates common downstream players, such as genes involved in cell wall synthesis, cell wall-loosening, and cell polarity processes. Recently, promoter analysis has identified typical cis-elements for root hair (RHE) in several model plants with different root hair patterning types (Kim et al., 2006). This finding supports the concept of a "root hair regulon".

Arabidopsis thaliana is a typical type III plant. The *Arabidopsis* root has a simple architecture. It is consist of only four types of tissues; epidermis, cortex, endodermis, and vascular tissues (**Figure. I.6.B.**). Epidermis, cortex, and endodermis are formed by single layers

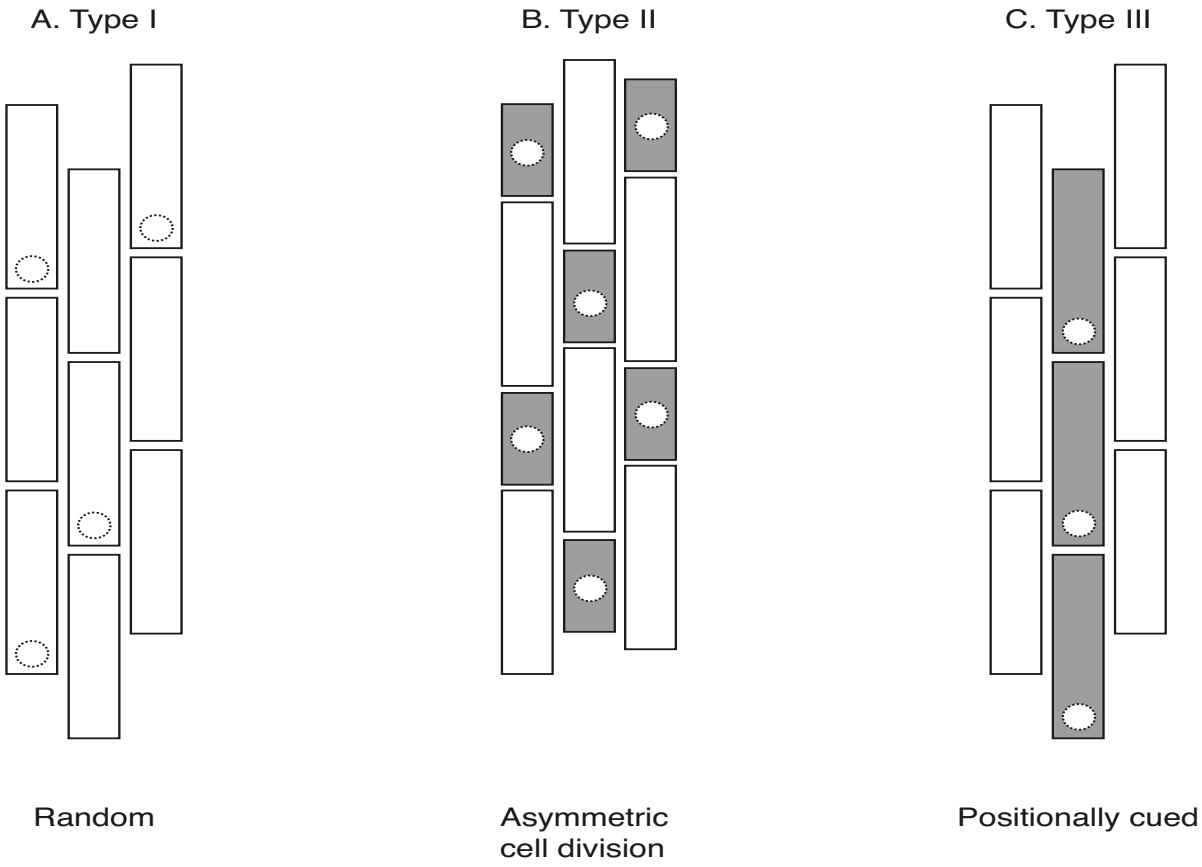

Figure I.7. Three types of root hair patterning in plants

Simplified figures explaining three types of root hair patterning in higher plants (after Kim *et al.*, 2006)

A. Random distribution of root hairs. Among model plants, maize and *Medicago truncatula* are in this type.

B. Asymmetric cell division on root epidermal cells. Plants in this type display two types of epidermal cells in different sizes. Rice and wheat are in this type.

C. Positionally cued. Position of epidermal cell relative to cortex cell decides the fate of epidermal cell to produce root hairs. Genetic mechanism of this type has been well studied in Arabidopsis thaliana. Cabbage and *Impatiens balsamina* also fall into this group.

of cells; the vascular tissue also is composed of a simple set of cells. Normally, viewed in cross section of the *Arabidopsis* primary root has eight cortex cells while epidermis produces eight trichoblasts and approximately 11-14 atrichoblasts. The molecular genetic basis of root hair patterning on the epidermis has been extensively studied with *Arabidopsis thaliana*.

I.3.2. Early embryonic fate determination mechanism of root hair cells

In *Arabidopsis*, the ultimate fate of epidermal cells relies on their position relative to the cortex (Galway et al., 1994). Epidermal cells are smaller than cortex cells so two kinds of epidermal cells can be generated based on their position relative to the cortex. Epidermal cells attached to two cortical cells always differentiate as hair-producing cells resulting in eight root hair cells since Arabidopsis has eight cortical cell files (**Figure. I.6.B.**). Forward genetic approaches have led to the identification of many genes that regulate root hair patterning in *Arabidopsis* (Bernhardt et al., 2005; Kirik et al., 2004a; Kirik et al., 2004b; Lee and Schiefelbein, 1999; Masucci et al., 1996; Masucci and Schiefelbein, 1996; Schellmann et al., 2002). Most of the genes encode transcription factors that regulate downstream genes involved in root hair epidermis differentiation and, with single and double mutants and promoter-reporter analysis, a well-supported signal transduction model has been developed (**Figure I.8.**). This mechanism is very interesting in three aspects; at first, upstream regulators show position-specific expression patterns, so that stripe-like patterns have been observed with promoter-reporter analysis (Galway et al., 1994; Lee and Schiefelbein, 1999; Masucci and Schiefelbein, 1996; Schellmann et al., 2002). Secondly, some transcription factors in the middle of signal transduction cascades can travel to neighboring cells where the proteins actually function (Bernhardt et al., 2005).

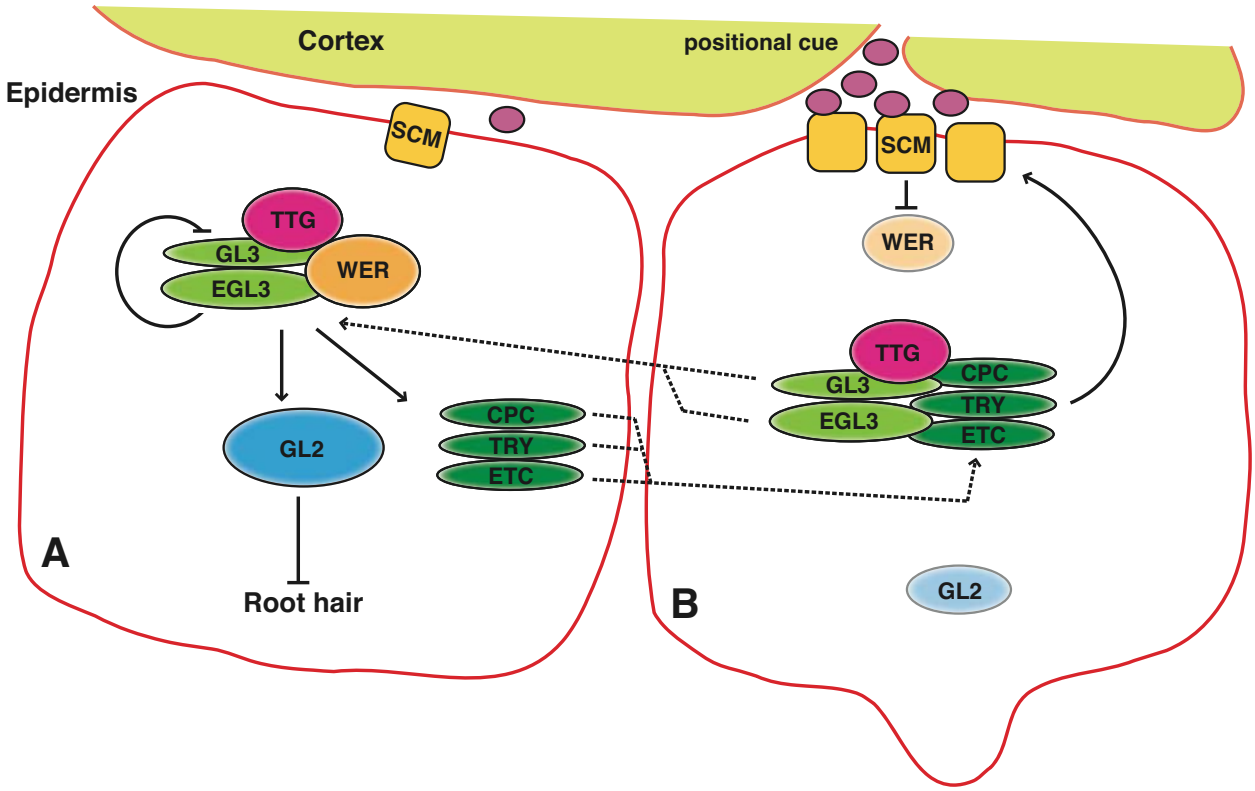

Figure I.8. Schematic mechanism of transcriptional regulation of root hair positioning

Simplified diagram of root hair positional cued signal cascade on root epidermal cells of *Arabidopsis thaliana* (after Guimil and Dunand, 2007; Kwak *et al.*, 2008; Schiefelbein *et al.*, 2009)

A. N-cell

B. H-cell

Finally, gene expression in the early steps of this pathway is regulated by the expression of later steps of the pathway in **a** feedback loop (Kwak and Schiefelbein, 2008; Lee and Schiefelbein, 2002).

There are nine major regulators that have been identified by their mutant phenotype and that have been characterized by double mutant analysis and promoter-reporter analysis. Mutations in *TRANSPARENT TESTA GLABRA* (Schellmann et al.), *GLABRA2* (*GL2*), *GLABRA3* (*GL3*), *ENHANCER OF GLABRA3* (*EGL3*), and *WEREWOLF* (*WER*) caused plants to produce more root hairs in N-cells (Bernhardt et al., 2003; Galway et al., 1994; Lee and Schiefelbein, 1999; Masucci and Schiefelbein, 1996), while mutations in *CAPRICE* (*CPC*), *TRIPTYCHON* (Moriau et al.), and *ENHANCER OF TRY AND CPC* (*ETC1*) showed less (or no) root hairs even on H-cells (Kirik et al., 2004a; Schellmann et al., 2002; Simon et al., 2007; Wada et al., 2002). Recently, *SCRAMBLED* (*SCM*) was discovered to be involved in this root epidermal cell patterning (Kwak and Schiefelbein, 2007). It is remarkable that *SCM* encodes a leucine-rich repeat receptor-like kinase localized at the plasmamembrane of the root epidermis which might receive positional signals from cortical cells (Kwak and Schiefelbein, 2008). In H cells, SCM might repress *WER* transcription (Kwak et al., 2005), thus, *WER* is expressed mainly in N-cells (**Figure. I.8.A.**). *WER* encodes a R2R3 MYB-domain transcription factor which forms a complex with TTG, GL3, and EGL3 in N-cells. Several gene expression and genetic studies up to date suggests that the complex with GL3, EGL3, TTG, and WER in N-cells activates the expression of GL2, a homeo domain-leucine-zipper transcription factor which down-regulates several downstream genes involved in root hair formation (Bernhardt et al., 2005; Lee and Schiefelbein, 1999; Masucci et al., 1996; Masucci and Schiefelbein, 1996; Tominaga-Wada et al., 2009). *TTG* encodes a small protein which has WD40 repeats and *GL3* and *EGL3* encode

related basic helix-loop-helix (bHLH) transcription factors. Interestingly, gene expression of *GL3* and *EGL3* occurs in H-cells although proteins actually function in N-cells. It has been suggested that GL3/EGL3 proteins move to N-cells for their position-specific function. The presence of EGL3/EGL3 in N-cells can inhibit the expression of their own genes in N-cells which provides a feedback loop to control gene expression (Bernhardt et al., 2005). Besides activation of *GL2* expression and self-repression of their own genes, the GL3/EGL3 complex can activate three genes, *CPC*, *TRY*, and *ETC*, in N-cells, the encoded proteins of which have also been shown to travel to neighboring cells (H-cells). These three genes encode small one-repeat MYB proteins that appear to have a lack of transcriptional activity which inhibits GL3/EGL3 activity by competing with WER for binding to the GL3/EGL3 proteins (**Figure. I.8.B.**) (Tominaga et al., 2007)

I.3.3. Plasticity from environmental factors

Several studies have shown that the length and density of root hairs can be modified in response to differences in environmental factors, including nutrient deficiency and hormonal changes (Bates and Lynch, 2000a; Bates and Lynch, 2000b; Müller and Schmidt, 2004; Zhang et al., 2003). Limitation of essential nutrients can lead to abnormal root development and additional root hair production to increase uptake of these nutrients (Lopez-Bucio et al., 2003). Primarily, phosphorus and iron can change growth rates of the roots as well as root architecture. Under limiting iron and phosphorus, wild type *Arabidopsis* produce more root hairs on both H-cells and N-cells than under normal conditions (Müller and Schmidt, 2004). Observation of the effects of iron and phosphorus deficiency on root hair formation in wild type and several mutants involved

in root hair formation allowed the effect of iron (Fe) to be distinguished from that of phosphorus (P) deficiency. Although in wild type both Fe and P deficiency caused relatively similar increases of root hair numbers, in mutants of *GL2* and downstream genes, Fe and P display distinct effects suggesting that an additional pathway related to P deficiency might exist (**Figure. I.9.**) (Guimil and Dunand, 2006; Müller and Schmidt, 2004).

Mutant analyses revealed the involvement of hormones in determining root epidermal cell fates. For example, *ctr1* mutants of *Arabidopsis*, which have a mutation in *CTR1* that encodes a protein kinase involved in ethylene signaling, displayed root hairs on every root epidermal cell (Kieber et al., 1993). It also has been shown that the lack of root hairs on several mutants related to auxin and ethylene synthesis can be rescued by providing exogenous hormones (Masucci and Schiefelbein, 1994; Tanimoto et al., 1995). Although the molecular mechanism of hormones involved in root hair patterning is still unknown, it is likely that these hormones function either independently or downstream of *GL2* in the type III pathway (Masucci and Schiefelbein, 1996). Recently, it has been shown that sucrose signaling is partly involved in sensing phosphate deficiency (Jain et al., 2007). It is likely that auxin and sucrose signaling contribute to sensing phosphate deficiency not in the primary root but in lateral roots. However, a detailed mechanism for how these independent signaling pathways can intertwine on root hair patterning still remains to be investigated.

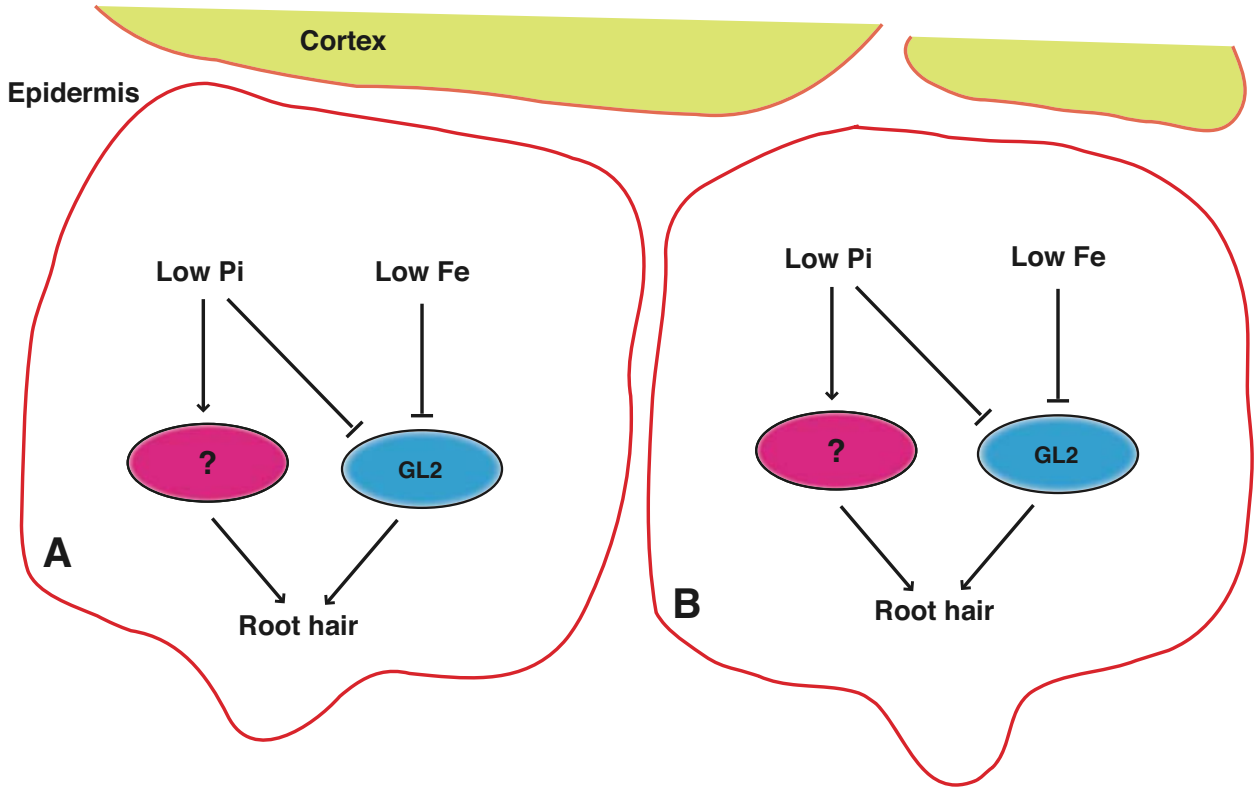

Figure I.9. Schematic pathway of root hair positioning with environmental factors

Simplified diagram of the control of root hair positioning by phosphorus and iron deficiency in *Arabidopsis thaliana* (after Müller and Schmidt. 2004; Guimil and Dunand, 2006)

A. N-cell

B. H-cell

I.3.4. Conclusion

Mutant analysis combined with ectopic gene regulation and determination of expression patterns has resulted in a detailed pathway leading to normal root hair patterning in *Arabidopsis* (Schiefelbein et al., 2009). However, there still are many things to be clarified. For example, it is unclear how proteins expressed in a specific cell (CPC/TRY/ETC in N-cells and GL3/EGL3 in H-cells) can move to their neighboring cells. It has been suggested that CPC proteins might move through plasmodesmata based on indirect evidence from SHORTROOT and KNOTTED1. These are also MYB transcription factors like CPC and are known to travel between cells through plasmodesmata (Schiefelbein et al., 2009; Wada et al., 2002). However, there is no direct experimental evidence to date. In addition, biochemical evidence for protein interactions in the complex are not sufficient. Recent computational modeling of mechanism of intracellular movement of CPC and GL3 would help to establish the pathway (Savage et al., 2008). Except for competition of binding on MYB transcription factor between CPC and WER, all protein complexes in the model are only predicted based on genetic evidence with mutants and gene expression in the mutants. Finally, the mechanism by which SCM, a receptor on the plasmamembrane of root epidermis can repress the gene expression of WER is still in question. The nature of the ligand of SCM is also unknown. Identification of additive mutants using existing mutants is also necessary to figure out the entire signaling mechanism of root hair positioning. The interaction of the positionally cued pathway and regulation by environmental factors also needs to be investigated further. In this context, it might be helpful to carefully observe the effects of hormones or nutrient deficiency on the mutants involved in positional pattern formation.

I.4. RATIONALE OF THIS STUDY

Fast and efficient deposition of cell components upon internal or external signals is essential to plant development. In a small cell, distribution might be possible by free diffusion of individual components. However, in a large cell or highly polarized cell, such as root hairs, faster and directional delivery is more effective than slow and random diffusion. Acto-myosin cytoskeleton has been suggested to serve this fast and directional trafficking (Yalovsky et al., 2008). Several studies showed examples of intracellular trafficking of molecules, or membrane compartments. For example, the auxin-efflux carrier PIN1 cycles between the plasma membrane and an endosomal compartment in an actin-dependent manner (Geldner et al., 2001). Compared to the study of the function of the acto-myosin cytoskeleton in trafficking of molecules in a single cell, there are not many studies to provide direct evidence for the involvement of acto-myosin cytoskeleton in plant development. There might be two explanations for this lack of functional studies of acto-myosin cytoskeleton in plant development. First, this could be because this system is highly fundamental, thus during phenotypic mutant screening it might be difficult to isolate the corresponding mutants since they might be lethal or give a pleiotropic phenotype. On the other hand, gene duplication in this essential system could have resulted in elevated gene redundancy which would also make it difficult to isolate mutants.

Recent advances in bioinformatics and genomics offer a possible solution. The *Arabidopsis* genome project revealed that 13 genes of class XI myosins are encoded in the *Arabidopsis* genome (Reddy and Day, 2001). In addition, microarray databases for gene expression provide excellent preliminary information for designing an experiment to characterize the gene function as well as quality control for gene expression studies (Zimmermann et al.,

2004). The most powerful genomic tool is a genome wide insertional mutagenesis in *Arabidopsis* (Alonso et al., 2003). This collection provides insertional mutants of genes of interest and thus offers the opportunity to observe a global phenotype of individual myosin mutants and facilitate the generation of multiple gene mutants in the myosin family. Combined with an advantage of *Arabidopsis* as a model plant, providing accessibility to detailed understanding of many developmental pathways and easy transformability to introduce new genes into the genome, it is now possible to approach myosin function with a reverse genetic approach.

This study will employ a combination of reverse genetic experiments and additional cell biological studies of organelle trafficking in mutants and wild type to address in detail the contribution of dynamic intracellular transport by myosin in plant cell growth and development.

CHAPTER II. Phylogenetic analysis of class XI plant myosins and Class XI myosin gene expression survey in Arabidopsis

◆ *Phylogenic analysis of this chapter has been studied as a term project of the functional genomics class (PS605, 2006). As genome projects are updated, more myosin genes in a various species are available to date. Moreover, rice genome sequences in this study have been also updated with a better gene annotation. However, a new analysis has not been conducted and methods and results for this part remains as they were in the report submitted to PS605 class, 2006. New findings after the analysis are rather discussed in Chapter VI. Conclusion.*

II.1. INTRODUCTION

To date, 35 classes of myosin have been classified from 328 eukaryotic species (Odronitz and Kollmar, 2007). Among them, plant-specific myosins are grouped in only two classes, VIII and XI. Class XI myosins have six IQ motifs and a tail with structural similarity to class V myosin in animal and fungi. Phylogenetic analysis showed that class XI has the same ancestor as class V suggesting that class XI might have same functions in plant as class V in non-plant species (Odronitz and Kollmar, 2007). Two genes in the class XI myosin were, at first, identified by PCR screening in *Arabidopsis* and named *MYA1* and *MYA2* (Kinkema et al., 1994) and later more myosins have been predicted based on the genome sequencing database, named XI-A through XI-K (Reddy and Day, 2001). The relatively large number of myosin XI isoforms present within a single plant species suggests that the possibility of functional redundancy within isoforms. It is also conceivable that certain myosins might have specific functions in certain tissues (or cell type) or in a certain developmental stage. Thus, it would be necessary to examine their similarity of amino acids and spatial and temporal gene expression pattern to postulate the functional redundancy in plant development.

In this study, to inform the guidance of the function of class XI myosin, phylogenic tree with 13 myosins in *Arabidopsis* and 11 myosins in rice were resolved. This relatively large number of isoforms may be related to their functional redundancy. In the tree, most of isoforms paired with one of inner species isoform or intra species isoforms. In addition, promoter-reporter analysis showed a diverse expression pattern of myosins over tissues and developmental stages to support that possible functional redundancy might exist on the various tissues and yet distinct

function on each isoforms might occur. This phylogenic analysis and expression survey might help to understand which isoforms may have function on specific developmental aspects and whether they share some functional redundancy.

II.2. MATERIALS AND METHODS

II.2.1. Myosin gene search in *Arabidopsis* and rice

Arabidopsis myosin sequences identified by Reddy and Day (2001) were modified based on the ESTs and the sequences of gene-specific PCR products. Rice myosins were, initially, searched by multiple BLASTs with 13 *Arabidopsis* myosins using Bioedit (http://www.mbio.ncsu.edu/BioEdit/Bioedit.html) with whole genome annotation sequences of rice downloaded fro rice genome project ver. 2.0 (http://rice.plantbiology.msu.edu/). Initially, the cut-off E-value to isolate candidate genes was set to *E=1-E0.5* and proofread sequences manually based on domain structure of myosins. Amino acid sequences of the class VIII myosins of *Arabidopsis* and *Chara* myosin XI were obtained from the myosin homepage (http://www.mrclmb.cam.ac.uk/myosin/myosin.html).

II.2.2. Identification of motifs in the putative myosin sequences

Motor and dilute domains in the putative myosins were identified using Pfam (http://www.sanger.ac.uk) with E=0.05. The IQ motif was identified with E=2. Coiled coil regions were detected by web-based program (http://theory.lcs.mit.edu).

II.2.3. Sequence alignment and phylogenetic analysis

For a preliminary alignment, Clustal X (ftp://ftp-igbmc.ustrasbg.fr/pub/ClustalX) was used. The aligned amino acids sequences were then modified by removing sections of low similarity part with Bioedit to allow resolution of a more accurate tree. To obtain the tree with motor domain only, amino acids sequences of motor domain defined by Pfam were taken and aligned by Clustal X. Maximum-likelihood analysis was performed using PHYML (http://atgc.lirmm.fr/phyml/) and bootstrap values were estimated with 1000 replicates for both full-length trees and motor domain only trees. The resulting phylogenetic relationships were visualized using TREEVIEW 1.6.0.

II.2.4. Expression profile and gene duplication profile

Gene expression profiles were examined by using the Gene Atlas function in Genevestigator 1.0 (Zimmermann et al., 2004). Gene duplications were surveyed with the MAtDB genome viewer (http://mips.helmholtzmuenchen.de/plant/athal/index. jsp). Rice gene expression information was obtained from Jiang and Ramachandran (2004).

II.2.5. Promoter-GUS analysis

Promoter sequences were predicted from gene bank (http://www.arabidopsis.org/) and cloned by PCR on the upstream of GUS reporter gene in pBIN20 binary vector by Dr. Xue Cai in this lab. These constructs were transformed into plants with the help of *Agrobacterium tumefaciens* by dipping methods (Weigel and Glazebrook, 2002). After initial screening of T1

lines by kanamycin selection, gene expression patterns were observed in T2 and T3 plants by GUS staining. Staining for GUS activity, the protocol from Blazquez et al. (1997) was modified as below. Plants were pre-fixed with ice-cold 90% acetone at 4°C for 30min and incubated in the staining buffer containing 100mM $NaPO_4$ (pH7.0), 10mM EDTA, 0.1% Triton X-100, 5mM $K_3Fe(CN)_6$, 5mM $K_4Fe(CN)_6$, and 2mM X-Gluc (5-bromo-4-chloro-3-indolyl-ß-glucuronide) at 37°C overnight. After clearing with serial concentration of ethanol (final concentration at 95%) for at least 4 hours, pictures of plants were taken under a stereomicroscope (Leica MZ16FA, http://www.leica-microsystems.com) equipped with digital camera (Leica DFC420) and Leica FW4000 image acquisition software.

II.3. RESULTS

II.3.1. Identification of myosins in Arabidopsis and Rice

Preliminary amino acids sequences for 13 of myosin XI in *Arabidopsis* were obtained from Reddy and Day (2001). The sequences were then corrected based on ESTs and PCR products available in our lab (**Table II.1**). Total of 129 genes were retrieved from the rice genome database within *E=1-E05* by multiple blast search with 13 *Arabidopsis* myosin amino acid sequences. 87 retrieved sequences were excluded since they were partial sequences of myosins or non-myosin proteins which have similarity with partial sequences of myosins, mostly the coiled coil domain. Among the 42 remaining results, many of the sequences were redundant or structurally imperfect and could not encode a complete myosin protein. In the end, 11 rice class

Table II.1. Summary of cDNA information

Gene name	EST accession number	Clone name	Length of cDNA	Covered domain
MYA1		MYA1		Full length
MYA2		MYA2		Full length
XI-A				
XI-B	BE526400.1	M66H16STM	~1000bp	dilute
XI-C	R30087.1	165B7T7	~1100bp	dilute
XI-D	BE528549.1	M79H19STM	~2500bp	tail +3'UTR
XI-E				
XI-F				
XI-G				
XI-H				
XI-I	AV530204.1	APZL62d09F	~2500bp	tail
XI-J		MYA3		
*XI-K**	BE526400.1	M65012STM	~ 2900bp	IQ + full tail +3'UTR
*XI-K**	AV546218.1	RZL10e06F	~3800bp	5' UTR+ SH3 + half tail

* Two EST overlapped in the beginning of tail region resulting in full length of XI-K.

Table II.2. Myosins from *Arabidopsis* and Rice

Species	Gene name	Chr	AGI	AA size	Note
Arabidopsis	*MYA1*	I	*At*1g17580	1520	
	MYA2	V	*At*5g43900	1505	
	XI-A	I	*At*1g04160	1723	
	XI-B	I	*At*1g04600	1500	
	XI-C	I	*At*1g08730	1572	
	XI-D	II	*At*2g33240	1611	
	XI-E	I	*At*1g54560	1529	
	XI-F	II	*At*2g31900	1556	
	XI-G	II	*At*2g20290	1502	
	XI-H	IV	*At*4g28710	1516	
	XI-I	IV	*At*4g33200	1510	
	XI-J	III	*At*3g58160	1242	
	XI-K	V	*At*5g20490	1531	
Rice	*OsMyoXI-A*	I	*Os*1g51630	2286	
	OsMyoXI-B	II	*Os*2g57190	1495	
	OsMyoXI-C	II	*Os*2g53740	1507	
	OsMyoXI-D	II	*Os*2g34080	1510	
	OsMyoXI-E	III	*Os*3g53660	1491	3 isoforms from different tissues (sizes are slightly different)
	OsMyoXI-F	III	*Os*3g48140	1529	
	OsMyoXI-G	III	*Os*3g64290	1445	
	OsMyoXI-H	V	*Os*5g46030	2159	
	OsMyoXI-J	VI	*Os*6g29350	1529	
	OsMyoXI-L	X	*Os*10g25560	1601	Wrong annotation, different N-terminal domain (NAM domain)
	OsMyoXI-K	X	*Os*10g19860	1339	Manually searched (> E < 2.1-e405)

XI myosins sequences could be obtained (**Table II.2**). Jiang and Ramachandran (Jiang and Ramachandran, 2004) identified 12 class XI myosins in rice and named *XI-A* to *XI-L*, however, *XI-I* genes from their study was not identified in my screening. Thus based on the information from them, potential genomic segment for *XI-I* gene was manually searched, however, there was no myosin gene found.

II.3.2. Genomic Distributions of Myosins in Rice and *Arabidopsis*

The genome distributions of *Arabidopsis* myosins and rice myosins were analyzed. In *Arabidopsis*, chromosome 1 contains genes for five isoforms (*XI-A*, *XI-B*, *XI-C*, *XI-E*, and *MYA1*) whereas chromosome 3 carries only one myosin gene, *XI-J* (**Figure II.1**). To obtain the evolutionary relationships of the 13 myosins, *Arabidopsis* genome duplication map was obtained from MAtDB genome viewer (http://mips.gsf.de/proj/thal/ db) and myosin gene positions were verified on the genome. **Figure II.2.** shows the distribution of recent genome duplication events that occurred in the *Arabidopsis* genome. *XI-H* and *XI-G* genes are located in duplicated segments in chromosomes 2 and 4. Similarly, *XI-A* and *XI-D* genes are also positioned in duplicated segments on chromosomes 1 and 2. However, several genes that are located in duplicated genome segments do not have an equivalent counterpart in the duplicated part on the other chromosome. For example, *MYA1* lies on the left arm of the chromosome 1 and this part is duplicated at the end of the same chromosome. However, no myosin gene is located in the duplicated chromosome region. In case of rice myosins, they are located on chromosome 1,2,3,5,6,7,and 10 while no isoforms were found on chromosome 4,8,9,11,and 12 (**Figure II.3.**). Jiang and Ramachandran (Jiang and Ramachandran, 2004) showed the gene distribution of 12

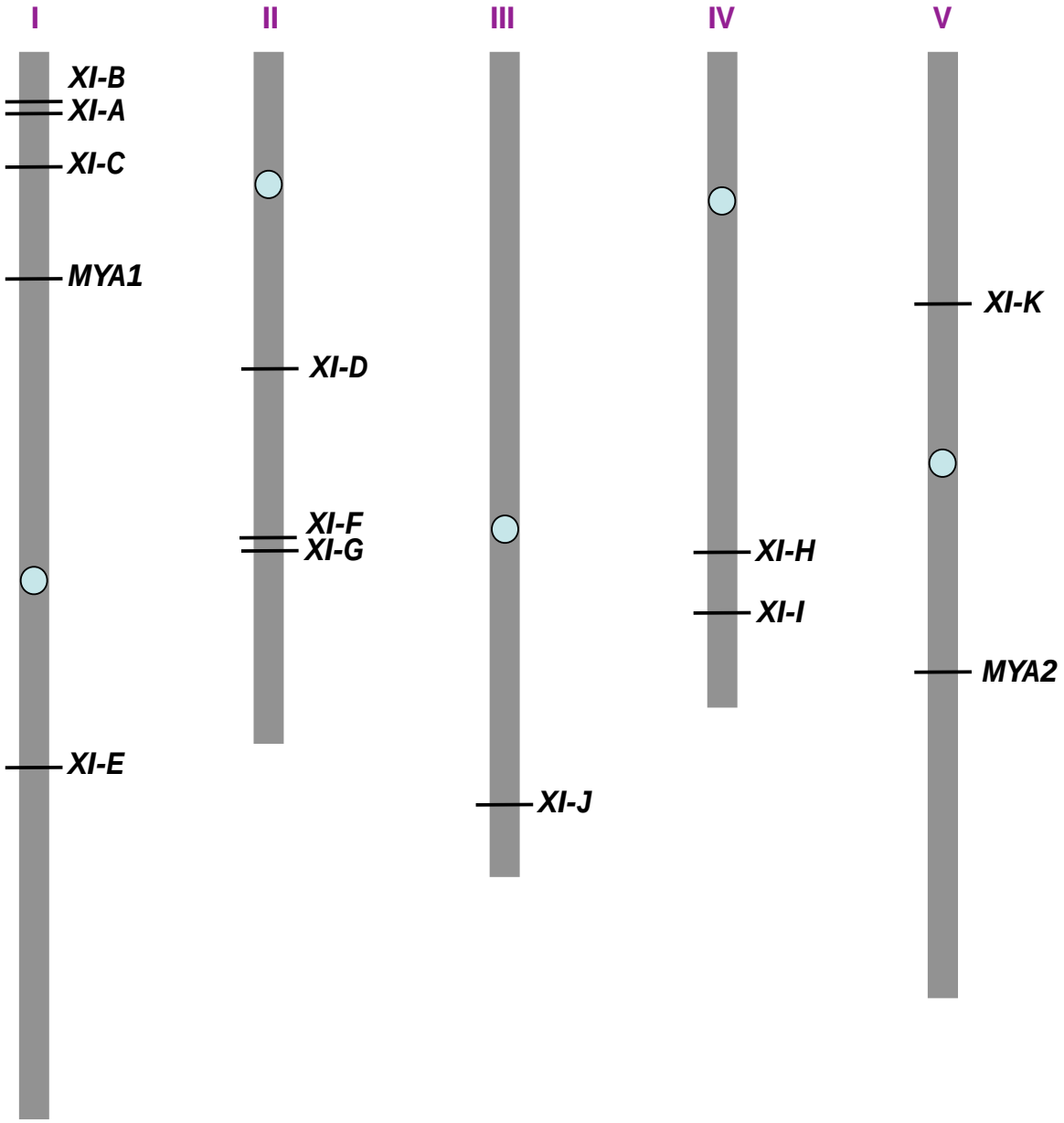

Figure II.1. Myosin gene distribution on *Arabidopsis* chromosomes

Sky blue circles indicate the position of centromeres.

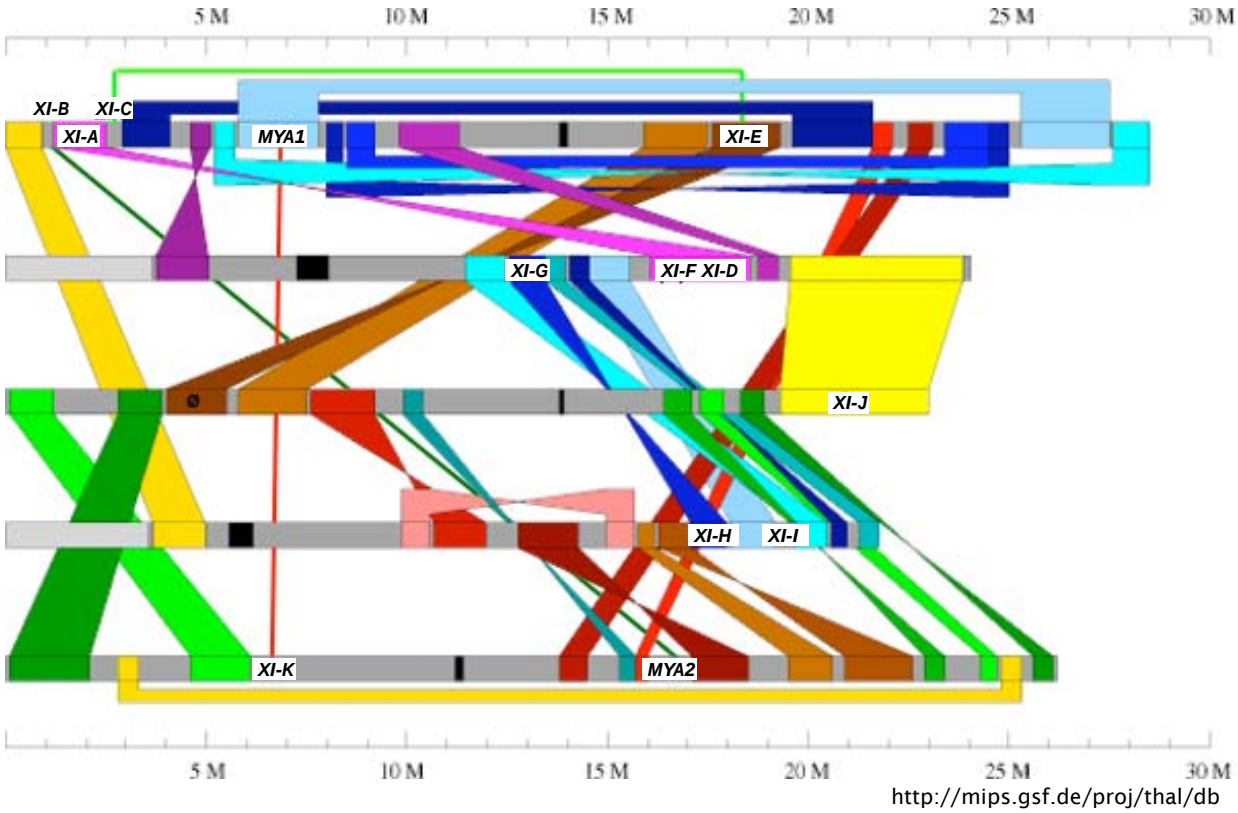

Figure II.2. Genome duplication map of class XI myosins in *Arabidopsis thaliana*

Colors on chromosomes indicate that those segments appeared to be formed by genomic duplication. Approximate positions of myosin genes are named on the relative position of chromosomes. Three thin lines connected two isoforms (light green, dark green, and red) are drawn to indicate two isoforms are similar but not formed by genome duplication (light green line for *XI-C* and *XI-E*, e.g.). Genome duplication map was obtained from MIPS (http://mips.gsf.de/proj/thal/db) and positions of myosins are manually confirmed.

Figure II.3. Myosin gene distribution in the rice genome

Chromosome map has been outlined in Jiang and Ramachandran (2004). Based on the analysis in this study, corrections are marked as red comments. Position of *OsMyoXI-I* is wrong and no myosin-like sequences were found nearby (red X mark on the map). *OsMyoXI-L* and OsMyo*XI-K* gene annotation is not correct.

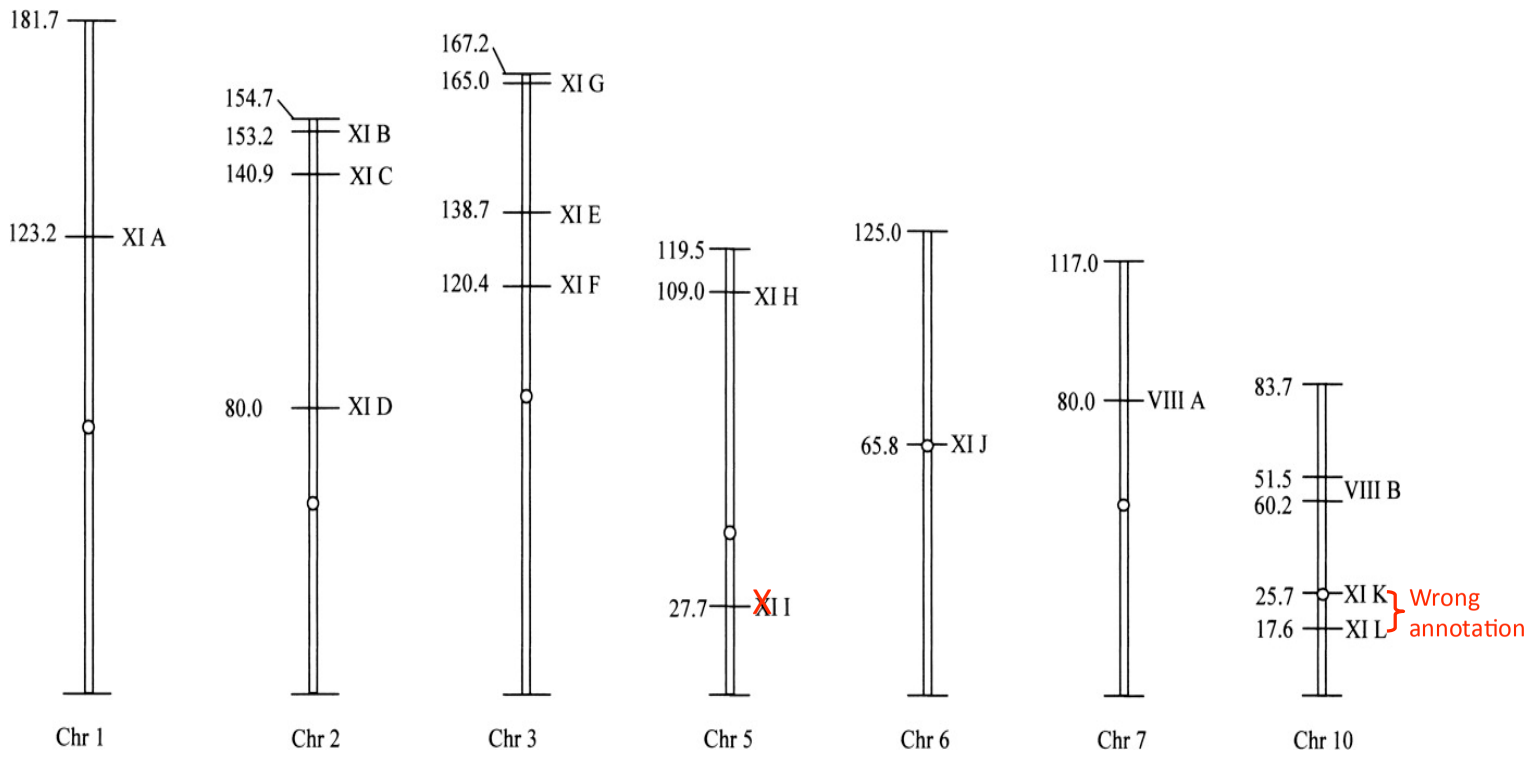
181.7
123.2
XI A
Chr 1
154.7
153.2
XI B
140.9
XI C
80.0
XI D
Chr 2
167.2
165.0
XI G
138.7
XI E
120.4
XI F
Chr 3
119.5
109.0
XI H
27.7
XI I
Chr 5
125.0
65.8
XI J
Chr 6
117.0
80.0
VIII A
Chr 7
83.7
51.5
VIII B
60.2
25.7
XI K
17.6
XI L
Wrong annotation
Chr 10

class XI myosins in rice, however, one of the myosins was actually miss-interpreted as two isoforms which located on different chromosomes since the BAC clone which contained the gene were biased in wrong position of chromosome (**Figure II.3.**).

II.3.3. Characterization of Myosin protein structures

Typical class XI myosins have a domain structure with an N-terminal SH3-like domain with unknown function, a motor domain whose function is to walk along actin filaments, six IQ motifs that are bind to calmodulins as light chains, a coiled coil region for dimerization, and a dilute domain which might be involved in organelle binding (Kinkema and Schiefelbein, 1994). Most family members have this typical domain structure, however, some isoforms have a distinct structure (**Figure II.4.**). Unlike most of the class XI myosins which have SH3-like domain in the N-terminus, OsMyoXI-H show the different N-terminal domain, NAM domain, known as a DNA binding domain of transcription factors involved in apical meristem development (Sablowski and Meyerowitz, 1998). OsMyoXI-L has a relatively long coiled coil region, similar to a class XI myosin in *Chara*. Moreover, XI-J in *Arabidopsis* does not have a dilute domain. Since the dilute domain is a signature of the class XI myosin and the other plant specific myosin, class VIII, does not have the dilute domain, XI-J could be considered as a member of class VIII despite of some structural resemblance to be class XI, like the presence of the N-terminal SH3-like domain and 6 IQ motifs in XI-J.

To clarify the class assignment of these distinct members, phylogenetic trees were constructed with *Arabidopsis* and rice class XI myosins. Class VIII myosins and *Chara* myosin XI were also included as outgroups. Since the C-terminus of myosins is less conserved, it could

Figure II.4. Class XI myosin domain structure

MYA1 showed a typical domain composition of class XI myosin. Domain information were searched from pFam (http://pfam.sanger.ac.uk/) with standard cut-off (*E=1*). Others class XI myosins shown in this figure have different domain structure than conventional class XI myosins. Domains are displayed in different shaped-colors (SH3-like, green; motor, red; IQ motif, yellow; dilute, plum; NAM, light green)

be difficult to be aligned properly. Thus phylogenetic tree was also constructed based only on the motor domain that is highly conserved (> 68% similarity). Some of the myosins clustered as a pair in a species (e.g. XI-A and XI-D; *Os*MyoXI-G and *Os*MyoXI-D), while many of them formed onto specific clusters like XI-F and OsMyoXI-Es (**Figure II.4.**). Interestingly, although the domain structure of XI-J suggested that it might be classified as a class VIII, both phylogenetic trees with full-length myosins and with the motor domain only resolved XI-J in class XI. Moreover, XI-J was clustered with OsMyoXI-A, OsMyoXI-F, and OsMyoXI-H which have the typical structures (except for long coiled coil region in OsMyoXI-H) in the full-length tree. In the tree based only on the motor domain, XI-J was grouped with XI-C, XI-E, and OsMyoXI-J. Thus, XI-J is clearly a member of Class XI. Major change of the trees is the position of XI-A and XI-D. In the full-length tree the XI-A and XI-D pair was branched out from a cluster that contained XI-G and XI-H, MYA2 and XI-B, and OsMyoXI-B, OsMyoXI-G, and OsMyoXI-D. However, in the tree with motor domain only, XI-A and XI-D were grouped with the OsMyoXI-B, OsMyoXI-G, and OsMyoXI-D (**Figure II.4. and 5.**).

II.3.4. Expression profile survey from Genevestigator

To evaluate spatial and temporal gene expression patterns at various developmental stages, gene expression profiles determined by Affymetrix chip analysis were searched in Genevestigator (**Figure II.7.**). Since no data set was included for *XI-K*, expression levels of 12 myosins in *Arabidopsis* developmental stages were obtained (Zimmermann et al., 2004). Interestingly, some myosins that resolved as a relatively duplicated gene pair in the phylogenetic tree, e.g. *MYA2* and *XI-B*, showed very distinct expression patterns (**Figure II.7.**). *MYA2* showed

broad expression in several developmental stages with particularly high expression in senescent leaves, whereas *XI-B* was expressed only in stamen and pollen. *OsMyoXI-J* was found to mostly be expressed in panicles that is a similar structure to inflorescences of Arabidopsis (Jiang and Ramachandran, 2004). Interestingly, *XI-C* and *XI-E*, which grouped with *OsMyoXI-J* in the phylogenetic analysis, also showed specific expression in stamen and pollen (**Figure II.5.** and **II.8 C, E, and F**).

II.3.5. Promoter-GUS analysis

Gene expression patterns were then confirmed with promoter-reporter assays. Promoter sequences have not been identified yet, thus, intergenic genomic sequences from the second exon of myosin gene to the end of upstream gene were cloned by PCR. These PCR fragments were used to drive expression of a GUS reporter gene by Dr. Xue Cai in this lab and transformed into plants. Once kanamycin resistant seedlings from T1 seeds were isolated, GUS staining was carried out with the tissues of adult plants, i.e. leaves from T1 plants. Stems, and flowers were tested and GUS staining on seedlings was performed with T2 seedlings. Most staining patterns are consistent with gene expression profiles from Genevestigator (compare **Figure II. 7, 8, 9, 10, and 11**). Of the 13 genes, promoter-GUS analyses were conducted for 11 genes but not for *XI-I* and *XI-H*. Four genes are exclusively expressing in stamens especially in anthers and pollen. *XI-C* and *XI-E* showed highest degree of sequence similarity among all myosins (**Figure II.4 and 5**) and both of them are expressed only in anthers (**Figure II. 8**). However, while the *XI-C* upstream sequences expressed on pollen in mature anthers exclusively, those of *XI-E* expressed only young anthers before they dehisced (**Figure II. 8. B and C for *XI-C* and E and F for *XI-E***). *XI-*

Jpro:GUS plants showed strong GUS staining in mature pollen. Staining was visible only anthers of mature flowers (**Figure II. 8. M-O**).

XI-B and *MYA2* are closely related paralogs (**Figure II.4 and 5**) and mutants of both genes showed short root hairs (Peremyslov et al., 2008). Both *XI-Bpro:GUS* and *MYA2pro:GUS* plants displayed GUS expression in roots (**Figure II. 8. H and II. 11.A**). In addition to roots, *XI-Bpro:GUS* presented GUS expression only in flowers (**Figure II.8.G-I**) while *MYA2pro:GUS* showed strong expression on most tissues throughout the all developmental stages (**Figure II.11. A-F**). *XI-Apro:GUS* and *XI-Dpro:GUS* also showed different expression patterns despite their sequence similarity. *XI-Apro:GUS* expressed only in pollen strongly (**Figure II.8.J-L**), while *XI-Dpro:GUS* expressed moderately in several tissues (**Figure II.11.G-L**). However, the gene expression profile of *XI-D* from Genevestigator did not concur with the GUS staining pattern. The gene expression profile by microarray showed exclusive gene expression in stamen and pollen (**Figure II.7.C**).

XI-Fpro:GUS displayed a unique expression pattern. *XI-Fpro:GUS* was expressed only in upper inflorescence stems and pedicels of flowers (**Figure II. 9. A-C**). *XI-Gpro:GUS* is also interesting due to its exclusive expression in the root cap (**Figure II. 9. D**). Expression levels of *XI-G* based on the Genevestigator profiles are extremely low in every tissues, but the highest expression is in roots (data not shown), suggesting that XI-G might have a function in the root tip.

MYA1 and *XI-K* were in the same group on the phylogenetic tree (**Figure II.4 and 5**). They both showed broad expression gene patterns with a slight difference. *MYA1pro:GUS* showed the strong expression in young leaves and shoot apical meristem and the expression became weak in the old leaves (**Figure II. 10. A-E**). Moderate gene expression was detected in

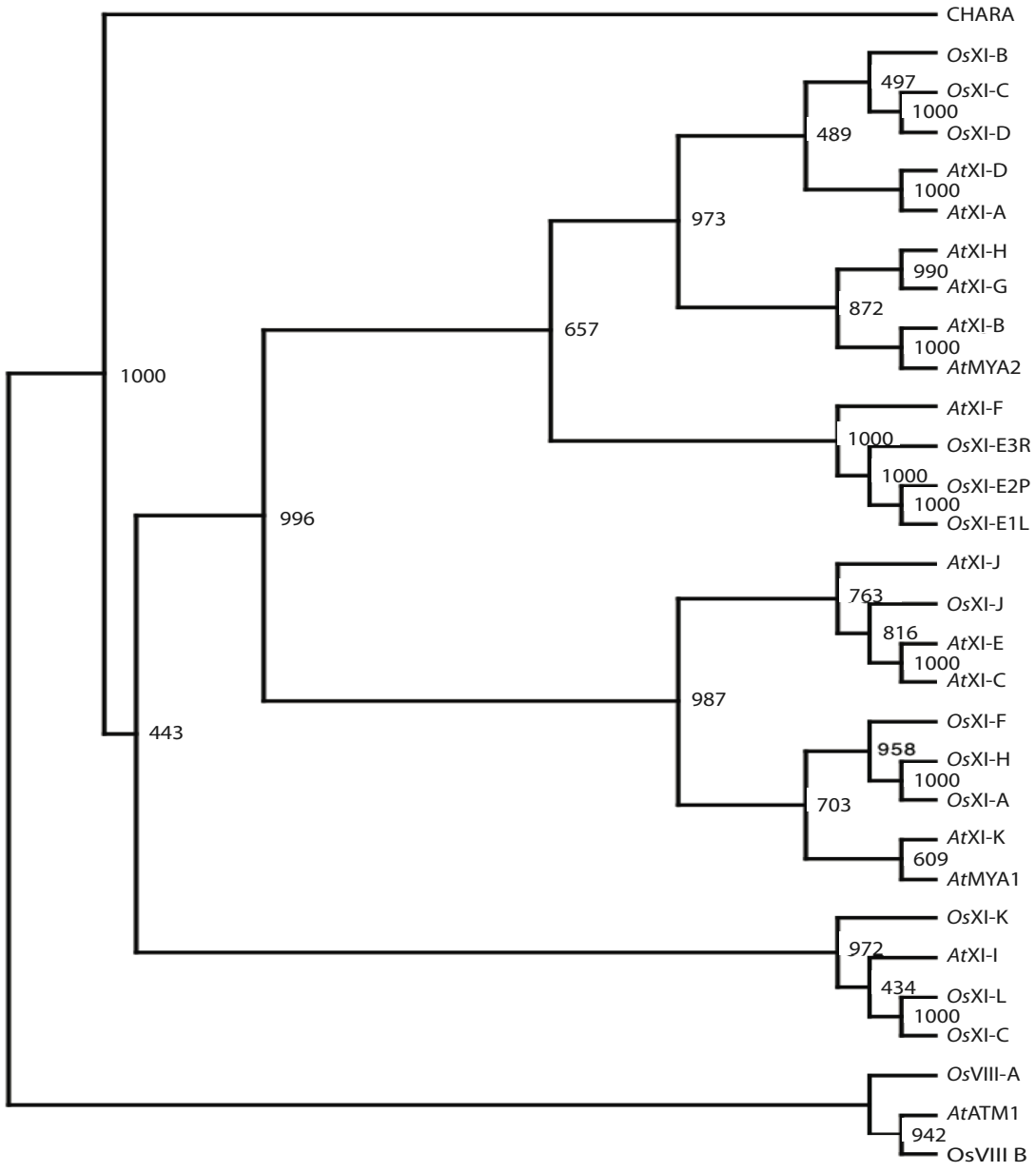

Figure II.5. Phylogenetic tree of myosins in *Arabidopsis* and rice based on motor domain sequences

Tree was resolved in the Maximum-likelihood methods with 1000 bootstraps and visualized with TreeView.

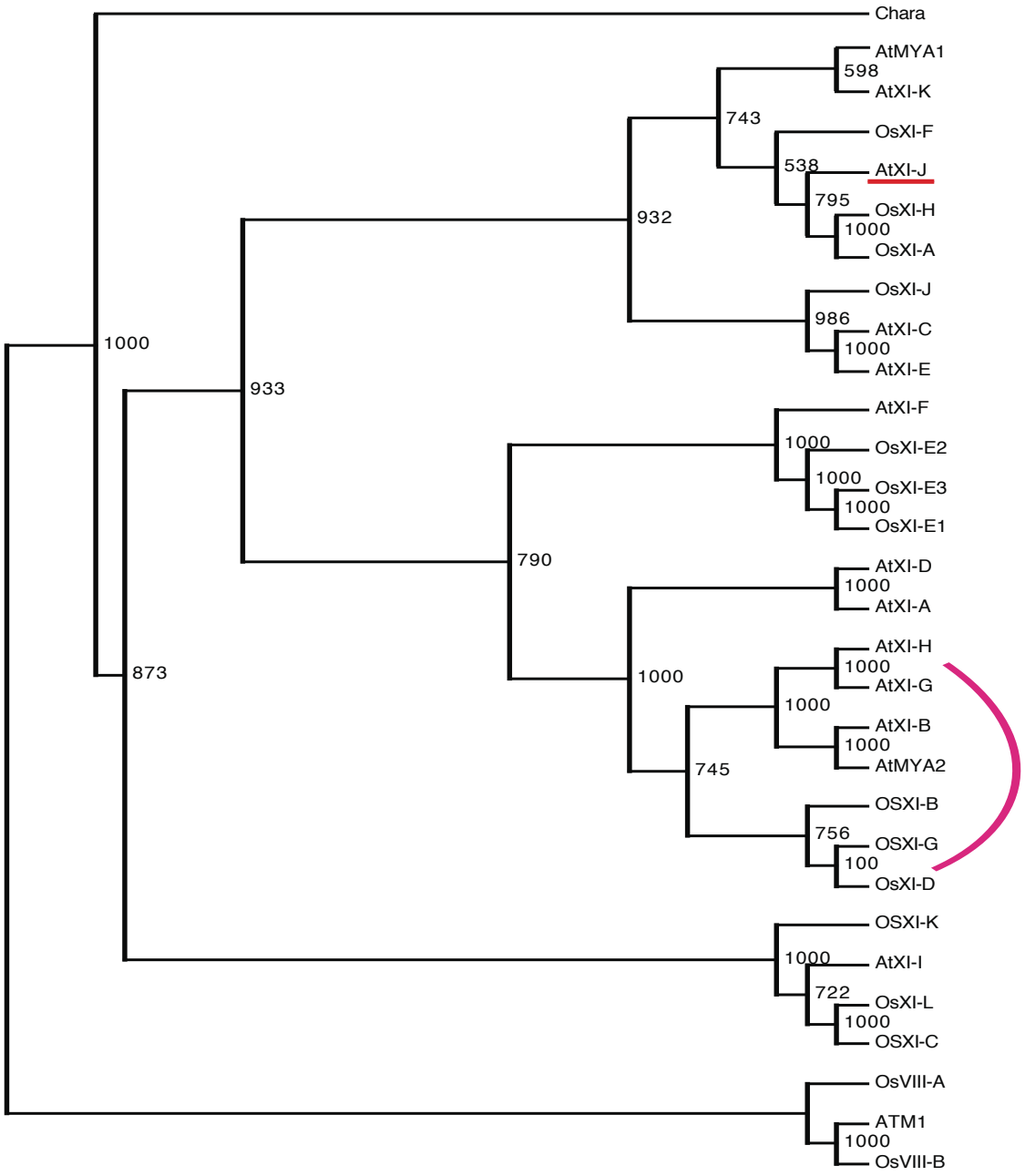

Figure II.6. Phylogenetic tree of myosins in *Arabidopsis* and rice based on full-length amino acid sequences

Differences with Figure II.5. are marked in red underline on *At*XI-J and magenta strip over the group.

Figure II.7. Myosin gene expression survey from microarray database

Gene expression profiles surveyed from Genevestigator were visualized individually with Gene Atlas too (Zimmermann et al., 2004). Among twelve gene profiles, three genes are shown.

A-B. XI-B and MYA2 have a high degree of sequence similarity but showed different expression patterns

C. Profile for XI-D. This gene is only case that appear to be different between its gene expression profile and its promoter-GUS analysis (compare with **Figure II. 11. G-L**)

A

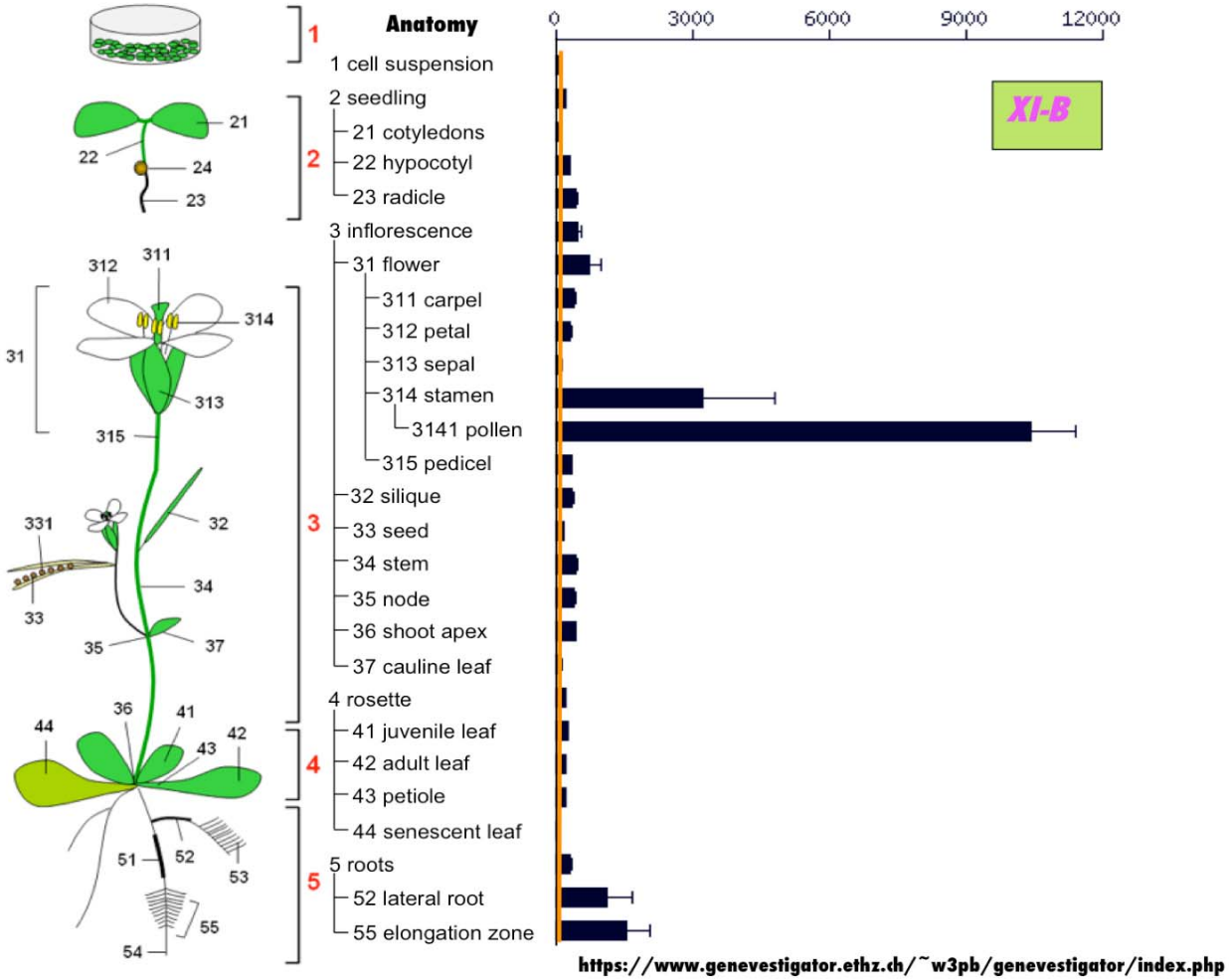
Anatomy
1 cell suspension
2 seedling
21 cotyledons
22 hypocotyl
23 radicle
3 inflorescence
31 flower
311 carpel
312 petal
313 sepal
314 stamen
3141 pollen
315 pedicel
32 silique
33 seed
34 stem
35 node
36 shoot apex
37 cauline leaf
4 rosette
41 juvenile leaf
42 adult leaf
43 petiole
44 senescent leaf
5 roots
52 lateral root
55 elongation zone
0
3000
6000
9000
12000
XI-B
https://www.genevestigator.ethz.ch/~w3pb/genevestigator/index.php

B

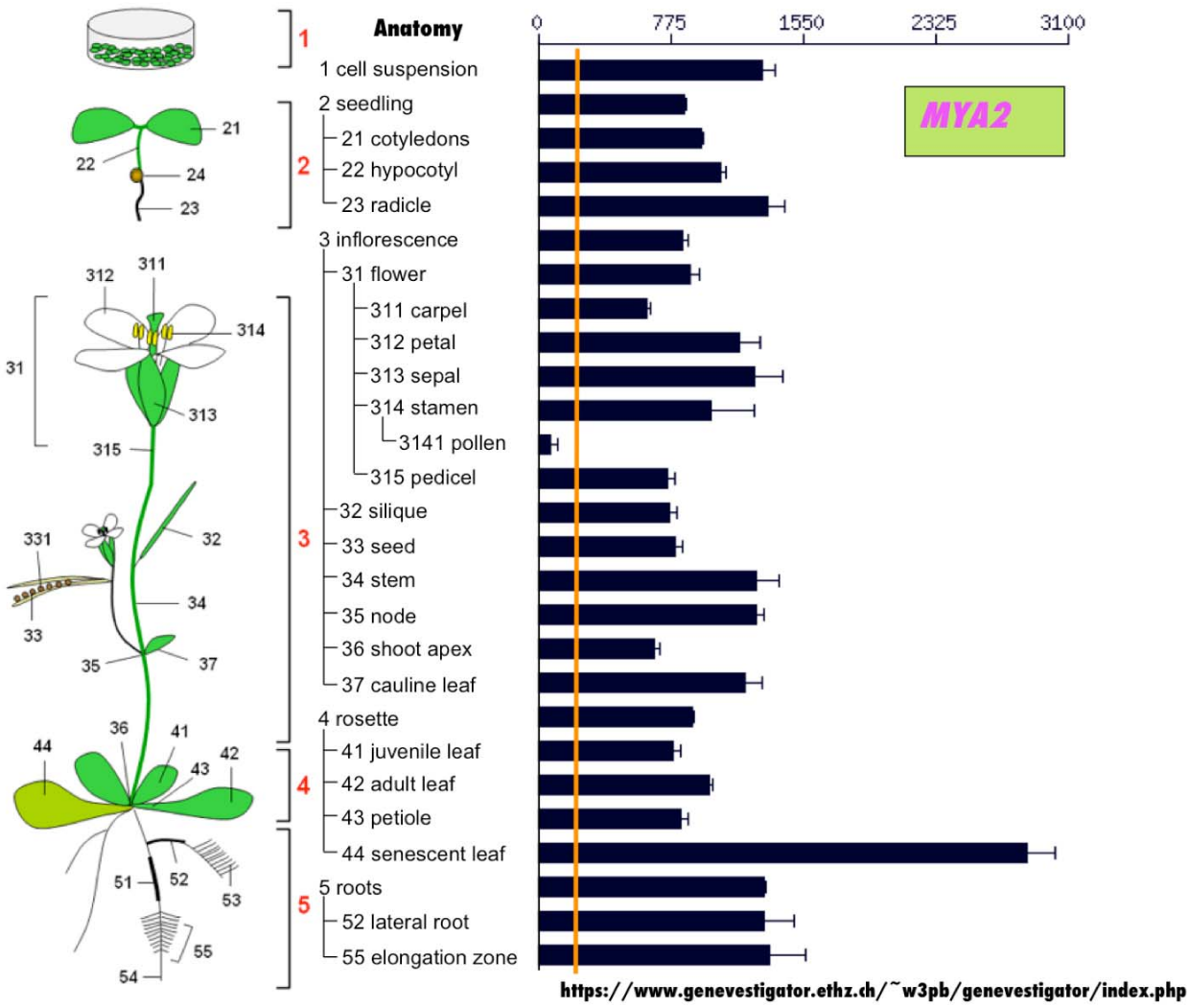

Figure II.7. Genevestigator results-continued

C

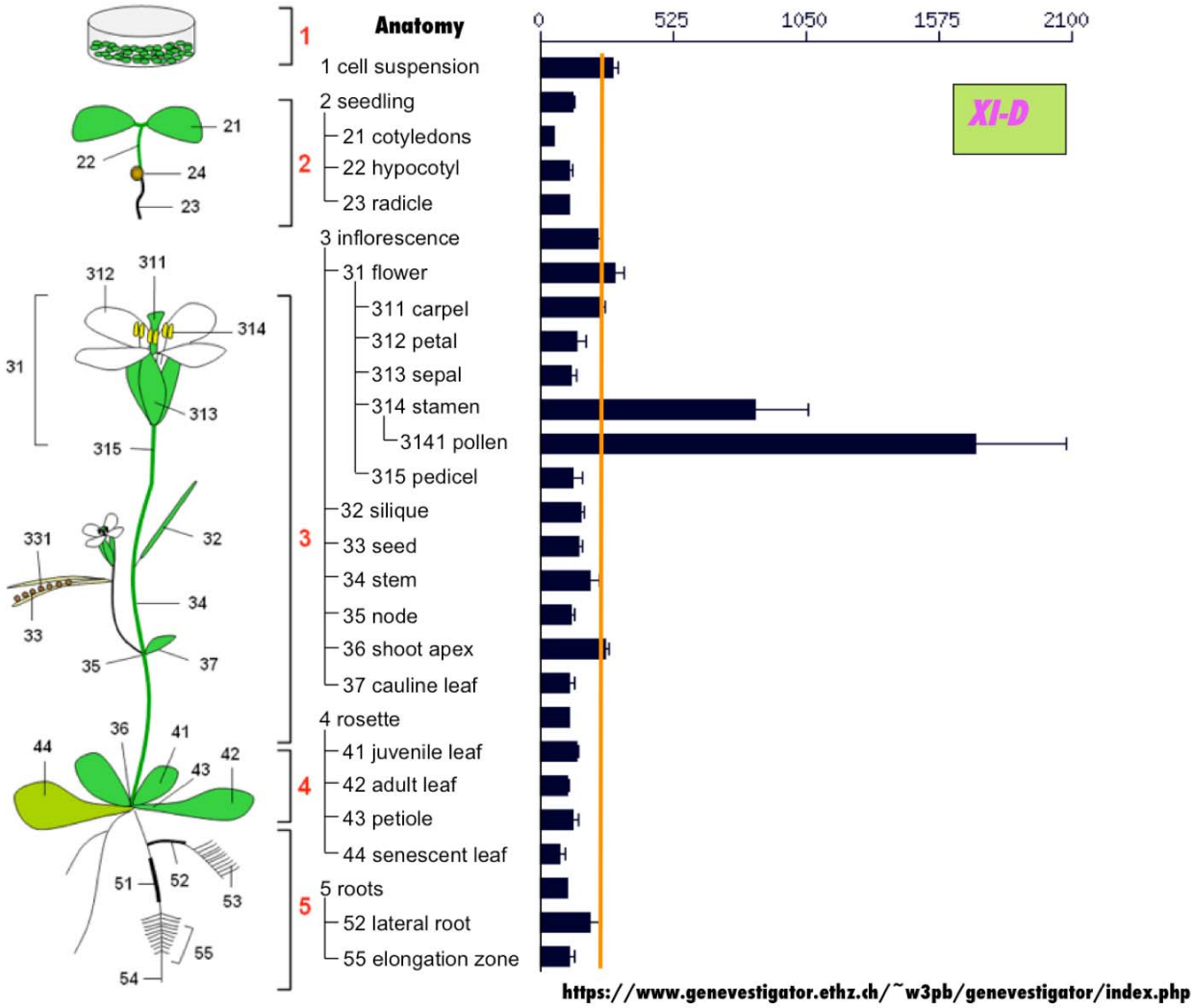

Figure II.7. Genevestigator results-continued

Figure II.8. Flower specific gene expression of five myosins

A-C. *XI-Cpro:GUS* plants showed GUS staining only at the flower, especially pollen. Pollen grain inside of anther showed very strong blue staining (yellow arrow in **C**).

D-F. *XI-Epro:GUS* plants showed GUS staining on young anther before dehiscence happen. Anther after dehiscence does not have staining (yellow arrow in **E**).

G-I. Unlike other genes which specifically expressed on stamen and pollen, *XI-Bpro:GUS* showed staining on other organ of flower (yellow arrows in **I**). Consist with microarray profile (**Figure II.6.A.**), Root showed moderate staining (white arrow in **H**). Unexpectedly, first true leaves on seedling also showed relatively strong staining (inset of **H**).

J-L. *XI-Apro:GUS* plants showed very strong staining on pollen and young anther (**K** and **L**).

M-O. Extremely strong staining on pollen and mature anther was observed in *XI-Jpro:GUS* plants.

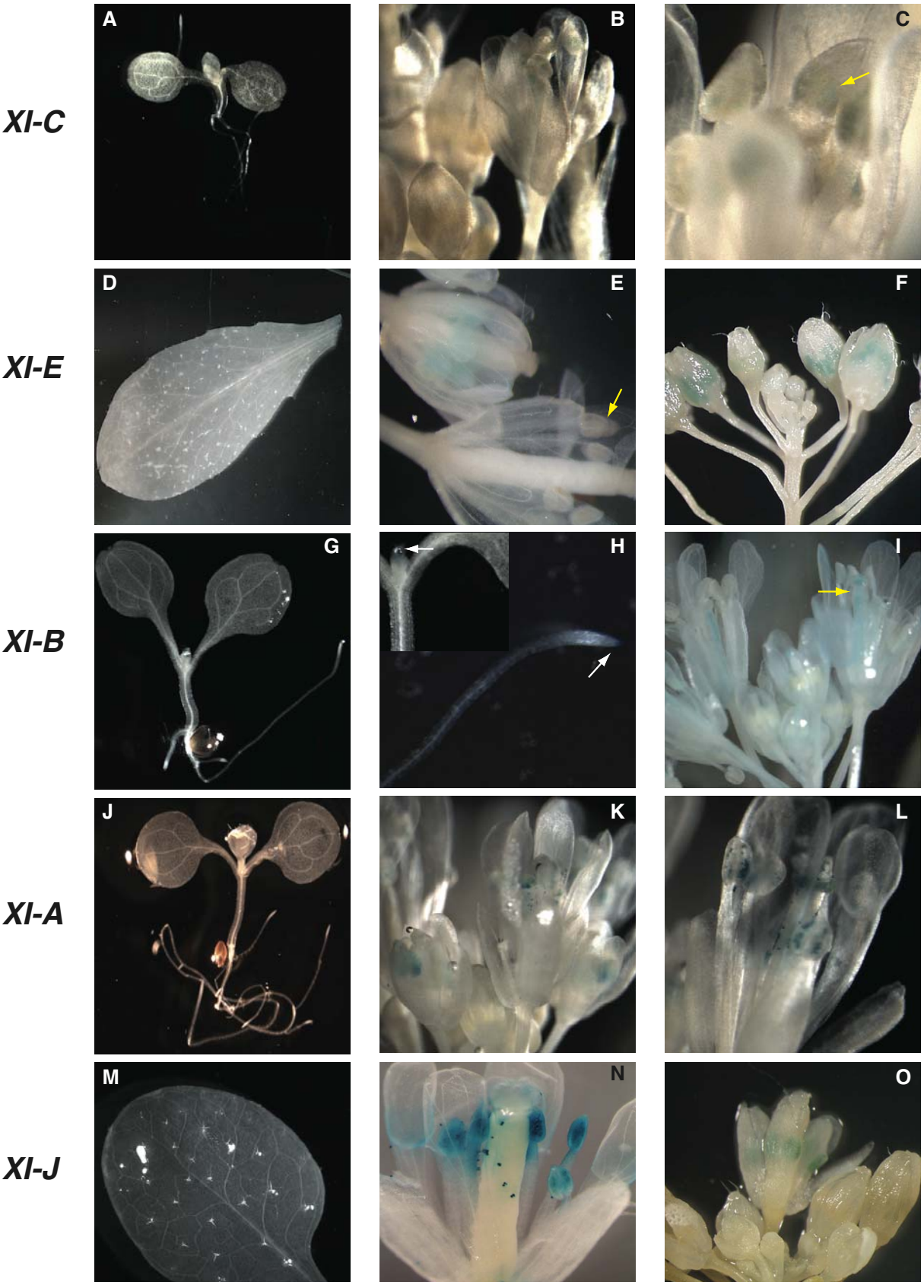
XI-C
XI-E
XI-B
XI-A
XI-J
A
B
C
D
E
F
G
H
I
J
K
L
M
N
O

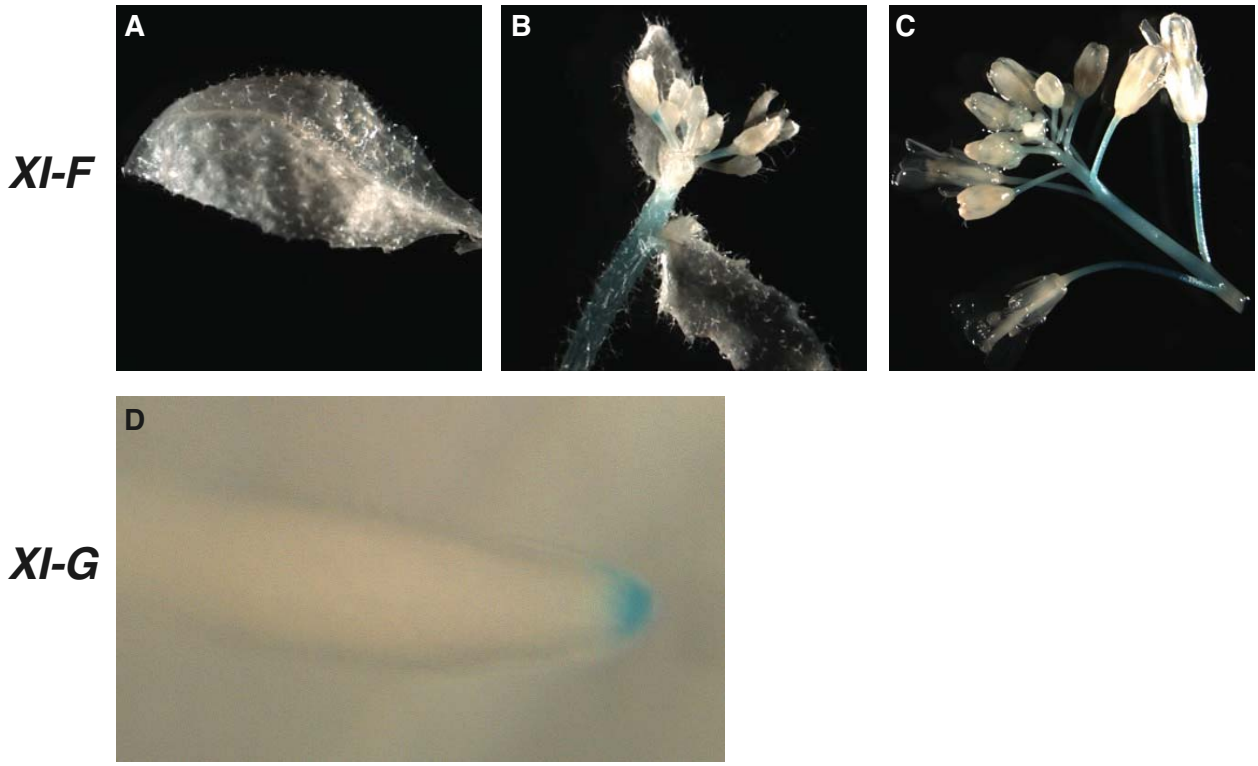

Figure II.9. *XI-F* and *XI-G* expression in specific vegetative tissues

A-C. *XI-Fpro:GUS* plants showed GUS staining in inflorescence stems and pedicles.

D. Only lateral root cap staining was visible in *XI-Gpro:GUS* seedlings.

Figure II.10. Broad expression of *MYA1* and *XI-K* in many tissues

A-I. *MYA1pro:GUS* plants showed GUS staining in various tissues at different developmental stages. Panel **A** showed strong staining in every tissue of a young plant. **B** to **D** are magnified images of a part of **A**. strong expression in trichomes and veins are shown on juvenile leaves (**B**). Interestingly, guard cells (yellow arrow in **C**) and shoot apical meristem (yellow dashed area in **D**) showed strong staining. Old leaves do not show strong expression as in young leaves (**E**). Expression in inflorescence stem (**F**), and flowers (**G** and **H**) are relatively moderate. Young flower (**G**) and old flower (**H**) showed slight different expression. Weak staining in seeds in young siliques are shown (**I**).

J-O. *XI-Kpro:GUS* plants showed GUS staining in various tissues relatively even. Strong staining in seedlings was observed (**J**). Note that root tip doesn't have *XI-Kpro:GUS* expression (white arrow in **K**). Old leaves showed moderate GUS expression in vein and surrounding tissues (**L**). Inflorescence stem (**M**) and flowers (**M**, **N**, and **O**) showed relatively strong expression but anther (white arrows in **N** and **O**).

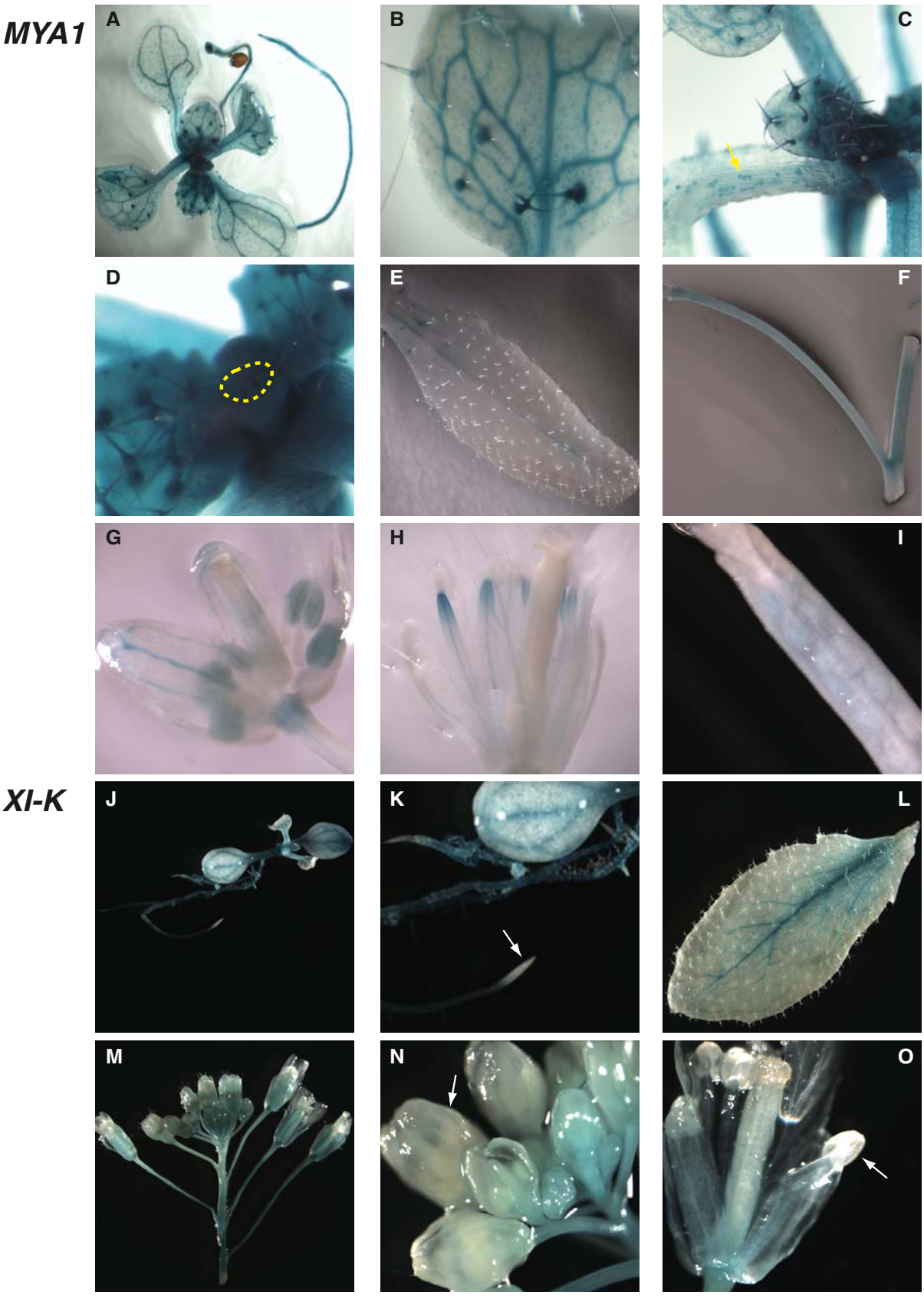
MYA1
A
B
C
D
E
F
G
H
I
XI-K
J
K
L
M
N
O

Figure II.11. *MYA2* and *XI-D* expressed in a various tissues

A-F. *MYA2pro:GUS* plants showed strong GUS staining in almost all tissues at various developmental stages. Strong GUS staining was observed in every tissues of seedling including root tip (**A**). This strong expression was maintained on tissues on later developmental stages, such as young leaves (**B**), inflorescence stems (**C**) and flowers (**D** and **E**). Even it was detectable in old siliques (**F**).

G-L. *XI-Dpro:GUS* plants showed broad expression in many tissues. Expression in seedlings is weak (**G** and **H**). Old leaves showed relatively moderate staining in entire tissues (**I**). Inflorescence stem also showed moderate staining (**J**). Young flowers showed stronger expression than old flowers (**L**). Stamens were lack of *XID* expression (Yellow arrow in **K**) while carpel showed GUS staining (white arrow in **L**).

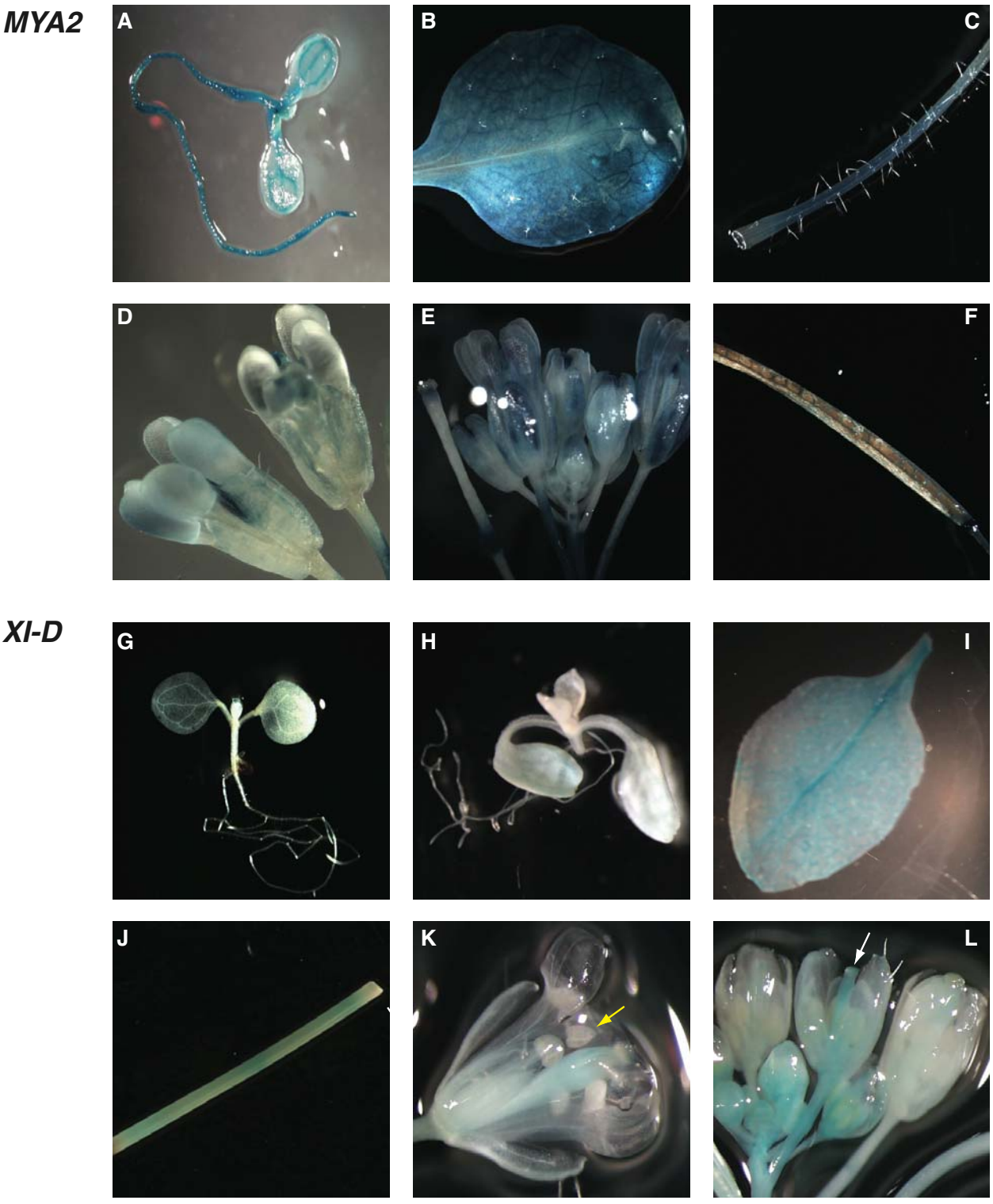
MYA2
A
B
C
D
E
F
XI-D
G
H
I
J
K
L

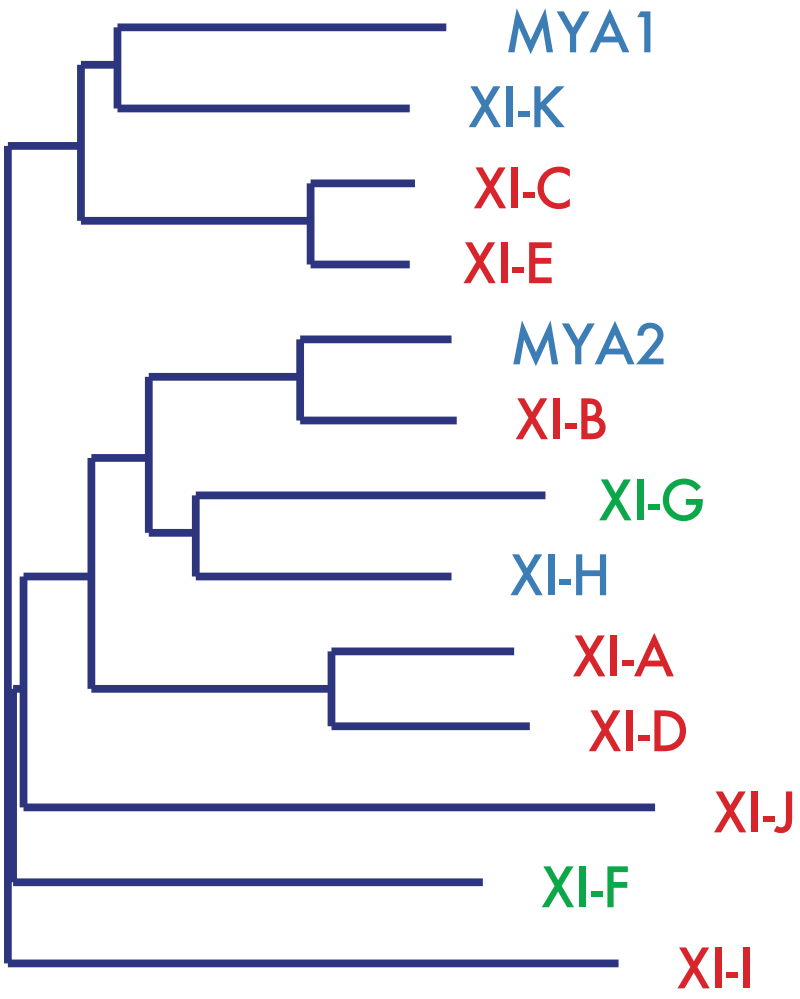

Figure II.12. Simplified cladogram of Arabidopsis Class XI Myosin

Blue colored isoforms express broadly across tissues in various developmental stages. Among isoforms expressed in specific tissues, the red color indicates flower, mainly stamen including pollen, specific expression, while green color-coded isoforms are expressing in vegetative tissues, lateral root cap and stems, respectively.

inflorescence stems and flowers and seeds (**Figure II.10.F-I**). *XI-Kpro:GUS* showed moderate expression evenly in every tissues throughout the development. Neither *MYA1pro:GUS* nor *XI-Kpro:GUS* showed expression in pollen, although both of them expressed in the filaments of stamen (**Figure II. 10. H and O**). A major difference between the gene expression of *MYA1pro:GUS* and *XI-Kpro:GUS* was the expression pattern at the root tip. Both genes are expressed in the entire root including root hairs. However, while *MYA1* expressed highly at the meristematic zone of root, *XI-Kpro:GUS* displayed the lack of staining on the meristematic zone of root tips (**Figure II. 10. A and K**).

II.4. DISCUSSION

Myosins are eukaryotic actin-dependent molecular motors that have various functions such as muscle contraction, vision, cell motility or vesicle trafficking. 35 groups of myosin have been identified, to date, from apicomplexan to human. Among them, plant myosins are grouped in 2 classes, class XI and VIII (Odronitz and Kollmar, 2007). Domain organizations are mostly identical within a class (N-terminal domain, motor domain, IQs or light chain binding domain, and various c-terminal structures). Class XI myosins are characterized by a SH3-like domain in N-terminus, 6 IQ motifs and a dilute domain at the C-terminus (Kinkema and Schiefelbein, 1994). However, *XI-J* and *OsMyoXI-L* deviate from this pattern and either lack the dilute domain or have a different N-terminal domain. These different domain structures could have arisen by evolution or could be an artifact from wrong prediction of gene. Myosins are large genes whose cDNA sequences are more than 3500bp long. Moreover, myosin genes contain more than 31

introns spread out over more than 8kb of genome fragment. Thus, there is ample opportunity for misannotation. For example, *OsMyoXI-L* in the original rice gene annotation lacked its motor domain and *OsMyoXI-K* was predicted to consist only of the dilute domain. These sequences could be corrected by careful analysis of the genome sequence, however, low sequence similarity of C-termini made this correlation diffused. Thus, to obtain a precise phylogenetic tree, isolation of full-length cDNAs is required. So far, only four genes in *Arabidopsis* (Kinkema and Schiefelbein, 1994; Kinkema et al., 1994; Ojangu et al., 2007) and three genes in rice (Jiang and Ramachandran, 2004) were identified with their full cDNA information.

Gene diversity of myosin in the species has been suggested to have arisen before the majority of plant species diverged (Richards and Cavalier-Smith, 2005). The tree in this study shows the presence of Arabidopsis and rice myosin genes in all major branches, suggesting that at least some classification of class XI isoforms already happened before the split between monocot and dicot. However, several gene duplication events took place after the monocot-dicot split, making it impossible to identify simple orthologous pairs. Other groups also reported a similar conclusion (Goodson and Dawson, 2006; Richards and Cavalier-Smith, 2005).

Highly similar isoforms could suggest functional redundancy within the myosin gene family and this could explain why knockout mutants do not show a strong phenotype (Hashimoto et al., 2005; Ojangu et al., 2007; Peremyslov et al., 2008). Thus, information of similarity of genes and overlapping expression patterns in this chapter will support the effort to select the candidate isoform for a further characterization of mutants.

CHAPTR III. Reverse genetic analysis of class XI myosin functions in Arabidopsis development

♦ *Peter Anthopolos, an undergraduate student who earned research credit in this lab from 2004 to 2005, isolated knockout mutants of two myosins, XI-B and XI-C, and another undergraduate student, Nilou Soltanian, has participated extensively in measurement of the root hair length from 2006 to 2008.*

III.1. INTRODUCTION

Myosins in non-plant organisms have been extensively characterized, however, less is known about their functions in plant cells. However, the possible functions of myosin in plants can be postulated indirectly based on the roles of actin since myosins are moving along actin filaments (Liu et al., 2001; Tominaga et al., 2000). The actin cytoskeleton is known to be involved in many processes such as signaling, cell division, organelle trafficking and morphogenesis in plants, suggesting that myosins may also function in a wide variety of processes. (Hepler et al., 2001; Liu et al., 2001).

A function of myosin in intracellular organelle trafficking has been suggested based on several pieces of evidence. First, treatment with a myosin inhibitor drug interferes with cytoplasmic organization and vesicle trafficking (Forer and Fabian, 2005; Šamaj et al., 2000; Tominaga et al., 2000). Immunolocalization studies using animal myosin antibodies in several plant species also showed that several different sized myosin isoforms are localized on the surface of organelles, the vegetative nuclei, generative cells in pollen grains and tubes and plasmodesmata in root tissues (Miller et al., 1995; Radford and White, 1998).

Class XI myosin was first identified as *MYA1* and *MYA2* in a PCR screening of *Arabidopsis* (Kinkema and Schiefelbein, 1994) and later has been found in several species (Odronitz and Kollmar, 2007). Immunolocalization studies using a class XI myosin specific-antibody raised against the head domain of a myosin protein in *Zea mays* showed that these myosins are associated with several organelles in the cells (Wang and Pesacreta, 2004). Recently, several studies showed colocalization of various myosin isoforms with several

organelles using fluorescent protein fused to C-terminus of myosins without motor domain (Li and Nebenführ, 2007; Reisen and Hanson, 2007; Sparkes et al., 2008). Mutant analyses with *xi-k* knockouts and RNAi assays of myosins in tobacco leaves showed the myosins function in organelle movements (Avisar et al., 2008b; Peremyslov et al., 2008). However, a relationship between myosin XI and specific organelles was not identified, leaving the precise function of myosin XI in organelle movement unclear.

Among the 13 myosins in Arabidopsis, ten of the genes form five pairs of closely related sister sequences (Odronitz and Kollmar, 2007). Spatial and temporal gene expression patterns overlapped highly (Discussed in Chapter II.). This relatively large number of isoforms may be related to a high degree of specialization among plant myosins or to a significant functional overlap and redundancy in plant development. Indeed, a mutation of *MYA2* in *Arabidopsis* showed no strong phenotype on plant growth (Hashimoto et al., 2005), suggesting that other(s) isoform of class XI myosin might have functional redundancy.

To address the question of isoform specificity versus functional overlap, in this study, several myosin mutants were isolated from T-DNA insertion lines of the 13 myosin XI genes. Most mutants did not show a significant phenotype, however, detailed observation of different cell types revealed defects in the development of trichomes and in root hair development in *xi-k* and more mutants. Additive root hair phenotype in double mutants of *mya1* and *xi-k* suggests their functional redundancy in root hair growth. Peroxisome movements in *mya1 xi-k* were slower than those in wild type.

III.2. MATERIALS AND METHODS

III.2.1. Mutant identification and confirmation

T-DNA insertion plants were carefully reviewed and selected from SIGnAL T-DNA express (Alonso et al., 2003). A total of 69 putative insertion lines for all 13 myosin genes were obtained from the ABRC (www.arabidopsis.org) and at least 4 plants for each line were grown to confirm the presence of a T-DNA insertion (**Table III.1.**). Seeds were surface sterilized with 75% EtOH with 0.1% TritonX-100 and washed with sterilized water four times. Seeds were then plated on ½X MS with 1% sucrose (pH 5.8) solidified with 0.21% phytagel. Five-day old seedlings were transplanted to soil and one fresh rosette leaf (about 1.5 cm long) was harvested later for PCR genotyping.

Genomic DNA was extracted with extraction buffer (200mM Tris-Cl, pH7.0, 250mM NaCl, 25mM EDTA, and 0.5% SDS) and precipitated with iso-propanol. The genomic DNA samples were then dissolved in 100 μl of ddH_2O and 1-2 μl of DNA was used for PCR. To confirm a T-DNA insertion, specific primers flanking the predicted T-DNA insertion site were designed with a web-based design tool (http://signal.salk.edu/tdnaprimers.2.html) (**Table III.2.**). Three sets of amplification (1) with two gene-specific primers (xx-LP+ xx-RP), (2) with one gene-specific primer (xx-LP) and T-DNA left border primer (T-LBa-1 for SALK lines or LB1-SAIL for SAIL lines), or (3) with the other gene-specific primer (xx-RP) and T-DNA primer were performed the following conditions: initial denaturation at 94°C for 2 min, followed by 30 cycles with 94°C (15 s), 62°C (15 s), 72°C (1 min), and a final extension for 5 min at 72°C (PCR

Table III.1. List of T-DNA insertion plants

Gene	Stock name	Line name	Position of insertion [a]	Comments
MYA1	SALK_022140	*mya1-1*	Exon	
	SALK_129098	*mya1-2*	Intron	
	SALK_129106	*mya1-3*	Exon	No T-DNA found
	SALK_134363	*mya1-4*	Intron	
	SALK_022140	*mya1-5*	Exon	
	SAIL_832_D02	*mya1-6*	Intron	
MYA2	SALK_084023	*mya2-1*	Promoter	
	SALK_037542	*mya2-2*	Intron	No T-DNA found
	SALK_127984	*mya2-3*	Intron	
	SALK_055785*	*mya2-4*	Exon	
XI-A	SALK_110436	*xi-a-1*	Exon	No T-DNA found
	SALK_086989	*xi-a-2*	Intron	
	SALK_086981	*xi-a-3*	Intron	No T-DNA found
	SALK_117717	*xi-a-4*	Exon	
	SALK_010100	*xi-a-5*	Exon	No T-DNA found
XI-B	SALK_021378	*xi-b-1*	Intron	No T-DNA found
	SALK_113062*	*xi-b-2*	Exon	
	SALK_016579	*xi-b-3*	Exon	
	SALK_054029	*xi-b-4*	Intron	No T-DNA found
	SALK_087951	*xi-b-5*	Intron	
XI-C	SALK_097302	*xi-c-1*	5' UTR	
	SALK_002170	*xi-c-2*	Intron	
	SALK_118329	*xi-c-3*	Exon	No T-DNA found
	SALK_118334	*xi-c-4*	Intron	No T-DNA found
	SALK_104026	*xi-c-5*	Exon	
XI-D	SALK_129738	*xi-d-1*	Promoter	
	SALK_082078*	*xi-d-2*	Exon	
	SALK_029987	*xi-d-3*	Intron	
	SALK_029988	*xi-d-4*	Exon	No germination
	SALK_094036	*xi-d-5*	Exon	No T-DNA found
XI-E	SALK_122989	*xi-e-1*	Exon	No T-DNA found
	SALK_119881	*xi-e-2*	Intron	
	SALK_025293	*xi-e-3*	Exon	
	SALK_044890	*xi-e-4*	Exon	
	SALK_044875	*xi-e-5*	Intron	

[a] Information of insertion site was obtained from SIGnAL database.

[*] Homozygous T-DNA insertions were identified by Peremyslov *et al*. 2008.

Table III.1. Continued

Gene	Stock name	Line name	Position of insertion [a]	Comments
XI-F	SALK_094787	*xi-f-1*	Intron	
	SALK_133869	*xi-f-2*	Exon	
	SALK_118541	*xi-f-3*	Exon	
	SALK_117832	*xi-f-4*	Exon	
	SAIL_568_H01	*xi-f-5*	Intron	
XI-G	SALK_051949	*xi-g-1*	Promoter	No T-DNA found
	SALK_091589	*xi-g -2*	Promoter	
	SALK_018032*	*xi-g -3*	Exon	
	SALK_009154	*xi-g -4*	Intron	
	SALK_109435	*xi-g -5*	Exon	No T-DNA found
	SAIL_97_E09	*xi-g -6*	Intron	
XI-H	SALK_020159	*xi-h-1*	Promoter	
	SALK_026839	*xi-h -2*	Promoter	No T-DNA found
	SALK_020788	*xi-h -3*	Promoter	No T-DNA found
	SALK_014709	*xi-h -4*	Exon	No T-DNA found
	SAIL_365_D03*	*xi-h-5*	Intron	
	SAIL_429_C07	*xi-h-6*	Exon	
XI-I	SALK_029565	*xi-i-1*	Promoter	
	SALK_025181	*xi-i-2*	5'UTR	
	SALK_092026	*xi-i-3*	Intron	
	SALK_069273	*xi-i-4*	Intron	
	SALK_100199	*xi-i-5*	Intron	No T-DNA found
	SAIL_186_D11	*xi-i-6*	Intron	
	SAIL_1271_E11	*xi-i-7*	Intron	
XI-J	SALK_026367	*xi-j-1*	5'UTR	
	SALK_048730	*xi-j-2*	Exon	No T-DNA found
	SALK_063159*	*xi-j-3*	Exon	No T-DNA found
	SALK_067361	*xi-j-4*	Intron	No T-DNA found
	SALK_066827	*xi-j-5*	Intron	No T-DNA found
XI-K	SALK_028822	*xi-k-1*	Promoter	
	SALK_059031	*xi-k-2*	Promoter	
	SALK_136682[§]	*xi-k-3*	Intron	No T-DNA found
	SALK_067972*[§]	*xi-k-4*	Exon	
	SALK_018764[§]	*xi-k-5*	Exon	

[a] Information of insertion site was obtained from SIGnAL database.

[*] Homozygous T-DNA insertions were identified by Peremyslov *et al*. 2008.

[§] Homozygous T-DNA insertions were analyzed in Ojangu et al. 2007.

Table III.2. Primers for the genotyping

Primer name	Sequences [a]	PCR product [b]	Comments
T-LBa1	TGGTTCACGTAGTGGGCCATCG		T-DNA specific for
T-LBb1	GCGTGGACCGCTTGCTGCAACT	500bp*	SALK lines
LB1-SAIL	CAGAAATGGATAAATAGCCTTGCTTCC		T-DNA specific for
LB3-SAIL	TGAATTTCATAACCAATCTCGATACAC		SAIL lines
1Ta-LP	AGATCATCTACAATCGTGTTGC	920bp	Used for *mya1-2, -3 and mya1-4*
1Ta-RP	ACATCTTGTCATCTTGAACCTAT		
1T5-LP	TCCACAAAGTGCTGGATTCCC	913bp	
1T5-RP	TGTGTACCGTATTTGTCGTCCCA		
1T6-LP	GCAGGTGCTTAGCATTCAGCAA	1187bp	
1T6-RP	ATGGCGGCAGTAACACCTTGA		
M1102-pro-F1	CGAGACGTCGGCGTTACGCGTTTGATCAG	1365bp	Used primers for *MYA2pro* for *mya2-1*
M1102-pro-R2	GCAACCGTAGCAACCTGTAGAGCAAAAGTG		
2T2-LP	ATATGGAGAATGGCTGCCACG	923bp	
2T2-RP	TGGTCGAATATTCATTTCGGCTG		
2T3-LP	GCTCCAGTTGATTTCCTCTTTCT	924bp	
2T3-RP	TTCCAGCTGCGATGAAAAAGC		
2T4-LP	TCGTTTTTCAGCAGAGTTTGTCA	943bp	
2T4-RP	TCAAAATTGCAGAAGTGTCGCA		
AT1-LP	TGCACCAGAACAGGTAAGCCC	916bp	
AT1-RP	TGTCAGTGAAAACAAAAGCATACCG		
AT2-LP	TGCAACAACATTTCAACCAGG	921bp	
AT2-RP	TCCGTGGTGCTCAAACTCTCC		
AT3-LP	TGACAAACGAGAAGCTGCAACA	920bp	
AT3-RP	TCTCCAGCAAAGATTGCAGTTG		
AT4-LP	CGTTCAACCTCTTCCCCGAAT	977bp	
AT4-RP	GGATCCTACGAACTGCATTCAAGA		
AT5-LP	CCAACAAAACCTCCACAGCCA	957bp	
AT5-RP	CGTTGACTGCCTGGAAAGTTGA		
BT1-LP	TTTGTCGGTGTATTGGAAGGC	920bp	
BT1-RP	GCAGAGGAACAACTGGCAAGC		
BT2-LP	TTCCAGTGGCCTAGATTGGCTT	857bp	
BT2-RP	TTTACATGAGAAGCTCGGCGG		
BT3-LP	AATTTGACCAATCGGGGAGGA	965bp	
BT3-RP	TCAACGAGCCTGCATAGACAGAA		
BT4-LP	TGGATGTCGTCGGGATCAGTT	890bp	
BT4-RP	CACTGCCTTGACGATGAAATGG		
BT5-LP	TGGATTCGAGAGTTTCAAGACAAA	929bp	
BT5-RP	AAAACACAAGCAAGGATTAGCAA		

[a] All primer sequences are in the 5' to 3' direction.

[b] This PCR product size assumes amplification of wild type alleles.

[*] This primer occasionally generated ~500bp false PCR product without a second primer.

Underlined nucleotides indicate restriction sites for gene cloning in different experiments.

Table III.2. CONTINUED

Primer name	Sequences [a]	PCR product [b]	Comments
CT1-LP	CTCTGGTGCTGCGCAGAGTTA	931bp	
CT1-RP	GCAAACAAGTGTGGCACATGAA		
CT2-LP	TTCATGTGCCACACTTGTTTGC	905bp	
CT2-RP	TGTAACAGCACGACCTCCCAA		
CT3-LP	ATCCCGTCCTTGAAGCCTTTG	848bp	
CT3-RP	TGCCTTTAAATCACACCTGAAACG		
CT4-LP	AAGCCTTTGGGAACGCAAAAA	931bp	
CT4-RP	CCGTCTCTGCTGGTTACAGCACT		
CT5-LP	CTGCGATTAATGGCTGGAACG	927bp	
CT5-RP	GGCAGCCTTTGTTTGCTTCCT		
DT1-LP	CCCAATCAGCTGGTGTTTCCA	901bp	
DT1-RP	CCACCACCACCATCATCTTCA		
DT2-LP	CCCTGGTTCATGCAAATACGC	908bp	
DT2-RP	ATATTCCGAGGGAAAACGCGA		
DT3-LP	CCGACGAGCAATCGCATAGAA	911bp	
DT3-RP	TTTTCCGGTGATTCTCACCATGT		
DT4-LP	TCGCTGCTTTTCTCTTTCGTCC	898bp	
DT4-RP	GGGGTCATGGAAGCCATTAGG		
DT5-LP	TGTCCGTGCCTGCTTCTGAAT	902bp	
DT5-RP	TGCATCAACTTAGGTGTGGGG		
ET1-LP	TGCAAGCAGAAGTTACAGGCG	947bp	
ET1-RP	AAAATTGCAGGGAACTCCGGT		
ET2-LP	TGTTATTCCTGACAGTTTTGGCG	887bp	
ET2-RP	AGGTTCAAGCCACAAACGGAA		
ET3-LP	TTCAAAACTGCAGGAGATCGCT	929bp	
ET3-RP	TGATTGTCATTGAAAACTCTTGGCA		
ET4-LP	CCTTGGCGCAGTAGACATTCC	955bp	
ET4-RP	CAGATTTCTGATCCAGAGCGCA		
ET5-LP	TGTGAAACTCAGGGGAAATGGTT	960bp	
ET5-RP	GGGTCATCCCAAGACGTTTCA		
FT1-LP	GAACAACACTCTCGGCGAAGC	946bp	
FT1-RP	TTGGTCCAGAAGGGCCAAGAT		
FT2-LP	GAACAACACTCTCGGCGAAGC	958bp	Used for genotyping of *xi-f-3 and xi-f-4*
FT2-RP	TTGGTCCAGAAGGGCCAAGAT		
FT5-LP	CCACAGATTTTTCGTTATCAAACC	976bp	
FT5-RP	AGTTTGAAGTGAAATGTTTTGCAC		
GT2-LP	TGCCTCCTCTGGATCTTGCAC	963bp	
GT2-RP	CGTCTTTGTTAAATTTGGATTTTCC		

[a] All primer sequences are in the 5' to 3' direction.

[b] This PCR product size assumes amplification of wild type alleles.

[*] This primer occasionally generated ~500bp false PCR product without a second primer.

Table III.2. CONTINUED

Primer name	Sequences [a]	PCR product [b]	Comments
GT3-LP	CACTGCCAAATTTCAATGCAG	956bp	
GT3-RP	AGCCGCTTTGGGAGAATTGAG		
GT4-LP	TCAAATACCAAGCTCGTCTGGC	913bp	
GT4-RP	TTGCCACTATGCTGGTGATGTG		
GT5-LP	CAAACCATAAATGGGTGGAGACAA	969bp	
GT5-RP	TTGCGTCTGCAACAGCTCATC		
GT6-LP	TTACAAAGAGAATCTTCCAGTGCC	1185bp	
GT6-RP	TCAAGGTGAATGTAACACACACAC		
HT1-LP	GCACCCCCTCGAAGTAAAAGA	967bp	
HT1-RP	ACCACCGGAGGAGGCTTATCA		
HT2-LP	GGTTTGTTCTTTGCAGTTAGTTGCT	907bp	
HT2-RP	ACCACCGGAGGAGGCTTATCA		
HT3-LP	GGTTTGTTCTTTGCAGTTAGTTGCT	907bp	
HT3-RP	ACCACCGGAGGAGGCTTATCA		
HT4-LP	TCGGAGAAATCGGATGGTGAG	976bp	
HT4-RP	TGCGGTAGTCTTCTAAAAGGGTTT		
HT5-LP	TCTAAATCTTTTGATCGGGGATC	1117bp	
HT5-RP	CACCACTTACCAGAATTGATTGAC		
HT6-LP	CGACGAGAATGTTGTACATTTAGC	1001bp	
HT6-RP	TGTGTTCTTGAAGGGACAGTACAC		
IT1-LP	TGAGGTTGCGCCAGAGAATTT	894bp	
IT1-RP	TGTACGTGGTTGATGATATTGTTGC		
IT2-LP	TCGTCAGGATCCCTCCGAAAT	858bp	
IT2-RP	ATTGCCTTCTACATTTTTGACTTAC		
IT3-LP	TGCTTCATTAGCAACCTGCAAGA	927bp	
IT3-RP	CTTCATCTCTGCACGGGCTTC		
IT4-LP	TCAACCCAATCAAACCTCCCA	993bp	
IT4-RP	CCAGCTCTGCTTCATATGACTTG		
IT5-LP	TGCTGCACACAACAACAACCA	902bp	
IT5-RP	GCAGGAACATCTTGGCACGAG		
IT6-LP	TATTACCTCGTTGAAATGTTGCTG	1060bp	
IT6-RP	ATGTTCTTATTTTGCTTAGGACGC		
IT7-LP	ATGAAGGATGCACATCAATCTCTTG	1261bp	
IT7-RP	ATGATGCTACATTGAAAGCAGAG		
JT1-LP	CTTCAGAAGCGGGAGGACCAT	962bp	
JT1-RP	TGAAATGGCATTAGACACAAAAGCA		
JT2-LP	TTGGGGATATACCCCTGCCTG	861bp	
JT2-RP	TGAATCAGCATCTTCTCCCTTCG		

[a] All primer sequences are in the 5' to 3' direction.

[b] This PCR product size assumes amplification of wild type alleles.

[*] This primer occasionally generated ~500bp false PCR product without a second primer.

Table III.2. CONTINUED

Primer name	Sequences [a]	PCR product [b]	Comments
JT3-LP	TCAACTTGCAGGCGTATTGGC	895bp	
JT3-RP	CATCTCAACTTCTGCAGTGAGGGA		
JT4-LP	TCCCTCACTGCAGAAGTTGAGATG	882bp	Used for genotyping of *xi-j-5*
JT4-RP	TCGAAGCCCCCTTCCTTATCA		
M11K-pro-F1	ACGTCCGGACAGATGCCAATTGAAGACGATG	2093bp	Used primers for *XI-K pro* for *xik-1* and *xik-2*
M11K-pro-R1	GCAAGATCTGACTGGGCCAACCTACAAAAG		
KT3-LP	TCTGCAATGGCAAACACATGG	977bp	
KT3-RP	TATTGTCCTGGTTTTGCGGGA		
KT4-LP	GGAAAGTGGTGCTGGTAAGAC	921bp	
KT4-RP	TCATGTGATTTAAAGCAGAACGCC		
KT5-LP	CCATATATCTTCTCGAGGAATGCA	857bp	
KT5-RP	CGGGAACCAGAGTCTGAGGAGA		

[a] All primer sequences are in the 5' to 3' direction.

[b] This PCR product size assumes amplification of wild type alleles.

[*] This primer occasionally generated ~500bp false PCR product without a second primer.

Underlined nucleotides indicate restriction sites for gene cloning in different experiments.

condition named A62E60D). PCR products were separated by electrophoresis in a 1% (w/v) agarose gel and stained with ethidium bromide to visualize under ultraviolet light.

Once plants were confirmed as homozygous lines, they were backcrossed with wild type plants to eliminate potential secondary T-DNA insertions in other positions of the genome.

To confirm whether homozygous insertion lines are target-gene knockout mutants, RT-PCR was performed with gene-specific primers. First, cDNAs were generated by using Superscript III (Invitrogen) with total RNA extracted from either seedlings or flowers with Trizol (Sigma) and then amplified by PCR with gene-specific primers (**Table III.3.**).

III.2.2. Phenotypic analysis

Confirmed homozygous lines were observed under various conditions and at different developmental stages to find a difference from the wild type as listed below.

a. Whole plant growth

Seedlings were first observed carefully to check if they have any growth defects, and then moved to soil to examine their development. Five features were observed; time for germination, size of leaves, height of plant at maturity, flowering time, and inflorescence stem branching pattern.

b. Trichome development

Trichomes on adult leaves and inflorescence were observed under a stereomicroscope (Olympus SZX12) and photographed with a digital camera DP10 operated by Olympus camera software ver. 3.1.

c. Leaf venation

Table III.3. Gene specific primers for RT-PCR

Target gene	Primer name	Sequences [a]	PCR condition[b]	PCR product
MYA1	M11.1-D-F1 SIL-MYA1-R1	CGAGGATCCGCTCCAAAACCGATG ATTGCT GCATCTAGAATCAACGCATGGACA CAACA	A60E90D	718bp
MYA2	M11.2-D-F1 M11.2.STOP-R1	ACGTCCGGACCCAGATCTTCTAAA GGAGG GCAGCGGCCGCAACAATCACAGA GGAAGAGAGC	A61E90D	739bp
XI-J	JT4-LP JT4-RP	TCCCTCACTGCAGAAGTTGAGATG TCGAAGCCCCCTTCCTTATCA	A62E90D	467bp
XI-K	11.K-D-F3 11.K-STOP-R1	ACGTCCGGACCAAGGACATCAAG GGCAAG GCAGCGGCCGCCGAGGGCAGTTAC GATGATGTAC	A61E90D	729bp

[a] All primer sequences are in the 5' to 3' direction.

b PCR condition named as the way described in section III.2.1.

Underlines indicate restriction site for gene cloning in different experiments

One cotyledon or first true leaf was detached and immersed in fixative (ethanol:acetic acid [3:1]) to clear of chlorophyll and then incubated in 100% ethanol at 4°C overnight (Carland et al., 2002). Samples mounted in 50% glycerol were observed and photographed with the stereomicroscope described above.

d. Hypocotyl growth

Hypocotyl lengths of dark-grown seedlings were measured. Plates wrapped with aluminum foil were stratified in 4°C for one day and placed at room temperature for about 30 minutes before transfer to a dark room to minimize precipitation from sudden temperature changes. Five-day old seedlings grown in the dark were then photographed under a stereomicroscope (see above) and the hypocotyl lengths were measured with ImageJ (NIH, http://rsbweb.nih.gov/ij/).

e. Root hair growth

Sterilized seeds were grown on the surface of 1/4X MS medium containing 1% sucrose in pH 5.7 solidified with 0.5% phytagel. After one-day stratification, plates were transferred in a vertical orientation into a growth chamber with continuous light at 22°C. Images of 5-day-old seedlings were captured on a Leica stereomicroscope (Leica MZ16 FA, http://www.leica-microsystems.com) equipped with a digital camera (Leica DFC420) under 7.1 X magnification or 23X magnification. Lengths of 10 root hairs per plant were counted from more than 15 plants in each genotype and the number of root hairs was counted from more than 15 plants in each genotype with ImageJ. Prism 5 was used for statistical analysis (www.graphpad.com).

f. Root gravitropism

Vertically oriented square plates (medium as above) containing 3 day old etiolated

seedlings were rotated 90° to the right to initiate a root gravitropic response. After 3 more days of growth in dark, seedlings were photographed under the stereomicroscope described above and their bending angles were measured with a protractor.

III.2.3. Double mutant analysis

Several crosses were initiated to obtain double mutants and seeds were harvested from individual siliques from successful crosses. F1 seeds were grown on MS media and seedlings were transplanted to soil to harvest self-fertilized seeds. About 100 F2 seedlings were grown to maturity and their genotype identified by PCR with the primer pairs used for verification of T-DNA insertion.

III.2.4. Organelle movement analysis

Motility of organelles was tested using either single organelle markers generated in this lab (Nelson et al., 2007) or a triple organelle marker which contains peroxisome-CFP, Mitochondria-YFP and Golgi-mCherry within a single binary vector. Single organelle markers, peroxisome-CFP, Mitochondria-YFP, Golgi-YFP, and Golgi-mCherry, were transformed with *Agrobacterium tumefaciens* into wild type and mutants (Weigel and Glazebrook, 2002). Two types of triple organelle markers were constructed by combining either Golgi-Tomato or Golgi-mCherry with Mitochondria-YFP and Peroxisome-CFP under individual 35S promoters in a binary vector, pFGC19. Several stable T1 plants per genotype were isolated and movements of organelles were observed in the T2 generation.

For the tracking of organelle movement in plants, time-lapse image sequences were captured with an Axiovert 200 M microscope (Zeiss, http://www.zeiss.com) equipped with filters for YFP, CFP fluorescence, and Texas red (filter set: 52017, YFP/CFP; 62002, Texas red, Chroma, http://www.chroma.com). Growing root hair cells were observed with a 63X (1.4 NA) plan-apo oil immersion objective and image sequences were captured in 1 (or 2) sec interval with a digital camera (Orca ER; Hamamatsu Photonics, http://www.hamamatsu.com) controlled by Openlab software (Improvision, http://www.improvision.com) for 60 to 120 sec. After background subtraction to remove camera noise, contrast of images was enhanced to increase signal intensity. Organelles in the root hairs were manually tracked with Openlab software. Data were analyzed and visualized with Prism 5.

III.3. RESULTS

III.3.1. Confirmation of T-DNA insertions

To investigate myosin function in plant development, 4-7 T-DNA insertion lines for each gene were obtained from the Arabidopsis stock center (**Table III.1.**) (Alonso et al., 2003). Insertion of T-DNA was confirmed by amplification with primers specifically designed for verifying T-DNA insertion in a target gene (**Table III.2.**). In summary, 64 of the 69 myosin T-DNA insertion lines were tested. The exceptions are 5 lines, which were ordered recently for additionally screening (*xi-f-5*, *xi-g-6*, *xi-i-6*, and *xi-i-7*) and one line (*xi-d-4*) that did not germinate. For several lines, T-DNA insertion in the genome could not be detected, thus only 39 lines were confirmed to have a T-DNA insertion (see **Figure III.2.** for examples, **Table III.4.** for detail, and **Table III.5.** for

Table III.4. Results of T-DNA identification

Gene	Line name	Genotype	T-DNA insertion[a]	Knock-outs[b] (by RT-PCR)
MYA1	*mya1-1*	homozygous	T	N
	mya1-2	homozygous	T	N
	mya1-3	-	-	-
	mya1-4	homozygous	T	N
	mya1-5	homozygous	T	KO
	mya1-6	homozygous	S	N
MYA2	*mya2-1*	hemizygous	nd	N
	mya2-2	-	-	-
	mya2-3	homozygous	S	KO
	mya2-4	homozygous	T	KO
XI-A	*xi-a-1*	-	-	-
	xi-a-2	homozygous	T	nt
	xi-a-3	-	-	-
	xi-a-4	homozygous	S	nt
	xi-a-5	-	-	-
XI-B	*xi-b-1*	-	-	-
	xi-b-2	homozygous	nd	KO
	xi-b-3	homozygous	nd	KO
	xi-b-4	-	-	-
	xi-b-5	homozygous	nd	N
XI-C	*xi-c-1*	homozygous	nd	KO
	xi-c-2	homozygous	nd	N
	xi-c-3	-	-	-
	xi-c-4	-	-	-
	xi-c-5	homozygous	nd	KO
XI-D	*xi-d-1*	homozygous	S	nt
	xi-d-2	homozygous	T	nt
	xi-d-3	homozygous	T	nt
	xi-d-4	no germination	-	-
	xi-d-5	-	-	-
XI-E	*xi-e-1*	-	-	-
	xi-e-2	homozygous	nd	nt
	xi-e-3	homozygous	nd	nt
	xi-e-4	homozygous	nd	nt
	xi-e-5	-	-	-

[a] nd: number if insertion was not determined; S: single insertion was confirmed.; T: tandem repeat T-DNA insertion was confirmed;

[b] N: RT-PCR with a product; KO: RT-PCR without a PCR product; nt: not tested

Table III.4. Continued

Gene	Line name	Genotype	T-DNA insertion[a]	Knock-outs[b] (by RT-PCR)
XI-F	*xi-f-1*	-	-	-
	xi-f-2	-	-	-
	xi-f-3	homozygous	nd	nt
	xi-f-4	hemizygous	nd	nt
	xi-f-5	nt	-	-
XI-G	*xi-g-1*	-	-	nt
	xi-g -2	homozygous	T	-
	xi-g -3	homozygous	T	nt
	xi-g -4	homozygous	S	nt
	xi-g -5	-	-	-
	xi-g -6	nt	-	-
XI-H	*xi-h-1*	homozygous	S	nt
	xi-h -2	-	-	-
	xi-h -3	-	-	-
	xi-h -4	-	-	-
	xi-h-5	homozygous	nd	nt
	xi-h-6	homozygous	nd	nt
XI-I	*xi-i-1*	homozygous	T	nt
	xi-i-2	homozygous	T	nt
	xi-i-3	homozygous	T	nt
	xi-i-4	homozygous	S	nt
	xi-i-5	-	-	-
	xi-i-6	nt	-	-
	xi-i-7	nt	-	-
XI-J	*xi-j-1*	homozygous	T	N
	xi-j-2	-	-	-
	xi-j-3	-	-	-
	xi-j-4	-	-	-
	xi-j-5	-	-	-
XI-K	*xi-k-1*	homozygous	S	N
	xi-k-2	homozygous	S	N
	xi-k-3	-	-	-
	xi-k-4	homozygous	S	N
	xi-k-5	homozygous	S	KO

[a] nd: number if insertion was not determined; S: single insertion was confirmed.; T: tandem repeat T-DNA insertion was confirmed;

[b] N: RT-PCR with a product; KO: RT-PCR without a PCR product; nt: not tested

Table III.5. Summary of mutant identification

Gene	Insertion tested line	Insertion confirmed	Homozygotes	Inverted repeat insertion	Knock-outs (by RT-PCR)
MYA1	6	5	5	4	1
MYA2	4	3	2	1	2
XI-A	5	3	3	1	nt
*XI-B**	5	3	3	nt	2
*XI-C**	5	3	2	nt	2
XI-D	4	2	2	2	nt
XI-E	5	3	3	nt	nt
XI-F	4	2	2	0	nt
XI-G	5	3	3	2	nt
XI-H	6	5	3	0	nt
XI-I	5	4	4	3	nt
XI-J	5	1	1	1	0
XI-K	5	4	4	0	2

nt Not tested.

* Isolation of homozygous mutants and confirmation of knockout was completed by Peter Anthopolos.

summary). Before observing the phenotype of homozygous mutants, they were backcrossed with wild type to eliminate potential additional T-DNA insertions beside the target myosin gene. It is possible that there is more than one T-DNA insertion in the plants, for example, *xi-j-4* failed to amplify T-DNA PCR products but plants were kanamycin resistant suggesting there is no T-DNA insertion in *XI-J* but in an unexpected region of genome. Most of the homozygous plants were backcrossed to wild type and homozygotes were reisolated, except lines of *xi-a*, lines of *xi-e*, and two lines of *xi-h* (*xi-h-5* and *xi-h-6*) due to the late isolation of homozygous plants. During this step, *mya2-1* and *xi-f-4* could not be isolated as homozygous plants. Thus overall, 37 homozygous plants for 13 myosin genes were isolated with several insertion lines per gene (**Table III.5.**).

While plants were backcrossed to remove potential second-site insertions, several homozygous plants were identified that had tandem T-DNA insertion in a myosin gene. With a single insertion, we would expect a PCR product either with the LBa/b-1plus LP or with the LAa/b-1 plus RP combination, but not with both (**Figure III.1.**). However, some homozygous lines generated two PCR products in different sizes with three primers (LP+RP+LBa-1). These results were different from the information provide from the SIGnAL. Thus, instead of PCR with three primers, PCR with a pair of primers, LBa/b-1+ LP and LBa/b-1+RP, were performed and PCR products were sequenced to verify their precise insertion region (**Figure III.2.** as examples). Four lines including *mya1-5* amplified PCR product with both combinations and sequencing of the PCR product revealed their exact insertion site of genome (**Figure III.3.A**). Other lines for all myosins were examined in same way and the results summarized in **Table III.4**.

Homozygous plants were then checked for their gene expression by RT-PCR. T-DNA

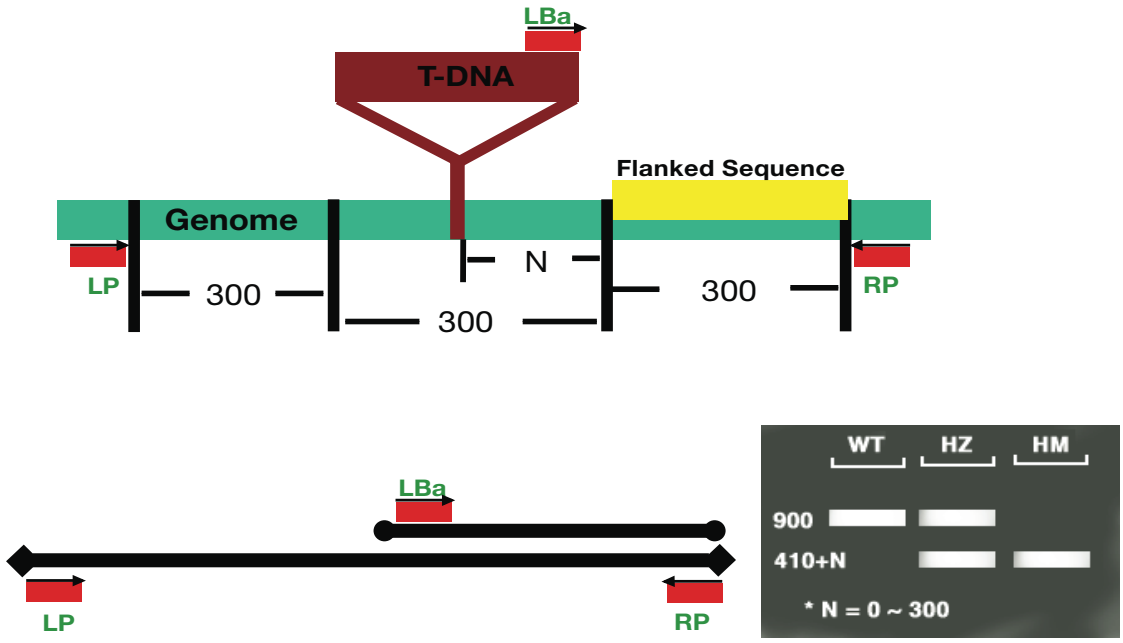

http://signal.salk.edu/tdnaprimers.html

Figure III.1. Diagram of the experiments to verify T-DNA insertion

Genomic primers (LP and RP) can amplify a 900bp product for wild type alleles, but not after insertion of T-DNA. In contrast, LBa/b and RP (or LBa/b and LP in case of reverse orientation of T-DNA) will amplify a product of about 410 to 710bp for mutant alleles. The gel diagram illustrates the banding pattern expected from wild type (Shane et al.), hemizygous (HZ), and homozygous (HM) mutant plants when all three primers are included in the PCR reaction. Note that a recent update of the primer-designing tool in the database now includes the information of directionality of T-DNA. This was not available when the research for this chapter was conducted.

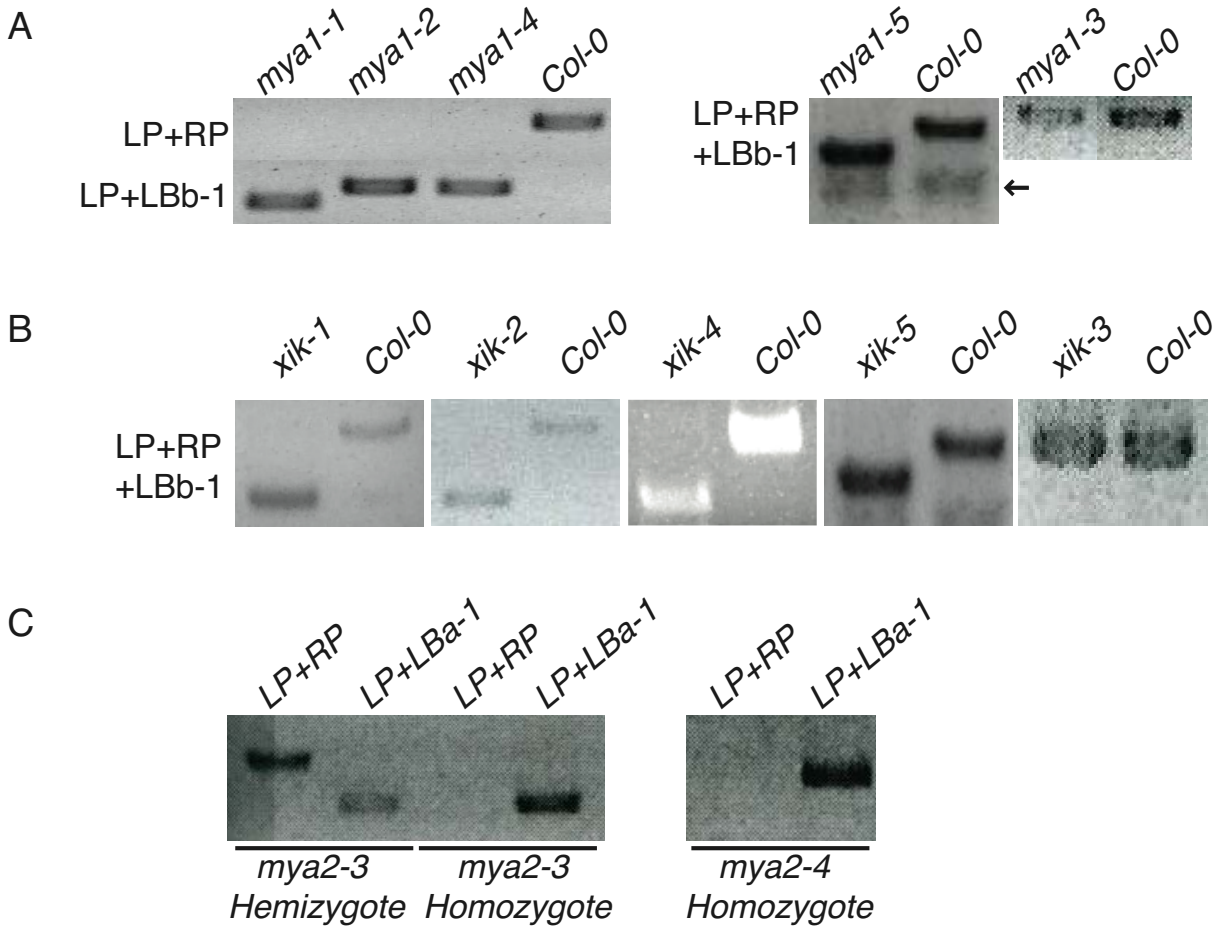

Figure III.2. Verification of T-DNA insertion by PCR

A. Presence of T-DNA was confirmed in *mya1* mutants. *mya1-3* plants have no T-DNA in their genome. Occasionally, TLBb-1 primers could generate around 500bp PCR product which is not related to myosin genes (arrow).

B. Identification of insertion alleles of *XI-K*. *xi-k-3* plants have no T-DNA in the genome.

C. *mya2-3* hemizygous plant amplified PCR products both with two gene specific primers and with a gene specific LP and T-DNA LBa-1 primer.

Figure III.3. T-DNA insertion sites in gene maps and confirmation of gene knockout by RT-PCR

Precise T-DNA insertion sites in the genome were identified by sequencing of PCR product with TLBa-1 and LP (or RP). Many insertion lines contained two insertions of T-DNAs. Disruption of gene expression was confirmed with RT-PCR.

A. Representative genomic maps of T-DNA insertion in myosins. Several lines of *mya1* contained tandem repeats of T-DNA insertions. Two arrows indicate the approximate primer binding region used for RT-PCR.

B. Confirmation of gene knockout by RT-PCR. RT-PCR with gene specific primers confirmed one-knockout mutant in each gene. In case of *MYA2* PCR in *mya2-4*, depending on the location of primer binding site, small amount of PCR product appeared only after 40 cycles of amplification (*mya2-4*^{b}).

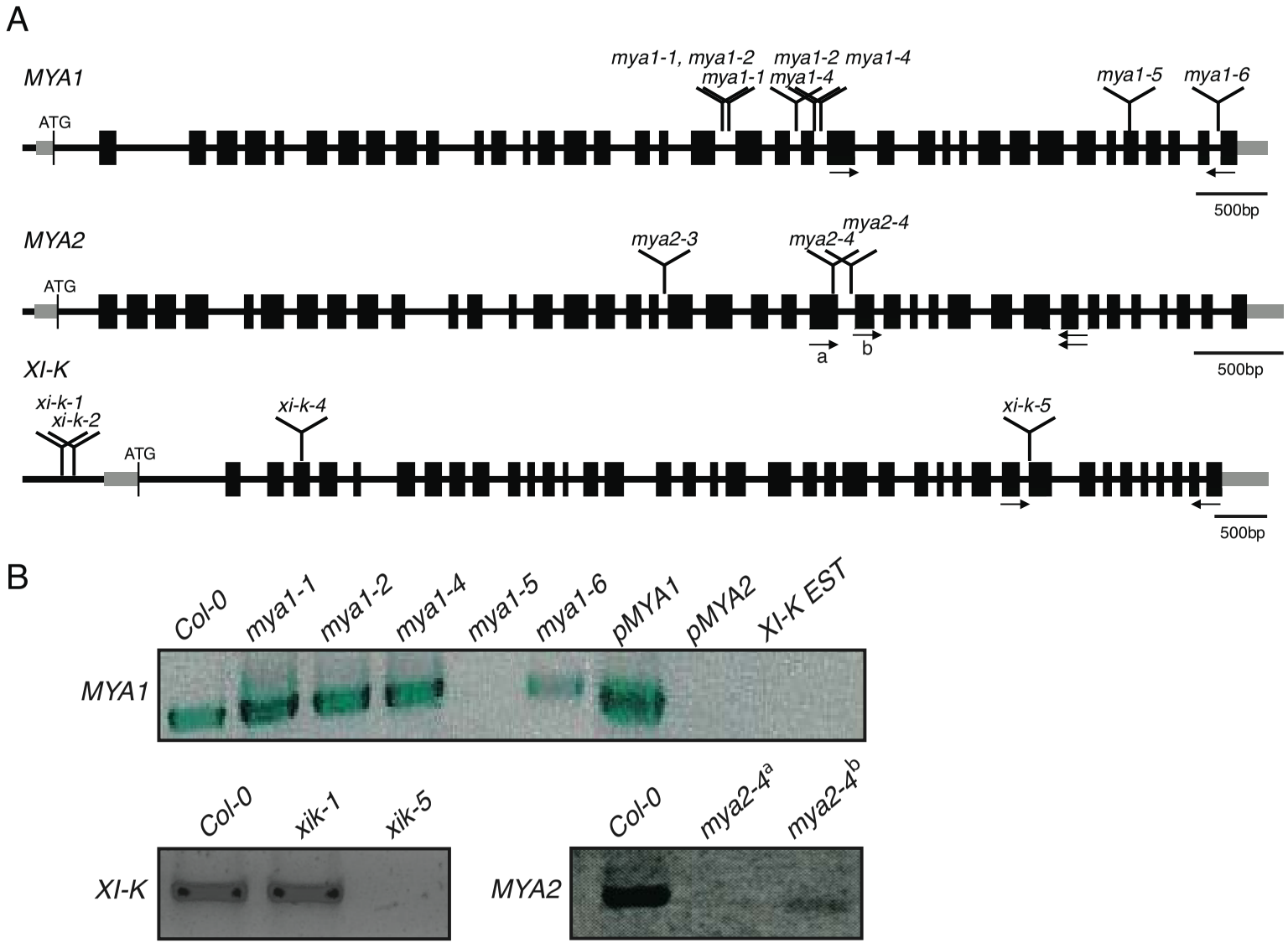
A
MYA1
mya1-1, mya1-2
mya1-1
mya1-2 mya1-4
mya1-4
mya1-5
mya1-6
ATG
500bp
MYA2
mya2-3
mya2-4
mya2-4
ATG
a
b
500bp
XI-K
xi-k-1
xi-k-2
xi-k-4
xi-k-5
ATG
500bp
B
Col-0
mya1-1
mya1-2
mya1-4
mya1-5
mya1-6
pMYA1
pMYA2
XI-K EST
MYA1
Col-0
xik-1
xik-5
XI-K
Col-0
mya2-4a
mya2-4b
MYA2

integration in a gene is normally expected to disturb proper gene expression. However, depending on the site of T-DNA insertion region, it is possible that no or only mild effects on gene expression are observed. In fact, among the five alleles of *mya1* mutants, four alleles still showed specific PCR products in RT-PCR experiments (**Figure III.3.B**). Amplified PCR fragments were also observed with cDNA from seedlings of three different alleles. Interestingly, RT-PCR of *mya2-4* gene fragments showed different results depending on the position of primers in the coding region. PCR with primers that span the T-DNA insertion site in *mya2-4* failed to generate a PCR product (**Figure III.3.B.** *MYA2* PCR **a**), while PCR with primers downstream of the T-DNA insertion site amplified to an extremely low level with 40 cycles (**Figure III.3.B.** *MYA2* PCR **b**). *mya1-1* also showed a PCR product with a pair of primers that failed to amplify with *mya1-5* cDNA (**Figure III.3.B**). However, with a different pair of primers which span the T-DNA insertion region, no PCR product was generated with cDNA of *mya1-1* suggesting that the mRNA in *mya1-1* might include abnormal sequences due to T-DNA insertion. In addition, more knockout mutants of *XI-B* (*xi-b-2* and *xi-b-3*) and *XI-C* (*xi-c-1* and *xi-c-5*) were identified and confirmed by the absence of amplification from corresponding cDNA in mutants by Peter Anthopolos. Thus, gene-specific RT-PCR could confirm loss of gene expression in *mya1-5*, *xi-k-5*, *xi-b-2*, *xi-b-3*, *xi-c-1*, *xi-c-5*, and *mya2-4*, supporting that those lines are gene knockout mutants (**Table III.5.**). Meanwhile, *xi-k-5* and *mya2-3* were isolated as knockout mutants from several other groups (Hashimoto et al., 2005; Ojangu et al., 2007; Peremyslov et al., 2008).

III.3.2. Phenotype survey

Once homozygous T-DNA insertion lines were confirmed by genotype PCR, plants were carefully examined to detect potential mutant phenotypes. At first, overall plant growth was observed during the entire development. None of the insertion mutants showed detectable morphological differences, suggesting that myosin genes might have functional redundancy. Thus, more detailed observation of different tissues or responses to special environmental signals were performed (**Table III.6.**). First, trichome morphology was observed on adult leaves and inflorescence stems. Normally, trichomes on leaves have three branches while trichomes on the inflorescence stem are not branched (Ishida et al., 2008; Pesch and Hulskamp, 2004). Among the observed lines, only *xi-k-5* showed distorted trichomes on stems, while, interestingly, trichomes on leaves did not show significant defects (**Figure III.4.**). This phenotype of *xi-k-5* was also observed by Ojangu et al. 2007. However, in their results, trichomes on leaves also showed distorted or abnormally branched trichomes (Ojangu et al., 2007).

Two characteristics of root hair development, root hair positioning and root hair growth, were also examined for several myosin mutants. To observe the two phenotypes, seedlings were grown on square plates positioned vertically in a growth chamber. Interestingly, *mya1-5* and *xi-h-1* plants were observed to produce more root hairs than wild type. This phenotype could be observed in different alleles of *mya1* and *xi-h*, *mya1-1*, *mya1-4*, *mya1-6*, and *xi-h-5* (See chapter V.)(**Figure III.5.A**). There was no significant difference of root hair length between wild type and *mya1-5* statistically (*Col-0*: 0.61 ±0.11, n= 730; *mya1-5*: 0.61 ±0.17, n= 311). On the other hand, root hair lengths of *xi-k-5* and *xi-b-2* were shorter than those of wild type (*xi-k-5*: 0.32

Table III.6. List of phenotype survey

Phenotypic analysis	Tested lines	Comments
Whole plant growth	all	No visible phenotype
Trichome development	*mya1*, *mya2*, *xi-f*, *xi-h*, *xi-i*, *xi-k*	*xi-k*
Leaf epidermal cell shape	*mya1*, *mya2*, *xi-i*, *xi-k*	No visible phenotype
Leaf venation	*mya1*, *mya2*, *xi-f*, *xi-h*, *xi-i*, *xi-g*, *xi-k*	No visible phenotype
Hypocotyl growth	*mya1*, *xik-5*, *mya1 xi-k*, *mya2*, *xi-i*	No visible phenotype
Root hair growth	*mya1*, *xi-b*, *mya1 xi-k*, *xi-i*, *xi-k*, *mya2*	*xi-k*, *mya1 xi-k*, *xi-b*, *mya2*
Root gravitropism	*mya1-5*, *xik-5*, *mya2*, *xi-i*, *xi-h*	No visible phenotype
Root hair positioning	*mya1*, *xi-k*, *mya1 xi-k*, *xi-h*	*mya1*, *xi-h*

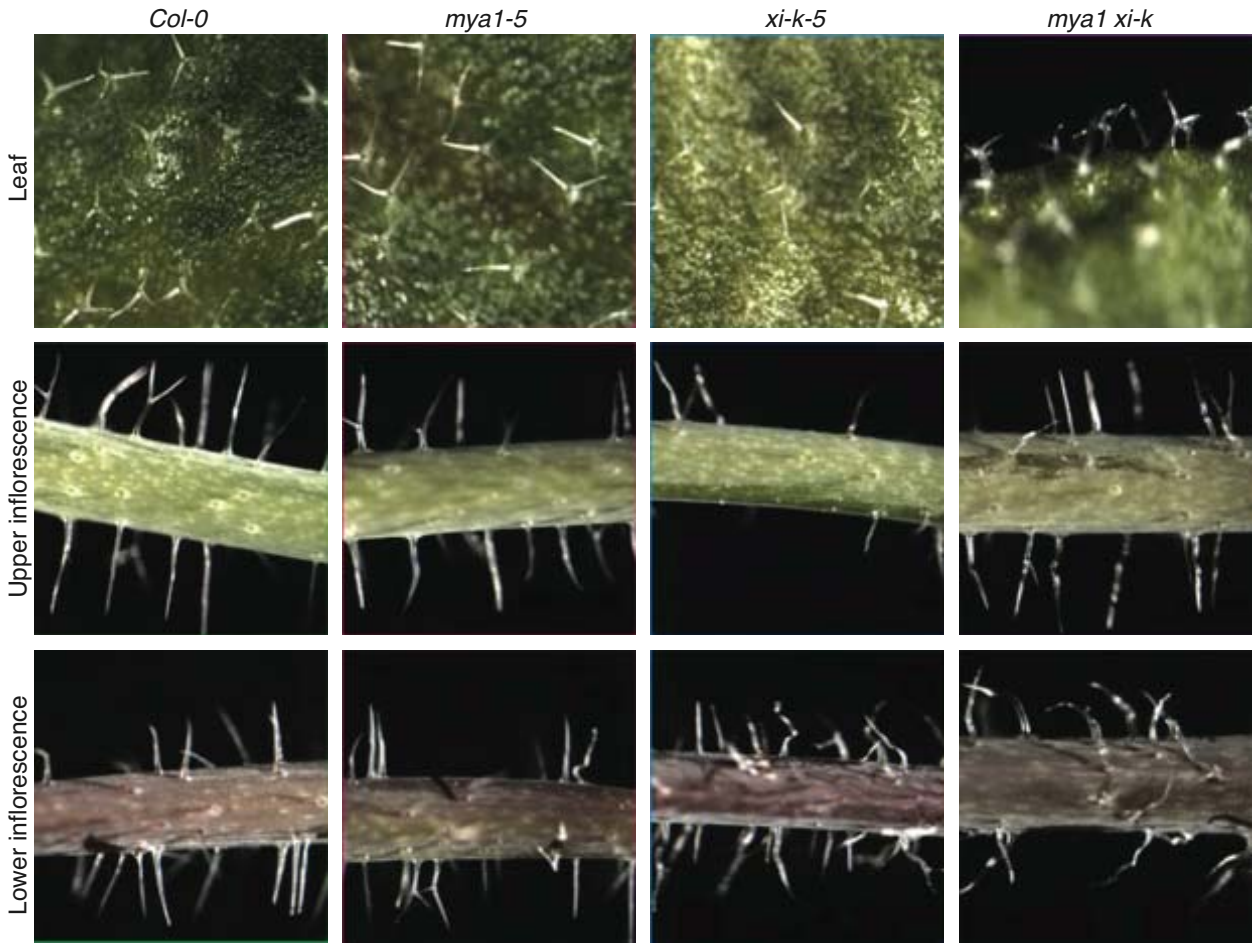

Figure III.4. Trichome morphology

Trichomes on leaves and inflorescence were compared in wild type and mutants. Trichomes on the inflorescence stem of *xi-k-5* were not straight and this phenotype was more severe in *mya1 xi-k* double mutants. However, there was no visible phenotype in trichomes on leaves.

Figure III.5. Root hair phenotypes of selected myosin mutants

Several alleles of *mya1* and *xi-h* produced more root hairs than wild type, while *xi-k* and *mya2* as well as *mya1 xi-k* double mutant showed shorter root hairs than wild type.

A. Mutants that displayed additional root hairs. Note the "bushy" appearance of the mutants compared to *Col-0*.

B. Mutants whose root hairs are shorter than wild type.

C. Comparison of root hair length on *xi-k* and *mya1 xi-k* with *Col-0* and *mya1.* Bars showed average length of at least 300 root hairs. Error bar indicate SE.

D. Short root hairs on *xi-b* mutants. Note that the phenotype is milder than in *xi-k*.

A

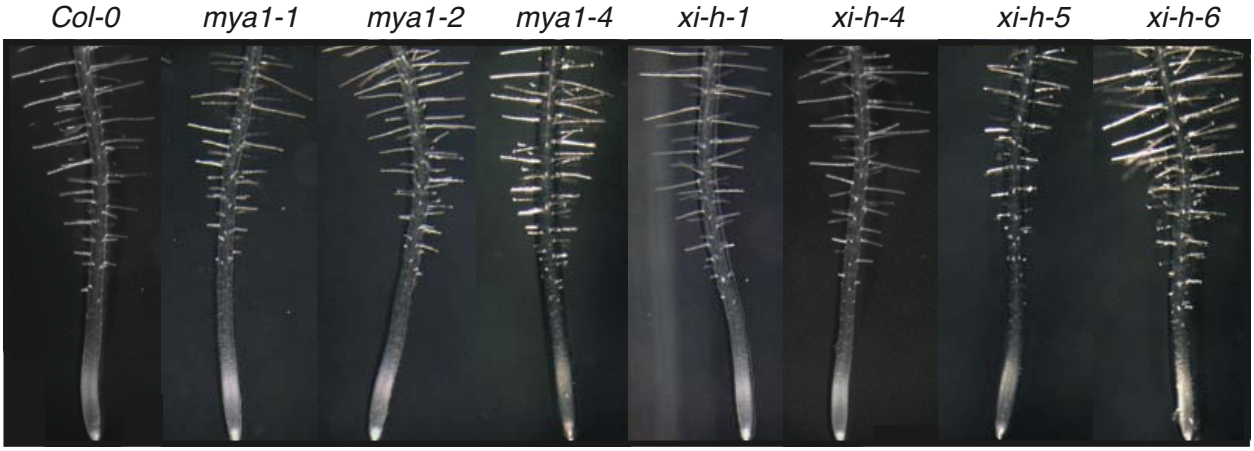
Col-0
mya1-1
mya1-2
mya1-4
xi-h-1
xi-h-4
xi-h-5
xi-h-6

B

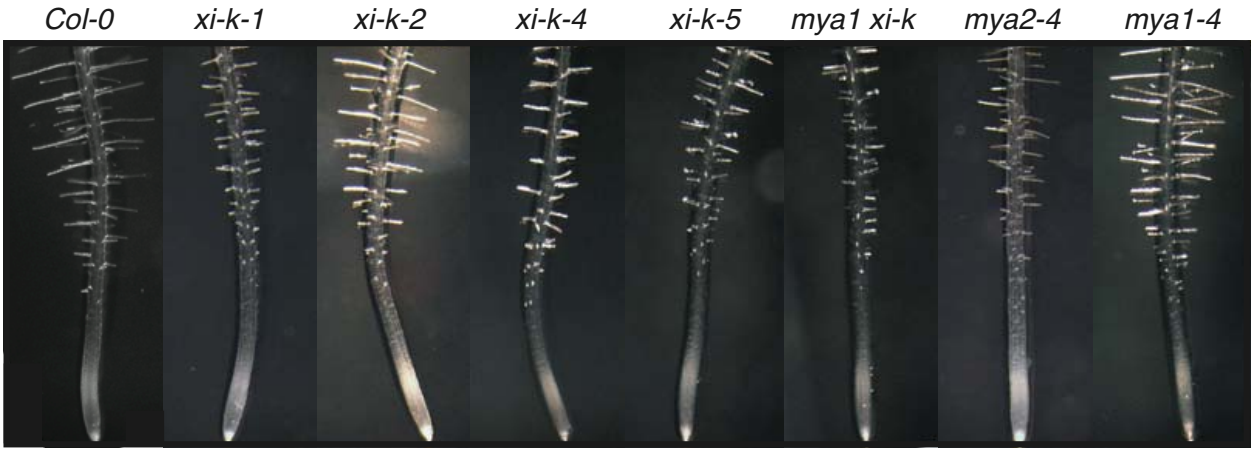
Col-0
xi-k-1
xi-k-2
xi-k-4
xi-k-5
mya1 xi-k
mya2-4
mya1-4

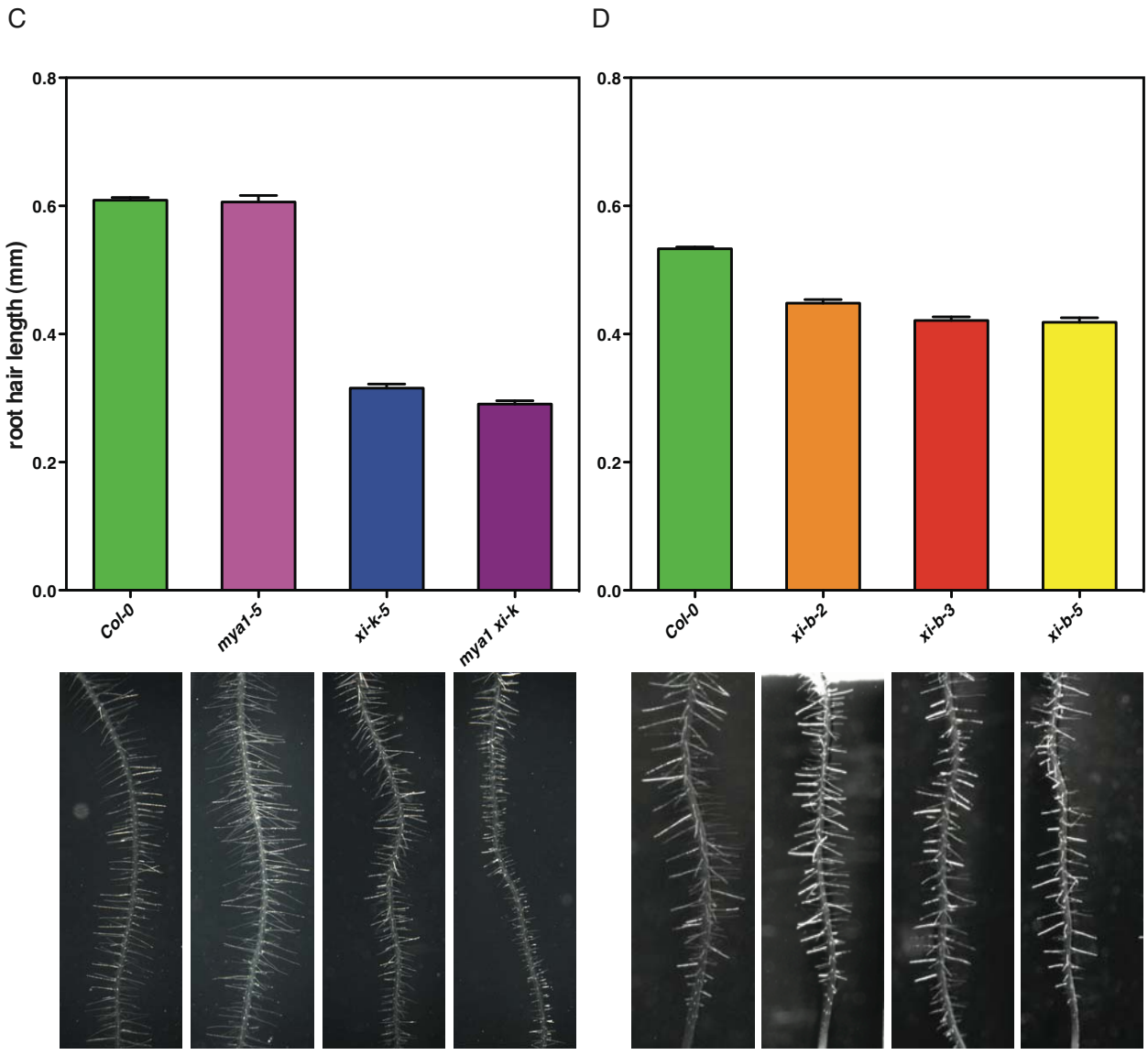

Figure III.5. Continued.

±0.12, n=370; *xi-b-2*: 0.45 ±0.12, n=475; *xi-b-3*: 0.42 ±0.11, n=387) (**Figure III.5.C and D**). It is remarkable that root hairs in *xi-k-5* could grow to only around 50% of root hair length in *Col-0*, while *xi-b* root hairs could grow around 70% of wild type (**Figure III.5.B, C, and D**). Other alleles of *xi-k*, *xi-k-1*, *xi-k-2*, and *xi-k-4*, also showed shorter root hairs consistent with descriptions from two publications (**Figure III.5.B**) (Ojangu et al., 2007; Peremyslov et al., 2008). No visible phenotype was detected for several myosin mutants. Also, some of the characteristics examined did not yield any differences between wild type and any of the myosin mutants. For example, measurement of hypocotyl elongation in dark grown seedlings did not show any difference in myosin mutants (**Figure III.6.**). Hypocotyl lengths from 10 seedlings of each genotype were measured 6 days after germination. Wild type showed average hypocotyl length of 7.3 mm (±0.71 SD), while seedlings of *mya1-5*, *xi-k-5*, *mya2-3*, and *xi-i-1* had no significant difference (7.9 ±1.1, 8.1 ±0.75, 8.3 ±1.0, 8.2 ± 0.92 mm, respectively).

III.3.3. Double mutant screening

The presence of highly similar pairs of myosin paralogs in the myosin class XI gene family suggests that these genes might be functionally redundant (**Figure II.4 and 5.**). To test this hypothesis, mutants of two highly similar myosins were crossed to generate a double mutant. For example, MYA1 and XI-K are most similar to each other and knockout mutant of both genes has been isolated. Thus, to investigate functional relationship of *MYA1* and *XI-K*, *mya1-5* and *xi-k-5* were crossed and double mutants were identified by genotype PCR in F2 plants. Among 98 individual F2 plants, 3 plants of *mya1 xi-k* double mutant were isolated. *mya1* single mutants showed additional root hairs compare to wild type while *xi-k* mutants had shorter root hairs than

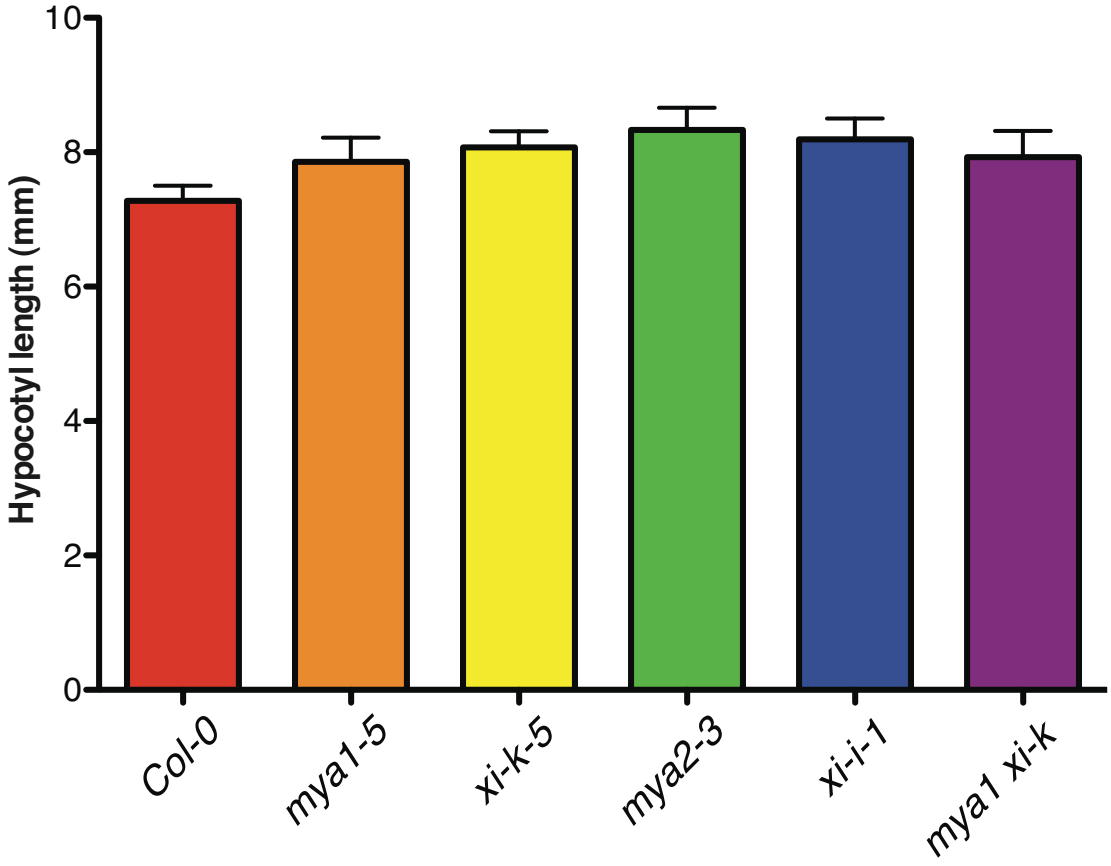

Figure III.6. Hypocotyl lengths of several myosin mutants are not different

Hypocotyl length in etiolated seedlings of *mya1-5*, *xi-k-5*, *mya1 xi-k*, *mya2-4*, and *xi-i-1* were compared with those of wild type. There was no significant difference between any of tested lines ($p > 0.05$).

wild type. A total of 476 root hairs from more than 30 double mutants were observed whether they show both phenotype of root hair positioning and root hair growth (**Figure III.5.**). Root hairs of *mya1 xi-k* double mutants were significantly shorter than the root hairs of *xi-k* (*mya1 xi-k*: 0.29 ±0.11, n=476 ; *xi-k*: 0.32 ±0.12, n= 370, p=0.0013). Interestingly, this was most pronounced in the lower (younger) part of the root (**Figure III.5.C**). This suggests that MYA1 and XI-K show some overlapping activity regarding root hair growth at least in this specific region of the root.

III.3.4. Organelle movements in a double mutant

To identify the cause of the root hair growth defect in *xi-k* and *mya1 xi-k*, organelle markers were transformed into several genotypes, including *Col-0*, *mya1-5*, *xi-k-5*, and *mya1 xi-k*. Since organelle movements are very sensitive to the environment, one binary vector containing three organelle markers (TOM) labeled with different fluorescence proteins (Peroxisome-CFP, Mitochondria-YFP, and Golgi-mCherry/Tomato) were cloned (**Figure III. 7.A**) and root hairs of stable transgenic plants in wild type and *mya1 xi-k* were observed with time-lapse photography. Image sequences for each organelle marker were analyzed for organelle movements in root hairs (**Movie III.1-8* and Figure III.7.B**).

Peroxisome movements in wild type showed a faster average speed than those in *mya1 xi-k* (**Figure III.7.C**). In *Col-0*, the mean velocity of peroxisome was 0.56 ±0.02 μm/sec with 923 individual time intervals and the average maximum speed was 2.44 ±0.41 μm/sec within 13 cells analyzed. In *mya1 xi-k*, both mean velocity of all tracks and average maximum speed were

---

* Movie files are included as attachments separately. Quick time player or an equivalent video player is necessary to open these files.

Figure III.7. Organelle movement analysis

Organelle movements were traced with a triple organelle marker (TOM) in wild type and *mya1 xi-k* double mutant.

A. Plasmid map of triple organelle marker. Three available organelle markers were inserted in a single binary vector, pFGC19, each with their own 35S promoters and nos terminators. Two variants of TOM were generated with different Golgi markers, either Golgi-tdTomato or Golgi-mCherry.

B. Images of TOM in wild type and *mya1 xi-k* double mutants were collected in three channels sequentially for 60 sec with 1-2sec intervals. Then images from the three channels were separated and used for tracking organelles. Peroxisome-CFP (PX-CFP) was pseudo-colored in blue, while mitochondria-YFP (MT-YFP) and Golgi-tdTomato (Go-Tomato) were pseudo-colored in green and red, respectively.

C. Cumulative distribution function plots of the speed of organelles in wild type and *mya1 xi-k* double mutants. Measurement of the speed of each organelle from several cells of each genotype were combined and displayed as a percentage of the cumulative distribution of speeds. While Golgi and mitochondria movements in double mutants were not significantly different, peroxisome movements in double mutants were slower than in wild type.

A


35Spro
Peroxisome-CFP
nos 3'
Mitochondria-YFP
Golgi-mCherry

B

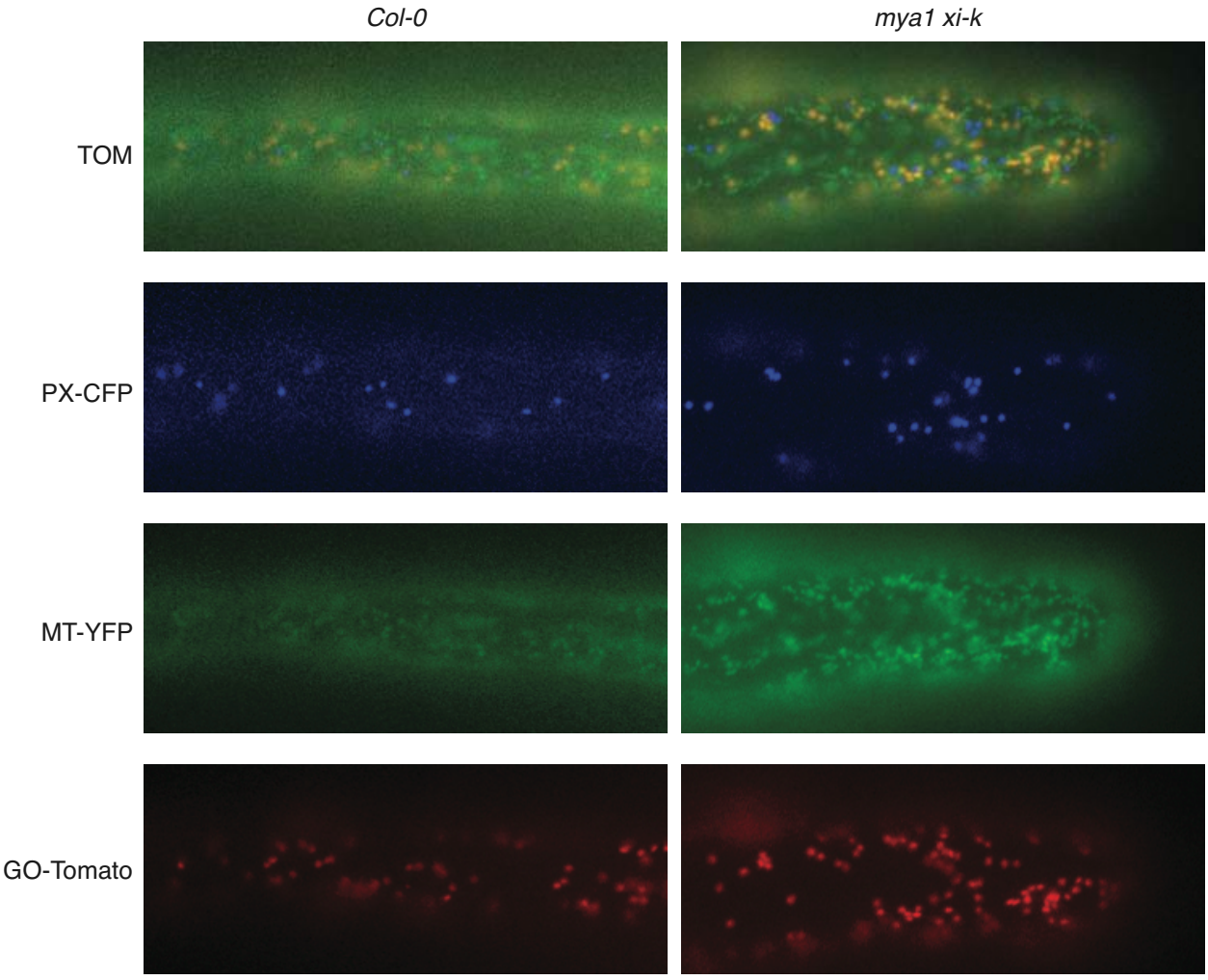
Col-0
mya1 xi-k
TOM
PX-CFP
MT-YFP
GO-Tomato

C

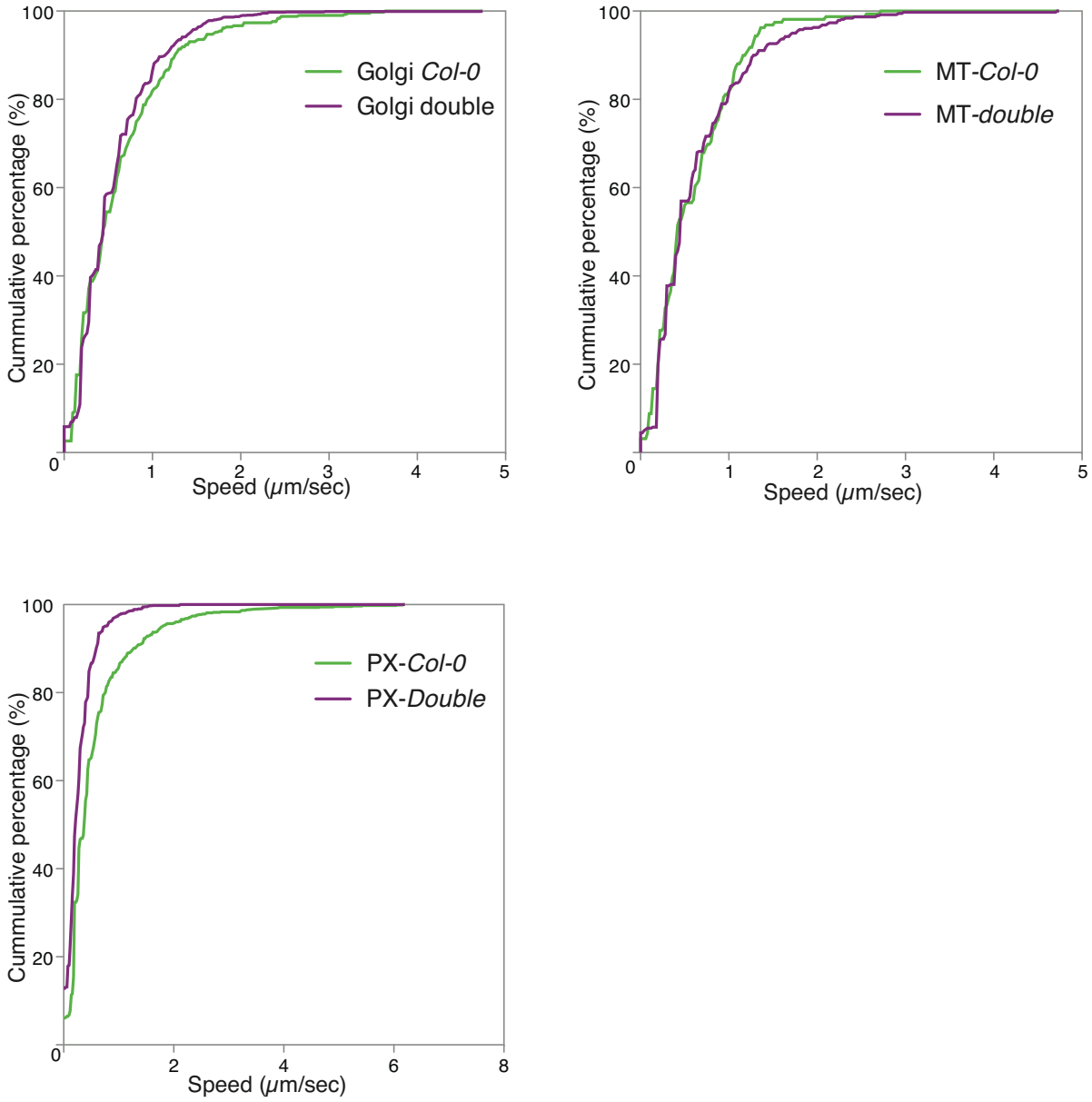

Figure III.7. Continued

slower than in wild type (0.28 ±0.007 μm/sec (n=1109) and 1.24 ±0.11 μm/sec (n=14), respectively). These results suggest that peroxisomes in *mya1 xi-k* double mutants are moving less overall (U test: $p < 0.0001$).

On the other hand, Golgi stack and mitochondria movement in *mya1 xi-k* did not show significant differences in either mean velocity or average maximum speed to those in *Col-0* (**Figure III.7.C**). Mean velocity of Golgi in *Col-0* was 0.61 ±0.03 μm/sec (n=420) and average maximum speed was 1.92 ±0.28 μm/sec (n=11), while mya1 and xi-k double mutants showed similar speeds in both criteria (0.54 ±0.01 μm/sec (n=1112) for mean velocity and 1.67 ±0.16 μm/sec (n=27) for average maximum speed, U-test: p=0.92). Mitochondria movement was also similar in wild type and *mya1 xi-k* double mutant with mean velocities of 0.58 ±0.037 μm/sec (n=159) and 0.63 ±0.029 μm/sec (n=381) and average maximum speeds of 2.47 ±0.18 μm/sec (n=5) and 2.81 ±0.21 μm/sec (n=10), respectively (U-test: p=0.64).

III.4. DISCUSSION

Compared with the intensive studies in non-plant organisms, including human cells, functional study of plant myosins has been very limited until recent (Avisar et al., 2008b; Harries et al., 2009; Ojangu et al., 2007; Peremyslov et al., 2008; Richards and Cavalier-Smith, 2005; Sparkes et al., 2008). This might be because the functional redundancy within the gene family makes it difficult to find a mutant by phenotypic screening. In fact, none of the single mutants of myosins analyzed here showed visible defects on whole plant growth. Individual cell types, like root hairs and trichomes, showed a phenotype suggesting that some isoforms function

predominantly in certain developmental processes. However, different isoforms might still share their function in at least root hair growth, since *mya1 xi-k* double mutants showed a stronger phenotype, although *mya1* single mutants did not show a root hair growth defect. It will be interesting to observe the phenotype of other multiple mutants, for example, *mya2 xi-b* and *mya1 xi-h*.

The observation of the phenotypes of myosin mutations may also have been difficult since myosin may function intensively in specific cells which are very sensitive to slight environmental changes. For example, three studies including two recent publications and this study about the *xi-k* mutant showed quantitatively different expression of the mutant phenotype (Ojangu et al., 2007; Peremyslov et al., 2008). Difference in phenotype of *xi-k* trichomes between my results and published results from Ojangu et al. (2007) might be caused by differences of growth condition. Slight differences of growth condition, for example, soil, light, or humidity, might cause variable growth defects. In fact, the average lengths of root hairs of wild type were different between my experiments and those of the other groups. Root hairs in my and Ojangu's experiments were about twice as long as the root hairs described by Peremyslov *et al*. (Ojangu et al., 2007; Peremyslov et al., 2008). Ojangu et al. also did not include sucrose in the growth media causing the plants to produce longer root hairs. The average length of root hairs grown on sucrose-free conditions in their results was similar to those in my results. Since plants were grown on quarter strength MS in my experiments, limitation of nutrients might stimulate root hair growth. Thus, variations in growth conditions may lead to different expression of mutant phenotype.

Different growth conditions might also partially explain the differences of organelle movements described in this study and elsewhere (Peremyslov et al., 2008). Root hair growth is

extremely sensitive to environmental changes (Bibikova et al., 1997; Monshausen et al., 2007). Slight changes of pH or nutrient contents in the medium can cause cessation of growth or even root hair rupture (personal communication with Monshausen and own observations). This suggests that organelle movements in root hairs might also be sensitive to environmental differences, so that different growth conditions could generate different effects on organelle movements. This should be examined in more detail in the future with tightly controlled environmental parameters. However, it may still be hard to explain why peroxisome movements were slower in both experiments while two other organelles showed different sensitivity to *xi-k* mutants.

In fact, it is difficult to track individual spots from root hairs since the organelle population is very dense and organelle tracks sometimes overlap. For example, the population of mitochondria is large thus occasionally several mitochondria move together in a same track, making it difficult to track an individual spot in the next image (**Movie III. 7.** and **8.**). In addition, it has been well known that organelles have a typical stop and go movement (Nebenführ et al., 1999). For example, Golgi stacks have about 20-45 sec periods of stop and go episodes in BY-2 cells (Nebenführ et al., 1999). In my observations, they showed about 20 to 35 sec long of one stop and go episode (data not shown). Since I tracked individual spots longer than 45 sec, my tracking results contain at least one stop and go episode. However, the other group tracked organelle movements only in 25 sec long, suggesting that they could track only a partial episode of stop and go movements. This might result in inaccurate measurement of movements. For example, Golgi stacks showed shorter moving periods than stop periods in my experiments (data not shown). Moreover, organelles that are not in major tracks are not moving or move more slowly than those in major tracks. Thus, it might be necessary to analyze the

organelle movement in those regions separately to examine organelle dynamics more accurately.

Overall, the high population density of mitochondria and complex moving behavior of organelles might exaggerate potential experimental errors in automatic tracking by computer. In my experiment, although data sample sizes are smaller than automatic tracking by computer, since I carefully selected organelles which showed fast movements and tracked them long enough to observe their behavior, my results are more accurate than automatic tracking. Since there is no maximum speed of organelles given by other group, we cannot conclude whether my interpretation is correct or not. Overall, a more sophisticated method should be developed to analyze this complex movement.

CHAPTER IV. XIK is required for root hair tip growth in Arabidopsis

♦ *The results presented in this chapter are currently being prepared for publication.*

IV.1. INTRODUCTION

Functional studies of class XI myosin in plants are relatively limited compared with studies on myosins in other classes. Recently, using fluorescent-tagged truncated myosin tails, localization information of several myosin in class XI was gathered (Avisar et al., 2009; Li and Nebenführ, 2007; Sparkes et al., 2008). Overexpression of motor-less myosins also revealed a potential myosin function in organelle trafficking (Avisar et al., 2009; Avisar et al., 2008b; Sparkes et al., 2008). However, there have been few studies to investigate a developmental function of class XI myosin.

Mutant analysis revealed a few myosin functions in plant development. Myosin *XI-B* in rice (*OsMyoXIB*) might control pollen development (Jiang et al., 2007), given that *osmyo-xib* mutants were male sterile under short day condition. Last year, two studies showed potential functions of *MYA2* for a plant virus movements in tobacco leaves (Harries et al., 2009) and movements of plastid stromules (Natesan et al., 2009). An antibody raised against an isoform of class XI myosin purified from cultured tobacco BY2-cells suggested that myosin might function in ER movement during mitosis (Yokota et al., 2009). At last, as already mentioned in the chapter III of this study, *xi-k* mutants had much shorter root hairs than wild type and *mya1 xi-k* double mutant analysis revealed defects in peroxisome and Golgi stack movements. In addition, two other groups showed the same mutant phenotype of *xi-k* mutation (Ojangu et al., 2007; Peremyslov et al., 2008) and one of them also showed defects in multiple organelle movement in *xi-k* mutants (Peremyslov et al., 2008). However, it is still unclear what is a direct function of *XI-K* in the mechanism of root hair growth. Root hairs are long tubular outgrowths of root epidermal

cells that increase the root surface by growing only at their tip. This tip growth is regulated by an extremely complicated self-organizing feedback mechanism with dynamic cytoskeleton, vesicle trafficking, and signaling factors (see chapter I.2 for detail.). Although many regulatory factors were identified in this mechanism, there are still a lot of unknown aspects to be investigated. For example, it has been shown that a unique cytoskeletal organization of root hairs leads to massive accumulation of vesicles containing cell wall material to the apex of root hairs (**Figure I. 5**, for review). However, how these vesicles are delivered is still unknown.

In this study, the tip growth defect myosin mutant, *xi-k*, was characterized in detail to identify XI-K function in the tip growth mechanism of root hairs. The reduced growth of root hairs in *xi-k* was tightly correlated with the accumulation of RabA4b labeled vesicles at the tip of growing root hairs. This study also showed XI-K localization at an unidentified type of vesicle at the root hair tip, partially colocalized with RabA4b-labeled vesicles. With a lack of knowledge of myosin function in root hair tip growth, this study provides significant new details about the mechanism of root hair tip growth.

IV.2. MATERIALS AND METHODS

IV.2.1. Plant growth and transformation

Col-0 was used as wild type and *xi-k-5* (SALK_018764), identified in Chapter III, was used for a mutant. Plants were grown in a growth chamber at 22°C in 16hr light and at 20°C in 8hrs dark with about 60% humidity (Weigel and Glazebrook, 2002). For root hair length

measurements, seeds were germinated on square plates of 1/4 strength MS with 1% sucrose pH adjusted to 5.7 and solidified with 0.5% phytagel (Sigma-Aldrich). Plates were incubated at 10° off vertical in a growth chamber with continuous light. 5 day-old seedlings were used for the measurements. Constructs used in this study were transformed into plants by the floral-dip method (Weigel and Glazebrook, 2002). Stable transgenic plants were screened with appropriate antibiotics or herbicides and observed under a fluorescence microscope.

IV.2.2. XI-K complementation test

The construct for the complementation test was composed with *XI-K* native promoter, which extends approximately 1kb upstream of the *XI-K* start codon and includes the first exon and intron of *XI-K*. This sequence was also used to construct the *XI-Kpro:GUS* expression reporter in chapter II (see table II.1. for primer information). The promoter was followed by *YFP* (yellow fluorescent protein) conjugated with a short linker DNA encoding ELYGGOGGSGSA and *XI-K* cDNA in the binary plasmid pPZP221. This construct was transformed into *xik-5* mutants. Full length *XI-K* cDNA was assembled by combining two EST clones, BE526400 and AV546218, which cover the full length of the gene including the 5' UTR and 3'UTR.

Root hair lengths were measured in images of 5-day-old seedlings that were captured under a Leica stereomicroscope (Leica MZ16 FA, http://www.leica microsystems.com) equipped with digital camera (Leica DFC420) under 7.1 X magnification or 23X magnification. Images were acquired with Leica FW4000 software. More than 150 root hair lengths from 15 or more plants in each genotype were measured with ImageJ (NIH, http://rsb.info.nih.gov/ij/) and statistically analyzed in Prism 5 (www.graphpad.com).

IV.2.3. Root hair growth rate measurements

To measure root hair growth rate, seeds were surface sterilized and stratified in water for 2 days and then transferred to special devices as described in (Kawamura et al., 2006) with a modification to maintain plants healthy during observation. Briefly, 2 seeds were moved to a cover glass-bottomed culture dish (Electron Microscopy Sciences) and covered with 2ml of media containing 1/4 strength MS salt, 1% sucrose, and 0.7% type VII agarose (Sigma-Aldrich) in pH 5.7. Culture dish chambers were sealed and placed in the growth chamber for a day. The culture dish chambers were tilted 30° off vertical so that roots could grow along the cover glass. DIC images of root hairs were taken in 30 sec intervals for 45min or 1 hour under a 100X objective with binning turned off to minimize pixelation errors. Time-lapse capture was repeated 5-7 times to observe entire growth of a root hair from shortly after bulging to fully-grown. Length of root hairs was measured with measurement option in OPENLAB (Improvision). Data were analyzed and visualized with Prism 5.0.

IV.2.4. Constructs and plant transformations

Constructs and their transgenic plants were listed in **Table IV. 1**. Briefly, *YFP-RABA4B*, *YFP-RABF2A*, and *YFP-hFAPP1* in *pCambia* were kindly provided by E. Nielsen from the University of Michigan. An actin marker, *YFP-FABD2* in pFGC19, was reconstructed based on *35Spro:GFP-FABD2* donated by Dr. Carola Holweg in Germany. *YFP/mCherry-ROP2* was generated from amplified cDNA sequences based on the sequence information from Fu *et al* (Fu

et al., 2002). *YFP/CFP-RHD4* was constructed from amplified cDNA sequences with primer information from Thole *et al*. (Thole et al., 2008). Constructs were transformed into wild type and *xi-k-5* mutants by Agrobacterium-mediated transformation (Weigel and Glazebrook, 2002).

For *EXP7pro:YFP/mCherry*, promoter sequence information of *EXPANSIN 7* (*EXP7*) was obtained from Kim *et al*. (Kim et al., 2006). DNA fragment containing *EXP7* promoter was obtained by PCR from genomic DNA with *EXP7pro-F* (5'-GCTAGCTTAGTTTATCTTTGGA AACGAAACGTAA-3') and *EXP7pro-R* (5'-CCATGGTTCTAGACCTAGCCTCTTTTTCTTT ATTCTT-3'). The PCR product was cloned in pGEM-Teasy vector and sequenced, then moved to a binary vector, *pFCG19* with XbaI (on primer) and EcoRI (from T-vector) restriction. YFP with nos 3' terminator was introduced downstream of the promoter.

IV.2.5. Analysis of YFP-RabA4b accumulation

35Spro: YFP-RABA4B in pCAMBIA, kindly provided by E. Nielsen (University of Michigan, Ann Arbor, MI) was transformed independently into *Col-0* and *xi-k-5*. Homozygous T3 seeds were germinated on vertical plates as described above and moved to the observation chamber four days after germination. After three hours incubation in the observation chamber to allow growth of new young root hairs, images of YFP fluorescence and DIC were collected with a Hamamatsu ORCA-ER digital camera sequentially every 10 sec for 30 min with a 63X (1.4 NA) plan-apo oil immersion objective with no binning on an Axiovert 200M microscope (Zeiss, http://www.zeiss.com) equipped with filters for YFP and CFP fluorescence (filter set 52017; Chroma, http://www.chroma.com). Background was subtracted with Openlab from all YFP images to remove camera background.

Table. IV.1. List of constructs transformed into plants

Name	Localization Information	Selection marker	Comments
XIKpro:YFP-XI-K	Vesicles at root hair tips[A]	Gentamicin	This study[B]
35Spro:YFP-RABA4B	Vesicles at root hair tips	Hygromycin B	E. Nielsen lab (Preuss et al., 2006)
35Spro:CFP-RABA4B	Vesicles at root hair tips	Hygromycin B	E. Nielsen lab (Preuss et al., 2006)
35S:YFP-PH$_{FAPP1}$	Plasma membrane at root hair*	Hygromycin B	E. Nielsen lab (Vermeer et al., 2009)
35S:CFP-HDEL	Endoplasmic reticulum	Basta	Nebenführ lab (Nelson et al., 2007)
35Spro:YFP-FABD2	Actin filaments	Basta	This study[B]
35Spro:YFP-RHD4	Root hair tip accumulation	Basta	This study[B]
35Spro:CFP-RHD4	Root hair tip accumulation	Basta	This study[B]
EXP7pro:mCherry	Cytoplasmic localization	Basta	This study[B]
EXP7pro:YFP	Cytoplasmic localization	Basta	This study[B]
EXP7pro:YFP-ROP2	Plasma membrane at root hair	Basta	This study[B]
35Spro:YC3.6	Calcium dynamics	Basta	S. Gilroy lab (Monshausen et al., 2007)

* YFP-PH$_{FAPP1}$ at the shank of root hairs can label Golgi stacks

[A] This information was shown in this study

[B] constructs were generated by author of this study

The time-lapse sequences of YFP and DIC were then separated and analyzed using ImageJ. YFP image sequences from individual root hairs were bleach corrected using a plug-in in ImageJ (ImageJ> plug-in> Stacks-T-function> bleach correction) with a decay constant calculated from whole image sequences based on fitting of an exponential decay curve ($R^2 >$ 0.68, overall). To measure accumulation of YFP fluorescence at the root hair tip, an oval area of about 2.1 μm^2 was selected within 4μm from the tip of the root hair and average fluorescence intensity was measured over time. Coefficient of variation of mean intensity was taken as a measure for the consistency of YFP accumulation at the tip of root hairs. DIC image sequences captured along with YFP images were used to measure root hair growth rate. Due to the limited pixel resolution of images, every third DIC image was selected and used for the measurement of root hair tip position. Statistical analyses and visualization of result were performed with Prism 5.0.

IV.2.6. YFP-XI-K localization analysis

XI-Kpro:YFP-XI-K xi-k-5 plants were observed for their YFP expression in root hairs. Microscope setting was identical to the analysis of RabA4b accumulation except that long exposure times were used. Sequential images were obtained under 63X with 2X binning for 1 min with 1sec intervals.

For drug treatment, 5-day-old seedlings grown as described above were transferred to the observation chambers. Inhibitors were diluted in liquid media and applied underneath solid media bed covering the root of a seedling in the observation chambers (10μg/ml final concentration of BFA from a 5mg/ml stock in EtOH and 100nM of Latrunculin B from 1mM

stocks in DMSO). EtOH was used for mock treatment. Images were taken for 60 min with 10sec interval (BFA and EtOH) or 30sec interval (LatB) and processed as described above.

For colocalization test, *35Spro:CFP-RHD4*, *EXP7pro:mCherry-ROP2*, and *EXP7pro:mCherry* were transformed into homozygous *XI-Kpro:YFP-XI-K xi-k-5* plants. T1 seedlings were screened on media with double selection and moved to a vertical plate without selection for additional growth for a day to allow normal growth of root hairs. Once seedling started producing normally shaped root hairs, they were moved to an observation chamber and sequential dual color images were acquired for one minute in 1sec intervals.

IV.2.7. Analysis of cytosolic Ca^{2+} dynamics at the tip of root hairs

35S-driven YC3.6 in the binary vector pEarleyGate100 was kindly donated by Dr. Simon Gilroy at the University of Wisconsin and transformed into wild type and *xi-k*. Successful transformants were isolated in a screen and T2 seeds were harvested. Imaging of cytosolic Ca^{2+} levels was performed by fluorescence resonance energy transfer (FRET). 5-day old seedlings were transferred to a minimal media plate described in Monshausen et al. 2008. After 3 hours of growing on the minimal media plate, agar surrounding the seedling was cut out and transferred to the observation chamber with 200µl of sterilized water. CFP, FRET, and YFP images were acquired using a dichroic mirror with two-transmission windows, 476/40nm and 550/50nm, under CFP excitation and YFP excitation sequentially. Separate images in CFP channel and YFP channel were recorded simultaneously through a beam splitter. These image acquisitions were repeated every 2 sec for 3 min. Images were manipulated in Openlab and normalized FRET was calculated with NFRET algorithm developed by (Xia and Liu, 2001) using the FRET module in

Openlab software. Bleed-through constants were determined experimentally to be 0.8 for donor and 0.01 for acceptor. Input thresholds were set up by averaging 5 randomly picked background intensities for each image. NFRET values were visualized and analyzed statistically with Prism 5.0.

IV.2.8. Analysis of Actin dynamics

An actin marker, YFP-FABD2, was transformed into both wild type and *xik* mutant and stable transgenic plants were screened for reliable fluorescence expressions. Time-lapse images of 15 growing root hairs were taken in 1 sec interval for 1 min under microscope with a microscope setting described in the section IV.2.6. Images were then analyzed and visualized with ImageJ.

To differentiate dynamic actin movements, subtraction of sequential images using ImageJ plug-in (ImageJ> plug-in> Stacks-T-function> Delta F up) was performed. Individual images were background subtracted with high stringency and then differentiated image sequences were generated. For statistical analysis, the relative area of the actin cytoskeleton the showed differences above a threshold was calculated. Statistical analysis was performed with Prism 5.0. For visualization, four image sequences in 5-second intervals were pseudo-colored in rainbow spectrum (red, yellow, green, and blue) and merged in one image.

IV.3. RESULTS

IV.3.1. Tip growth is altered in the root hairs of *xi-k* mutants

As described in chapter III, *xi-k* mutants showed shorter root hairs than wild type (**Figure III.5. B and C**). Root hairs of *xi-k* usually grew to about 60% of root hair length in wild type. This phenotype may have resulted from two different mechanisms: Mutant root hairs might have grown normally but stopped growing earlier than wild type, or they might have grown more slowly than wild type for the same time period. To identify the cause of these short root hairs, root hair growth rates were measured over time. A seedling was moved to an observation chamber and photographed sequentially every 30 sec for up to one hour. The microscope stage was then moved to start tracking the same root hair until it stopped growing. *xi-k* mutants could grow for 4-5 hours under these conditions while wild type could grow up to about 7 hours. This experiment was repeated four times and one representative result is shown in **Figure IV.1**. Complete image sequences are available online in **Movie IV. 1-7** for *Col-0* and **Movie IV. 8-12** for *xi-k*. Both wild type and mutants showed growth rate oscillations which also has been reported (Monshausen et al., 2007). As root hairs got older, their growth rate dropped down and eventually became zero. However, comparison of growth rates of root hairs with similar length revealed that growth rates of *xi-k* were much smaller than those of wild type (**Figure IV.1.A**). Interestingly, growth rates of *xi-k* root hairs were similar to those of wild type root hairs that were 2 hours older (**Figure IV.1.A and B**) suggesting that root hairs in *xi-k* grew more slowly than in wild type. Maximum root hair growth rate in *xi-k* in this condition was 1.67μm/min while wild type showed 2.33μm/min of maximum growth rate suggesting that root hairs in *xi-k* grow slower from their initiation (**Figure IV.1.C**). Overall, average growth rates were 1.26 ±0.53μm/min and 0.918 ±0.21(SD) μm/min in wild type and *xi-k*, respectively. This difference

of root hair growth rates of wild type and xi-k mutants was statistically significant ($p < 0.001$). As a result, *xi-k* mutants produced shorter root hairs than wild type since root hairs in *xi-k* mutants grew more slowly and also stopped growing earlier than in wild type (**Figure IV.1.D**).

IV.3.2. YFP-RABA4B accumulation is impaired in the *xi-k* mutant

YFP-RABA4B has been used as a marker for growing root hairs (Preuss et al., 2006; Preuss et al., 2004; Thole et al., 2008). When root hairs are growing, YFP-RABA4B accumulates at the tip of root hairs; when root hairs stop growing this accumulation disappears (Preuss et al., 2004). Since root hairs in *xi-k* mutants are growing more slowly and stop growing earlier than in wild type, the effect of the *xi-k* mutation on YFP-RABA4B accumulation was observed in mutants. Root hairs from both wild type and *xi-k* mutants displayed accumulation of YFP-RABA4B at the tip of growing root hairs (**Figure IV.2.A**). However, interestingly, tip accumulation of YFP-RABA4B of *xi-k* frequently displayed a stochastic loss and recovery at the tip of root hairs, while the accumulation was more consistent in wild type (**Figure IV.2.A** and **Movie IV.13-26**). To investigate the relationship between the rate of root hair growth and the accumulation of YFP-RABA4B at the tip of root hairs, YFP fluorescence at the tip of root hairs and root hair growth were monitored over time. Mean intensities in the tip area of growing root hairs are changing spontaneously over time even in wild type, however, the variation of mean intensity in wild type was not as large as in *xi-k* (**Figure IV.2.B-E**).

Figure IV.1. Root hairs in *xi-k* mutants are growing more slowly and stop growing sooner than in wild type

A. Montage of DIC image sequences of Col and *xik* during one hour. Young root hairs in *xi-k* grew more slowly than wild type root hair at the same stage.

B. Growth rate of three root hairs shown in panel A were compared. Root hair growth oscillated over time, however, growth rates of young root hairs in wild type (light green) were higher than those of *xi-k* root hairs at the same developmental stage (magenta), while about two hours older root hairs of wild type (dark green) showed a similar growth rate as younger *xi-k* root hairs.

C. Overview of growth rate from after root hair initiation to termination of root hair growth. Root hairs in *xi-k* mutant (magenta) cannot grow as fast as in wild type from the beginning and eventually stop growing earlier than wild type (green).

D. Cumulative growth over time. Wild type is shown in green while *xi-k* is shown in magenta.

A

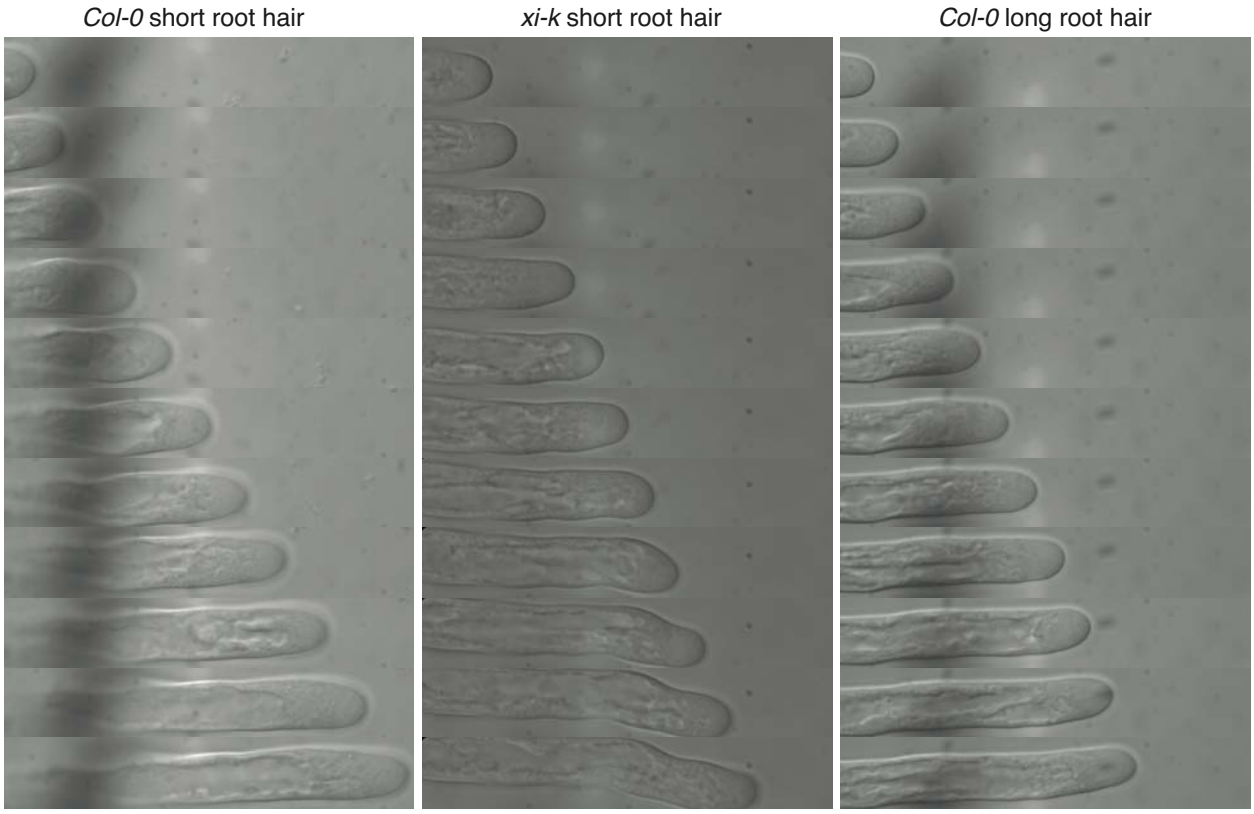
Col-0 short root hair
xi-k short root hair
Col-0 long root hair

B

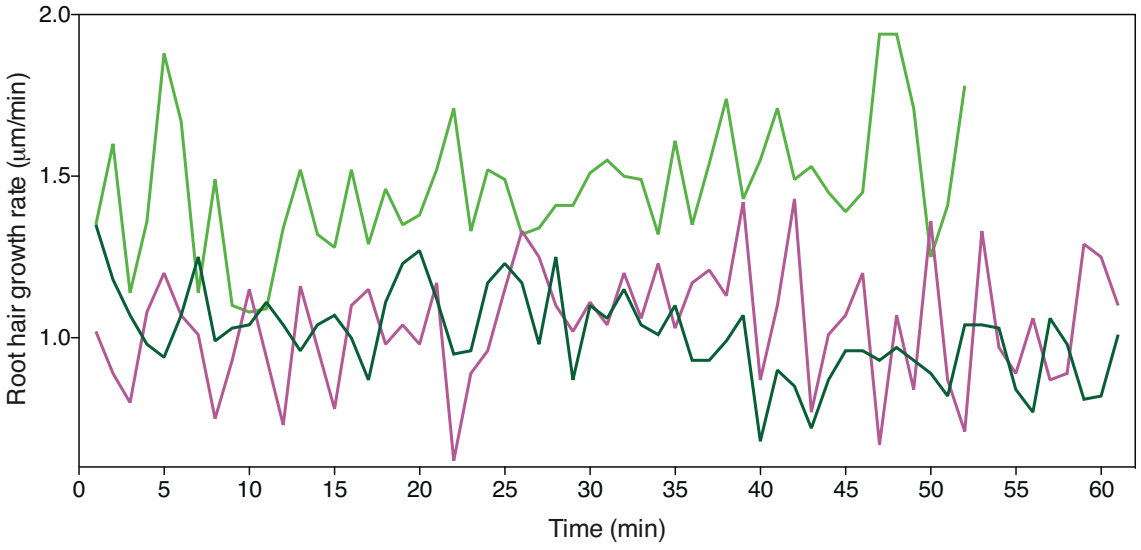
Root hair growth rate (μm/min)
2.0
1.5
1.0
0
5
10
15
20
25
30
35
40
45
50
55
60
Time (min)

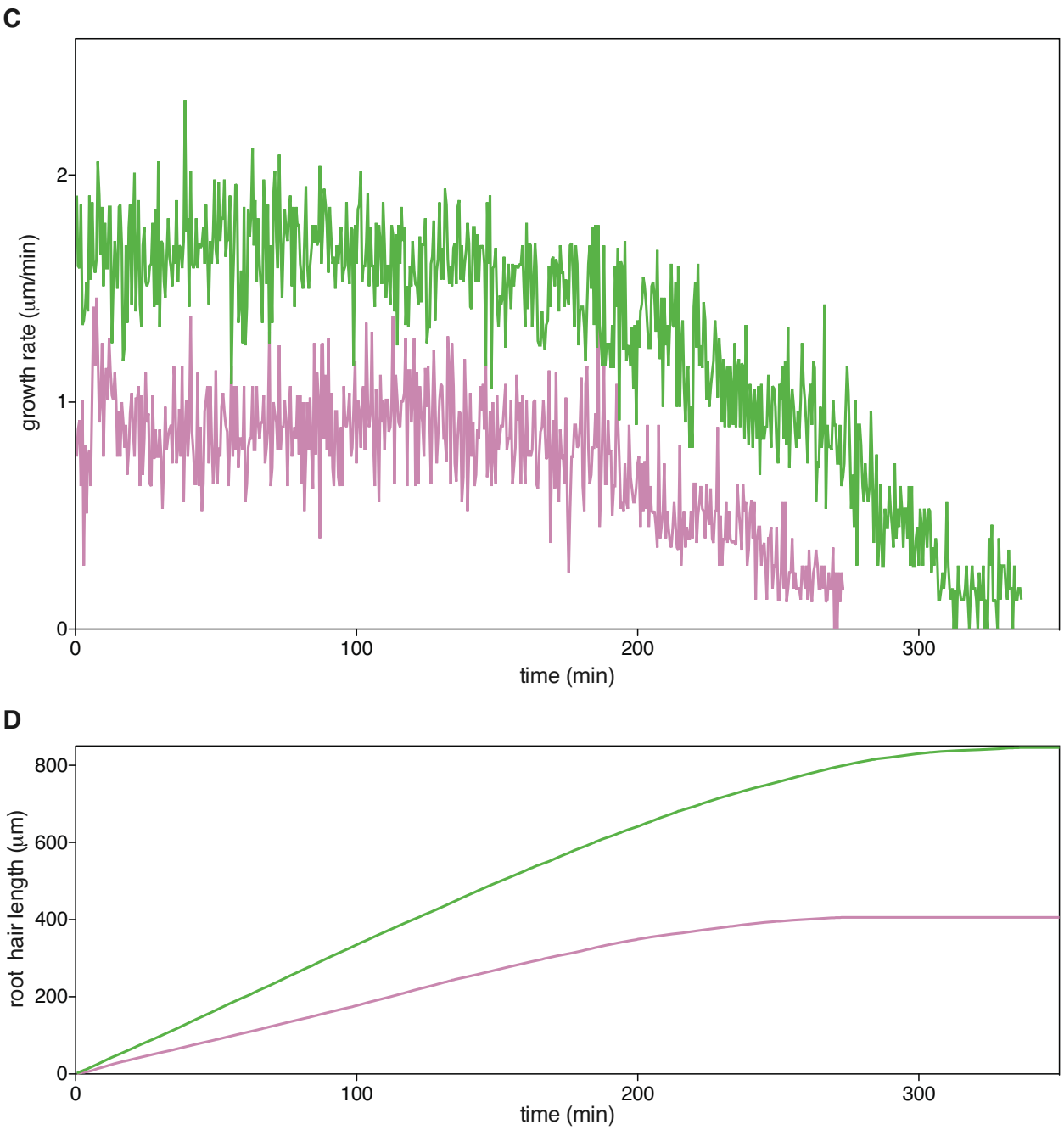

Figure IV.1. Continued

With comparing two root hairs from wild type and *xi-k* with similar average growth rate over time (**Figure IV.2.B and C**), coefficients of variation of the growth rates of *xi-k* root hairs were larger than those of wild type root hairs. While the coefficient of variation of wild type root hairs were 8.62% (green in **Figure IV. 2.B**), 14.71% (green in **Figure IV.2.C**), and 7.02% and 10.79% (**Figure IV. 2.C**), *xi-k* showed higher coefficient of variation than any of wild type (17.65%, magenta in **Figure IV.2.B**; 26.11%, magenta in **Figure IV.2.C**; 20.96%, **Figure IV.2.E**). This result suggests that YFP-RabA4b accumulation in *xi-k* is less stable than in wild type.

To understand the relationship of YFP-RabA4b accumulation and growth rate, growth rates from each sample were compared with their YFP-RabA4b accumulation (**Figure IV.2.F-I**). Although we frequently observed similar changes in RabA4b accumulation and growth rate of root hairs (**Figure IV. 2. F-I**, black arrows), there were also occasional counter examples (**Figure IV. 2. F-I**, yellow arrows), suggesting that there is only a loose correlation of YFP-RAbA4b accumulation and growth rate. However, growth rates of *xi-k* mutants fluctuated more than those of wild type similar to the unstable YFP-RabA4b accumulation in the root hairs of *xi-k* mutants. While coefficients of variation of the growth rates of wild type root hairs are 20.28% (average growth rate: 0.88 ±0.18μm/min, **Figure IV.2.F**) and 30.56% (average growth rate: 0.71 ±0.21μm/min, **Figure IV.2.G**), *xi-k* mutants had coefficients of variation of the root hair of 32.39% (average growth rate: 0.90 ±0.30μm/min, **Figure IV.2.H**) and 31.61%(average growth rate: 0.78 ±0.25μm/min, **Figure IV.2.I**).

Figure IV.2. YFP-RabA4b accumulation at the tip of growing root hair is impaired in *xi-k* mutants

A. Montage of YFP-RabA4b image sequences of Col and *xi-k*. Yellow arrows point to reduced YFP-RABA4b signal at the root hair tip in *xi-k* mutants.

B – E. Coefficient of variation plot of RabA4b accumulation at the root hair tip over time in wild type (green) and *xi-k* (magenta). Grey area indicates the range of variation of RabA4b intensity in wild type. Cumulative growths over time are superimposed with a black line and a grey line for Wild type and *xi-k*, respectively. Panel **B** and **C** show root hairs from wild type and xi-k that showed relatively similar growth rates. Panel **D** showes two wild type root hairs whose growth is almost finished. Note that they still showed relatively consistent accumulation of RabA4b at the tip. Interestingly, very young root hairs (panel **E**) in *xi-k* also showed large variation of YFP-RabA4b accumulation.

F-I. Comparison of RabA4b variation and growth rate per min. Overall, there was only a loose correlation between in both wild type (green) and *xi-k* (magenta). Black arrows indicate the periods that showed a good match of variation of growth rate with RabA4b variation. Yellow arrows indicate the periods that showed a no match of variation of growth rate with RabA4b variation.

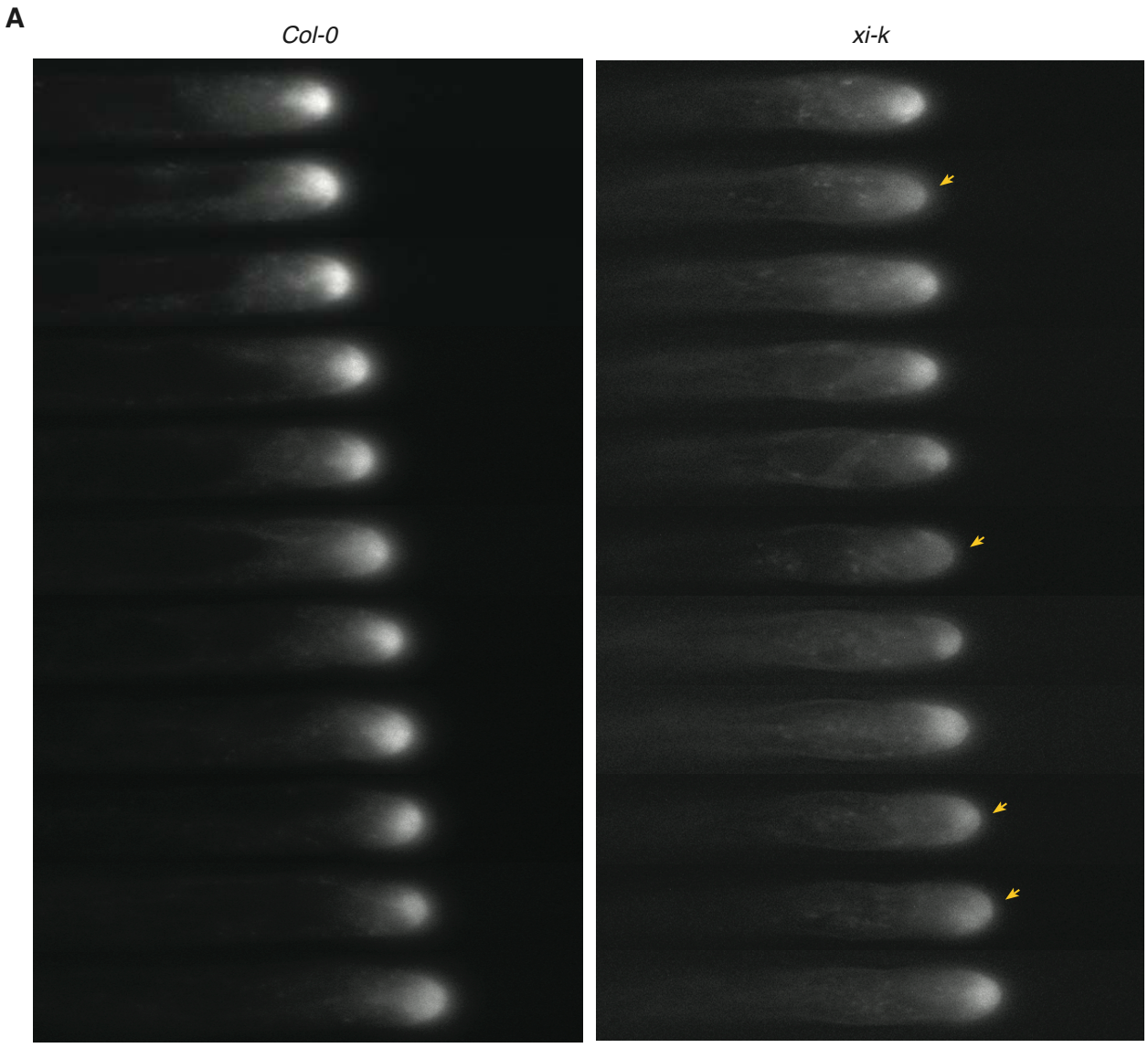
A
Col-0
xi-k

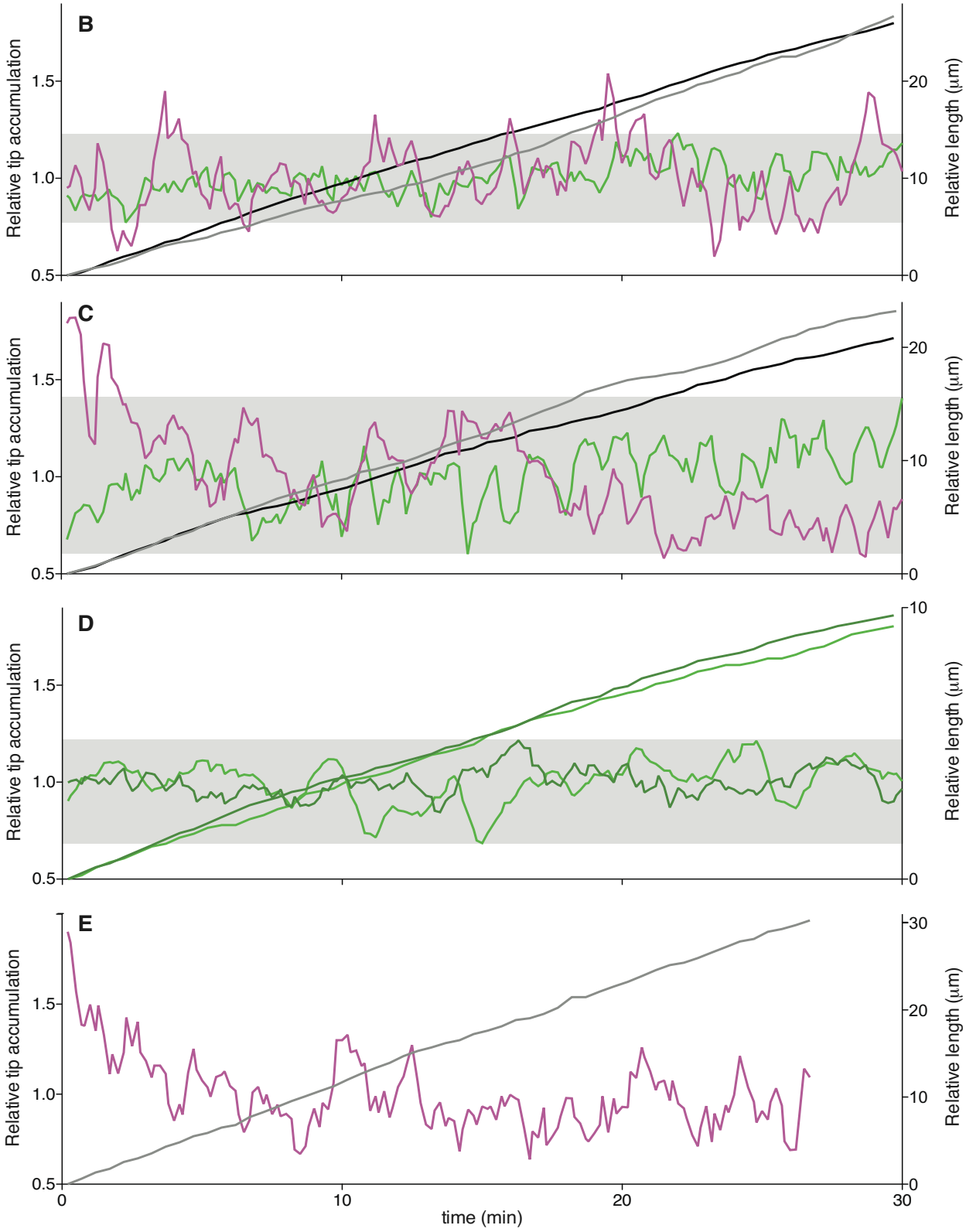

Figure IV.2. Continued

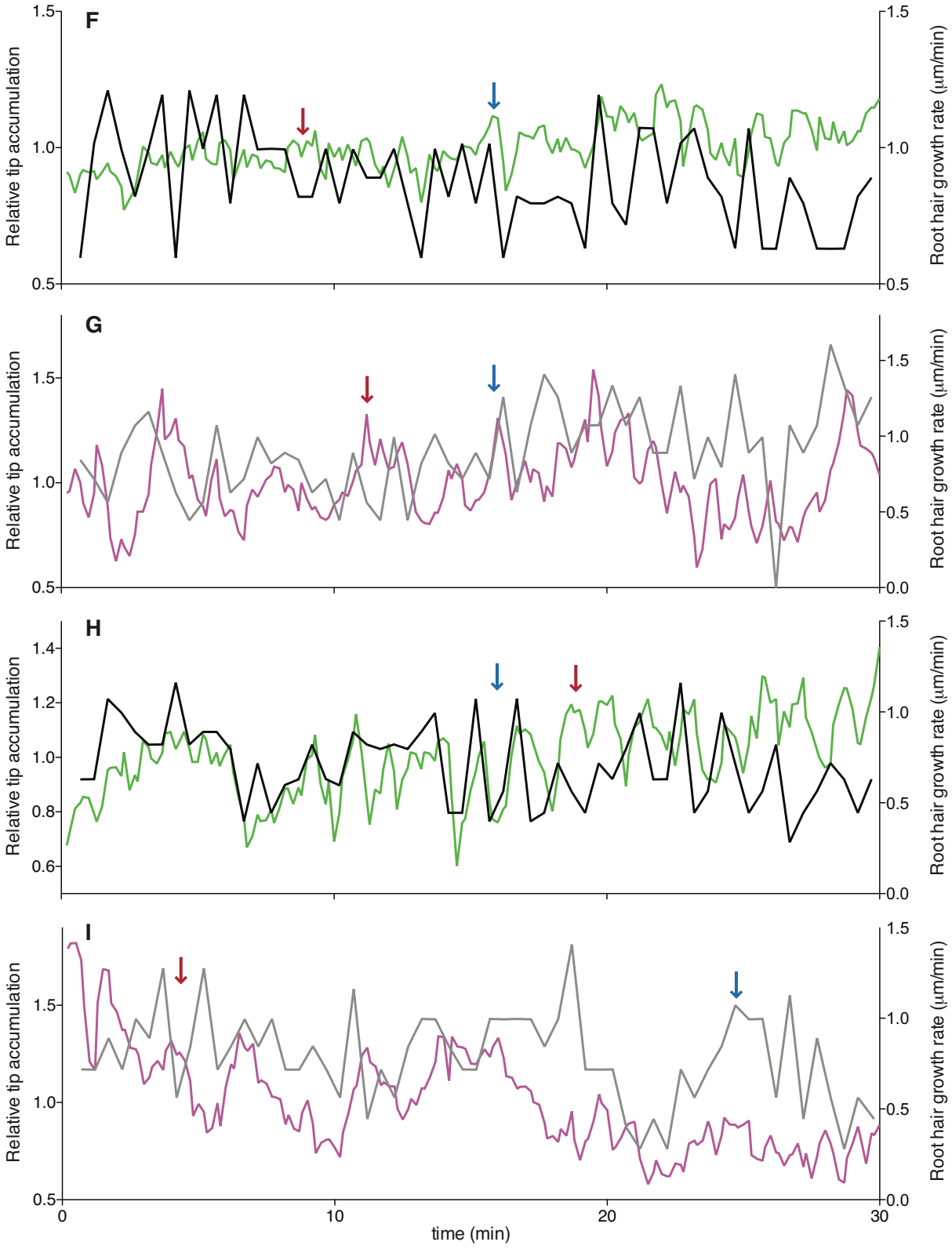

Figure IV.2. Continued

Although we failed to detect a tight correlation between YFP-RabA4b accumulation and root hair growth rate, overall results suggest that growth rate in *xi-k* were more variable that in wild type consistent with the instability of the YFP-RabA4b accumulation at the tip of growing root hairs in *xi-k*.

IV.3.3. PtdIns4P and ER localization were normal in *xi-k* root hair

PtdIns4P kinase is a known effector of RabA4b and their colocalization at the tip of growing root hair has been shown (Preuss et al., 2006). Since RabA4b accumulation at the tip of root hairs in *xi-k* was altered (**Figure IV. 2**), PtdIns4P distribution was observed in the root hairs of *xi-k* using the pleckstrin homology domain of the human phosphatidylinositol-4-phosphate adaptor protein-1 (FAPP1) (Vermeer et al., 2009). However, there was no visible difference between wild type and *xi-k* (**Figure IV. 3.A**) suggesting that the reduced accumulation of RabA4b in xi-k root hairs does not affect the availability of PI4P at the plasma membrane.

Previously, it was suggested that XI-K might localize to the ER, based on results with fluorescently labeled truncated XI-K without motor domain (Sparkes et al., 2008). To test the prediction that XI-K might be involved in ER dynamics, ER distribution was observed in the root hairs of *xi-k* and overall their localization was not different between in wild type and *xi-k* mutants (**Figure IV. 3.B**).

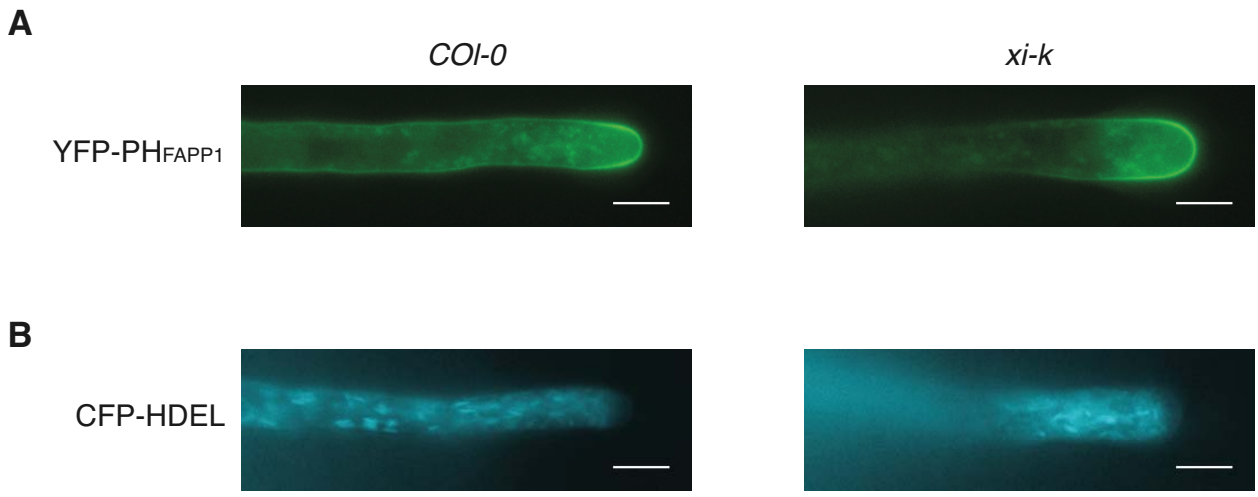

Figure IV.3. No differences of PtdIns4P and ER localization in *xi-k*

A. YFP-PH$_{FAPP1}$ in wild type and *xi-k*. This marker can visualize PI4P lipid in the plasmamembrane particularly stronger at the tip of root hairs.

B. CFP-HDEL in wild type and *xi-k*. This marker labels the ER lumen. Not that this marker does reach into the apex of both wild type and *xi-k* root hair.

IV.3.4. Intracellular Ca^{2+} dynamics during root hair growth in *xi-k*

It has been reported that calcium concentrations in the root hair tip oscillate with 5 sec intervals and are tightly correlated with root hair growth (Monshausen et al., 2008). To define the relationship of XI-K function with calcium oscillations, calcium dynamics were measured by a FRET-based calcium tracker, YC3.6., in wild type and *xi-k* mutants (**Figure IV.4.**). Due to a large variation of data among the samples, it is difficult to conclude whether there is a difference between the genotypes or not. Only a subset of the samples could be fit with low stringency to a sine wave. In particular, only four out of eight observations in wild type root hairs and three out of nine observations in mutant root hairs showed clear oscillations (**Figure IV.4.**). Among these root hairs, the averages of the coefficient of variation of amplitude in wild type and *xi-k* mutants showed statistically no difference (8.20 ±0.032% and 8.71 ±0.026%, respectively. T-test =0.254). Thus, *xi-k* might not have a significant difference in calcium oscillation events during root hair growth.

IV.3.5. Actin dynamics in *xi-k* did not show significant difference from wild type

The actin cytoskeleton is highly dynamic during root hair tip growth (see section I.2. for detail.). As described in chapter III of this study as well as other studies, *xi-k* mutants showed defects in the movements of several organelles (Peremyslov et al., 2008). Since XI-K localization does not match with any of these organelles, actin filament dynamics were observed to determine whether secondary effects of *xi-k* on actin dynamics existed. Similar to calcium

Figure IV.4. Calcium dynamics in *xi-k*

Dynamic calcium changes were monitored at the tip of root hair with the calcium indicator YC3.6. Each sample was grouped based on the genotype (wild type in green and *xi-k* in magenta) and how well its variation could be fit to a sine wave.

A. Wild type group with oscillations

B. *xi-k* group with oscillations

C. Wild type group without clear oscillations

D. *xi-k* group with without clear oscillations

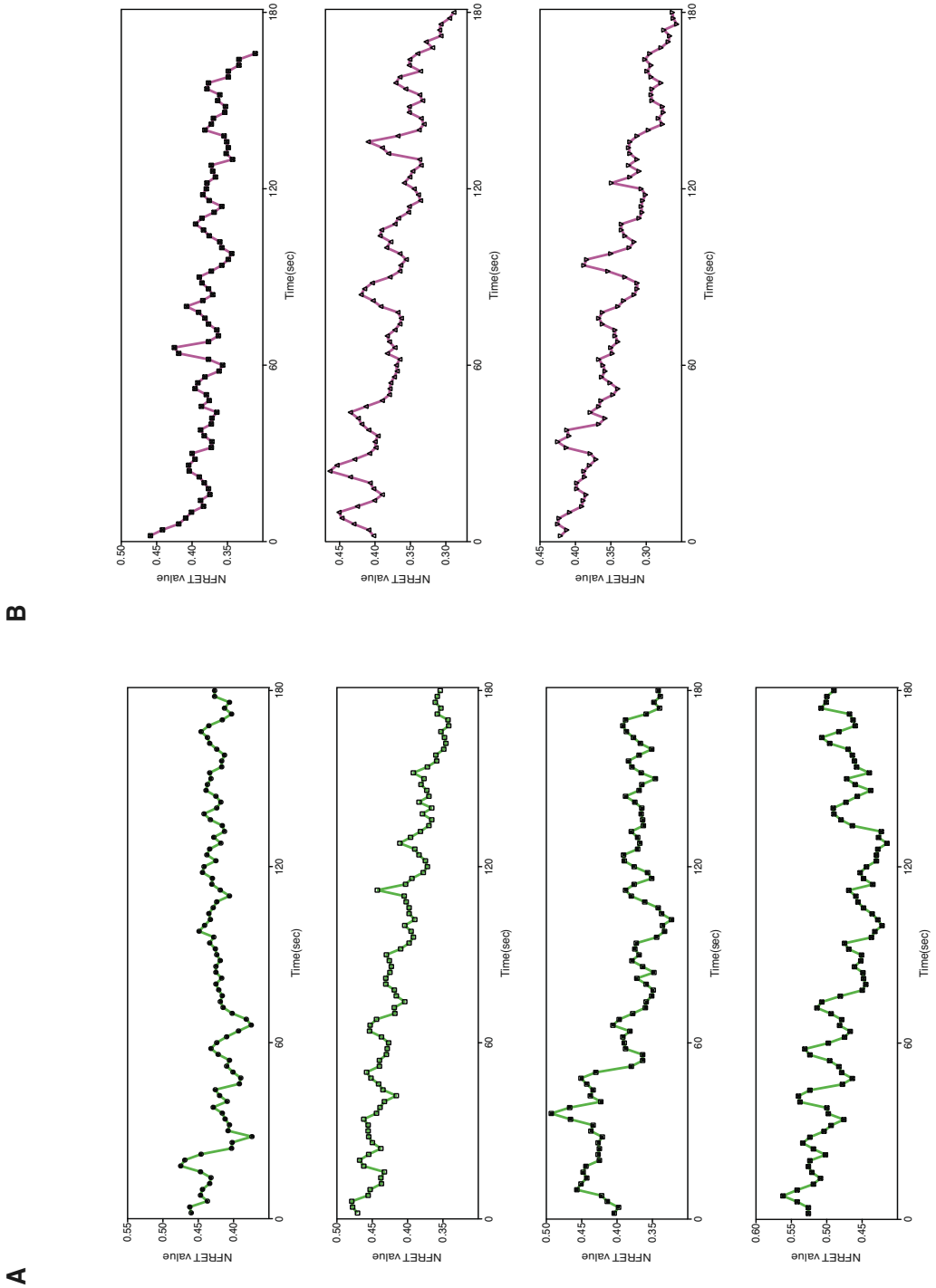
A
B
NFRET value
Time(sec)
0
60
120
180

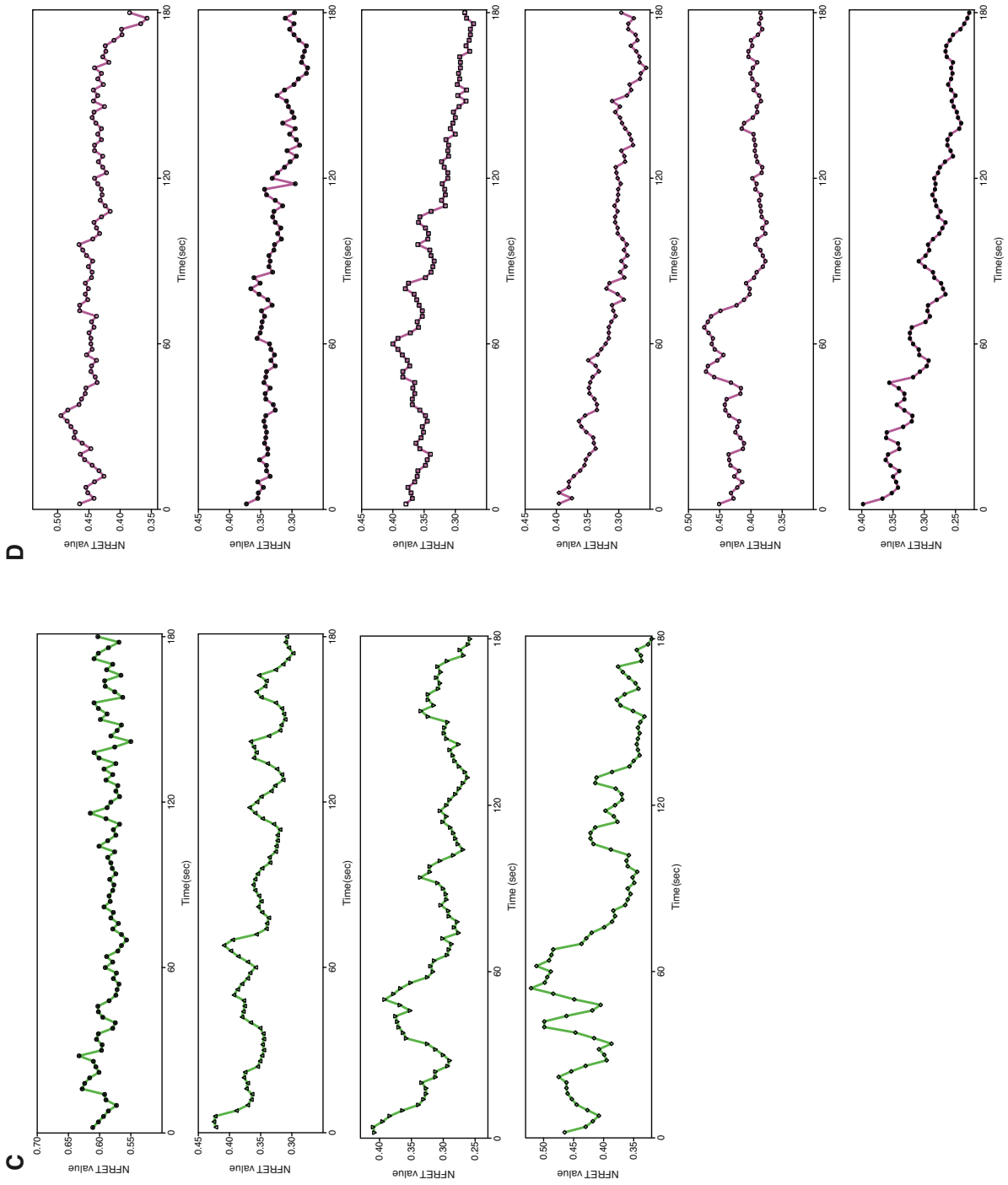

Figure IV.4. Continued

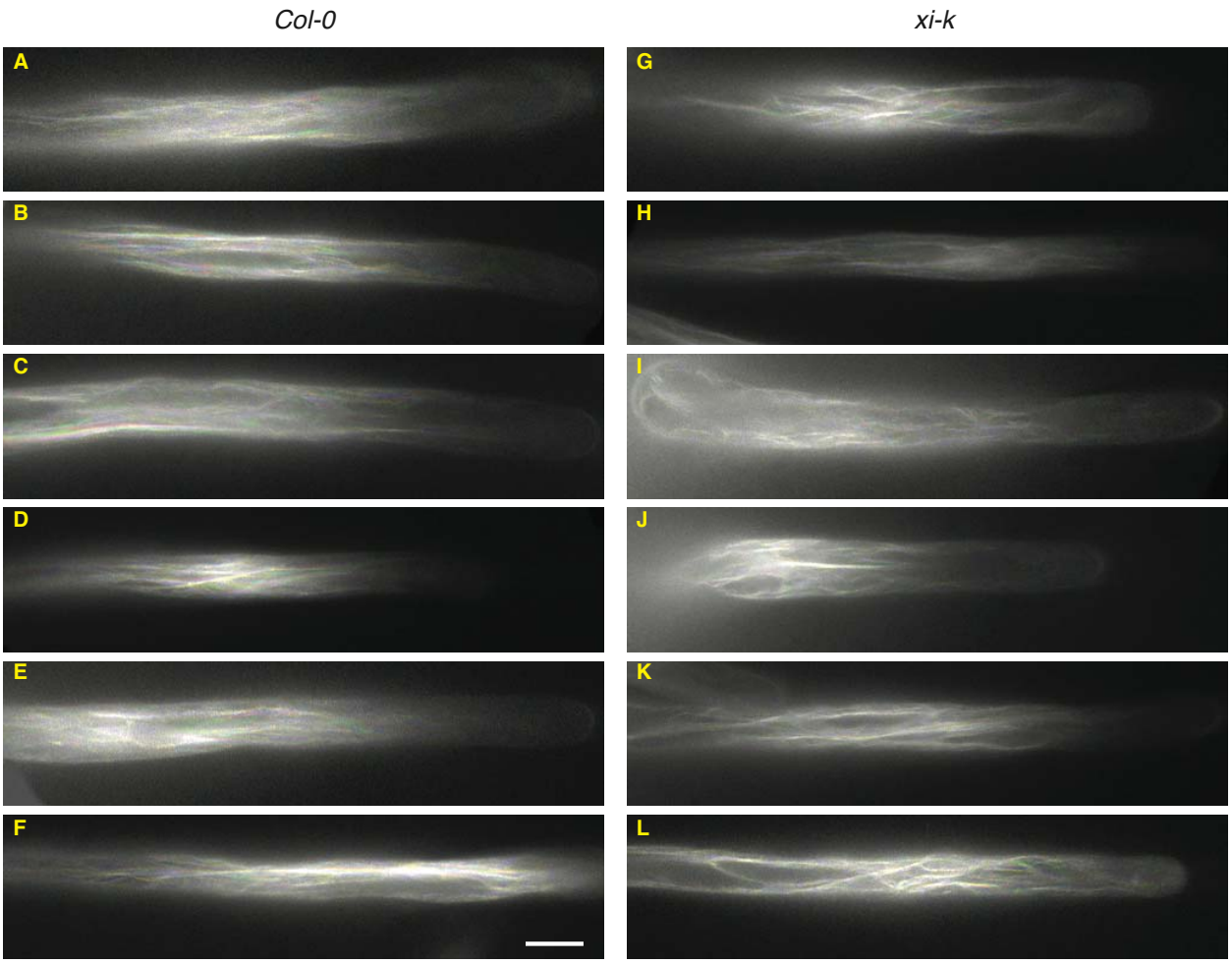

Figure IV.5. Actin dynamics

Actin filaments are visualized with YFP-FABD2 and shown as superimposition of 4 images taken in 5sec interval. Individual images were a pseudo-colored with rainbow spectrum to reveal movements (red, yellow, green, and blue). White indicates no change of position.

A-F. Different samples of wild type

G-L. Different samples of wild type

dynamics, sample to sample variation was very large (**Figure IV.5.**). Differences of pixel brightness from second to second over a one-minute observation period were calculated and coefficients of variation of each time lapses were compared within wild type and *xi-k* mutants. Statistically, there was no difference between wild type and *xi-k* mutants (12.8 ±0.038% and 14.40 ±0.043, respectively. T-test = 0.075), although visual inspection of the time-lapse seemed to suggest reduced activity in *xi-k* mutants (**Figure IV.5.**).

IV.3.6. *XI-Kpro:YFP-XI-K* can complement the short root hair phenotype of *xi-k*

To confirm that the root hair growth defect was caused by knockout of *XI-K*, a wild type XI-K cDNA was transformed into *xi-k* mutant under the control of its native promoter. In addition, YFP was conjugated in front of XI-K cDNA to observe the localization of *XI-K*. Three individual transgenic lines were identified and measured their root hair length. In all cases, *XI-Kpro:YFP-XI-K* could complement *xi-k* root hair growth (**Figure IV.6.A and B**). While an average root hair length of *xi-k* were 0.32 ±0.06mm (SD, n= 370), *XI-Kpro:YFP-XI-K xi-k* had an average root hair length of 0.62 ±0.006mm (SD, n=660) similar to those in wild type (0.61 ±0.004mm, n=730), This suggests that the slower growth of root hairs in *xi-k* mutants resulted from the lack of XI-K motor proteins. In addition, this could also confirmed that YFP-XI-K can function normally in plants, so that we can use these transgenic plants to observe XI-K localization in cells.

IV.3.7. XI-K localizes to BFA-sensitive vesicles at the tip of growing root hairs

YFP-XI-K expression was observed in root hairs. Interestingly, high accumulation of YFP was observed at the tip of growing root hairs, similar to the distribution of YFP-RAbA4b (**Figure IV.7. A** and **Movie IV. 27.**). This accumulation of YFP-XI-K was stable while root hairs are growing, but disappeared when root hairs were fully grown (data not shown). Occasionally, distinct small spots appeared in the shank of root hairs (arrows in **Figure IV.7.A**). The YFP-labeled compartments at the tip of root hairs could have resulted from diffuse cytoplasmic labeling since the root hair tip has a thick cytoplasm unlike the rest of the root hair. Thus, an actin filament inhibitor, LatB, and a vesicle trafficking inhibitor, BFA, were used to observe their effects on YFP-XI-K labeled compartments. Root hairs in ethanol treatments continued to show tip focused YFP-XI-K during the entire hour of observation and root hairs could grow normally (**Figure IV. 7.B** and **Movie IV. 28.**). At the relatively low concentrations of LatB (100nM), tip accumulations of YFP-XI-K dispersed throughout the root hairs with some very large clumps of YFP combined with a stop of root hair growth (**Figure IV. 7.C and Movie IV. 29.**). This suggests that YFP-XI-K localization at the tip of root hairs is actin cytoskeleton dependent.

Interestingly, treatment of 10μg/ml of BFA for 30min showed a gradual loss of YFP-XI-K at the tip of root hairs and the appearance of bigger spots of YFP-XI-K in the shank of root hairs (**Figure IV. 7.D** and **Movie IV. 30.**), suggesting that YFP-XI-K transports small post-Golgi, or endocytic vesicles normally accumulate at the tip of root hairs for root hair growth.

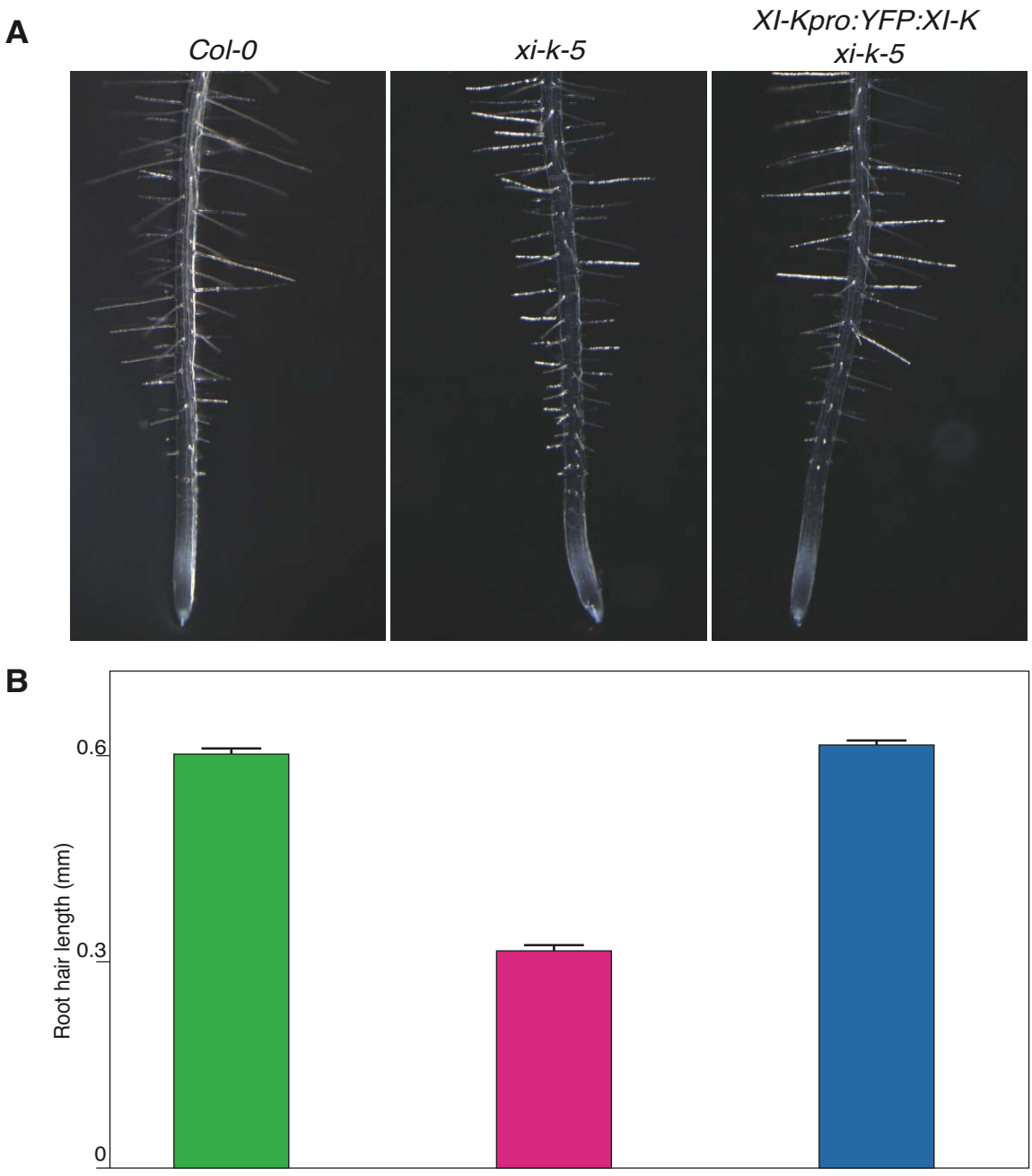

Figure IV.6. *XI-Kpro:YFP-XIK* complements the *xi-k* phenotype

A. Root hairs in transgenic plants showed recovery of root hair growth to levels similar to wild type.

B. Measurement of root hairs lengths in Wild type (green), *xi-k* (magenta), and complemented plants (blue)

Figure IV.7. YFP-XI-K localizes at the tip of growing root hairs

A. YFP-XI-K accumulation at the tip of growing root hairs. Occasionally, small punctate spots (white and yellow arrow in different time point) appear in the shank of root hairs while the tip focused fluorescence is more broadly localized. Scale bar indicate 10 μm.

B. Ethanol treatment did not have any effect on YFP-XI-K accumulation at the tip of growing root hairs.

C. 100nM LatB treatment released YFP-XI-K accumulation at the tip within 30 min. YFP-XI-K then accumulated in large undefined structures throughout the root hairs.

D. 10 μg of BFA treatment led to the gradual release of YFP-XI-K from the tip of root hair. Interestingly, many large spots are resulted from BFA treatment (white arrow).

A

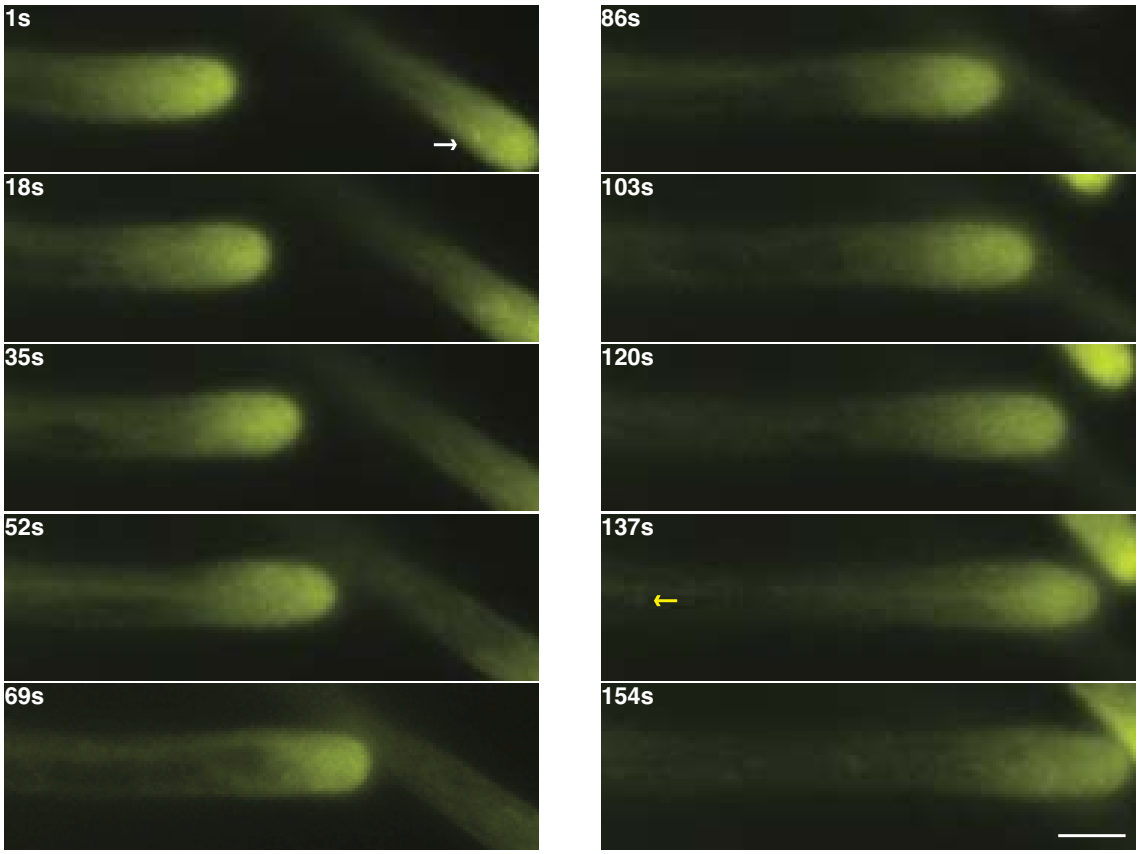

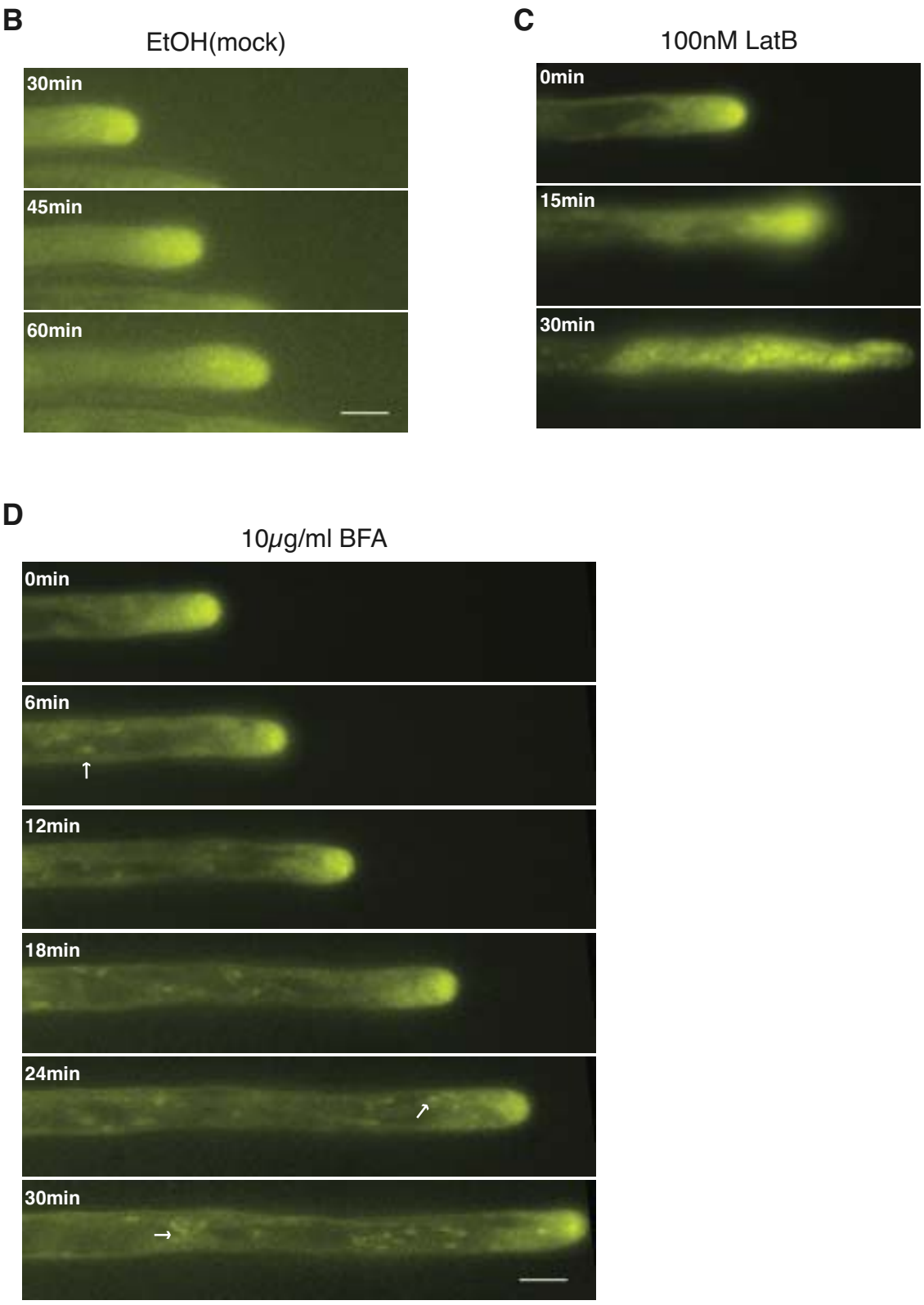

Figure IV.7. Continued

IV.3.8. YFP-XI-K vesicles partially colocalize with YFP-RabA4b vesicles at the tip of root hairs

Several kinds of vesicles were known to accumulate at the tip of growing root hairs (see section I.2. for detail.). Recently, YFP-RHD4 has been shown to accumulate at the tip of growing root hairs and *rhd4-1* showed stochastic YFP-RabA4b fluctuation similar to those in *xi-k* (Thole et al., 2008). Thus, to test for colocalization of YFP-XI-K and CFP-RHD4 or CFP-RabA4b, which are well known to accumulate at the growing root hairs, root hairs of double transgenic plants were observed. While cytoplasmic mCherry was diffuse throughout in the cytoplasm and appeared evenly in the root hair tip, YFP-XI-K was more accumulated at the apical region of root hair tip, confirming that YFP-XI-K is not freely diffusing in the cytoplasm consistent with the results from the previous section. (**Figure IV. 8.A.** and **Movie IV. 31.**). CFP-RHD4 was partially colocalized with YFP-XI-K in the tip region. However, CFP-RHD4 did not accumulate in the apex of the root hair tip, while YFP-XI-K was highly accumulated in that area (**Figure IV. 8.B.** and **Movie IV. 32.)** Interestingly, CFP-RabA4b and YFP-XI-K were colocalized at the apex which is the area whose RHD4 does not localize (**Figure IV. 8. C.**). However, CFP and YFP could be distinguished clearly in different spots along the shank frequently. In addition, tip accumulation of YFP-XI-K and CFP-RabA4b ocassionally were temporally and spatially separated (**Movie IV.33.**), suggesting that vesicles that XI-K attached to might be different from the YFP-RabA4b labeled vesicles. mCherry-ROP2 clearly highlighted the plasmamembrane of root hairs as well as a diffuse distribution in the cytoplasm, as reported previously (Fu et al., 2002) and YFP-XI-K was lack on the plasmamembrane (**Figure IV. 8.D**).

IV.4. DISCUSSION

One isoform of class XI myosin, XI-K, has been identified in the previous chapter of this study as well as by other groups as being involved in root hair growth in *Arabidopsis* (Ovecka et al., 2005; Peremyslov et al., 2008). Shorter root hair length in *xi-k* is due to both slow growth of root hairs and early termination of root hair growth in *xi-k* mutants (**Figure IV. 1.D**).

Information from the colocalization analysis of YFP-XI-K and observation of the localization of other markers demonstrate the presence of YFP-XI-K labeled vesicles at the apex of root hair (**Figure IV. 9.A**). Since root hairs can only grow with a massive delivery of vesicles which provide cell wall materials and membrane lipid to the tip (Guimil and Dunand, 2007), XI-K might deliver important vesicles to control actual cell growth. It is unclear whether XI-K can deliver one kind of vesicles or multiple types of vesicles. There are many vesicle markers which can label an intermediate membrane compartment in secretory pathway. For example, YFP-RabA4b and YFP-PH$_{FAPP1}$ were found in the TGN in addition to secretory vesicles and at the plasmamembrane, respectively (Preuss et al., 2004; Vermeer et al., 2009) Partial colocalization of YFP-XI-K and CFP-RabA4b suggested the existence of new kind of vesicles which XI-K might transport to the tip of root hair, however, we cannot exclude the possibility that XI-K might be able to transport multiple types of vesicles, including RabA4b-labeled vesicles. Careful observation of behavior of YFP-XI-K and CFP-RabA4b in time-lapse images during the treatment with inhibitors to distinguish vesicles from crowded root hair apex might give more information.

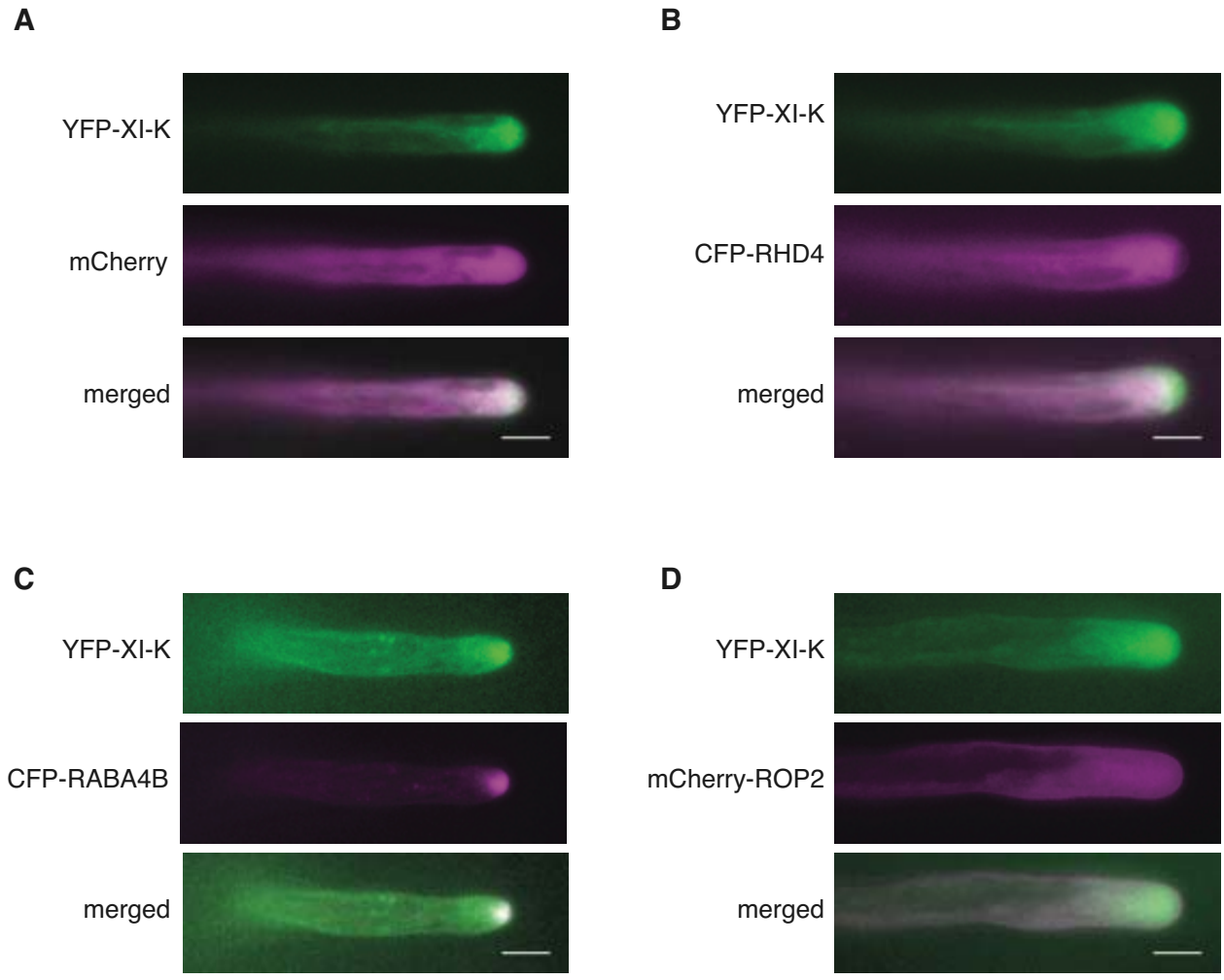

Figure IV.8. YFP-XI-K colocalization information

Colocalization of YFP-XI-K with several markers.

A. *EXP7pro:mCherry*. mCherry signal was diffuse in the entire cytoplasm.

B. *35Spro:CFP-RHD4*.YFP- XI-K and CFP-RHD4 partially overlapped in the subapex of the root hair.

C. *35Spro:CFP-RabA4b*. RabA4b signal largely overlapped with YFP-XI-K at the apex of root hair.

D. *EXP7pro:mCherry-ROP2*. ROP2 labeled the plasma membrane and was clearly distinct from YFP-XI-K

Unlike the tight correlation of tip growth rate with calcium and ROS oscillation (Monshausen et al., 2009), RabA4b accumulation appeared to have only a loose correlation with root hair growth rate (**Figure IV.2**). This might be explained by the difference of time scale between RabA4b accumulation variation and calcium oscillations. Calcium oscillation has been reported with a wave length of about 20 sec and root hair growth rate also oscillate with a similar frequency, although with 5 sec lag behind calcium oscillations (Monshausen et al., 2008). On the other hand, fluctuations of growth rate in this study and of RabA4b accumulation in this study and in previous reports (Preuss et al., 2004; Thole et al., 2008) were observed on the minute scale. Thus, the contributions of calcium and ROS signaling on the one hand and of secretory vesicle trafficking by myosin on the other hand might be different temporal event. This assumption can be supported with the results of calcium dynamics in *xi-k* (**Figure IV.4.**). Although our results included a large variation, we could observe no difference of calcium dynamics between wild type and *xi-k*. This suggests that XI-K functions in a different event of the regulatory mechanism of tip growth and operates on a different time scale than calcium.

The distinctive actin organization and dynamics during tip growth are known to be controlled by multiple factors (reviewed in section 2 of chapter I.). Although there are few studies about the temporal regulation of actin cytoskeleton yet, lack of significant differences of actin dynamics in wild type and in *xi-k* in this study (**Figure IV.5.**) might be explained with the different temporal regulation mentioned above. It might be helpful to more carefully examine longer-term changes of calcium and actin organization in *xi-k* since several studies suggested that vesicle trafficking regulates calcium oscillations and global actin organization (**Figure I.5** for review).

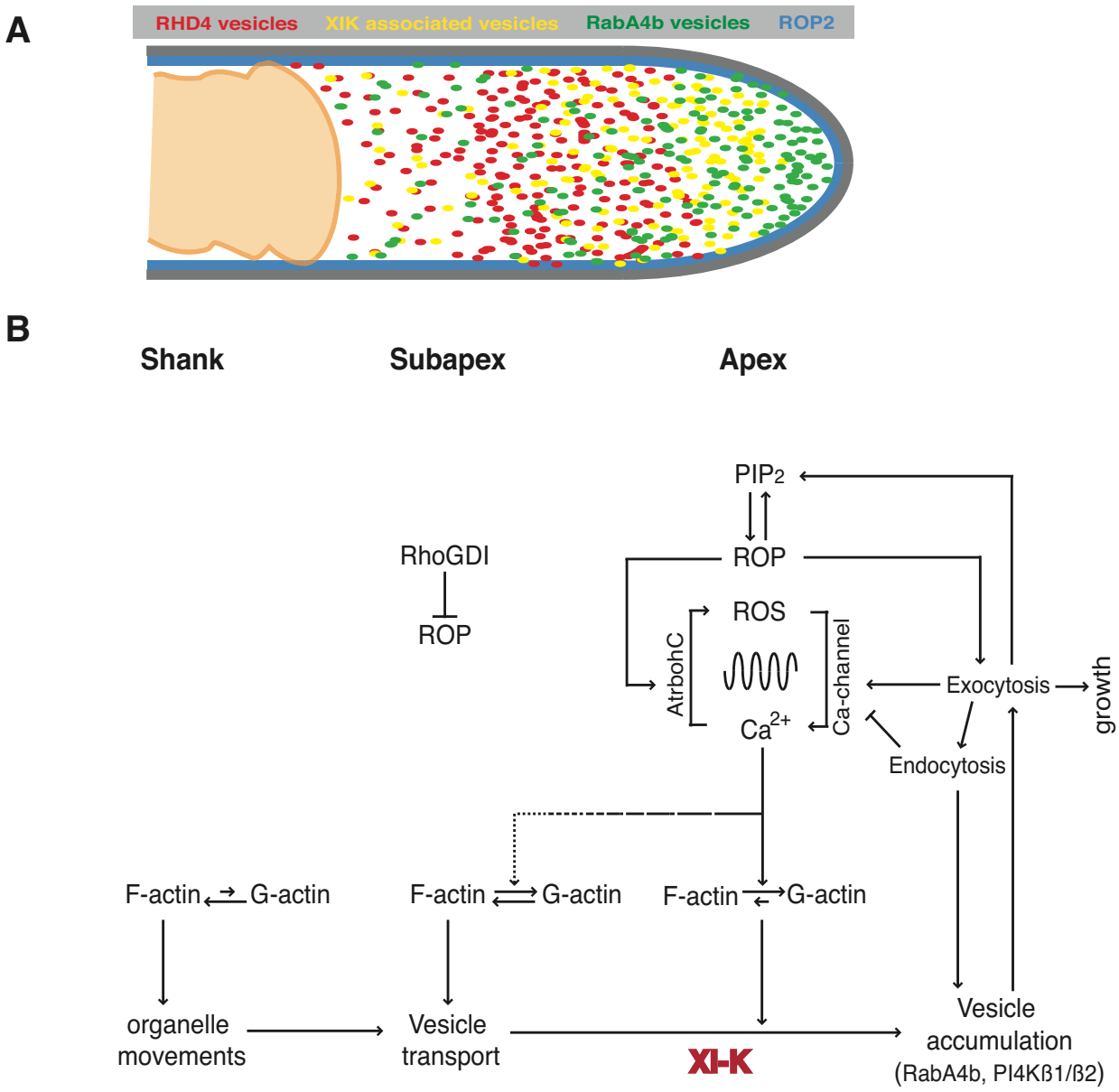

Figure IV.9. Working model of myosin function in root hair tip growth

A. Relative position of markers including YFP-XI-K at the tip of root hairs based on the evaluation of time lapse movies with root hairs in double transgenic plants.

B. Schematic model of XI-K function in root hair tip growth. Results presented in this study that myosin XI-K functions specifically in the delivery of secretory vesicles from the sub apex to the apex.

Due to the lack of information of potential XI-K functions in root hair tip growth, it was not possible to explain the connection between a mutation of *xi-k* and altered organelle movements during tip growth of root hairs. In this chapter, more information about XI-K function in root hair tip growth has been obtained and we proposed a potential myosin function in root hair tip growth (**Figure IV.9.B**). While many studies using various approaches have enforced the relationship of calcium and ROS with root hair tip growth (Monshausen et al., 2007; Monshausen et al., 2009; Monshausen et al., 2008; Takeda et al., 2008), it was relatively unclear how vesicles are transported to the apex of root hairs and how this transport regulates root hair growth in detail. It has been well known that vesicle trafficking in root hairs is actin dependent. This study showed for the first time direct evidence for the myosin dependent vesicle movement to the root hair.

CHAPTER V. Root hair positioning and class XI myosin

◆ *This chapter introduces background and experimental design with some preliminary data. Many of the preliminary data in this chapter have been collected by undergraduate students under the author's guidance (Nilou Soltanian, Annabel Rodriguez, and Kevin Kuo,). Some students presented their research in posters at the conference of undergraduate research (K. K. and A. R.) and will write an honor thesis (K. K.). N.S. contributed to isolating root epidermal cell specific markers in mutant background and K.K. confirmed homozygous mutants with a marker and analyzed GUS expression patterns. A.R. generated results from phosphate deficiency test. The author was involved in developing hypothesis, designing experiments, generating preliminary results. Similar to chapter III in this dissertation, the studies described in this chapter will be from the bases for a future project in this lab.*

V.1. INTRODUCTION

Class XI myosin is generally considered to transport intracellular molecules along actin filaments (Liu et al., 2001). Intracellular trafficking of vesicles and proteins is one of the key regulatory processes for development of multicellular organisms (Šamaj et al., 2006). Although there is up to now not much direct evidence, it is assumed that class XI myosins transport cargo that has which have critical roles for plant development (Campanoni and Blatt, 2007).

As mentioned in the previous chapter, two mutants of class XI myosins in *Arabidopsis thaliana*, *mya1* and *xi-h*, showed an increase of frequency of root hairs on root epidermis (Chapter III.3.3.). *Arabidopsis* normally has type III root hair positioning plan that displays a "stripe" pattern of root hairs which depends on the relative position of epidermal cell files on cortical cells. Molecular and genetic mechanisms of root hair patterning have been extensively studied with several mutants and corresponding gene expression patterns (Schiefelbein et al., 2009). However, the contribution of myosins to the determination of cell fate in the root epidermis has not been studied. Based on the biochemical function of myosin which transports cargo in the cell, we can hypothesize that MYA1 and XI-H transports factor(s) which is (are) involved in cell patterning process of root epidermis.

Based on the pathway established for positionally cued patterning and environmental factors (**Figures I.8. and 9.**), it is possible to hypothesize that myosin is involved in one of two events (**Figure V.1.**). First, myosin might be involved in the trafficking of GL3/EGL3 transcription factors (**Figure V.1.A.**). Although it is predicted that GL3/EGL3 travel from H-cells to N-cells for their function, there is no study about how these proteins move from cell to

Figure V.1. Two hypotheses of myosin involvement in root hair positioning

A. Potential myosin function in GL3/EGL3 trafficking from H-cells to N-cells.

B. Potential myosin function in phosphate perception in root epidermis.

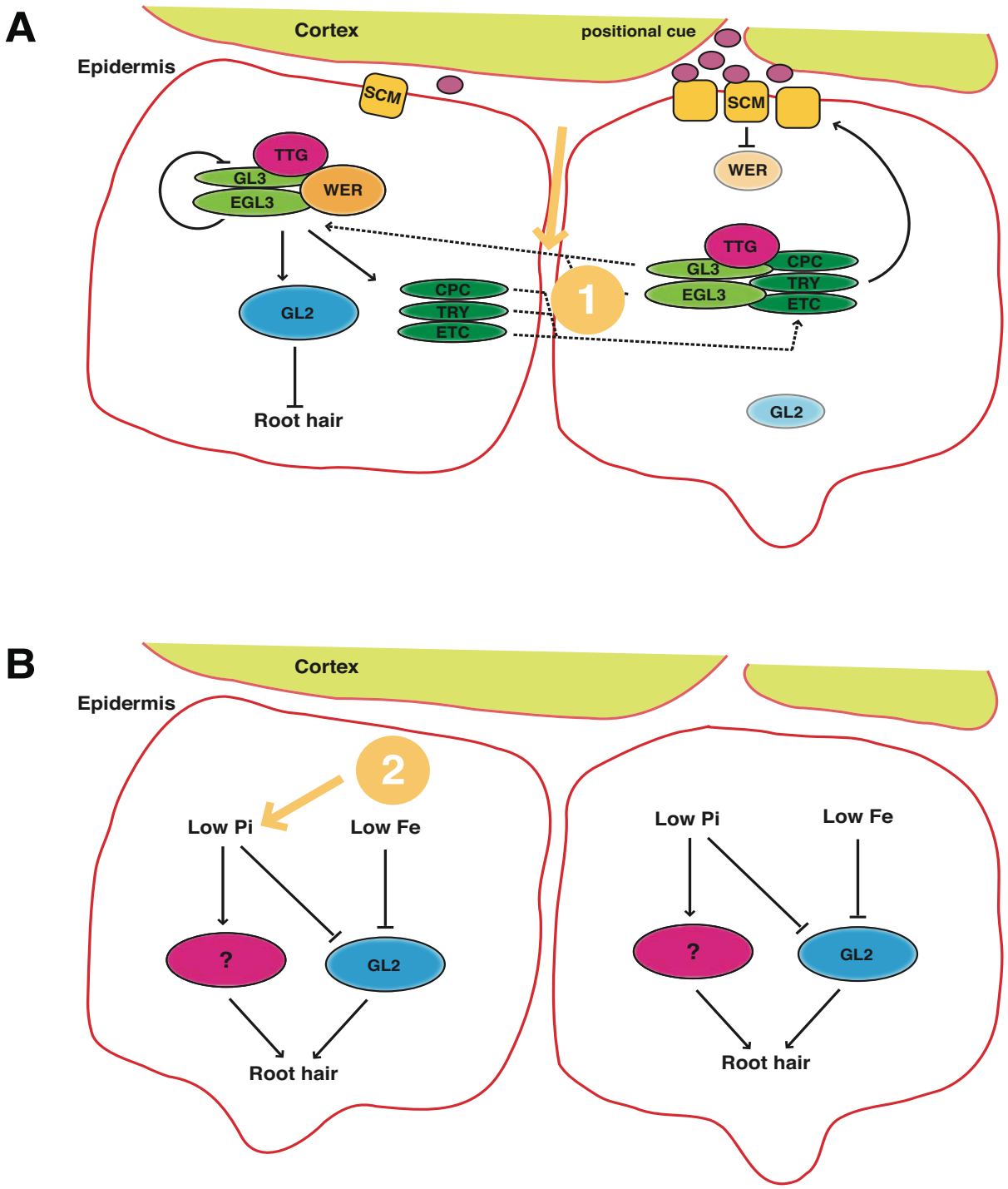
A
Cortex
positional cue
Epidermis
SCM
SCM
TTG
GL3
EGL3
WER
WER
TTG
CPC
GL3
TRY
EGL3
ETC
GL2
CPC
TRY
ETC
1
Root hair
GL2
B
Cortex
Epidermis
2
Low Pi
Low Fe
Low Pi
Low Fe
?
GL2
?
GL2
Root hair
Root hair

cell. CPC, a transcription factor that is assumed to travel from N-cells to H-cells, was proposed to travel through plasmodesmata based on the studies of the related of proteins, e.g. SHORTROOT which has been shown to travel through plasmodesmata (Wada et al., 2002). Whether GL3/EGL3, bHLH transcription factors, can move through the plasmodesmata has not been demonstrated yet.

As a second possibility of myosin function in root hair positioning mechanism, myosin might be involved in phosphate uptake or perception in the root epidermis (**Figure V.1.B.**). Ectopic root hairs on N-cells have been observed in phosphate limitation (Bates and Lynch, 2000b; Müller and Schmidt, 2004; Zhang et al., 2003). Furthermore, it has been shown that this mechanism is independent of the cell fate determining mechanism by a positional cue based on studies with several mutants involved in root hair positioning (Müller and Schmidt, 2004). However, mechanism of this signaling has not known in detail. Since myosin *mya1* and *xi-h* mutants produce ectopic root hairs on N-cells, it is necessary to verify myosin involvement in the phosphate-signaling pathway on root hair positioning.

In this study, two myosin mutants have been used to investigate the role of myosins on root hair positioning mechanism. At least two alleles of *mya1* and *xi-h* mutants were observed for root hair production in N-cells as well as H-cells and crossed with promoter:GUS plants of major genes involved in positional signaling cascade, *WERpro: GUS*, *EGL3pro: GUS*, and *GL2pro: GUS*. In addition, sensitivity of phosphate deficiency was tested to test for possible myosin involvement in root hair production mechanism in response to phosphate deficiency. because of the lack of functional study of myosins in plant development, this study might be significant as a preliminary contribution to investigate myosin function in plant root development.

V.2. MATERIALS AND METHODS

V.2.1. Mutant phenotype analysis

Four lines of *mya1* and two lines of *xi-h* were confirmed as homozygous for T-DNA insertion (**Table II. 4.** in chapter II.). Images of 5-day-old seedlings grown on vertical plates described in the previous chapter were captured with a Leica stereomicroscope (Leica MZ16 FA, http://www.leica-microsystems.com) equipped with a digital camera (Leica DFC420) under 23X magnification or 75X magnification. The number of root hairs were counted over 5mm length of root for each genotype and statistically analyzed by Prism 5 (www.graphpad.com).

V.2.2. Root hair positioning markers

Homozygous plants containing root hair specific promoter:GUS constructs were obtained from the Schiefelbein lab, the Unversity of Michigan (Schiefelbein, 2003). Since they were in different ecotypes- *WERpro:GUS* in *Col-0*, *EGL3pro:GUS* in *Ler*, and *GL2pro:GUS* in *WS*, they were crossed to *Col-0* as well as *mya1-5* and *xih-1*. Genotypes of F2 plants were confirmed by PCR with primers for detecting T-DNA insertion (TLba-1, 1T5-LP, and 1T5-RP; see chapter III for primer sequences) and GUS staining. Conventional GUS staining was modified to yield better distribution between expressing and non-expressing cells. Plants were pre-incubated in staining buffer containing without X-Gluc (100mM $NaPO_4$ (pH7.0), 10mM EDTA, 0.1% Triton X-100, 5mM $K_3Fe(CN)_6$, and 5mM $K_4Fe(CN)_6$) for 15minutes at room temperature followed by incubation in the staining buffer (with 2mM X-Gluc) for 20 min at 37°C. After clearing with

serial concentration of ethanol for at least 4 hours, pictures of plants are taken under the stereomicroscope (Leica MZ16FA, http://www.leica-microsystems.com) equipped with digital camera (Leica DFC420) and Leica FW4000 image acquiring software.

V.2.3. Phosphate deficiency test

Col-0, *mya1-5*, and *xi-h-1* seeds were germinated on one-quarter strength MS media containing different concentrations of phosphate. Phosphate concentrations were chosen based on the previous research (Müller and Schmidt, 2004). Briefly, MS media without phosphate (Caisson laboratories Inc.) were solidified with 0.5% phytagel including 1% sucrose and five different concentrations of phosphate (1 μM, 10 μM, 30 μM, 100 μM, and 300 μM) adjusted pH to 5.7. After two days of stratification, plates were placed vertically in a growth chamber at 22°C under long day conditions (16 light, 8 dark). Pictures were taken seven days after germination with a stereomicroscope at a magnification of 23X. Root hairs on 5 mm of roots were then counted with ImageJ (NIH).

V.2.4. MYA1 localization test

For myosin localization and mutant complementation test, full-length *MYA1* fused with YFP under control of its native promoter was assembled by several lab members and transformed into plants by *Agrobacterium*-mediated transformation. Stable transgenic plants were selected on hygromycin B selection media followed by fluorescence observation in T2 or T3 generations.

V.2.5. Tissue specific complementation test

For tissue specific complementation, GAL4-UAS two components systems were designed (**Figure V. 2**). Epidermis or cortex-specific enhancer trap plants were selected in a catalog from Haseloff lab at the University of Cambridge and ordered from the Haseloff and Poethig collections in ABRC (http://www.arabidopsis.org). These enhancer trap plants were already confirmed for GAL4 activity in specific tissues of root. J0481 (CS9093) and Q1220 (CS9224) have confirmed GFP expression only in epidermal cells, while J0571 (CS9094) showed exclusive GFP expression in the cortex. Those plants were then crossed with *mya1-5* to yield mutants with the GAL4 construct.

To construct the other component, five repeats of GAL4 responsive upstream activation sequences (UAS) were obtained from the plasmid pUAST by PCR with UAS-F (5'- CGGAGCT CCCTGCAGGTCGGTCGGAGTAC -3') and UAS-R (5'-CGGTCGACCCCAATTCCCTATTC AGAG -3'). A minimal plant prove to, i.e. a sequence of the -90 region of 35S promoter was also amplified using primers (35S(-90)-F; 5'-GAGCTCGCCTCGAGACATCTCCACTGACGTAAG G -3' and 35S(-90)-R; 5'- ACTAGTGGATCC GGTCGACGATCTGGGCTGTCCTCTCC -3'). The UAS PCR fragment and 35S(-90) PCR fragment were then inserted into the plasmid pBS-KSII. Full-length *MYA1* was ligated behind the 35S(-90) fragment.

V.3. RESULTS

V.3.1. The number of root hairs is increased in *mya1* and *xi-h* mutants

In chapter III of this dissertation, it was described that *mya1* mutants and *xi-h* mutants showed more root hairs than wild type. To confirm whether they produce more root hairs, different alleles of *mya1* and *xi-h* mutants were grown on the vertical plates for 5 days and photographed. The number of root hairs on a 5 mm long segment of root were counted in individual seedlings (**Figure V.3.**). Wild type seedlings displayed 24.48 ± 2.47 root hairs per mm of root. Four alleles of *mya1* mutants showed different results. While *mya1-1* produced 26.15 ± 1.53, which is not significantly different from *Col-0*, on the other hand, *mya1-2*, *mya1-4*, and *mya1-5* produced 26.84 ± 1.53, 29.0 ± 1.74, and 29.69 ± 4.17, root hairs per mm, respectively. These members are significantly different from wild type ($P < 0.002$). *mya1 xi-k* double mutants also showed increased numbers of root hairs compared with wild type, as expected. Interestingly, two alleles of *xi-h*, *xi-h-1* and *xi-h-5*, showed a dramatic increase of root hair numbers over wild type (36.29 ± 1.24 and 36.86 ± 4.84, respectively). In summary, *mya1* and *xi-h* mutants produced more root hairs than wild type in the same growth condition.

V.3.2. Increase in root hair numbers resulted from ectopic root hairs on atrichoblast cells

The increase in root hair numbers could be caused by two different mechanisms. First, it is possible that root epidermis lost their fate to be non-hair cells thus non-hair cells could

Figure V.2. Schematic diagram of GAL4-UAS two components system

To test MYA1 function, targeted expression system was introduced. System was adopted by Haseloff laboratory in University of Cambridge from similar system widely used in *Drosophila*.

A. *GAL4* activator with *UAS-GFP*$_{ER}$ construct. This construct contains *GAL4-VP16* transcription factor gene as well as ER targeted-mGFP5 under control of *UAS* elements. Plants containing this construct can express *GAL4* based on a plant-driven enhancer upstream of the integration site of this construct. Then GAL4 transcription factor can activate *GFP,* resulting in localized expression of GFP as controlled by the plant enhancer.

B. *UAS-MYA1* construct. As a counterpart of GAL4 activator construct, this construct contains six repeats of upstream activation sequences (UAS) and a minimal promoter region GAL4 can specifically bind to the UAS elements to activate the downstream gene, i.e. *MYA1*. Full length *MYA1* introduced *UAS* for targeted expression by GAL4.

C. Experimental strategy. GAL4 activator constructs were randomly transformed into plants and categorized by their GFP expression patterns. Pre-selected three lines which show GFP expressions only in either root epidermis (Q1220 and J0481) or cortex and endodermis (J0571) were crossed to *mya1* to integrate GAL4 activation in *mya1* mutants. Meanwhile the construct containing *MYA1* under *UAS* will be generated and transformed into *mya1*. Crossing two transgenic plants in *mya1* mutant background then leads to *MYA1* expression only in the targeted tissue.

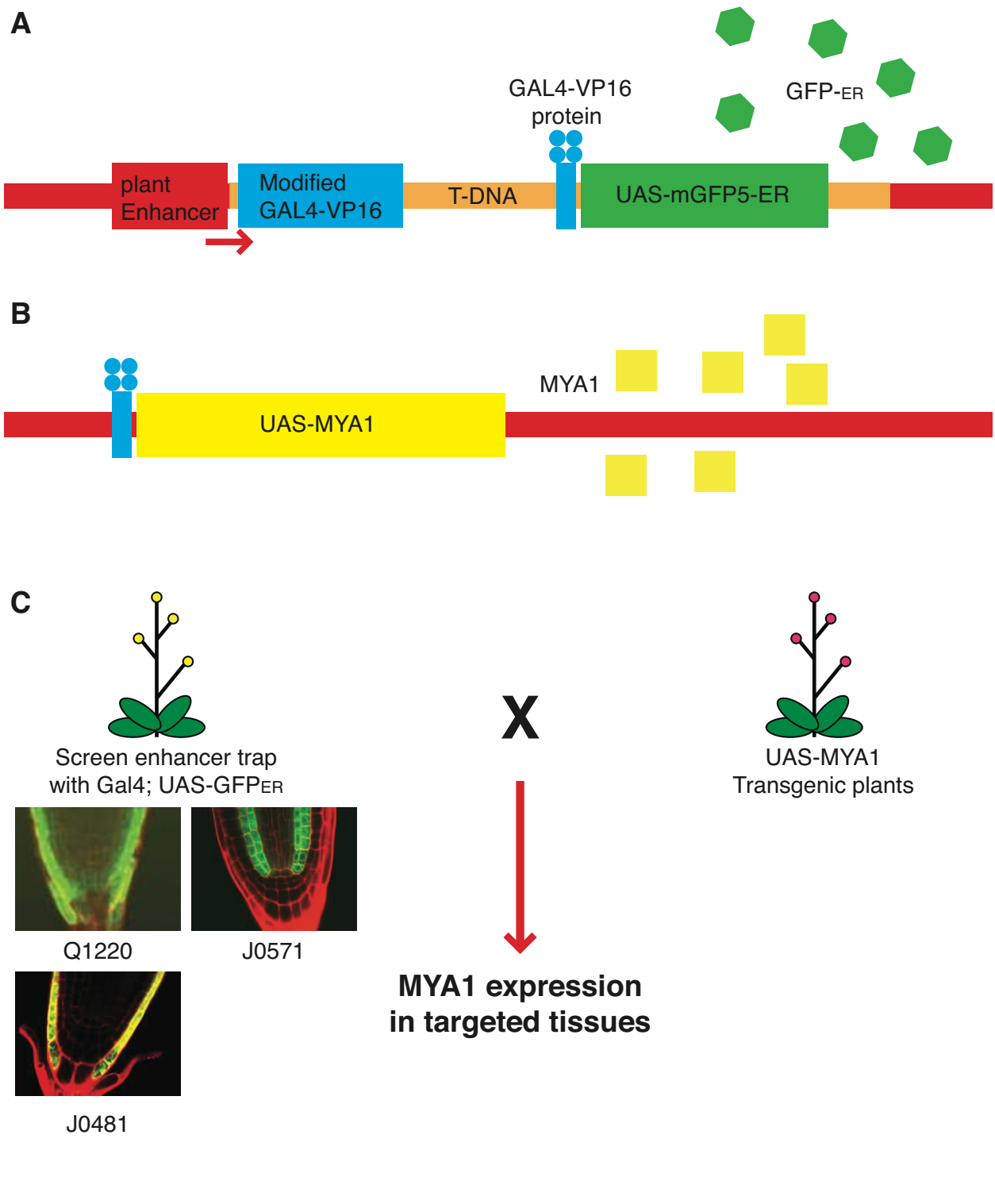
A
GAL4-VP16
protein
GFP-ER
plant
Enhancer
Modified
GAL4-VP16
T-DNA
UAS-mGFP5-ER
B
MYA1
UAS-MYA1
C
X
Screen enhancer trap
with Gal4; UAS-GFPER
UAS-MYA1
Transgenic plants
Q1220
J0571
J0481
MYA1 expression
in targeted tissues

produce root hairs. On the other hand, hair cells might have a defect on maintaining planar polarity, so that an additional root hair grows at a different site on a single hair-producing root epidermal cell. Based on pictures used for root hair counting (23X magnification), mutants seemed to have ectopic root hairs in N-cells but not more root hairs from single H-cells. However, it was not always possible to distinguish individual epidermal cells. Thus, to clarify the cause of increase of root hair numbers in mutants, images were taken at a higher magnification under stereomicroscope (75X magnification) and root hair position on epidermis was observed carefully (**Figure V.4.**). Interestingly, N-cells of mutants occasionally produced root hairs (white arrows in **Figure V.4.B** and **C**) while individual H-cell (ectopic root hair producing N-cell, as well) did not have multiple root hairs (yellow arrows in **Figure V.4.B** and **C**). In addition, position of N-cell and H-cell files were often shifted, so that N-cell pile started producing root hairs and changed to a H-cell file later while a neighbored H-cell eventually became N-cell file resulting two root hair cell files in parallel (**Figure V.4.B. and C.**). This observation suggests that, in *mya1* and *xi-h* mutants, the cells fate determination machinery in the root epidermis is not functioning properly.

V.3.3. Mutation of *MYA1* affects the normal patterning of root hairs.

The genetic mechanism of determining root hair epidermal cell fate depending on positional cues has been studied extensively (see chapter I.3 in this dissertation and Schiefelbein et al. 2009 for detail). To understand a potential myosin function on fate determination in the root epidermis, we develop two hypotheses of myosin function in the root hair positioning signaling pathway (**Figure V. 2.**).

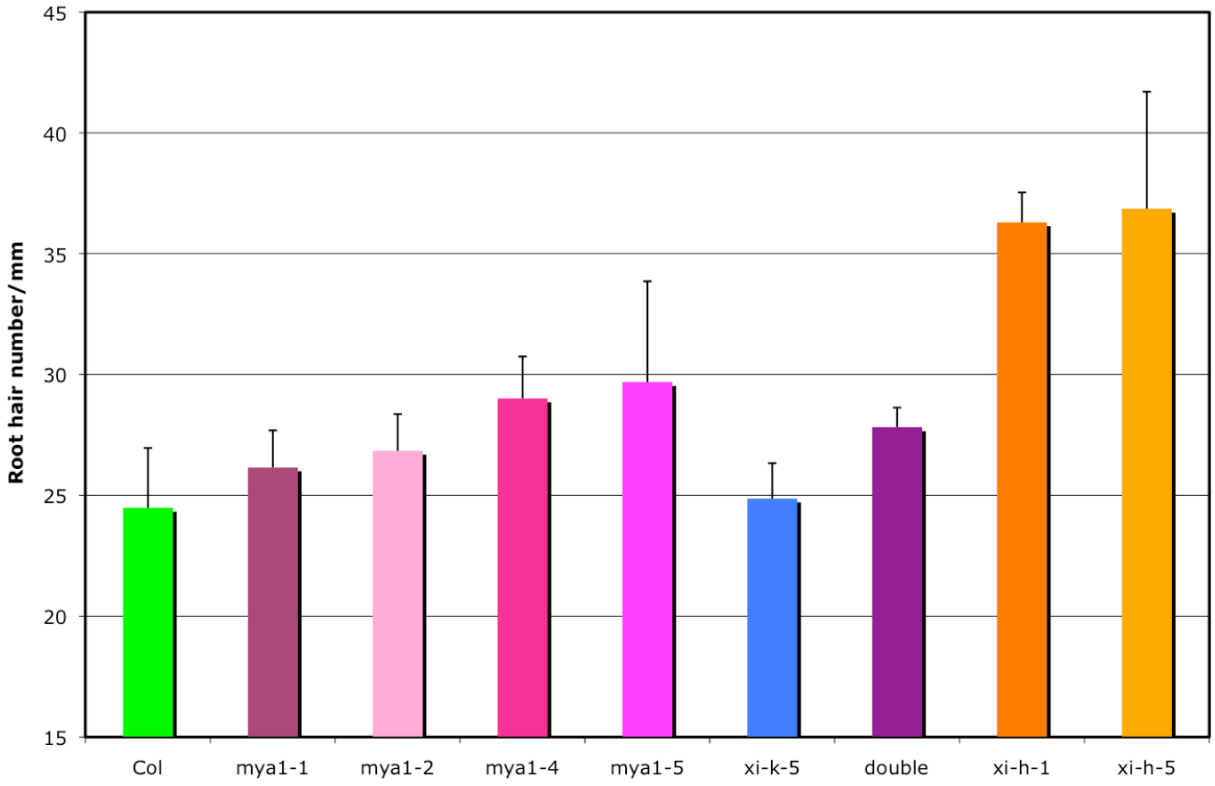

Figure V.3. *mya1* and *xi-h* mutants show more root hairs than wild type.

Several alleles of *mya1* (*mya1-1*, *mya1-2*, *mya1-4*, and *mya1-5*) and *xi-h* (*xi-h-1* and *xi-h-5*) were counted their root hair frequency. *xi-k-5* does not produce more root hairs but shorter root hairs. Double mutation of *MYA1* and *XI-K* still retain both *mya1* and *xi-k* phenotypes.

Figure V.4. *mya1* and *xi-h* mutants have ectopic root hairs on non-hair cells

A. *Col-0*. Root hairs are growing on H-cell files resulting a longitudinal array of root hairs. Cell files adjacent to H-cells did not produce root hairs.

B. *mya1-5*. While yellow arrows indicate normal root hairs from H-cells, white arrows indicate additional root hairs from N-cells. Unlike in wild type, two cell files produced root hairs.

C. *xi-h-1*. While yellow arrows indicate normal root hairs from H-cells, white arrows indicate additional root hairs from N-cells.

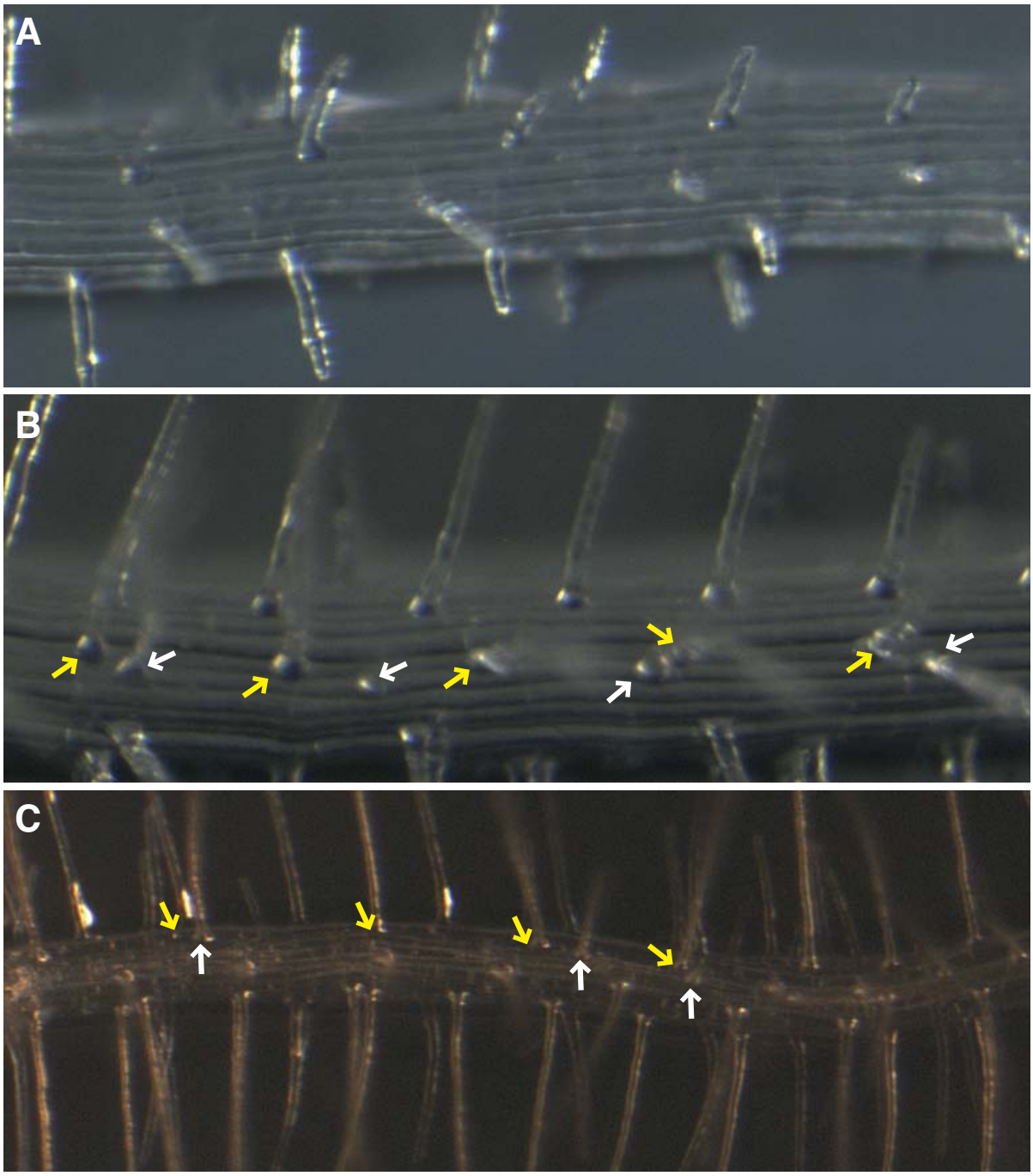
A
B
C

To evaluate these hypotheses, three markers of root hair positioning were obtained from Schiefelbein lab. WER, EGL3, and GL2 are key players in positional signaling for cell fate determination and their cell file-specific expression is well established (Bernhardt et al., 2003; Lee and Schiefelbein, 1999). *WERpro:GUS* in *Col-0*, *EGL3pro:GUS* in *Ler*, and *GL2pro:GUS* in *WS* ecotype of *Arabidopsis* were crossed with *mya1-5* plants. F2 plants from this cross were genotype by PCR with primers for identifying T-DNA insertion in *MYA1*. So far, we could obtain *GL2pro:GUS mya1*. The pattern of *GL2pro:GUS* expression were observed by GUS staining with seedlings (**Figure V. 5.**). To eliminate possible effect from different ecotype, F2 progenies identified to have *MYA1*/+*; GL2pro:GUS*/+ were used as controls. Interestingly, homozygous *mya1* seedlings showed misplaced GUS expression. Although range of disarrangement of the GUS staining is large in individual seedlings and wild type plants also displayed irregular patterns of GUS staining occasionally, frequency of disarrangement and strength of irregularity in *mya1* background are significant larger than those in wild type, suggesting that MYA1 might function upstream of GL2 expression. This experiments were don by Kevin Kuo.

V.3.4. *mya1-1* and *xi-h-1* mutants showed different responses to phosphate deficiency

In addition to increase of the frequency of root hairs, *mya1* and *xi-h* mutants showed slightly longer root hairs than wild type. Since root hair length is also variable in wild type, the increase of length in mutants was not statistically significant (data not shown). However, it has been reported that *Arabidopsis* roots produce longer root hairs in limited phosphate condition as

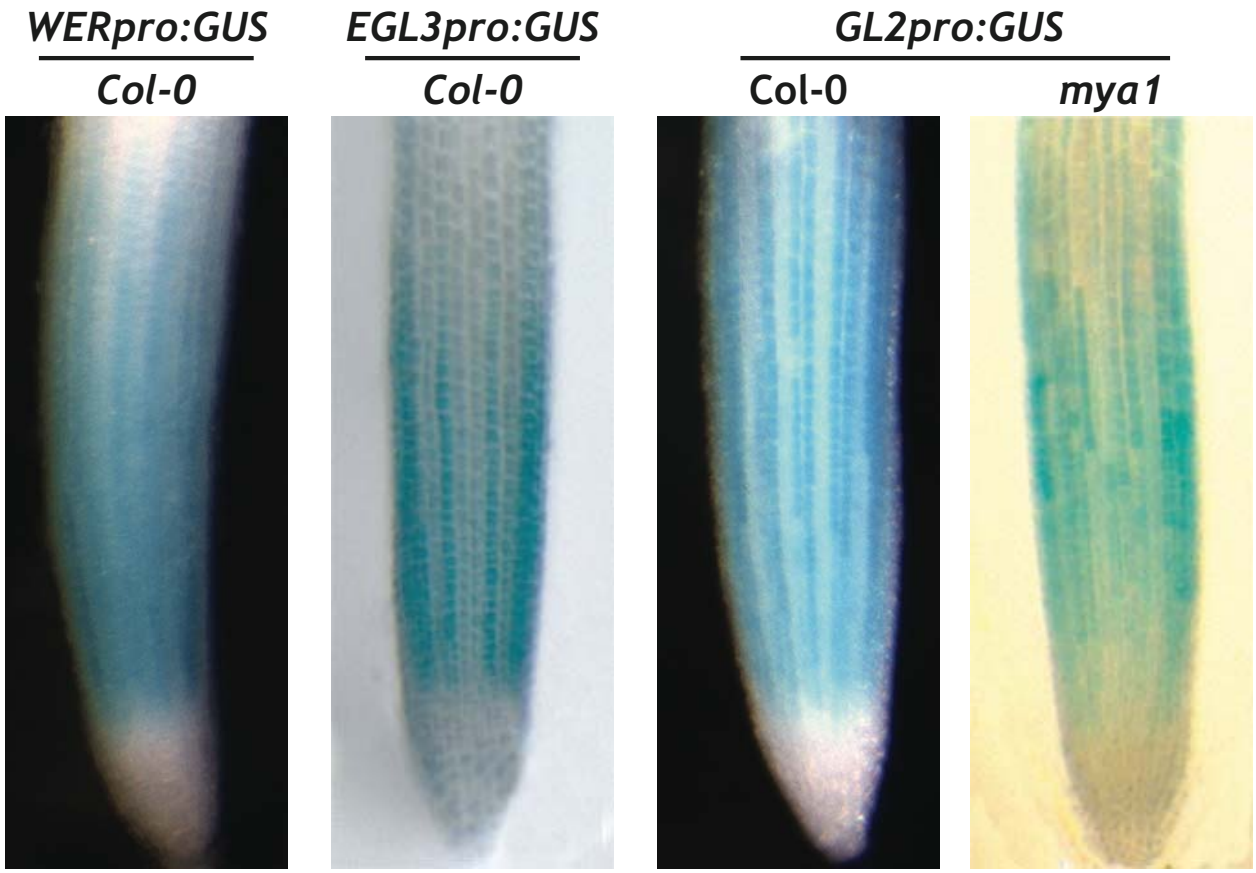

Figure V.5. Expression patterns of several regulators of epidermal cell fate

WERpro:GUS, EGL3pro:GUS and *GL2pro:GUS* show characteristic expression patterns. *GL2pro:GUS* expression seems to be more variable in some *mya1* plants, but quantitative analysis of staining patterns does not reveal a statistically significant difference to wild type. Images with light background were provided by Keven Kuo.

well as more root hairs on N-cells (Müller and Schmidt, 2004) which is similar to *mya1* and *xi-h* grown under normal condition.

To test whether MYA1 and XI-H are involved in phosphate perception or uptake from environment, *mya1-5* and *xi-h-1* were grown on MS media containing various concentration of phosphate (**Figure V. 6.**). Root hair frequency of wild type increased depending on limitation of phosphate availability, however, root hair frequency significantly decreased on 1 μM phosphate medium, the lowest concentration tested (**Figure V.7.**). Interestingly, *mya1* and *xi-h* showed distinct responses to the limited availability of phosphate. Root hair frequency of *mya1* grown in a concentration of 100 μM of phosphate decreased significantly, however, root hair density in *mya1* was inconsistent at lower concentrations of phosphate. *xi-h-1* showed insensitivity of phosphate deficiency. Interestingly, their root hair frequency remained fairly constant across the concentrations suggesting that XI-H might be involved in phosphate perception mechanism of root epidermis. This experiment has been done by Annabel Rodriguez.

V.3.5. MYA1 localization in root cells

Localization of MYA1 was observed with stable transgenic plants containing YFP fused full-length MYA1 under native promoter (Chapter III.3.5. for more information). Since MYA1 seemed to be involved in two developmental mechanisms in roots, MYA1 expression in root cells has been observed carefully. YFP-MYA1 showed colocalization with tiny punctate structures throughout cytoplasm. YFP-MYA1 expression on root of *Arabidopsis* seedlings was relatively stronger than those in shoot. Root epidermal cells showed punctate YFP-MYA1 localization in addition to root hairs (**Figure V. 8.**). YFP-MYA1 expression in roots of

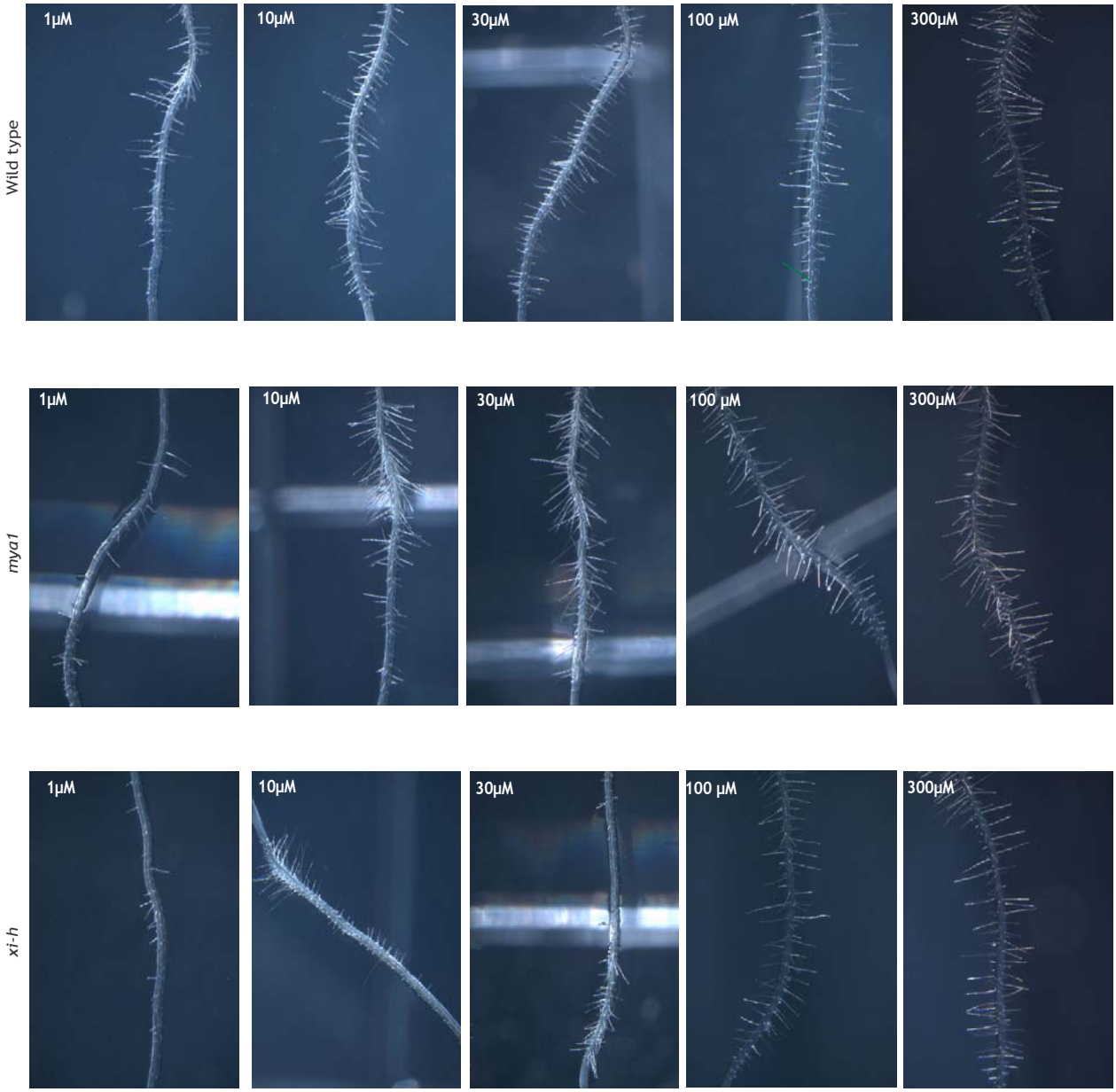

Figure V.6. Roots of five-days-old seedlings on a series of phosphate-limited media

Wild type, *mya1-5*, and *xi-h-1* were germinated on MS plates containing 1 μM, 10 μM, 30 μM, 100 μM, or 300 μM of phosphate. Images were taken by Annabel Rodriguez in her own experiment.

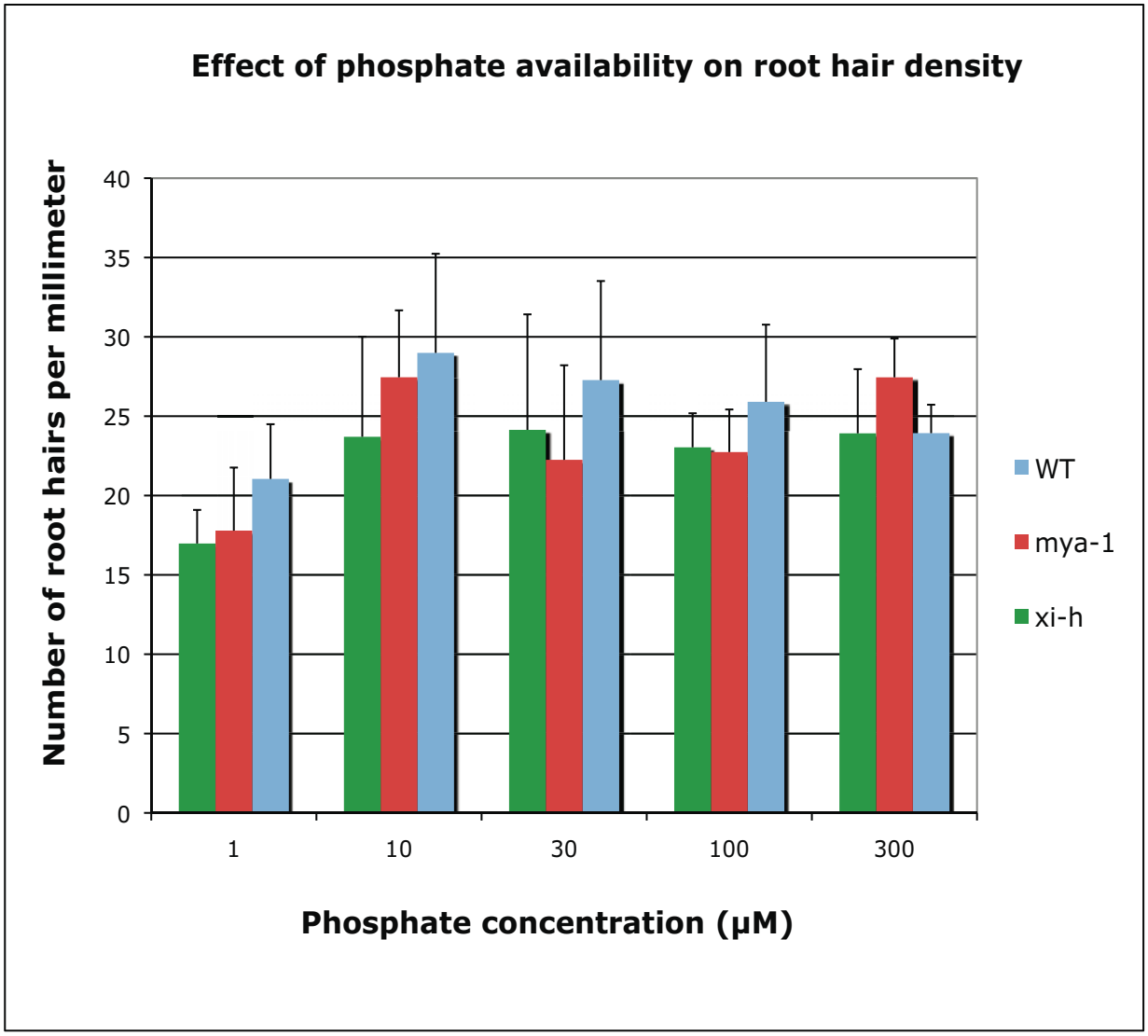

Figure V.7. Effect of phosphate availability on root hair density

Wild type plants produced more root hairs on phosphate deficient plates while *mya1* and *xi-h* mutants showed insensitivity to phosphate deficiency. This graph was generated by Annabel Rodriguez based on her own results.

Arabidopsis seedlings was stronger than in shoot (**Figure V. 8.D-F**). Punctate spots of visible size were detected in every cell that showed YFP-MYA1 expression. Since YFP fusion to truncated MYA1 without the N-terminal motor domain occasionally showed colocalization with peroxisomes (Li and Nebenführ, 2007), colocalization of YFP-MYA1 with peroxisomes were observed in double transgenic plants, *YFP-MYA1 PX-CFP* in *mya1* or *mya1 xi-k* backgrounds. Interestingly, YFP-MYA1 and PX-CFP were not colocalized (Figure III.8. E-H). Since they both were highly abundant in a cell, sometime they looked colocalized, however, careful observation of several spots confirmed YFP-MYA1 is not colocalized with PX-CFP (**Movie V.1, and Figure III.8. G and H**).

V.4. DISCUSSIONS

The mechanism of root hair positioning has been studied extensively in *Arabidopsis thaliana*. Research over several decades has established a detailed model for the genetically controlled mechanism by positional signaling from inner cortex cells to the epidermis. Additional pathways respond to basic nutrients and hormones, especially ethylene, phosphate, and iron, deficiency (Müller and Schmidt, 2004; Schiefelbein et al., 2009). Although major players of this pathway are clear since they have been identified with corresponding mutants and their molecular genetic relationship have been studied for a long time, there are still many aspects that remain to be identified. Particularly, information in biochemical interaction of proteins and mechanism of their trafficking cell to cell are still lacking. The higher frequency of

root hairs in *mya1* and *xi-h* mutants suggests a potential involvement of myosin in root hair fate determination. Since myosin proteins can deliver their cargo along actin filaments, investigation of myosin contribution in root hair positioning mechanism can enforce the weak point of the model. Occasionally, mutants which have a defect in genes related to hormone synthesis or signaling have been reported to produce more root hairs not only because of ectopic root hairs in N-cells but also because of multiple root hair initiation in a single H-cell (Lopez-Bucio et al., 2003; Masucci and Schiefelbein, 1994; Masucci and Schiefelbein, 1996; Müller and Schmidt, 2004). Neither *mya1* nor *xi-h* showed additional root hair initiation site in H-cells and increases of the root hair density of *mya1* and *xi-h* were only due to additional root hair production in N-cells. Therefore, possibility of direct involvement of myosin in hormone-related mechanism seems less likely.

In phosphate deficient condition, plants can produce more and longer root hairs to increase surface area for faster nutrient uptake (Lopez-Bucio et al., 2003). As expected, wild type seedlings produced more root hairs upon phosphate deficiency except that phosphate starvation condition (1 μM phosphate in this experiment) inhibited root hair production. We assume that plants might suspend normal plant growth resulting less root hairs as well as inhibition of root growth under these conditions. However, in this experiment, wild type and mutants failed to be statistically different, since variation between individual seedlings in same genotype was too high (**Figure V.7.**). In addition, root hair frequency of *xi-h-1* in normal condition (300 μM of phosphate) in this experiment was lower than previous observation in regular media condition (**Figure V.4**). Evaluating media condition and careful repeat of this experiment to increase sample size might help to resolve this apparent contradiction.

Figure V.8. YFP-MYA1 localization in a various tissues

MYA1pro:YFP-MYA1 was expressed in a various tissues.

A. YFP-MYA1 in leaf epidermal cells. Not every cell expresses YFP-MYA1. Yellow inset shows relatively strong expression of YFP-MYA1 in guard cells.

B. YFP-MYA1 in hypocotyl epidermis.

C. YFP-MYA1 in leaf pavement cells and guard cells

D. YFP-MYA1 in root tip. Most cells have clear YFP-MYA1 expression.

E. YFP-MYA1 (green) and peroxisome-CFP (magenta) in root epidermis

F. YFP-MYA1 (green) and peroxisome-CFP (magenta) in root hairs.

G. Sequential images of YFP-MYA1 and PX-CFP in a root hair and a root epidermal cell. In a root hair cell, white arrows track a peroxisome initially colocalized with one spot of YFP-MYA1 (yellow arrows), however they were clearly separated from tracking after 11 sec. Fast movement of peroxisome without YFP-MYA1 association tracked with orange arrows. In a root epidermal cell, sky blue arrows identify a YFP-MYA1 spot that seems to colocalize with a PX-CFP spot at 1s, However, tracking their movement over time confirmed they are not associated.

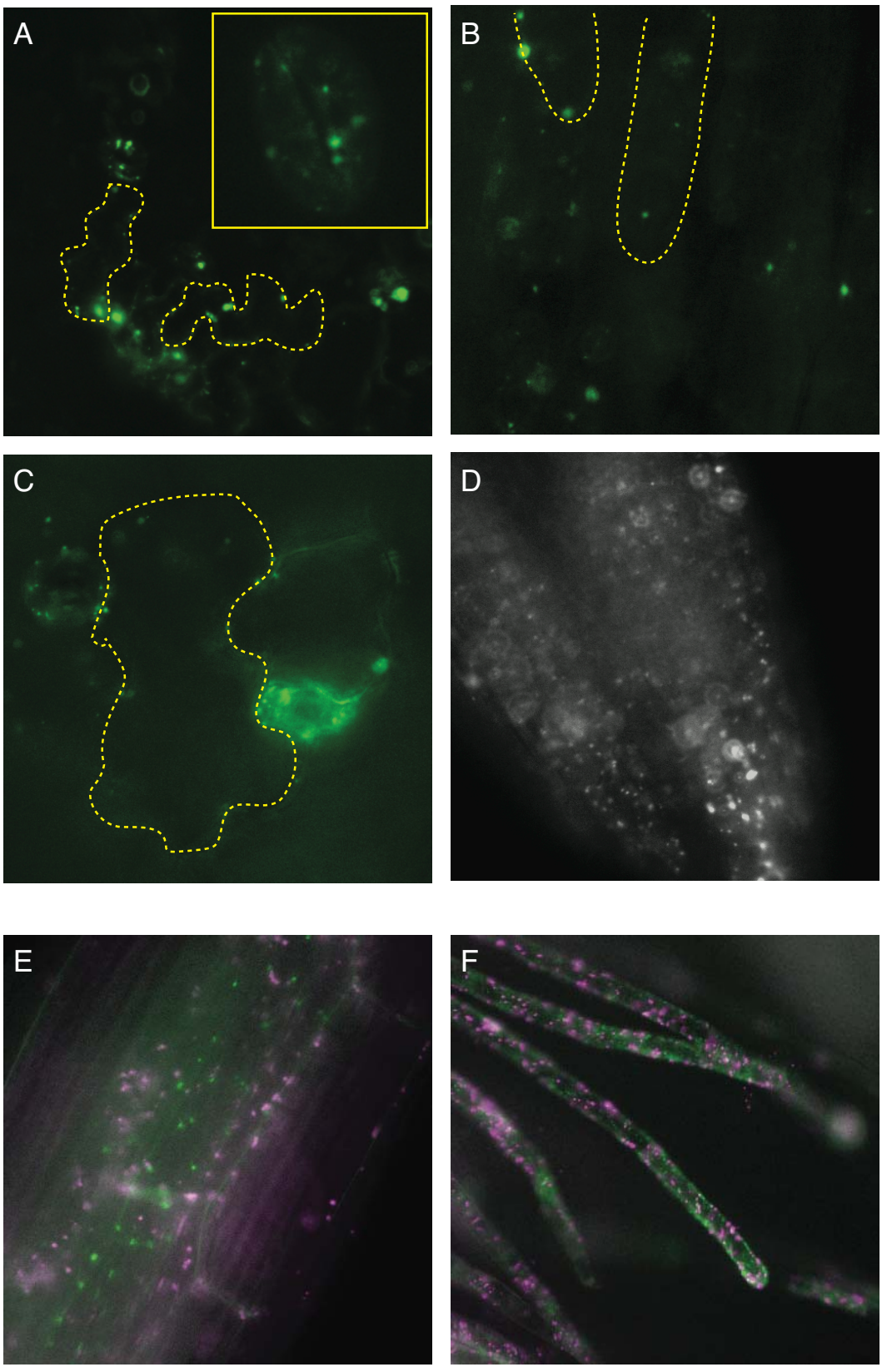
A
B
C
D
E
F

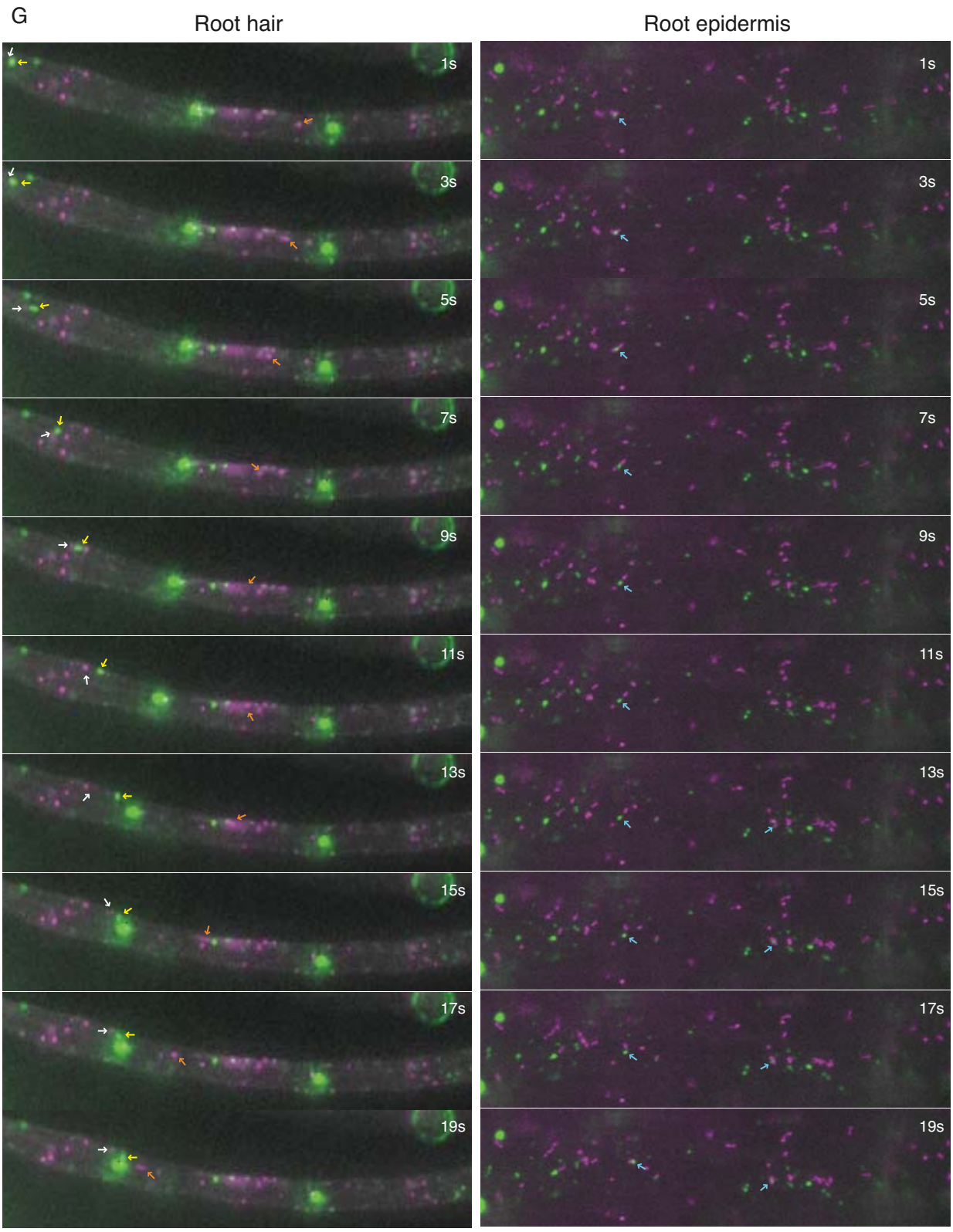

Figure V.8. Continued

CHAPTER VI. Concluding remarks

Myosin proteins function as molecular motors that drive the ATP-dependent movement of cellular components along actin filaments. Vascular plants encode two different types of myosin, referred to as class VIII and class XI (Odronitz and Kollmar, 2007). Although class XI myosin has been suggested to function in organelle movement and cytoplasmic streaming, little is known about their cellular function in detail. The *Arabidopsis* genome encodes 13 class XI myosin genes (Reddy and Day, 2001). The reasons for the relatively large number of myosin XI isoforms present within a single plant species are also unknown.

As a first step to investigate potential myosin function in plant growth and development, the sequence similarity of isoforms was examined in order to identify the phylogenetic relationships of myosins in *Arabidopsis* and rice. Interestingly, most of isoforms have a highly similar isoform which might lead to functional redundancy (**Figure. II.5.** and **6.**). 22 isoforms (12 from *Arabidopsis* and 8 from rice) of the 24 found in these species could be resolved in two large groups, a group including *MYA2* or the other group including *MYA1* (**Figure. II.5.** and **6.**). This might indicate functional differences between those two groups. However, further experimental support is essential to confirm this assumption. Interestingly, *mya2* and *xi-b* produce shorter root hairs than wild type (Peremyslov et al., 2008) supporting that they are functionally in a same group that the phylogenetic tree showed. However, *xi-k* showed same phenotype, but XI-K is most similar to MYA1 in a different group in the tree and *mya1* showed a redundant phenotype with *xi-k*. However, remarkably, *mya1* single mutants did not showed a difference in root hair length but a higher density of root hairs on epidermis, which is similar phenotype to *xi-h* mutants. XI-H is resolved in a same group as MYA2. These results could be interesting since two functionally separate groups, which are involved in either root hair tip growth or root epidermis patterning, are mixed in two different phylogenetic groups. This might

suggest that two different intracellular function of myosin contribute to a developmental process. However, there is not sufficient evidence to support this hypothesis yet.

MYA2-specific antibody has been shown to colocalize with peroxisomes in *Arabidopsis* leaf epidermis (Hashimoto et al., 2005), while YFP-XI-K colocalizes with undefined secretory vesicles at the root hair tip (**Figure. IV.8.**) and YFP-MYA1 colocalizes with undefined organelles throughout the cytoplasm but not peroxisomes (**Figure. V.8.**), suggesting that they are involved in different intracellular trafficking processes. Although the actual cargo binding happens at the globular tail domain (GTD) of myosins, coevolution of myosin domains within a class has been postulated (Foth et al., 2006; Korn, 2000; Odronitz and Kollmar, 2007). In this study, the phylogenetic tree with full-length myosins also showed same results (**Figure. II.6.**). as the one based on motor domains (**Figure. II.5.**) or the dilute domain in GTD (data not shown), suggesting that the phylogenetic tree with the motor domain is sufficient to represent the similarity of GTD in group. However, this assumption also should be supported by experiments, since there is an example of one myosin V that can bind to multiple cargoes (Karcher et al., 2002). Myosin Va in human was shown to have 6 binding partners in different tissues. Class V myosin has the same evolutionary origin as class XI myosin (Odronitz and Kollmar, 2007), suggesting that myosin cargo binding might not be solely related to protein sequence but rather depend on accessibility. However, more detailed studies should be conducted to test this hypothesis. Further analysis using YFP-XI-K and YFP-MYA1 to identify the nature of the vesicles that they transport will be an excellent system to inspect this hypothesis.

In fact, it is not easy to distinguish the vesicles from secretion and endocytosis. However, several proteins have been successfully used to differentiate membrane lipid composition (Vermeer et al., 2009), thus it will be informative to observe colocalization of those markers and

YFP-XI-K. In addition, identification of XI-K binding proteins might give a clue to define the vesicles that XI-K transports to the root hair tip. Recently, binding of GTD of class XI myosin from *Chara* to phospholipid vesicles were demonstrated using GST-Myosin GTD fusion protein and GST antibody (Nunokawa et al., 2007). In addition, two GTPases, AtRabD1 and AtRabC2a, were also identified as adaptor proteins of MYA2 binding to peroxisomes (Hashimoto et al., 2008). Thus, using *XI-Kpro:YFP-XI-K xi-k* transgenic plants, we might be able to conduct immunoprecipitation experiment to isolate adaptor proteins. At the same time, an EMS mutagenesis of *XI-Kpro:YFP-XI-K xi-k* transgenic plant and screening for mutants which show altered YFP-XI-K localization will genetically provide more details about the regulatory mechanism of YFP-XI-K function.

It is also necessary to determine the relationship of those myosins whose mutants showed similar phenotypes in a specific tissue. Since intracellular trafficking might be more active in a highly polarized cell, screening myosin mutants should be targeted to those cells which have an extreme polarity. For example, root hairs might be a good system since they are one of tip-growing cells in which active transport happens. It is not surprising that multiple myosin mutants showed phenotype in root hair growth. Since MYA2 and XI-B are most similar to each other and XI-K and MYA1 also most similar to each other in a different group of the phylogenetic tree, it will be interesting to check their overlapping function on root hair growth by checking the phenotype of double or triple mutants. It has been reported that MYA2 and XI-B show mild redundancy in a double mutant (Prokhnevsky et al., 2008), thus defining the functional relationship of them with XI-K and MYA1 is necessary. In addition, observation of XI-B localization in root hairs is also essential to figure out the functional relationship between these myosins.

As an independent approach to examine whether multiple intracellular trafficking pathways might contribute to a single developmental mechanism, we can also design another experiment to characterize myosin function in pollen tube growth. Pollen tube is the most polarized cell in plant and, interestingly, many myosins are specifically expressed in pollen tubes (**Figure. II. 8.**). Thus, identification of the functional relationship of these myosins on pollen tube growth using the mutants generated in chapter III, accompanied with characterization of their intracellular localization will be informative.

Combining a biochemical approach to identify myosin-cargo binding and a genetic and cell biological approach to understand myosin function in intracellular trafficking and its developmental effects, we can significantly increase our understanding of myosin function. The study in this dissertation has provided initial insights in this topic and also can serve as a critical resource to design future research more systematically.

List of references

Alonso, J.M., A.N. Stepanova, T.J. Leisse, C.J. Kim, H. Chen, P. Shinn, D.K. Stevenson, J. Zimmerman, P. Barajas, R. Cheuk, C. Gadrinab, C. Heller, A. Jeske, E. Koesema, C.C. Meyers, H. Parker, L. Prednis, Y. Ansari, N. Choy, H. Deen, M. Geralt, N. Hazari, E. Hom, M. Karnes, C. Mulholland, R. Ndubaku, I. Schmidt, P. Guzman, L. Aguilar-Henonin, M. Schmid, D. Weigel, D.E. Carter, T. Marchand, E. Risseeuw, D. Brogden, A. Zeko, W.L. Crosby, C.C. Berry, and J.R. Ecker. 2003. Genome-wide insertional mutagenesis of Arabidopsis thaliana. *Science*. 301:653-657.

Avisar, D., M. Abu-Abied, E. Belausov, E. Sadot, C. Hawes, and I.A. Sparkes. 2009. A comparative study of the involvement of 17 Arabidopsis myosin family members on the motility of Golgi and other organelles. *Plant Physiol*. 150:700-709.

Avisar, D., A.I. Prokhnevsky, and V.V. Dolja. 2008a. Class VIII myosins are required for plasmodesmatal localization of a closterovirus Hsp70 homolog. *J Virol*. 82:2836-2843.

Avisar, D., A.I. Prokhnevsky, K.S. Makarova, E.V. Koonin, and V.V. Dolja. 2008b. Myosin XI-K Is required for rapid trafficking of Golgi stacks, peroxisomes, and mitochondria in leaf cells of Nicotiana benthamiana. *Plant Physiol*. 146:1098-1108.

Baluska, F., F. Cvrckova, J. Kendrick-Jones, and D. Volkmann. 2001. Sink plasmodesmata as gateways for phloem unloading. Myosin VIII and calreticulin as molecular determinants of sink strength? *Plant Physiol*. 126:39-46.

Baluska, F., J. Salaj, J. Mathur, M. Braun, F. Jasper, J. Samaj, N.H. Chua, P.W. Barlow, and D. Volkmann. 2000. Root hair formation: F-actin-dependent tip growth is initiated by local assembly of profilin-supported F-actin meshworks accumulated within expansin-enriched bulges. *Dev Biol*. 227:618-632.

Baluska, F., and D. Volkmann. 2002. Pictures in cell biology. Actin-driven polar growth of plant cells. *Trends Cell Biol*. 12:14.

Baluska, F., P. Wojtaszek, D. Volkmann, and P. Barlow. 2003. The architecture of polarized cell growth: the unique status of elongating plant cells. *Bioessays*. 25:569-576.

Bao, Y., B. Kost, and N.H. Chua. 2001. Reduced expression of alpha-tubulin genes in Arabidopsis thaliana specifically affects root growth and morphology, root hair development and root gravitropism. *Plant J*. 28:145-157.

Bates, T.R., and J.P. Lynch. 2000a. The efficiency of Arabidopsis thaliana (Brassicaceae) root hairs in phosphorus acquisition. *Am J Bot*. 87:964-970.

Bates, T.R., and J.P. Lynch. 2000b. Plant growth and phosphorus accumulation of wild type and two root hair mutants of Arabidopsis thaliana (Brassicaceae). *Am J Bot*. 87:958-963.

Baxter-Burrell, A., Z. Yang, P.S. Springer, and J. Bailey-Serres. 2002. RopGAP4-dependent Rop GTPase rheostat control of Arabidopsis oxygen deprivation tolerance. *Science*. 296:2026-2028.

Berg, J.S., B.C. Powell, and R.E. Cheney. 2001. A millennial myosin census. *Mol Biol Cell*. 12:780-794.

Bernhardt, C., M.M. Lee, A. Gonzalez, F. Zhang, A. Lloyd, and J. Schiefelbein. 2003. The bHLH genes GLABRA3 (GL3) and ENHANCER OF GLABRA3 (EGL3) specify epidermal cell fate in the Arabidopsis root. *Development*. 130:6431-6439.

Bernhardt, C., M. Zhao, A. Gonzalez, A. Lloyd, and J. Schiefelbein. 2005. The bHLH genes GL3 and EGL3 participate in an intercellular regulatory circuit that controls cell patterning in the Arabidopsis root epidermis. *Development*. 132:291-298.

Bibikova, T.N., E.B. Blancaflor, and S. Gilroy. 1999. Microtubules regulate tip growth and orientation in root hairs of Arabidopsis thaliana. *Plant J*. 17:657-665.

Bibikova, T.N., T. Jacob, I. Dahse, and S. Gilroy. 1998. Localized changes in apoplastic and cytoplasmic pH are associated with root hair development in Arabidopsis thaliana. *Development*. 125:2925-2934.

Bibikova, T.N., A. Zhigilei, and S. Gilroy. 1997. Root hair growth in Arabidopsis thaliana is directed by calcium and an endogenous polarity. *Planta*. 203:495-505.

Braun, M., F. Baluska, M. von Witsch, and D. Menzel. 1999. Redistribution of actin, profilin and phosphatidylinositol-4, 5-bisphosphate in growing and maturing root hairs. *Planta*. 209:435-443.

Campanoni, P., and M.R. Blatt. 2007. Membrane trafficking and polar growth in root hairs and pollen tubes. *J Exp Bot*. 58:65-74.

Carland, F.M., S. Fujioka, S. Takatsuto, S. Yoshida, and T. Nelson. 2002. The identification of CVP1 reveals a role for sterols in vascular patterning. *Plant Cell*. 14:2045-2058.

Carol, R.J., and L. Dolan. 2002. Building a hair: tip growth in Arabidopsis thaliana root hairs. *Philos Trans R Soc Lond B Biol Sci*. 357:815-821.

Carol, R.J., S. Takeda, P. Linstead, M.C. Durrant, H. Kakesova, P. Derbyshire, S. Drea, V. Zarsky, and L. Dolan. 2005. A RhoGDP dissociation inhibitor spatially regulates growth in root hair cells. *Nature*. 438:1013-1016.

Clowes, F.A.L. 2000. Pattern in root meristem development in angiosperms. *New Phytologist*. 146:83-94.

Cole, R.A., and J.E. Fowler. 2006. Polarized growth: maintaining focus on the tip. *Curr Opin Plant Biol*. 9:579-588.

Collings, D.A., A.W. Lill, R. Himmelspach, and G.O. Wasteneys. 2006. Hypersensitivity to cytoskeletal antagonists demonstrates microtubule-microfilament cross-talk in the control of root elongation in Arabidopsis thaliana. *New Phytol*. 170:275-290.

Deeks, M.J., F. Cvrckova, L.M. Machesky, V. Mikitova, T. Ketelaar, V. Zarsky, B. Davies, and P.J. Hussey. 2005. Arabidopsis group Ie formins localize to specific cell membrane domains, interact with actin-binding proteins and cause defects in cell expansion upon aberrant expression. *New Phytol*. 168:529-540.

Dolan, L., and S. Costa. 2001. Evolution and genetics of root hair stripes in the root epidermis. *J Exp Bot*. 52:413-417.

Dolan, L., and K. Roberts. 1995. The development of cell pattern in the root epidermis. *Philos Trans R Soc Lond B Biol Sci*. 350:95-99.

Era, A., M. Tominaga, K. Ebine, C. Awai, C. Saito, K. Ishizaki, K.T. Yamato, T. Kohchi, A. Nakano, and T. Ueda. 2009. Application of Lifeact reveals F-actin dynamics in Arabidopsis thaliana and the liverwort, Marchantia polymorpha. *Plant Cell Physiol*. 50:1041-1048.

Felle, H.H., and P.K. Hepler. 1997. The Cytosolic Ca2+ Concentration Gradient of Sinapis alba Root Hairs as Revealed by Ca2+-Selective Microelectrode Tests and Fura-Dextran Ratio Imaging. *Plant Physiol*. 114:39-45.

Fischer, U., Y. Ikeda, and M. Grebe. 2007. Planar polarity of root hair positioning in Arabidopsis. *Biochem Soc Trans*. 35:149-151.

Foreman, J., V. Demidchik, J.H. Bothwell, P. Mylona, H. Miedema, M.A. Torres, P. Linstead, S. Costa, C. Brownlee, J.D. Jones, J.M. Davies, and L. Dolan. 2003. Reactive oxygen species produced by NADPH oxidase regulate plant cell growth. *Nature*. 422:442-446.

Forer, A., and L. Fabian. 2005. Does 2,3-butanedione monoxime inhibit nonmuscle myosin? *Protoplasma*. 225:1-4.

Foth, B.J., M.C. Goedecke, and D. Soldati. 2006. New insights into myosin evolution and classification. *Proceedings of the National Academy of Sciences of the United States of America*. 103:3681-3686.

Fu, Y., H. Li, and Z. Yang. 2002. The ROP2 GTPase controls the formation of cortical fine F-actin and the early phase of directional cell expansion during Arabidopsis organogenesis. *Plant Cell*. 14:777-794.

Galway, M.E., J.D. Masucci, A.M. Lloyd, V. Walbot, R.W. Davis, and J.W. Schiefelbein. 1994. The TTG gene is required to specify epidermal cell fate and cell patterning in the Arabidopsis root. *Dev Biol*. 166:740-754.

Geitmann, A., and A.M. Emons. 2000. The cytoskeleton in plant and fungal cell tip growth. *J Microsc*. 198:218-245.

Geldner, N., J. Friml, Y.D. Stierhof, G. Jurgens, and K. Palme. 2001. Auxin transport inhibitors block PIN1 cycling and vesicle trafficking. *Nature*. 413:425-428.

Gilliland, L.U., M.K. Kandasamy, L.C. Pawloski, and R.B. Meagher. 2002. Both vegetative and reproductive actin isovariants complement the stunted root hair phenotype of the Arabidopsis act2-1 mutation. *Plant Physiol*. 130:2199-2209.

Golomb, L., M. Abu-Abied, E. Belausov, and E. Sadot. 2008. Different subcellular localizations and functions of Arabidopsis myosin VIII. *BMC Plant Biol*. 8:3.

Goodson, H.V., and S.C. Dawson. 2006. Multiplying myosins. *Proc Natl Acad Sci U S A*. 103:3498-3499.

Grabski, S., E. Arnoys, B. Busch, and M. Schindler. 1998. Regulation of Actin Tension in Plant Cells by Kinases and Phosphatases. *Plant Physiol*. 116:279-290.

Grebe, M. 2004. Ups and downs of tissue and planar polarity in plants. *Bioessays*. 26:719-729.

Grebe, M., J. Friml, R. Swarup, K. Ljung, G. Sandberg, M. Terlou, K. Palme, M.J. Bennett, and B. Scheres. 2002. Cell polarity signaling in Arabidopsis involves a BFA-sensitive auxin influx pathway. *Curr Biol*. 12:329-334.

Guimil, S., and C. Dunand. 2006. Patterning of Arabidopsis epidermal cells: epigenetic factors regulate the complex epidermal cell fate pathway. *Trends Plant Sci*. 11:601-609.

Guimil, S., and C. Dunand. 2007. Cell growth and differentiation in Arabidopsis epidermal cells. *J Exp Bot*. 58:3829-3840.

Harries, P.A., J.W. Park, N. Sasaki, K.D. Ballard, A.J. Maule, and R.S. Nelson. 2009. Differing requirements for actin and myosin by plant viruses for sustained intercellular movement. *Proc Natl Acad Sci U S A*. 106:17594-17599.

Hashimoto, K., H. Igarashi, S. Mano, M. Nishimura, T. Shimmen, and E. Yokota. 2005. Peroxisomal localization of a myosin XI isoform in Arabidopsis thaliana. *Plant Cell Physiol*. 46:782-789.

Hashimoto, K., H. Igarashi, S. Mano, C. Takenaka, T. Shiina, M. Yamaguchi, T. Demura, M. Nishimura, T. Shimmen, and E. Yokota. 2008. An isoform of Arabidopsis myosin XI interacts with small GTPases in its C-terminal tail region. *J Exp Bot*. 59:3523-3531.

Hasson, T., and M.S. Mooseker. 1995. Molecular motors, membrane movements and physiology: emerging roles for myosins. *Curr Opin Cell Biol*. 7:587-594.

He, X., Y.M. Liu, W. Wang, and Y. Li. 2006. Distribution of G-actin is related to root hair growth of wheat. *Ann Bot*. 98:49-55.

Hemsley, P.A., A.C. Kemp, and C.S. Grierson. 2005. The TIP GROWTH DEFECTIVE1 S-acyl transferase regulates plant cell growth in Arabidopsis. *Plant Cell*. 17:2554-2563.

Hepler, P.K., L. Vidali, and A.Y. Cheung. 2001. Polarized cell growth in higher plants. *Annu Rev Cell Dev Biol*. 17:159-187.

Holweg, C., A. Honsel, and P. Nick. 2003. A myosin inhibitor impairs auxin-induced cell division. *Protoplasma*. 222:193-204.

Hu, Y., R. Zhong, W.H. Morrison, 3rd, and Z.H. Ye. 2003. The Arabidopsis RHD3 gene is required for cell wall biosynthesis and actin organization. *Planta*. 217:912-921.

Hussey, P.J., T. Ketelaar, and M.J. Deeks. 2006. Control of the actin cytoskeleton in plant cell growth. *Annu Rev Plant Biol*. 57:109-125.

Ishida, T., T. Kurata, K. Okada, and T. Wada. 2008. A genetic regulatory network in the development of trichomes and root hairs. *Annu Rev Plant Biol*. 59:365-386.

Jain, A., M.D. Poling, A.S. Karthikeyan, J.J. Blakeslee, W.A. Peer, B. Titapiwatanakun, A.S. Murphy, and K.G. Raghothama. 2007. Differential effects of sucrose and auxin on localized phosphate deficiency-induced modulation of different traits of root system architecture in Arabidopsis. *Plant Physiol*. 144:232-247.

Jiang, S., and S. Ramachandran. 2004. Identification and molecular characterization of myosin gene family in Oryza sativa genome. *Plant Cell Physiol*. 45:590-599.

Jiang, S.Y., M. Cai, and S. Ramachandran. 2007. ORYZA SATIVA MYOSIN XI B controls pollen development by photoperiod-sensitive protein localizations. *Dev Biol*. 304:579-592.

Kandasamy, M.K., E.C. McKinney, and R.B. Meagher. 2009. A single vegetative actin isovariant overexpressed under the control of multiple regulatory sequences is sufficient for normal Arabidopsis development. *Plant Cell*. 21:701-718.

Karcher, R.L., S.W. Deacon, and V.I. Gelfand. 2002. Motor-cargo interactions: the key to transport specificity. *Trends Cell Biol*. 12:21-27.

Kawamura, E., R. Himmelspach, M.C. Rashbrooke, A.T. Whittington, K.R. Gale, D.A. Collings, and G.O. Wasteneys. 2006. MICROTUBULE ORGANIZATION 1 regulates structure and function of microtubule arrays during mitosis and cytokinesis in the Arabidopsis root. *Plant Physiol*. 140:102-114.

Ketelaar, T., E.G. Allwood, and P.J. Hussey. 2007. Actin organization and root hair development are disrupted by ethanol-induced overexpression of Arabidopsis actin interacting protein 1 (AIP1). *New Phytol*. 174:57-62.

Ketelaar, T., R.G. Anthony, and P.J. Hussey. 2004. Green fluorescent protein-mTalin causes defects in actin organization and cell expansion in Arabidopsis and inhibits actin depolymerizing factor's actin depolymerizing activity in vitro. *Plant Physiol*. 136:3990-3998.

Kieber, J.J., M. Rothenberg, G. Roman, K.A. Feldmann, and J.R. Ecker. 1993. CTR1, a negative regulator of the ethylene response pathway in Arabidopsis, encodes a member of the raf family of protein kinases. *Cell*. 72:427-441.

Kim, D.W., S.H. Lee, S.B. Choi, S.K. Won, Y.K. Heo, M. Cho, Y.I. Park, and H.T. Cho. 2006. Functional conservation of a root hair cell-specific cis-element in angiosperms with different root hair distribution patterns. *Plant Cell*. 18:2958-2970.

Kinkema, M., and J. Schiefelbein. 1994. A myosin from a higher plant has structural similarities to class V myosins. *J Mol Biol*. 239:591-597.

Kinkema, M., H. Wang, and J. Schiefelbein. 1994. Molecular analysis of the myosin gene family in Arabidopsis thaliana. *Plant Mol Biol*. 26:1139-1153.

Kirik, V., M. Simon, M. Huelskamp, and J. Schiefelbein. 2004a. The ENHANCER OF TRY AND CPC1 gene acts redundantly with TRIPTYCHON and CAPRICE in trichome and root hair cell patterning in Arabidopsis. *Dev Biol*. 268:506-513.

Kirik, V., M. Simon, K. Wester, J. Schiefelbein, and M. Hulskamp. 2004b. ENHANCER of TRY and CPC 2 (ETC2) reveals redundancy in the region-specific control of trichome development of Arabidopsis. *Plant Mol Biol*. 55:389-398.

Knight, A.E., and J. Kendrick-Jones. 1993. A myosin-like protein from a higher plant. *J Mol Biol*. 231:148-154.

Korn, E.D. 2000. Coevolution of head, neck, and tail domains of myosin heavy chains. *Proc Natl Acad Sci U S A*. 97:12559-12564.

Kovar, D.R., B.K. Drobak, and C.J. Staiger. 2000. Maize profilin isoforms are functionally distinct. *Plant Cell*. 12:583-598.

Krendel, M., and M.S. Mooseker. 2005. Myosins: tails (and heads) of functional diversity. *Physiology (Bethesda)*. 20:239-251.

Kwak, S.H., and J. Schiefelbein. 2007. The role of the SCRAMBLED receptor-like kinase in patterning the Arabidopsis root epidermis. *Dev Biol*. 302:118-131.

Kwak, S.H., and J. Schiefelbein. 2008. A feedback mechanism controlling SCRAMBLED receptor accumulation and cell-type pattern in Arabidopsis. *Curr Biol*. 18:1949-1954.

Kwak, S.H., R. Shen, and J. Schiefelbein. 2005. Positional signaling mediated by a receptor-like kinase in Arabidopsis. *Science*. 307:1111-1113.

Lee, M.M., and J. Schiefelbein. 1999. WEREWOLF, a MYB-related protein in Arabidopsis, is a position-dependent regulator of epidermal cell patterning. *Cell*. 99:473-483.

Lee, M.M., and J. Schiefelbein. 2002. Cell pattern in the Arabidopsis root epidermis determined by lateral inhibition with feedback. *Plant Cell*. 14:611-618.

Li, J.F., and A. Nebenführ. 2007. Organelle targeting of myosin XI is mediated by two globular tail subdomains with separate cargo binding sites. *J Biol Chem*. 282:20593-20602.

Li, J.F., and A. Nebenführ. 2008. The tail that wags the dog: the globular tail domain defines the function of myosin V/XI. *Traffic*. 9:290-298.

Liu, L., J. Zhou, and T.C. Pesacreta. 2001. Maize myosins: diversity, localization, and function. *Cell Motil Cytoskeleton*. 48:130-148.

Lloyd, C.W., and B. Wells. 1985. Microtubules are at the tips of root hairs and form helical patterns corresponding to inner wall fibrils. *J Cell Sci*. 75:225-238.

Lopez-Bucio, J., A. Cruz-Ramirez, and L. Herrera-Estrella. 2003. The role of nutrient availability in regulating root architecture. *Curr Opin Plant Biol*. 6:280-287.

Masucci, J.D., W.G. Rerie, D.R. Foreman, M. Zhang, M.E. Galway, M.D. Marks, and J.W. Schiefelbein. 1996. The homeobox gene GLABRA2 is required for position-dependent cell differentiation in the root epidermis of Arabidopsis thaliana. *Development*. 122:1253-1260.

Masucci, J.D., and J.W. Schiefelbein. 1994. The rhd6 Mutation of Arabidopsis thaliana Alters Root-Hair Initiation through an Auxin- and Ethylene-Associated Process. *Plant Physiol*. 106:1335-1346.

Masucci, J.D., and J.W. Schiefelbein. 1996. Hormones act downstream of TTG and GL2 to promote root hair outgrowth during epidermis development in the Arabidopsis root. *Plant Cell*. 8:1505-1517.

McKillop, D.F., N.S. Fortune, K.W. Ranatunga, and M.A. Geeves. 1994. The influence of 2,3-butanedione 2-monoxime (BDM) on the interaction between actin and myosin in solution and in skinned muscle fibres. *J Muscle Res Cell Motil*. 15:309-318.

Miller, D., N.C. de Ruijter, T. Bisseling, and A.M. Emons. 1999. The role of actin in root hair morphogenesis: studies with lipochito-oligosaccharide as a growth stimulator and cytochalasin as an actin perturbing drug. *Plant Journal*. 17:141-154.

Miller, D.D., S.P. Scordilis, and P.K. Hepler. 1995. Identification and localization of three classes of myosins in pollen tubes of Lilium longiflorum and Nicotiana alata. *J Cell Sci*. 108 (Pt 7):2549-2563.

Molchan, T.M., A.H. Valster, and P.K. Hepler. 2002. Actomyosin promotes cell plate alignment and late lateral expansion in Tradescantia stamen hair cells. *Planta*. 214:683-693.

Molendijk, A.J., F. Bischoff, C.S. Rajendrakumar, J. Friml, M. Braun, S. Gilroy, and K. Palme. 2001. Arabidopsis thaliana Rop GTPases are localized to tips of root hairs and control polar growth. *EMBO J*. 20:2779-2788.

Monshausen, G.B., T.N. Bibikova, M.A. Messerli, C. Shi, and S. Gilroy. 2007. Oscillations in extracellular pH and reactive oxygen species modulate tip growth of Arabidopsis root hairs. *Proc Natl Acad Sci U S A*. 104:20996-21001.

Monshausen, G.B., T.N. Bibikova, M.H. Weisenseel, and S. Gilroy. 2009. Ca2+ regulates reactive oxygen species production and pH during mechanosensing in Arabidopsis roots. *Plant Cell*. 21:2341-2356.

Monshausen, G.B., M.A. Messerli, and S. Gilroy. 2008. Imaging of the Yellow Cameleon 3.6 indicator reveals that elevations in cytosolic Ca2+ follow oscillating increases in growth in root hairs of Arabidopsis. *Plant Physiol*. 147:1690-1698.

Moriau, L., B. Michelet, P. Bogaerts, L. Lambert, A. Michel, M. Oufattole, and M. Boutry. 1999. Expression analysis of two gene subfamilies encoding the plasma membrane H+-ATPase in Nicotiana plumbaginifolia reveals the major transport functions of this enzyme. *Plant J*. 19:31-41.

Müller, M., and W. Schmidt. 2004. Environmentally induced plasticity of root hair development in Arabidopsis. *Plant Physiol*. 134:409-419.

Natesan, S.K., J.A. Sullivan, and J.C. Gray. 2009. Myosin XI Is Required for Actin-Associated Movement of Plastid Stromules. *Mol Plant*. 2:1262-1272.

Nebenführ, A., L.A. Gallagher, T.G. Dunahay, J.A. Frohlick, A.M. Mazurkiewicz, J.B. Meehl, and L.A. Staehelin. 1999. Stop-and-go movements of plant Golgi stacks are mediated by the acto-myosin system. *Plant Physiol*. 121:1127-1142.

Nelson, B.K., X. Cai, and A. Nebenführ. 2007. A multicolored set of in vivo organelle markers for co-localization studies in Arabidopsis and other plants. *Plant J*. 51:1126-1136.

Nunokawa, S.Y., H. Anan, K. Shimada, Y. Hachikubo, T. Kashiyama, K. Ito, and K. Yamamoto. 2007. Binding of chara Myosin globular tail domain to phospholipid vesicles. *Plant Cell Physiol*. 48:1558-1566.

Odronitz, F., and M. Kollmar. 2007. Drawing the tree of eukaryotic life based on the analysis of 2,269 manually annotated myosins from 328 species. *Genome Biol*. 8:R196.

Ojangu, E.L., K. Jarve, H. Paves, and E. Truve. 2007. Arabidopsis thaliana myosin XIK is involved in root hair as well as trichome morphogenesis on stems and leaves. *Protoplasma*. 230:193-202.

Ovecka, M., I. Lang, F. Baluska, A. Ismail, P. Illes, and I.K. Lichtscheidl. 2005. Endocytosis and vesicle trafficking during tip growth of root hairs. *Protoplasma*. 226:39-54.

Paves, H., and E. Truve. 2007. Myosin inhibitors block accumulation movement of chloroplasts in Arabidopsis thaliana leaf cells. *Protoplasma*. 230:165-169.

Payne, R.J., and C.S. Grierson. 2009. A theoretical model for ROP localisation by auxin in Arabidopsis root hair cells. *PLoS One*. 4:e8337.

Peremyslov, V.V., A.I. Prokhnevsky, D. Avisar, and V.V. Dolja. 2008. Two class XI myosins function in organelle trafficking and root hair development in Arabidopsis. *Plant Physiol*. 146:1109-1116.

Pesch, M., and M. Hulskamp. 2004. Creating a two-dimensional pattern de novo during Arabidopsis trichome and root hair initiation. *Curr Opin Genet Dev*. 14:422-427.

Preuss, M.L., A.J. Schmitz, J.M. Thole, H.K. Bonner, M.S. Otegui, and E. Nielsen. 2006. A role for the RabA4b effector protein PI-4Kbeta1 in polarized expansion of root hair cells in Arabidopsis thaliana. *J Cell Biol*. 172:991-998.

Preuss, M.L., J. Serna, T.G. Falbel, S.Y. Bednarek, and E. Nielsen. 2004. The Arabidopsis Rab GTPase RabA4b localizes to the tips of growing root hair cells. *Plant Cell*. 16:1589-1603.

Prokhnevsky, A.I., V.V. Peremyslov, and V.V. Dolja. 2008. Overlapping functions of the four class XI myosins in Arabidopsis growth, root hair elongation, and organelle motility. *Proc Natl Acad Sci U S A*. 105:19744-19749.

Radford, J.E., and R.G. White. 1998. Localization of a myosin-like protein to plasmodesmata. *Plant J*. 14:743-750.

Ramachandran, S., H.E. Christensen, Y. Ishimaru, C.H. Dong, W. Chao-Ming, A.L. Cleary, and N.H. Chua. 2000. Profilin plays a role in cell elongation, cell shape maintenance, and flowering in Arabidopsis. *Plant Physiol*. 124:1637-1647.

Reddy, A.S., and I.S. Day. 2001. Analysis of the myosins encoded in the recently completed Arabidopsis thaliana genome sequence. *Genome Biol*. 2:RESEARCH0024.

Reichelt, S., A.E. Knight, T.P. Hodge, F. Baluska, J. Samaj, D. Volkmann, and J. Kendrick-Jones. 1999. Characterization of the unconventional myosin VIII in plant cells and its localization at the post-cytokinetic cell wall. *Plant J*. 19:555-567.

Reisen, D., and M.R. Hanson. 2007. Association of six YFP-myosin XI-tail fusions with mobile plant cell organelles. *BMC Plant Biol*. 7:6.

Richards, T.A., and T. Cavalier-Smith. 2005. Myosin domain evolution and the primary divergence of eukaryotes. *Nature*. 436:1113-1118.

Ringli, C., N. Baumberger, A. Diet, B. Frey, and B. Keller. 2002. ACTIN2 is essential for bulge site selection and tip growth during root hair development of Arabidopsis. *Plant Physiol*. 129:1464-1472.

Sablowski, R.W.M., and E.M. Meyerowitz. 1998. A Homolog of NO APICAL MERISTEM Is an Immediate Target of the Floral Homeotic Genes APETALA3/PISTILLATA. 92:93-103.

Sagi, M., and R. Fluhr. 2001. Superoxide production by plant homologues of the gp91(phox) NADPH oxidase. Modulation of activity by calcium and by tobacco mosaic virus infection. *Plant Physiol*. 126:1281-1290.

Sakai, T., H. Honing, M. Nishioka, Y. Uehara, M. Takahashi, N. Fujisawa, K. Saji, M. Seki, K. Shinozaki, M.A. Jones, N. Smirnoff, K. Okada, and G.O. Wasteneys. 2008. Armadillo repeat-containing kinesins and a NIMA-related kinase are required for epidermal-cell morphogenesis in Arabidopsis. *Plant J*. 53:157-171.

Šamaj, J., J. Muller, M. Beck, N. Bohm, and D. Menzel. 2006. Vesicular trafficking, cytoskeleton and signalling in root hairs and pollen tubes. *Trends Plant Sci*. 11:594-600.

Šamaj, J., M. Peters, D. Volkmann, and F. Baluska. 2000. Effects of myosin ATPase inhibitor 2,3-butanedione 2-monoxime on distributions of myosins, F-actin, microtubules, and cortical endoplasmic reticulum in maize root apices. *Plant Cell Physiol*. 41:571-582.

Sattarzadeh, A., R. Franzen, and E. Schmelzer. 2008. The Arabidopsis class VIII myosin ATM2 is involved in endocytosis. *Cell Motil Cytoskeleton*. 65:457-468.

Savage, N.S., T. Walker, Y. Wieckowski, J. Schiefelbein, L. Dolan, and N.A. Monk. 2008. A mutual support mechanism through intercellular movement of CAPRICE and GLABRA3 can pattern the Arabidopsis root epidermis. *PLoS Biol*. 6:e235.

Schellmann, S., A. Schnittger, V. Kirik, T. Wada, K. Okada, A. Beermann, J. Thumfahrt, G. Jurgens, and M. Hulskamp. 2002. TRIPTYCHON and CAPRICE mediate lateral inhibition during trichome and root hair patterning in Arabidopsis. *EMBO J*. 21:5036-5046.

Schiefelbein, J. 2003. Cell-fate specification in the epidermis: a common patterning mechanism in the root and shoot. *Curr Opin Plant Biol*. 6:74-78.

Schiefelbein, J., M. Galway, J. Masucci, and S. Ford. 1993. Pollen tube and root-hair tip growth is disrupted in a mutant of Arabidopsis thaliana. *Plant Physiol*. 103:979-985.

Schiefelbein, J., S.H. Kwak, Y. Wieckowski, C. Barron, and A. Bruex. 2009. The gene regulatory network for root epidermal cell-type pattern formation in Arabidopsis. *J Exp Bot*. 60:1515-1521.

Schiefelbein, J.W., and C. Somerville. 1990. Genetic Control of Root Hair Development in Arabidopsis thaliana. *Plant Cell*. 2:235-243.

Shane, M.W., G.R. Cawthray, M.D. Cramer, J. Kuo, and H. Lambers. 2006. Specialized 'dauciform' roots of Cyperaceae are structurally distinct, but functionally analogous with 'cluster' roots. *Plant Cell Environ*. 29:1989-1999.

Sheahan, M.B., C.J. Staiger, R.J. Rose, and D.W. McCurdy. 2004. A green fluorescent protein fusion to actin-binding domain 2 of Arabidopsis fimbrin highlights new features of a dynamic actin cytoskeleton in live plant cells. *Plant Physiol*. 136:3968-3978.

Sieberer, B.J., A.C. Timmers, F.G. Lhuissier, and A.M. Emons. 2002. Endoplasmic microtubules configure the subapical cytoplasm and are required for fast growth of Medicago truncatula root hairs. *Plant Physiol*. 130:977-988.

Simon, M., M.M. Lee, Y. Lin, L. Gish, and J. Schiefelbein. 2007. Distinct and overlapping roles of single-repeat MYB genes in root epidermal patterning. *Dev Biol*. 311:566-578.

Smith, L.G., and D.G. Oppenheimer. 2005. Spatial control of cell expansion by the plant cytoskeleton. *Annu Rev Cell Dev Biol*. 21:271-295.

Sparkes, I.A., N.A. Teanby, and C. Hawes. 2008. Truncated myosin XI tail fusions inhibit peroxisome, Golgi, and mitochondrial movement in tobacco leaf epidermal cells: a genetic tool for the next generation. *J Exp Bot*. 59:2499-2512.

Swarup, R., J. Friml, A. Marchant, K. Ljung, G. Sandberg, K. Palme, and M. Bennett. 2001. Localization of the auxin permease AUX1 suggests two functionally distinct hormone transport pathways operate in the Arabidopsis root apex. *Genes Dev*. 15:2648-2653.

Takahashi, H., K. Hirota, A. Kawahara, E. Hayakawa, and Y. Inoue. 2003. Randomization of cortical microtubules in root epidermal cells induces root hair initiation in lettuce (Lactuca sativa L.) seedlings. *Plant Cell Physiol*. 44:350-359.

Takeda, S., C. Gapper, H. Kaya, E. Bell, K. Kuchitsu, and L. Dolan. 2008. Local positive feedback regulation determines cell shape in root hair cells. *Science*. 319:1241-1244.

Tang, X.J., P.K. Hepler, and S.P. Scordilis. 1989. Immunochemical and immunocytochemical identification of a myosin heavy chain polypeptide in Nicotiana pollen tubes. *J Cell Sci*. 92 (Pt 4):569-574.

Tanimoto, M., K. Roberts, and L. Dolan. 1995. Ethylene is a positive regulator of root hair development in Arabidopsis thaliana. *Plant J*. 8:943-948.

Thole, J.M., J.E. Vermeer, Y. Zhang, T.W. Gadella, Jr., and E. Nielsen. 2008. Root hair defective4 encodes a phosphatidylinositol-4-phosphate phosphatase required for proper root hair development in Arabidopsis thaliana. *Plant Cell*. 20:381-395.

Timmers, A.C., P. Vallotton, C. Heym, and D. Menzel. 2007. Microtubule dynamics in root hairs of Medicago truncatula. *Eur J Cell Biol*. 86:69-83.

Tominaga, M., K. Morita, S. Sonobe, E. Yokota, and T. Shimmen. 1997. Microtubules regulate the organization of actin filaments at the cortical region in root hair cells of hydrocharis. *Protoplasma*. 199:83-92.

Tominaga, M., E. Yokota, S. Sonobe, and T. Shimmen. 2000. Mechanism of inhibition of cytoplasmic streaming by a myosin inhibitor, 2,3-butanedione monoxime. *Protoplasma*. 213:46-54.

Tominaga, R., M. Iwata, K. Okada, and T. Wada. 2007. Functional analysis of the epidermal-specific MYB genes CAPRICE and WEREWOLF in Arabidopsis. *Plant Cell*. 19:2264-2277.

Tominaga-Wada, R., M. Iwata, J. Sugiyama, T. Kotake, T. Ishida, R. Yokoyama, K. Nishitani, K. Okada, and T. Wada. 2009. The GLABRA2 homeodomain protein directly regulates CESA5 and XTH17 gene expression in Arabidopsis roots. *Plant J*. 60:564-574.

Traas, J.A., P. Braat, A.M. Emons, H. Meekes, and J. Derksen. 1985. Microtubules in root hairs. *J Cell Sci*. 76:303-320.

Tsai, S.L., P.J. Harris, and P.H. Lovell. 2003. The root epidermis of Echium plantagineum L.: a novel type of pattern based on the distribution of short and long root hairs. *Planta*. 217:238-244.

Van Bruaene, N., G. Joss, and P. Van Oostveldt. 2004. Reorganization and in vivo dynamics of microtubules during Arabidopsis root hair development. *Plant Physiol*. 136:3905-3919.

Vermeer, J.E., J.M. Thole, J. Goedhart, E. Nielsen, T. Munnik, and T.W. Gadella, Jr. 2009. Imaging phosphatidylinositol 4-phosphate dynamics in living plant cells. *Plant J*. 57:356-372.

Very, A.A., and J.M. Davies. 2000. Hyperpolarization-activated calcium channels at the tip of Arabidopsis root hairs. *Proc Natl Acad Sci U S A*. 97:9801-9806.

Voigt, B., A.C. Timmers, J. Samaj, J. Muller, F. Baluska, and D. Menzel. 2005. GFP-FABD2 fusion construct allows in vivo visualization of the dynamic actin cytoskeleton in all cells of Arabidopsis seedlings. *Eur J Cell Biol*. 84:595-608.

Wada, T., T. Kurata, R. Tominaga, Y. Koshino-Kimura, T. Tachibana, K. Goto, M.D. Marks, Y. Shimura, and K. Okada. 2002. Role of a positive regulator of root hair development, CAPRICE, in Arabidopsis root epidermal cell differentiation. *Development*. 129:5409-5419.

Wang, Y.S., C.M. Yoo, and E.B. Blancaflor. 2008. Improved imaging of actin filaments in transgenic Arabidopsis plants expressing a green fluorescent protein fusion to the C- and N-termini of the fimbrin actin-binding domain 2. *New Phytol*. 177:525-536.

Wang, Z., and T.C. Pesacreta. 2004. A subclass of myosin XI is associated with mitochondria, plastids, and the molecular chaperone subunit TCP-1alpha in maize. *Cell Motil Cytoskeleton*. 57:218-232.

Weigel, D., and J. Glazebrook. 2002. Arabidopsis : a laboratory manual. Cold Spring Harbor Laboratory Press, Cold Spring Harbor, N.Y. xii, 354 p. pp.

Whittington, A.T., O. Vugrek, K.J. Wei, N.G. Hasenbein, K. Sugimoto, M.C. Rashbrooke, and G.O. Wasteneys. 2001. MOR1 is essential for organizing cortical microtubules in plants. *Nature*. 411:610-613.

Wymer, C.L., T.N. Bibikova, and S. Gilroy. 1997. Cytoplasmic free calcium distributions during the development of root hairs of Arabidopsis thaliana. *Plant J*. 12:427-439.

Xia, Z., and Y. Liu. 2001. Reliable and global measurement of fluorescence resonance energy transfer using fluorescence microscopes. *Biophys J*. 81:2395-2402.

Xue, H.W., X. Chen, and Y. Mei. 2009. Function and regulation of phospholipid signalling in plants. *Biochem J*. 421:145-156.

Yalovsky, S., D. Bloch, N. Sorek, and B. Kost. 2008. Regulation of membrane trafficking, cytoskeleton dynamics, and cell polarity by ROP/RAC GTPases. *Plant Physiol*. 147:1527-1543.

Yang, G., P. Gao, H. Zhang, S. Huang, and Z.L. Zheng. 2007. A mutation in MRH2 kinesin enhances the root hair tip growth defect caused by constitutively activated ROP2 small GTPase in Arabidopsis. *PLoS One*. 2:e1074.

Yokota, E., S. Muto, and T. Shimmen. 2000. Calcium-calmodulin suppresses the filamentous actin-binding activity of a 135-kilodalton actin-bundling protein isolated from lily pollen tubes. *Plant Physiol*. 123:645-654.

Yokota, E., S. Ueda, K. Tamura, H. Orii, S. Uchi, S. Sonobe, I. Hara-Nishimura, and T. Shimmen. 2009. An isoform of myosin XI is responsible for the translocation of endoplasmic reticulum in tobacco cultured BY-2 cells. *J Exp Bot*. 60:197-212.

Yoo, C.M., J. Wen, C.M. Motes, J.A. Sparks, and E.B. Blancaflor. 2008. A class I ADP-ribosylation factor GTPase-activating protein is critical for maintaining directional root hair growth in Arabidopsis. *Plant Physiol*. 147:1659-1674.

Zhang, Y.J., J.P. Lynch, and K.M. Brown. 2003. Ethylene and phosphorus availability have interacting yet distinct effects on root hair development. *J Exp Bot*. 54:2351-2361.

Zheng, M., M. Beck, J. Muller, T. Chen, X. Wang, F. Wang, Q. Wang, Y. Wang, F. Baluska, D.C. Logan, J. Samaj, and J. Lin. 2009. Actin turnover is required for myosin-dependent mitochondrial movements in Arabidopsis root hairs. *PLoS One*. 4:e5961.

Zimmermann, P., M. Hirsch-Hoffmann, L. Hennig, and W. Gruissem. 2004. GENEVESTIGATOR. Arabidopsis microarray database and analysis toolbox. *Plant Physiol*. 136:2621-2632.

VITA

Eunsook Park was born in Seoul, Korea on November 20, 1973. Her interest of biology was raised when she met a new assistant professor, Ilha Lee, in March of 1999, after spending her undergraduate years with protesting for a better democracy and for improvement of the working environment of women in Seoul National University. Dr. Lee introduced the research of plant genetics using *Arabidopsis thaliana* and she joined his lab in 2000 as a graduate student. She received her degree of Master of Science at the division of Biological sciences in Seoul National University in February 2002. Eunsook moved to Knoxville, TN with her husband who entered the University of Tennessee for his Ph.D. in department of Botany. She started her Ph.D. program with Dr. Andreas Nebenführ in the department of Botany at the University of Tennessee, Knoxville in August 2003. Eunsook officially received her Ph.D. in March of 2010.